(2)

REPORT DOCUMENTATION PAGE

DTIC FILE COPY

1a. AD-A197 916

1b. RESTRICTIVE MARKINGS: N/A

2a. UNCLASSIFIED

DTIC ELECTE AUG 15 1988 D

3. DISTRIBUTION / AVAILABILITY OF REPORT: Approved for public release; distribution unlimited.

2b. DECLASSIFICATION / DOWNGRADING SCHEDULE: N/A

4. PERFORMING ORGANIZATION REPORT NUMBER(S): N/A

5. MONITORING ORGANIZATION REPORT NUMBER(S): AFOSR-TR- 88-0741

6a. NAME OF PERFORMING ORGANIZATION	6b. OFFICE SYMBOL (If applicable)	7a. NAME OF MONITORING ORGANIZATION
Pennsylvania State University		Air Force Office of Scientific Research

6c. ADDRESS (City, State, and ZIP Code)	7b ADDRESS (City, State, and ZIP Code)
Department of Electrical Engineering University Park, PA 16802	Bolling Air Force Base Washington, D.C. 20332

8a. NAME OF FUNDING / SPONSORING ORGANIZATION	8b. OFFICE SYMBOL (If applicable)	9. PROCUREMENT INSTRUMENT IDENTIFICATION NUMBER
Air Force Office of Sci. Res.	NE	AFOSR-84-0375

8c. ADDRESS (City, State, and ZIP Code)	10. SOURCE OF FUNDING NUMBERS			
	PROGRAM ELEMENT NO.	PROJECT NO.	TASK NO.	WORK UNIT ACCESSION NO.
Bolling Air Force Base Washington, D.C. 20332	61102F	2305	B4	

11. TITLE (Include Security Classification)

Studies of Optical Wave Front Conjugation and Imaging Properties of Nematic Liquid Crystal Films

12. PERSONAL AUTHOR(S)

Iam-Choon Khoo

13a. TYPE OF REPORT	13b. TIME COVERED	14. DATE OF REPORT (Year, Month, Day)	15 PAGE COUNT
Final	FROM 8/15/84 TO 5/14/88	June 30, 1988	

16. SUPPLEMENTARY NOTATION

17. COSATI CODES			18. SUBJECT TERMS (Continue on reverse if necessary and identify by block number)
FIELD	GROUP	SUB-GROUP	

19. ABSTRACT (Continue on reverse if necessary and identify by block number)

Optical nonlinearities of liquid crystals owing to laser induced molecular reorientation or laser induced thermal index change, were studied in the context of optical wave mixings and real time imagings. The basic mechanisms and the dynamics of the non-linearities were studied in detail in theories, and in experiments using lasers of various time scales and temporal characteristics. Quantitative documentation of nanosecond laser induced thermal grating was performed for the first time, and further established the optical imaging and switching capabilities of nematic liquid crystal film. The conversion of infrared images to visible images via real time optical wave mixing processes was also demonstrated. The capability of optical four wave mixing to generate amplified reflection and self-oscillation in nematic liquid crystal film was also demonstrated for the first time. Such a process will be useful for image processing as well as laser oscillator adaptive optics applications. New optical intensity switching effects and optical beam amplifications and infrared laser wave mixings were also experimentally demonstrated, that will find application in optical switching, image processing and power self-limiting.

UNCLASSIFIED

20. DISTRIBUTION / AVAILABILITY OF ABSTRACT	21. ABSTRACT SECURITY CLASSIFICATION
☐ UNCLASSIFIED/UNLIMITED ☐ SAME AS RPT ☐ DTIC USERS	UNCLASSIFIED

22a. NAME OF RESPONSIBLE INDIVIDUAL	22b. TELEPHONE (Include Area Code)	22c. OFFICE SYMBOL
	(202) 767-4931	NE

DD FORM 1473, 84 MAR — 83 APR edition may be used until exhausted. All other editions are obsolete.

SECURITY CLASSIFICATION OF THIS PAGE

"Studies of Optical Wave Front Conjugation and Imaging Properties of Nematic Liquid Crystal Films"

[AFOSR 840375]

By

Dr. Iam-Choon Khoo

Department of Electrical Engineering

Pennsylvania State University

University Park, PA 16802

June 30, 1988

Final Report

Prepared for

Air Force Office of Scientific Research

Bolling Air Force Base

Washington, D.C. 20332

Final Report

Table of Contents

Summary

Optical nonlinearities of liquid crystals owing to laser induced molecular reorientation or laser induced thermal index change, were studied in the context of optical wave mixings and real time imagings. The basic mechanisms and the dynamics of the nonlinearities were studied in detail in theories, and in experiments using lasers of various time scales and temporal characteristics. Quantitative documentation of nanosecond laser induced thermal grating was performed for the first time, and further established the optical imaging and switching capabilities of nematic liquid crystal film. The conversion of infra-red images to visible images via real time optical wave mixing process was also demonstrated. The capability of optical four wave mixing to generate amplified reflection and self oscillation in nematic liquid crystal film was also demonstrated for the first time. Such a process will be useful for image processing as well as laser oscillator adaptive optics applications. New optical intensity switching effects and optical beam amplifications and infrared laser wave mixings were also experimentally demonstrated, that will find applications in optical switching, image processing and power self limiting devices.

I. Introduction

Current research and development in optical imaging and signal processing have largely employed the nonlinear optical and electro-optical properties of certain crystals and thin film devices. In combination with new novel nonlinear optical processes, and cw or pulsed lasers covering the UV to far IR spectrum, useful high resolution imaging system with aberration correction capability and other image processing capabilities, optical light modulators, switches and various signal processing devices and adaptive optics applications have emerged. Nevertheless, the number of useful nonlinear (or otherwise) optical materials for meeting these new application demands is relatively limited.

This program is devoted to a detailed study of the special nonlinear optical properties of liquid crystal films for optical wave front conjugation and in related four-wave mixing processes. The fabrication of stable, high optical quality liquid crystal thin film has been established for many years. Commercially, an ever increasing number of liquid crystal of wide ranging physical characteristics are becoming available. These basic advantages, together with the recently discovered extraordinarily large optical nonlinearities make liquid crystals an attractive candidate for nonlinear optical switches and devices. We anticipate that some of the processes under study will in fact find immediate applications.

There are two distinct basic mechanisms for nonlinearity in liquid crystal. One is the optical field induced reorientation of the axially birefringent nematics. Perhaps the most important characteristics of liquid crystals is their large optical anisotoopy $\Delta\varepsilon$ ($\Delta\varepsilon=\varepsilon_{\parallel}-\varepsilon_{\perp}$ is the dielectric constant for optical field parallel, and perpendicular to the director (optical) axis of the liquid crystal, respectively). Typically $\Delta\varepsilon$ ranges from

0.4 to 1. Recent discovery by this investigator that it is possible to induce director axis reorientation with relatively low power lasers (with intensities on the order of watts/cm^2) had opened up a wide range of possibilities for nonlinear optical effects and applications. Most of the pioneer work have been conducted by this investigator in the past few years. Work done during the period supported by the Air Force Office of Scientific Research is detailed in the next section.

The other mechanism for optical nonlinearity is the naturally present high thermal index gradients of liquid crystal, especially near the nematic → isotropic phase transition temperature Tc. At temperatures far from Tc, both dn_e/dT and dn_o/dT (where n_e and n_o are the extraordinary and the ordinary refractive indices, respectively) are already higher than most high thermal index materials (e.g. cyclohexane). Near Tc, the magnitudes of these two increase by more than an order of magnitude. Since many nonlinear processes, e.g. optical wave mixings, wave front conjugations, self-phase modulation etc., depends on the laser induce thermal index changes, these effects can be observed in liquid crystals at much lower laser power (or energy). More importantly, since the required refractive index change can be achieved with high energy pulsed lasers, the (nonlinear) processes can also occur with a fast on-time.

II. Research Accomplishment

In the following paragraphs, we will summarize our research accomplishment into six broad categories. The related publications, conference presentations and other forms of research records are listed in the next section.

During the period 8/15/84 to 5/14/88:

1. We have conducted a thorough review of the theory and experiments on the orientational optical nonlinearity of liquid crystals in their nematic phase. We have compared and contrasted the nonlinearity with those observed previously in the liquid phases. A detailed examination of their dynamics (rise- and decay-times) and how these dynamics are affected by various liquid crystalline parameters (like viscosity, temperature, elastic constants, etc.) and geometrical configurations and laser intensity is performed. An important point that is borne out in actual experimentations is that the response of the liquid crystal reorientation can be faster if higher intensity lasers are used. Nanosecond response is possible with Megawatt/cm^2 optical intensity.

   The extraordinarily large optical nonlinearity associated with director reorientation has also been utilized to gain further insights into several nonlinear optical processes like self-focusing, self-phase modulation, optical bistability, nonlinear wave guiding and optical wave mixings. We have also developed a theory for the nonlocal dependence of the director axis reorientation with respect to the incident laser spot size, and conducted experimental measurements that substantiated the theoretical results. These nonlocal dependence

will be important in assessing the amount of cross talks in optical processing using multi-beams, and in the resolution limit in optical imaging processes.

2. We have also conducted a thorough theoretical analysis and experimental study of the basic mechanisms and the dynamics of laser induced thermal index change in nematic liquid crystals. In particular, we have performed a calculation based on current molecular theory of nematogen on both the ordinary and the extraordinary refractive index changes with temperature, and the index (holographic) grating associated with two laser beams mixings. Experimentally, we have employed nanosecond laser pulses to generate the thermal grating and studied its rise and decay time. Very interesting high frequency (GH_Z) interference effects associated with laser induced acoustic waves are observed in the first 100 ns of the rise part. The decay dynamics, and the anisotropy of the dynamics were found to be in agreement with the theoretical expectations. This detailed study has conclusively demonstrated that laser induced thermal grating and index change in nematic liquid can be a very useful mechanism for applications; future research on this is clearly call for.

3. In line with the thermal grating studies reported in item 2 above, we have also looked into the quasi steady state case where the thermal grating is induced by laser pulses on the order of ms, on the order of the thermal decay time constant. For this case, as discussed in the attached preprints, the grating associated with two beam mixings can be maximized if the grating spacing is large. In conjunction with the

extraordinarily large thermal nonlinearity, we have observed for the first time wave front conjugation with gain in a nematic liquid crystal film, and the related self-oscillations, using low power cw visible laser. This opens up a rather exciting new area, e.g., the possibility of image amplification, ring oscillator amplifier, etc., associated with these two wave mixing processes. Moreover, the obsorption constant of the liquid crystal can be increased with traces of disolved dye that absorbs in the IR regine, and thus one can extend all these studies to IR lasers.

4. Related to items 2 and 3 is the process of so-called nondegenerate four wave mixing, whereby the real time holographic grating is generated with lasers of one wavelength, and the image is reconstructed at another desired wavelength. We have, as an example, demonstrated the possibility of converting infra-red images to the visible. Obviously, the reverse is also possible. It is also possible to have an incoherent to coherent image conversion using a similar four wave mixing scheme, but it remains to be demonstrated. An interesting observation is that using liquid crystals "doped" with IR obsorbing dyes, IR laser energies on the order of $1mj/cm^2$ or so are sufficient for the wavelength conversion, and at a relatively fast time scale (nanoseconds on-time, microseconds off-time).

5. We have also followed up on our previous research expertise in transverse self-phase modulation and conducted studies on some novel transverse switching processes. This includes optical power limiting and laser self-bending effects. More recently, we have extended this

result to applications in the infrared regime, where there are relatively few room-temperature nonlinear materials.

6. We have experimentally and theoretically shown for the first time the possibility of obtaining large gain in Kerr media by degenerate multiwave mixing. This effect, which is previously thought possible only in photorefractive material, can be observed in any highly nonlinear thin film, and may be applied to various phase conjugation, beam/image amplification, oscillation, and wave-mixing based nonlinear optical devices.

III. List of Publications

III.A. Refereed Journals (reprints attached)

1. The mechanism and dynamics of transient thermal grating diffraction in nematic liquid crystal films I.C. Khoo and R. Normandin, IEEE J. Quantum Electronics, QE21, 329 (1985).

2. Liquid crystals--nonlinear optical properties and processes. I.C. Khoo and Y.R. Shen. (Invited paper) Optical Engineering, 24, 579 (1985).

3. Four wave mixing with gain using liquid crystal film. I.C. Khoo, T.H. Liu, R.R. Michael, G.M. Finn and J.Y. Hou, SPIE Vol. 613, 70 (1986).

4. Laser self-limiting and bending using nematic liquid crystal film. I.C. Khoo et al. Published in Proceedings of SPIE Optoelectronic Conference, SPIE Vol. 613, 43 (1986).

5. Infra-red to visible image conversion capability of nematic liquid crystal film. I.C. Khoo and R. Normandin, Appl. Phys. Letts. 47, 350 (1985).

6. Nonlinear optical properties of liquid crystal films for optical imaging processes. I.C. Khoo, Optical Engineering, 25, 198 (1986).

7. Wave front conjugation with gain and self-oscillation with a nematic liquid crystal film. I.C. Khoo, Appl. Phys. Letts. 47, 908 (1985).

8. Dynamic gratings and the associated self-diffractions and wave front conjugation processes in nematic liquid crystals. I.C. Khoo, Invited paper. IEEE Journal of Quantum Electronics. QE22, 1268 (1986).

9. Passive optical self-limiter using laser induced axially symmetric and asymmetric transverse self-phase modulations in a liquid crystal film. I.C. Khoo, G. Finn, R.R. Michael and T.H. Liu. Optics Letters 11, 227 (1986).

10. Theory and experiment on optically induced nematic axis reorientation and nonlinear effects in the nanosecond regime. I.C. Khoo, R.R. Michael and P.Y. Yan. IEEE J. Quant. Electronics. QE 23, 267 (1987).

11. Nonlocal transverse dependence of optically induced director axis reorientation of a nematic liquid cyrstal film--theory and experiment. I.C. Khoo, P.Y. Yan and T.H. Liu. J. of Optical Society of America B, Vol. 4, p. 115 (1987).

12. Transverse self-phase modulation optical bistability. Invited paper. Proceedings of the International Conference on Lasers '84, p. 196.

13. Probe beam amplification via two- and four-wave mixings in a nematic liquid crystal film. I.C. Khoo and T.H. Liu, IEEE J. Quantum Electronics, IEEE J. Quant. Electronics, JQE 23, 171 (1987).

14. Simultaneous occurrence of phase conjugation and pulse compression in stimulated scatterings in liquid crystal mesophases. I.C. Khoo et al., IEEE J. Quant. Electronics, JQE 23, 1344 (1987).

15. Transverse self-phase modulation and bistability in the transmission of a laser beam through a nonlinear thin film. I.C. Khoo et al. J. Opt. Soc. Am B4, 886 (1987).

16. Probe beam amplification via two- and four- wave mixing in a Kerr-like (liquid crystal) medium. I.C. Khoo and T.H. Liu, Mol. Crystal and Liquid Crystals, Vol. 143, 57 (1987).

17. Laser spot size dependence, nonlocality and saturation effect in transverse bistability. I.C. Khoo, T.H. Liu and P.Y. Yan and J.Y. Hou. Invited paper. Proceedings of the SPIE 1986 Quebec International Symposium on Optical Chaos, SPIE Vol. 667, p. 220 (1986).

18. Probe beam amplification via degenerate optical wave mixing in a Kerr medium. T.H. Liu and I.C. Khoo. IEEE J. Quantum Electronics JQE 23, 2020 (1987).

19. Optical multiwave mixings in silicon. I.C. Khoo and R. Normandin. Applied Physics Letters, 52, 525 (1988).

20. Nonlinear optical processes and applications in the infrared with nematic liquid crystals. Invited Paper. Proceedings of American Chemical Society Symposium on Electroactive Polymers (April 1987, Denver, CO).

21. Low power (10.6μm) laser beam amplification via thermal grating mediated degenerate four wave mixings in a nematic liquid crystal film. I. C. Khoo et al. J. Opt. Soc. Am. B5, p. 202 (1988).

III.B. Book Chapters

"Nonlinear Optics of Liquid Crystals" by I. C. Khoo in "Progress in Optics," Vol. XXVI, ed. E. Wolf (North Holland Press, 1988).

IV. Conference Presentations

1. Optical wave mixings in the mesophases of liquid crystals using nanosecond lasers. I.C. Khoo, Presented at the 1984 Annual Meeting of the Optical Society of America, October 1984.

2. Cavityless optical switching elements using nonlinear self-phase modulation. I.C. Khoo and T.H. Liu, Presented at the 1984 Annual Optical Society of America Meeting, October 1984.

3. Transverse self-phase modulation bistability in a nonlinear thin-film theory and experiment. I.C. Khoo, T.H. Liu and R. Normandin, International Conference on Lasers and Application--Laser, '84, November 1984.

4. Optical bistability of a dielectric cladded thin film near the total internal reflection state--theory and experiment--I.C. Khoo and J.Y. Hou. Presented at the Conference on Lasers and Electro-Optics, Baltimore, 1985.

5. Infra-red to visible image conversion using four-wave mixing in a liquid crystal film. I.C. Khoo and R. Normandin. Presented at the Conference on Lasers and Electro-Optics, 1985.

6. Nondegenerate four wave mixing and IR to visible image conversion in liquid crystal film. I.C. Khoo et al., Annual Meeting of Optical Society of America, Washington, D.C. (1985).

7. Nonlocal transverse dependence of liquid crystal directory reorientation and nonlinearity induced by a laser beam. I.C. Khoo et al., presented at the 1985 Annual meeting of the Optical Society of America, Washington, D.C.

8. Saturation and nonlocal effect in transverse self-phase modulation bistability. I.C. Khoo et al. Presented at the 1985 Annual meeting of the Optical Society of America, Washington, D.C.

9. Laser self-power limiting and self bending effect using nematic films. I.C. Khoo et al. presented at the SPIE Technical Conference, January 1986, Los Angeles, California.

10. Wave front conjugation with gain in a nematic liquid crystal film. I.C. Khoo. presented at the SPIE Technical Conference, January 1986, Los Angeles, California.

11. Laser spot size dependence, nonlocality and saturation effect in transverse bistability. Invited talk presented at the Quebec International Symposium on Optical Chaos, June 1986.

12. Nonlinear optics of nematic liquid crystal. Invited talk. Presented at the 1986 SPIE Annual International Symposium on Optical and Optoelectronic Applied Sciences and Engineering, August 1986.

13. Two and four wave mixing in liquid crystal. Invited talk. Presented at the 1986 SPIE Annual International Symposium on Optical and Optoelectronic Applied Sciences and Engineering, August 1986.

14. Beam amplification by two wave mixing via moving gratings in liquid crystal film. Invited talk. Presented at the International Topical meeting on Optics of Liquid Crystals, Italy, Napoli, July 1986.

15. Beam amplification via thermal and reorientational nonlinearities in liquid crystal films. Invited talk. Presented at Thomson CSF, Orsay, France, July 1986.

16. Phase conjugation and pulse compression via stimulated scattering in the isotropic and mesophases of liquid crystals, I.C. Khoo et al. Presented at Annual Meeting of the Optical Society of America, Oct. 1986, Seattle, Washington.

17. Beam amplification via dynamic wave mixings in liquid crystal film. I.C. Khoo and T.H. Liu. Presented at Annual Optical Society of America, October 1986, Seattle, Washington.

18. Theory of self-phase modulations, optical switching, and transverse bistability in the transmission of a laser through a nonlinear thin film. I.C. Khoo et al. Presented at the 1986 Annual Optical Society Meeting, Seattle, Washington, October 1981.

19. Theory and experiment on the nonlocal radial dependence of laser induced molecular reorientation in a nematic film. I.C. Khoo et al. Presented at 1986 Annual Optical Society Meeting, Seattle, Washington, October 1986.

20. Optical wave mixing and nonlinear optics of nematic liquid crystal film in the near- and far-infrared regime. I.C. Khoo, G.M. Finn and R.R. Michael. Conference on Lasers and Electro-Optics, Baltimore, April 1987.

21. Multiple nonlinear film for optical wave mixing. I.C. Khoo, G.M. Finn, T.H. Liu and R.R. Michael. CLEO, 1987, Baltimore.

22. Degenerate four wave mixing and beam amplification in a Kerr-medium T.H. Liu and I.C. Khoo. IQEC, 1987, Baltimore.

23. Nonlinear optical processes and applications in the infrared with nematic liquid crystals. Invited talk, American Chemical Society Symposium on Electroactive Polymers (April 5-10, 1987, Denver, CO).

24. Infrared optical wave mixing and amplification with liquid crystal nonlinearity. I.C. Khoo et al. SPIE Annual Optoelectronic Conference. San Diego, CA, August 1987.

25. 1.06μm nanosecond laser amplification via degenerate multiwave mixings in Si. I.C. Khoo et al. Presented at 1987 Annual Optical Society Meeting, Rochester, NY, October 1987.

26. Infrared laser amplification and switching using nematic liquid crystal films. I.C. Khoo et al. Presented at 1987 Annual Opt. Soc. Meeting, Rochester, NY, October 1987.

27. Beam amplification via multiwave mixing in stationary and transient thermal grating. I.C. Khoo et al. Presented at 1987 Annual Opt. Soc. Meeting, Rochester, NY, October 1987.

28. Optical bistabilities in liquid crystals. I.C. Khoo. Invited paper. International topical meeting on Optical Bistability, Chaos and Optical Computing, Peking University, August 1987.

29. Degenerate multiwave mixing and beam amplification in Si with nanosecond laser pulses. I.C. Khoo et al. Presented at the International Laser Science Conference, Atlantic City, NJ, November 1987.

30. Beam amplification via multiwave mixings in a nonlinear medium: New theoretical perspectives and experimental results. I.C. Khoo. Invited paper. Lasers '87, Lake Tahoe, December 1987.

31. New perspectives on multiwave mixing in Kerr-like and photorefractive semiconductor. I.C. Khoo. Presented at the Topical Meeting on Photorefractive Materials, UCLA, August 1987).

V. Personnel

The personnel involved in this research program includes the principal investigator and

(a) Four graduate students: T.H. Liu, R.R. Michael and G.M. Finn and P.Y. Yan.

The Mechanism and Dynamics of Transient Thermal Grating Diffraction in Nematic Liquid Crystal Films

IAM-CHOON KHOO, MEMBER, IEEE, AND RICHARD NORMANDIN

Abstract—We have studied the mechanism and the dynamics of degenerate four-wave mixing in a nematic liquid crystal film. Nanosecond laser pulses are used to generate an index grating associated with the changes in the density and in the order parameter. We have measured and analyzed the contributions from these two mechanisms, their interference effects rise and decay time constants, and have also performed a detailed analysis of the diffraction efficiency. This study quantitatively characterizes the potential usefulness of nematic films for four-wave mixing based applications.

Introduction

RECENT studies have demonstrated extraordinarily large optical nonlinearity of nematic liquid crystal arising from the optically induced reorientation of the molecular director axis [1]-[3]. The nonlinearity has been shown to be several orders of magnitude larger than that exhibited by a typical anisotropic liquid like CS_2 and is in the same order of magnitude as those observed in some nonlinear photorefractive crystals (e.g., $BaTiO_4$) or semiconductors. The response time of molecular reorientation in nematics is dependent on the optical intensity, ranging from seconds (optical intensity $\approx W/cm^2$) to microsecond or less (optical intensity $\approx MW/cm^2$), among other factors. Wavefront conjugation [4], optical bistability [5], and other optical processes [6] have been demonstrated using CW low-power lasers. In some nematic liquid crystals, e.g., MBBA (p-methoxybenzylidene-p-n-butylaniline), an equally large thermal indexing effect [1], [7] has been observed, due to the crystal's natural absorption and unusually high thermal index gradient dn/dT (where n denotes the refractive index and T the temperature). Laser induced thermal refractive index change in liquid crystalline media is a well-known effect, and has been studied in many other contexts [8]. Recently, thermal grating has received considerable attention in the study of degenerate four-wave mixing as a useful mechanism for high-power wavefront conjugation [9], [10]. Martin and Hellwarth, for example, have studied a wide variety of liquids with dissolved dyes in infrared-to-visible image conversion processes. Others have shown amplified reflections and high fidelity phase aberration corrected imaging results [11], [12].

In this paper, we present detailed experimental results and analysis of the basic mechanism for thermal indexing effects in nematic liquid crystals, whose refractive index in the nematic phase depends on the density ρ (as in liquid and crystals) and the order parameter S (unique for the liquid crystal phase). Degenerate four-wave mixing experiments are carried out with nanosecond laser pulses, and results for various parameters such as the diffraction efficiencies, the grating decay and on-set time, acoustic contribution, etc., are obtained. In the next section we will review the relevant theory of nematogen and some quantitative expressions for the laser induced density and order parameter gratings, and the roles played by various nematic, geometrical, and optical parameters. This is followed by detailed experimental results and an analysis.

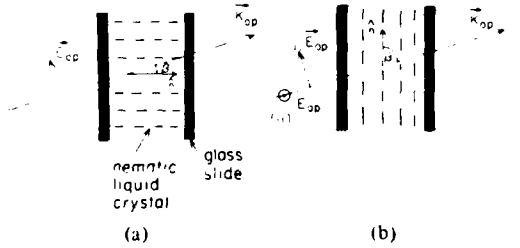

Fig. 1. Schematics of the laser nematic interaction in two typical nematic cell. (a) Homeotropically aligned nematics. (b) Planar nematic cell. Case (i) is for extraordinary ray. Case (ii) for ordinary ray ($\vec{E}_{op}$ is orthogonal to the nematic director axis).

Theoretical Considerations

Under excitation by nanosecond laser pulses, the thermal indexing effect in nematic is due to some finite absorption by the nematic at the wavelength of the laser. The absorption rate varies from material to material, and may often be aided by some dissolved dyes. It is perhaps more illuminating if we limit our attention to some exemplary geometries of interaction between the polarization of the laser and the director axis of the nematic, for two commonly occurring nematic cell alignments (planar and homeotropic). As depicted in Fig. 1(a) and (b), the optical propagation makes an angle β with respect to the nematic director axis $\vec{n}$. In Fig. 1(a), the beam propagates as an extraordinary ray with a refractive index n_e given by [13]

$$n_e = \frac{n_\perp n_\parallel}{(n_\parallel^2 \cos^2 \beta + n_\perp^2 \sin^2 \beta)^{1/2}}. \tag{1}$$

For Fig. 1(b), the beam propagates as an extraordinary ray in case (i), and as an ordinary ray with the refractive index $n_\perp$ in case (ii).

Manuscript received September 5, 1984; revised November 15, 1984. This work was supported in part by the National Science Foundation under Grant ECS8415387 and by the Air Force Office of Scientific Research under Grant AFOSR 840375.

I.-C. Khoo is with the Department of Electrical Engineering, The Pennsylvania State University, University Park, PA 16802.

R. Normandin is with the Division of Microstructural Sciences, the National Research Council of Canada, Ottawa, Ont., Canada K1A OR6.

0018-9197/85/0400-0329$01.00

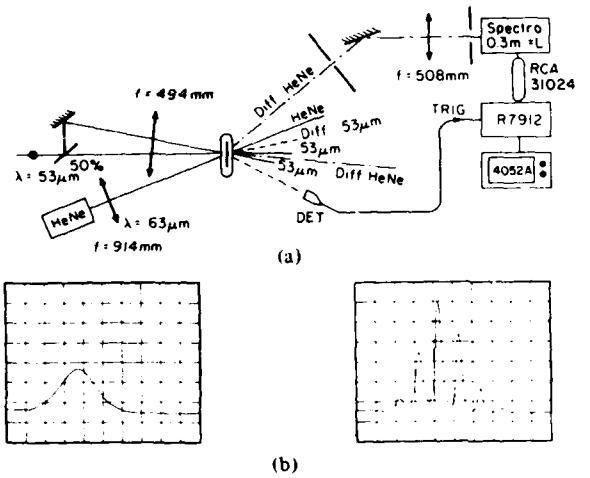

Fig. 2. Schematics of the experimental setup. Θ is the wave-mixing in air. (Θ in liquid crystal is 2/3 of Θ in air). The incident Nd:YAG SHG pulses and the He-Ne lasers are all in the same plane. (a) A single mode pump laser pulse. (b) A modulated two-mode pump laser pulse. Intensity profile as a function of time. Time scale: 10 ns/div.

Depending on the laser wavelength and intensity, the optically induced refractive index change originates from molecular reorientation and/or thermal heating. Pulsed laser induced molecular reorientation can occur in the configurations depicted in Fig. 1(a) and (b) [case (i)] [14], [15]. The basic mechanism is similar to that observed using a CW laser, with a rise time that depends on the laser intensity. Typically, one can estimate using well-known nematic theory that an optical intensity on the order of 100 MW/cm^2 is needed to see significant reorientation in the nanosecond time scale. Under this intensity, the accompanying thermal index effect is very large and tends to mask the reorientational effect. There is also a practical consideration not to involve the molecular reorientation, which is characterized by a very slow recovery time (typically about 1 s for a 40 μm thick sample).

For incident optical fields at $\beta = 0$, two distinct thermal index changes are induced $\Delta n_\parallel$ and $\Delta n_\perp$, corresponding to case (i) and case (ii), respectively. We shall henceforth limit our discussion to the planar sample depicted in Fig. 1(b). Similar results have been obtained for the homeotropic sample [Fig. 1(a)], where the thermal index gradient involved is $dn_\perp/dT$.

We are interested in a degenerate four-wave mixing configuration. As depicted in Fig. 2, the applied optical field consists of two lasers intersecting at a wave mixing angle θ in the xy plane and incident at an angle $\beta = 0$ on a planar sample with the polarization parallel to or perpendicular to the director axis. We have used wave mixing angles ranging from 1 to 12°, corresponding to optical grating constant ranging between about 34 μm (1°) to about 5 μm. The grating is characterized by a wave vector $\vec{q}(\vec{q} = \vec{k}_1 - \vec{k}_2)$. In case (i), $\vec{q}$ is *almost* normal to n while in case (ii), q is *almost* parallel to n. Obviously, for a finite wave mixing angle, the grating wave vector $\vec{q}$ is not exactly normal (or parallel) to n. However, since the wave mixing angle is small, the correction factor for components in the directions other than the ones stated is small and may be neglected.

Following standard nematic theory, the optical dielectric constants $\epsilon_\parallel(n_\parallel^2)$ and $\epsilon_\perp(n_\perp^2)$ are given by

$$\epsilon_\parallel = \epsilon_l(T) + 2/3\ \Delta\epsilon(T) \tag{2}$$

and

$$\epsilon_\perp = \epsilon_l(T) - 1/3\ \Delta\epsilon(T) \tag{3}$$

where $\epsilon_l(T)$ is the dielectric constant associated with the nematic in the zero-ordered phase ($S = 0$)

$$\epsilon_l = 1 + \frac{N\rho}{3\epsilon_0 M}(\alpha_l k_l + 2\alpha_T k_T); \qquad \epsilon_l \sim 1 + \text{const.}\ \rho. \tag{4}$$

ρ is the density of the nematic and $\alpha_{l,T}$ and $k_{l,T}$ are the longitudinal and transverse components of the molecular electronic polarization tensor α and the internal field tensor $\vec{K}$[13]. The dielectric anisotropy $\Delta\epsilon$ is given by

$$\Delta\epsilon = \frac{N\rho}{\epsilon_0 M}(\alpha_l k_l - \alpha_T k_T); \qquad \Delta\epsilon \sim \rho S \tag{5}$$

where S is the order parameter. The order parameter in most nematics is well approximated by the expression.

$$S = \left(1 - 0.98\frac{TV^2}{T_{Ni}V_{Ni}^2}\right)^{0.22} \tag{6}$$

where T_{Ni} is the nematic $\leftrightarrow$ isotropic phase transition temperature, and V's are the corresponding molar volumes. In general, therefore, the dielectric constant ϵ of a particular nematic is a function of ρ and S, which in turn depend on T.

Studies of thermal index change in nematics can be extremely complicated, since almost all the parameters mentioned so far (ρ, S, V), and other parameters (e.g., specific heat) that are important in wave mixing diffraction efficiency are temperature dependent. It is futile and probably meaningless to account for all temperature dependences. We shall focus here on the induced *density* and *order parameters* changes, whose effects dominate the wave mixing processes.

Equations (4) and (5) can be rewritten to give

$$\epsilon_l = 1 + C_1\rho \tag{4a}$$

and

$$\Delta\epsilon = C_2\rho S \tag{5a}$$

where C_1 and C_2 are constants deducible from (4) and (5). From known values of $\rho(\sim 1\ \text{gm}\cdot\text{cm}^{-3})$, $S(0.6)$, $\Delta\epsilon(0.65)$, and $\epsilon_\perp((1.53)^2)$ for PCB (at 20°C), we get $C_1 \sim 1.33$ and $C_2 \sim 1.12$. combining (4) and (5) and using $n^2 = \epsilon$, we get

$$\frac{dn_\perp}{dT} = 2n^{-1}\left[(1.33 - 0.37S)\frac{d\rho}{dT} - 0.37\frac{dS}{dT}\right]. \tag{7}$$

For PCB, S ranges from about 0.6 (at 20°C) to near vanishing value at T_{ni}. Notice that for $dn_\parallel/dT$, we get a similar expression as (7) with the numerical factor (-0.37) on the right-hand side replaced by (0.74). Both $d\rho/dT$ and dS/dT are negative. However, dS/dT is larger in magnitude and therefore $dn_\parallel/dT$ is negative and $dn_\perp/dT$ is positive.

Some numerical estimates may be illustrative. Consider PCB at 20°C. Using measured values of $d\rho/dT$ (6×10^{-4} gm/cm^{-3}

K^{-1}), ρ(1 gm/cm^{-3}), and the value of 0.37 dS/dT calculated from (6) (-6.9×10^{-3} K^{-1}), we get $dn/dT \sim (-2.7 \times 10^{-4} + +6.9 \times 10^{-4}) \sim 4.2 \times 10^{4}$ K^{-1}. This value agrees with the experimental value of 4×10^{-4} quite closely. Fig. 3 shows experimental values of $dn_{\parallel}/dT$ and $dn_{\perp}/dT$ and some theoretical points. Values calculated for other temperatures also agrees fairly with experimental results, although discrepancies arise as one approaches T_{ni}. There are several reasons for the discrepancies. One possibly is due to the breakdown of the mean field theory on which the expressions for S and ϵ are based. Secondly, we have not included any near-field corrections in our calculation. Nevertheless, the point to note from these plots is the largeness of dn/dT and its dramatic increase with temperature.

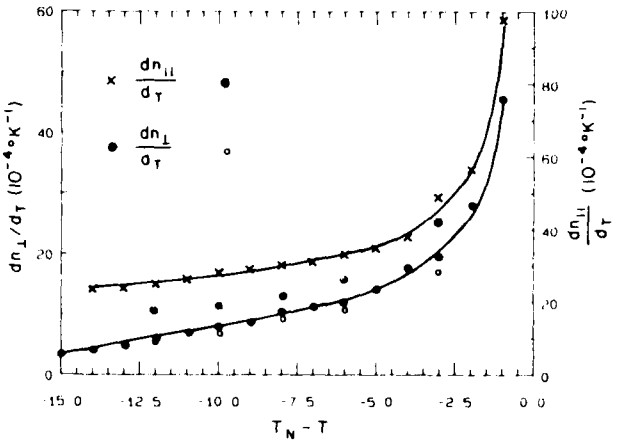

Fig. 3. Plot of $dn_{\parallel}/dT$ and $dn_{\perp}/dT$ for PCB as a function of temperature; data is deduced from [18]. Note that both dn/dT increase by an order of magnitude near T_{Ni}. The value of dn/dT of a high thermal index gradient liquid like cyclohexane is about 4×10^{-4} K^{-1}. Some sample theoretical estimates are also indicated (⊕ and ○).

Following a short laser pulse, a temperature grating $\Delta T(\vec{q}; t)$ is generated in the medium. The response of the medium as observed in our experiment follows the time-integrated intensity of the laser, and maximum diffraction is observed immediately following (within the laser pulsewidth) the laser. The resultant refractive index grating $\Delta n(\vec{q}; t)$ consists of two components. One is associated with the order parameter fluctuations $\Delta S(\vec{q}; t)$ while the other with the density fluctuation $\Delta S(\vec{q}; t)$. Under appropriate conditions (e.g., comparable magnitude of contribution in Δn from ΔS and $\Delta \rho$) the propagating $\Delta \rho$ grating will interfere with the nonpropagating (diffusive type) ΔS grating, leading to modulation in the diffraction from the grating [16], [17]. The period of modulation f_S^{-1} of the temporal behavior of the diffraction from the grating (of a CW probe laser) is simply given by $2\pi/|\vec{q}|\, C_s^{-1}$ (where Cs is the velocity of sound and $|\vec{q}| = 2|\vec{k}| \sin \theta/2$).

For a quantitative analysis of the diffraction efficiency, we note here an important point with respect to nematics, namely, that the thermal index gradient dn/dT is not a constant as a function of the temperature. As a matter of fact, it increases by more than one order of magnitude as one approaches the nematic ↔ isotropic phase transition [18] (cf., Fig. 3). Furthermore, values of the ρ, the heat capacity Cp, and the absorption coefficient α of the material needed for calculating the diffraction efficiency, are also sensitive to the temperature [19]. To get a good (and semiquantitative) insight into the diffraction efficiency, we choose for our theoretical calculations the parameters ΔT (rise in temperature), and Δn (the corresponding change in the refractive index), associated with the input pump energies. Both parameters can be easily measured experimentally. In the language of the usual four-wave mixing calculations [20], the two pump lasers set up an index grating Δn that oscillates spatially with a wave vector $\vec{q} = \vec{k}_1 - \vec{k}_2$. In conjunction with a probe laser (incident at $\vec{k}_1$, say), this generates a diffraction at $\vec{k}_4 = 2\vec{k}_1 - \vec{k}_2$. The maximum amplitude of the diffraction (corresponding to the maximum Δn, which, as a function of time, reaches a maximum value as the temperature of the sample rises to a maxima) is given by

$$E_D \cong \frac{k \Delta n E_1}{2n} \frac{(\sin \partial k\, d)}{\partial k} \tag{8}$$

assuming small absorption loss and small wave-mixing angles (valid in our case involving pure PCB). ∂k is the magnitude of the momentum mismatch. Equation (8) gives a maximum diffraction efficiency I_D/I_1 of

$$R \max \sim \frac{k^2}{4n^2} (\Delta n)^2 \left(\frac{\sin \partial k\, d}{\partial k}\right)^2. \tag{9a}$$

For typical experimental parameters ($\lambda = 0.53$ μm, $k_1 = k_2 = 2\pi n/\lambda$, θ (in air) = 2°, $d = 40$ μm), $\partial k \sim k\,\theta^2 \sim (39\ \mu\text{m})^2$, which is close to $d^2 = (40\ \mu\text{m})^2$. Equation (9) possesses an obvious overestimate factor of the experimentally realizable diffraction efficiency. Both the probe and the diffracted beam suffer scattering loss in traversing the sample (typically about 20 percent due to reflections at the glass-air, glass-nematic boundaries, and the nematic orientational fluctuation scattering). These losses in conjunction also with the "Gaussian" shape intensity profiles of the beam can easily contribute to at least an order of magnitude lower diffraction efficiency in the actual observed value.

Alternatively, one can also use the thin phase grating expression as in [9], by replacing all the temperature dependent parameters like dn/dT, C_p, and ρ, by their average values. In the temperature range involved (21-30°C), ρ and C_p varies only slightly (<10 percent), and thus can be assumed constant. On the other hand, dn/dT, (e.g., for n_1) changes by a factor of 2 (cf., Fig. 3), from ~0.0004 to ~0.001. The average dn/dT is thus taken to be 0.0007. The only unknown parameter for PCB is the absorption coefficient α. This is estimated from experimental observation of the temperature rise for a given incident laser energy. We found that $\alpha d \sim 3 \times 10^{-3}$, where d is the sample thickness ($d \sim 40$ μm). Following [9], the maximum diffraction efficiency is given

$$R_m \sim T D^2 U_1 U_2 \eta \tag{9b}$$

where T is the transmission coefficient at frequency ν of the third (probe) beam, $D = \nu_\rho^{-1} C_p^{-1}\, dn/dT$, and U_1 and U_2 are the energies (per centimeter^2) of the pump lasers, and $\eta \sim \alpha d$. We must remark here that both (9a) or (9b) are at best order of magnitude estimates of the diffraction efficiency.

The large change in the refractive index of liquid crystal over a small temperature rise is due to its inherently large thermal index. At 21°, $dn_\perp/dT$ is $\sim 4 \times 10^{-4}$, which is already larger than almost all high index liquids [21] (e.g., CS_2 and cyclohexane). Note, however, that $dn_\parallel/dT$ has an even larger magnitude $\sim 3 \times 10^{-3}$. Thus, utilizing $\Delta n_\parallel$ (or $\Delta n_\perp$ and $\Delta n_\parallel$ near Tc, where both increase by an order of magnitude) will greatly enhance the diffraction efficiency.

Experiment

We have conducted experiments with principally two kinds of nematics: MBBA (p-methoxybenzylidene-p-n-butylaniline) and PCB (pentyl-cyano-biphenyl). PCB absorbs very little at the 0.53 μm (SHG of Nd:YAG) wavelength used. To increase the absorption, we have also used PCB samples with traces of dissolved dyes (Rhodamine 6G). Comparative studies are made for samples with dissolved dyes and the pure samples to ascertain the roles of the dye molecules. MBBA absorption at 0.53 μm is considerably more than PCB's. However, as often noted, MBBA is rather unstable with the age of the sample. The overall results obtained for MBBA are, however, similar to those obtained with PCB, which appears to be stable over a period of months.

The typical sample used is 40 μm thick. Planar alignment is obtained by the rubbing method with lens tissues. Sample temperature is maintained at 21°. (The nematic ↔ isotropic transition temperature Tc of PCB is 35°.) At this temperature, $n_\perp \sim 1.52$, $n_\parallel \sim 1.72$, and $n_{liquid} \sim 1.58$. The experimental setup is schematically depicted in Fig. 2. The pump laser pulses are derived from the SHG of a Q-switch Nd:YAG laser. The output from this laser is either in the single [Fig. 2(a)] or a time-modulated two-mode [Fig. 2(b)] state. The laser pulse width (FWHM) is typically 20 ns, and the laser energies used lie in the range of a few millijoules to 35 mj. The incident lasers are weakly focused at the sample to a spot size of ~ 0.64 mm^2. The sample is oriented with the plane normal to the incident laser beams, with the director axis n oriented either parallel (||) or perpendicular (⊥) to the optical field polarization. A linearly polarized He-Ne laser is used to probe the grating and the diffraction following each *single* pump laser shot is monitored with a monochromator-PMT setup and analyzed by a transient waveform digitizer or a fast storage scope.

Results and Discussions

Depending on the wave-mixing angle and the type of pump-pulses used, there are essentially two types of time-dependence of the diffraction from the transient grating as probed by the He-Ne laser. Results quoted below involve the ordinary refractive index change Δn. One is depicted in Fig. 4(a), which is obtained using single-mode laser pulses [Fig. 2(a)]. We have a monotonic rise followed by a monotonic long-lived decay. The rise time is within the pulse length of the laser (which has a FWHM of about 20 ns). On the other hand, if the excitation is a time modulated [Fig. 2(b)] laser pulse, modulations due to the acoustic waves are observed during the first 100 ns or so of the diffraction, [as depicted in Fig. 4(b)] at an external wave-mixing angle = 2°. At other angles, modulations are also

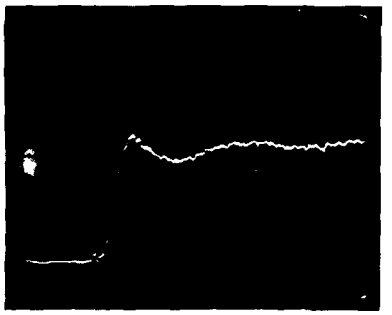

(a)

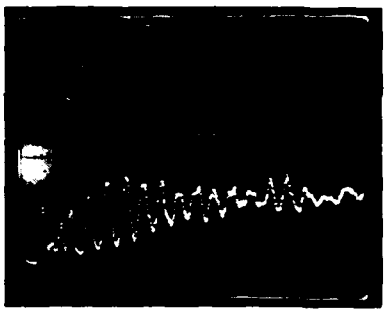

(b)

Fig. 4. The diffraction from the He-Ne as detected by the transient waveform digitizer. (a) Using single-mode Nd:YAG SHG as pump lasers. Time scale is 50 ns/dw, showing monotonic rise of the diffracted signal to a maximum within 50 ns from the start of the pump laser. (b) Modulated diffraction from the He-Ne. Time scale is 20 ns/dw.

observed but the modulation depth is less. The modulation is maximum at $\theta = 2°$ because the modulation frequency is "at resonance" with the acoustic frequency as confirmed in a recent report [12]. Fig. 4(b) also allows us to estimate the acoustic attenuation time constant in nematic liquid crystal to be about 100 ns at the acoustic frequency of 90 MHz (since the interference effects between the density (acoustic) and the order parameter gratings decay in a time scale of this order). This is probably the first direct time-dependent measurement of the acoustic attenuation time constant. The velocity of sound inferred from these experimental measurements ($\sim 1.53 \times 10^5$ cm/s) for nematic is in good agreement with known results.

More quantitative results of the density and order parameter can also be deduced from Fig. 4. The parameters used in the experiment for getting the results depicted in Fig. 4(b) are as follows. The energy in each of the pump beams is about 10 mj. The diffraction efficiency (associated with $dn_\perp/dT$) is measured to be 2 percent. The spot sizes of the incident laser beams are 0.6 mm^2. The initial temperature of the sample is 21°. Pulse duration is about 20 ns (FWHM). In a separate experiment, we have estimated that the rise in the temperature of the sample is about 9°C. (To determine the temperature rise due to the laser pulses, we noted the total pulse energy needed to just heat the sample to the isotropic phase (≈ 30 mj), i.e., 30 mj is needed to induce a 14° change in temperature. In our experiment, the *total* laser pulse energy is 20 mj, which gives us an estimate (by no means exact) of about 9° rise in temperature).

From known experimental data, this corresponds to a change in the refractive index Δn of 0.004. For the same tempera-

ture rise, the change in the refractive index $\Delta n_\perp(\rho)$ is -0.004, implying therefore $\Delta n(S)$ associated with the order parameter of 0.0008. Since $\Delta n_\perp(\rho)$ and $\Delta n_\perp(S)$ are comparable, one expects large modulations in the diffracted signal, which is indeed experimentally observed [cf., Fig. 4(b)]. In general, modulations are not detectable in samples where there is large induced temperature change (or refractive index change, equivalently) whence the $\Delta n(S)$ component dominates.

Using the experimental parameters ($\Delta n_\perp = 0.004$, $d = 40$ μm, $\lambda = 0.53$ μm, $\theta_{air} = 2°$), the forward diffracted efficiency as probed by the YAG laser pulses themselves can be estimated from (9a) to give $R_{max} \sim 2 \times 10^{-1}$. Using the expression (9b), with the parameters ($T \sim 1$), D(liquid crystal) $\sim 2 \times 10^{-2}$ (comparable to cyclohexane), $U_1 \sim U_2 \sim 1.6$ J/cm^2, $\eta \sim 3 \times 10^{-3}$, we also get $R_{max} \sim 2 \times 10^{-1}$. Experimentally we observe a diffraction efficiency of 2×10^{-2}. There are several reasons for the experimentally observed lower diffraction efficiency. Principally, we have not included losses (in both the pump and the probe, as well as the signal) in the liquid crystals, from scattering and reflection losses from the glass slides. Secondly, the grating builds up on the order of the laser pulse duration, and thus probing it with a time coincident pulse of the same duration may well not give the highest efficiency estimated in the theory. Finally, beam spot size, nonuniform spatial intensity distributions, etc., that normally lower the experimentally observed value (compared to theory) are all expected to contribute to some errors.

It is not our intention here, of course, to delve into a detailed quantitative exposition of the diffraction efficiency. Rather, noting that the parameters governing the diffraction efficiency and their roles, one can draw some conclusions regarding means of optimizing the four-wave mixing process.

One obvious way is to employ $dn_\parallel/dt$ (which is about seven times $dn_\perp/dt$ in the same temperature range), as we will presently see. Another way is by going to a slightly thicker sample. Our previous experiments have indicated that 100 μm thick samples are probably ideal in terms of stability (alignment) and losses (scattering). These two factors could easily increase the diffractions by two orders of magnitude.

For the same temperature rise, the change in the extraordinary refractive index $\Delta n_\parallel$ is much larger ($\Delta n_\parallel \sim 0.03$ for the same temperature rise). Under the same experimental situation, a diffraction efficiency of about 2×10^{-1} is observed (i.e., a ten-fold increase). At least a factor of two in the diffraction efficiency was also observed in thicker samples ($\approx$75 μm).

The decay behavior of the diffractions (from the He-Ne) is depicted in Fig. 5(a) and (b), for the case where $\vec{q}$ is normal to the director axis $\vec{n}$, and for $\vec{q}$ parallel to $\vec{n}$, respectively. Since the grating constant is about 17 μm (for $n_\perp$) at a 2° cross angle, while the sample thickens is 40 μm, the thermal diffusion may be approximated as a 1-dimensional problem along $\vec{q}$ (for this crossing angle at least). In that case, the decay time constants are given by $\tau_\perp = (D_\perp q_\perp^2)^{-1}$ and $\tau_{11} = (D_{11} q_{11}^2)^{-1}$, respectively. Using the value $D_\perp = 7.9 \times 10^{-4}$ cm^2/cm^{-1}, $D_{11} = 1.25 \times 10^{-3}$ cm^2/s^{-1}, and $q_\perp^2 \sim (2\pi/17\ \mu\text{m})^2$, and $q_{11}^2 \sim ((n_{11} \cdot 2\pi/n_\perp)/17\ \mu\text{m})^2$; we get $\tau_\perp \approx 110$ μs and τ_{11} of 55 μs. Experimentally, we obtain [from Fig. 5(a) and (b)] a value of 100 μs for $\tau_\perp$ and 50 μs for τ_{11}, showing remarkable

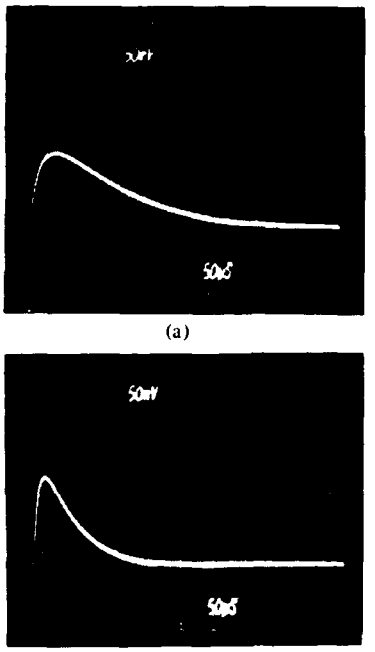

(a)

(b)

Fig. 5. (a) The decay of the thermal grating as monitored by the He-Ne diffraction. Time scale is 50 μs/dw. The grating wave vector $\vec{q}$ is perpendicular to the director axis n. (b) Thermal grating decay for $\vec{q}$ parallel to the director axis n. Decay is shorter by a factor of two.

agreement with the theoretical expectation. In general, the decay time constant decreases as we increase the wave-mixing angle θ (i.e., increase q), in a *roughly* q^{-2} dependence.

The rather large amount of pump energy needed to generate the observed diffraction is simply due to the fact that the liquid crystal used (PCB) absorbs very little at the pump laser wavelength (0.53 μm). The absorption can be easily increased by "doping" the PCB with traces of dissolved dyes. Using dyed samples, the same diffraction efficiency is observed using pump laser energies on the order of 3 or 4 mj. A detailed study of both the rise and the decay of the diffraction shows that there is hardly any difference compared to the "undyed" or pure nematic. This indicates that the dye molecules essentially act as absorbers and rapidly transfer the excitation to the nematic via some intermolecular relaxation processes.

In the case of dyed samples, the sample shows sign of heating through the nematic → isotropic transition at slightly elevated input energies (>10 mj). In that case, multiorder diffractions are observed. The decay is characterized by very long lifetime (cf., Fig. 6) on the order of ~150 ms. This is consistent with the fact that when the input energies are high, grating or "line" of liquid are produced [22]. When these lines cool through the isotropic-nematic point, the orientations of the director axes will be random. These lines of nematics (with a refractive index (~1.58) higher than the surrounding nematic $n_\perp \sim 1.52$) reorient themselves with a time constant characterized by the grating spacing λ_q of 17 μm, (which is much smaller than the thickness of the sample 40 μm). Using the well-known results for τ in terms of the viscosity ($\tau = \gamma \lambda_q^2/K\pi^2$), we get a reorientation time of $\approx$290 ms (using $K \sim 0.7 \times 10^{-8}$; $\gamma \sim 0.7$; $\lambda q = 17$ μm) in support of the above experimental observation.

Fig. 6. The decay behavior of the thermal grating of a "dyed" PCB sample when the grating maxima give rise to liquid phase. Time scale is 50 ms/div. The observed relaxation time of ~150 ms is consistent with the theoretical prediction based on reorientation mechanisms.

Further Remarks

Time dependence studies of thermal effects in liquid crystals are both interesting (and new) and necessary.

Our study has resulted in the determination of several key parameters needed for a quantitative determination of the suitability and superiority over other materials, of nematics for pulsed laser wave-mixing processes. Since the thermal decay constants are on the order of microseconds, pulsed lasers of considerably less power can be employed (e.g., a 10 mj, 10 μs laser with a power of 1 kW) for wavefront conjugation or other purposes. Microsecond lasers also eliminate complications from acoustic waves interference. The versatility of nematics can be widened, and the pump energy requirement reduced, if appropriate dyes are dissolved in the nematics. Operating near Tc (but not too near to induce instability) will also obviously improve the diffraction efficiency. Experimentally we have verified that the diffraction increases by more than an order of magnitude at temperatures near Tc. Utilizing $\Delta n_{\parallel}$ will also improve the diffraction efficiency by at least an order of magnitude over $\Delta n_{\perp}$, as we have demonstrated.

Using these new known experimental results on the dynamical constants of the wave-mixings and nematic parameters, we are currently investigating the actual optimum configurations for wavefront conjugation applications.

References

[1] I. C. Khoo, "Optically induced molecular reorientation and third order nonlinear processes in nematic liquid crystals," *Phys. Rev.*, vol. A23, pp. 2077–2081, 1981; see also I. C. Khoo and S. L. Zhuang, "Nonlinear light amplification in a nematic liquid crystal above the Freedericksz transition," *Appl. Phys. Lett.*, vol. 37, pp. 3–5, 1980; see also I. C. Khoo, "Theory of optically induced molecular reorientation and quantitative experiments on wave-mixings and self-focusing of light," *Phys. Rev.*, vol. A25, pp. 1636–1644, 1982.

[2] S. D. Durbin, S. M. Arakelian, and Y. R. Shen, "Optically induced birefringence and Freedericksz transition in nematic liquid crystal," *Phys. Rev. Lett.*, vol. 47, pp. 1411–1415, 1981.

[3] N. V. Tabiryan and B. Ya Zel'dovich, "The orientational optical nonlinearity of liquid crystals," *Mol. Cryst. Liq. Cryst.*, vol. 62, pp. 237–250; see also R. M. Hermen and R. J. Serinko, "Nonlinear optical processes in nematic liquid crystals near a Freedericksz transition," *Phys. Rev.*, vol. A19, pp. 1757–1769, 1979.

[4] I. C. Khoo and S. L. Zhuang, "Wavefront conjugation in nematic liquid crystals," *IEEE J. Quantum Electron.*, vol. QE-18, pp. 246–248, Feb. 1982; see also F. N. Leith, H. Chen, Y. Cheng, G. Swanson, and I. C. Khoo, "Wavefront conjugation with reduced coherence," in *Proc. 5th Rochester Conf. Coherence. Quantum Optics*, 1983.

[5] I. C. Khoo, P. Y. Yan, T. H. Liu, S. Shepard, and J. Y. Hou, "Theory and experiment on optical transverse intensity bistability in the transmission through a nonlinear thin (nematic liquid crystal) film," *Phys. Rev.*, vol. A29, pp. 2756–2764, 1984; see also I. C. Khoo, J. Y. Hou, R. Normandin, and V. C. Y. So, "Theory and experiment on optical bistability in a Fabry–Perot interferometer with an intracavity nematic liquid crystal film," *Phys. Rev.*, vol. A27, pp. 3251–3257, 1983.

[6] G. Barbero, F. Simoni, and P. Aiello, "Nonlinear optical reorientation in hybrid aligned nematics," *J. Appl. Phys.*, vol. 55, pp. 304–311, 1984; see also I. C. Khoo, "Optical-thermal induced total internal reflection to transmission switching at a glass-nematic liquid crystal interface," *Appl. Phys. Lett.*, vol. 40, pp. 645–648, 1982.

[7] I. C. Khoo and S. Shepard, "Submillisecond grating diffractions in nematic liquid crystal films," *J. Appl. Phys.*, vol. 54, pp. 5491–5493, 1983.

[8] F. J. Kahn, "IR-laser induced thermo-optic smectic liquid crystal storage displays," *Appl. Phys. Lett.*, vol. 22, pp. 111–113, 1973, and references therein; see also V. Volterra and I. Wiener Avnear, *Opt. Commun.*, "CW thermal lens effects in thin laser of nematic liquid crystal," *Opt. Commun.*, vol. 12, pp. 194–197, 1974.

[9] G. Martin and R. W. Hellwarth, "Infrared-to-optical image conversion by Bragg reflection from thermally induced index gratings," *Appl. Phys. Lett.*, vol. 34, pp. 371–373, 1979.

[10] I. O. Tocho, W. Sibbett, and D. J. Bradley, "Picosecond phase-cojugate reflection from organic dye saturable absorbers," *Opt Commun.*, vol. 34, pp. 122–126, 1980; see also "Thermal effects in phase cojugation in saturable absorbers with picosecond pulses," *Opt. Commun.*, vol. 37, pp. 67–71, 1981; see also R. C. Caro and M. C. Gower, "Phase conjugation by degenerate four-wave mixing in absorbing media," *IEEE J. Quantum Electron.*, vol. QE-18, pp. 1376–1380, Sept. 1982; see also "Amplified phase conjugate reflection of krf laser radiation," *Appl. Phys. Lett.*, vol. 39, pp. 855–857, 1981.

[11] M. H. Garrett and H. J. Hoffman, "Thermally induced phase conjugation efficiency and beam quality studies," *J. Opt. Soc. Amer.*, vol. 73, pp. 617–623, 1983.

[12] I. C. Khoo and R. Normandin, "Nanosecond laser induced four-wave mixings and ultrasonic waves in nematic liquid crystal films," *Opt. Lett.*, vol. 9, pp. 285–287, 1984.

[13] W. H. de Jeu, *Physical Properties of Liquid Crystalline Materials*, New York: Gordon and Breach, 1980, ch. 4 and references therein.

[14] H. Hsiung, L. P. Shi, and Y. R. Shen, "Time dependent laser induced molecular reorientation in a nematic liquid crystal film," *Bull. Amer. Phys. Soc.*, vol. 29, p. 394, 1984; see also *Phys. Rev.*, vol. A30, pp. 1453–1459, 1984.

[15] Using nanonsecond laser pulses, we have observed degenerate four-wave mixing signals associated with the molecular reorientation nonlinearity in a homeotropic sample (for the case $\delta = 0$).

[16] K. A. Nelson, R. J. Dwayne Miller, D. R. Lutz, and M. D. Fayer, "Optical generation of tunable ultrasonic waves," *J. Appl. Phys.*, vol. 53, pp. 1144–1149, 1982.

[17] R. C. Desai, M. D. Levenson, and J. A. Barber, "Forced Rayleigh scattering: Thermal and acoustic effects in phase conjugate wavefront generation," *Phys. Rev.*, vol. A27, pp. 1968–1976, 1983; see also I. P. Battra, R. H. Enns, and D. Pohl, "Stimulated thermal scattering of light," *Phys. Status Solidi*, vol. 48, pp. 11–63, 1971.

[18] R. G. Horn, "Refractive indices and order parameters of two liquid crystals," *J. de Phys.*, vol. 39, pp. 105–109, 1978; see for example, the refractive index of PCB at 6328 and 5890 Å as a function of temperature.

[19] G. R. Van Hecke and J. Stecki, "Pretransitional behaviour of the density of the nematic phase," *Phys. Rev.*, vol. A25, pp. 1123–1126, 1982; see also D. Armitage and I. P. Price, "Volumetric study of the nematic-isotropic pretransition region," *Phys. Rev.*, vol. A15, pp. 2496–2500, 1977.

[20] N. A. Bloembergen, *Nonlinear Optics*, New York: Benjamin, 1965.

[21] See, for example, M. F. Mack, "Stimulated thermal light scattering in the picosecond regime," *Phys. Rev. Lett.*, vol. 22, pp. 13–15, 1969, for some tabulated value of $\partial n/\partial T$; see also R. M. Herman and M. A. Gray, "The prediction of the stimulated thermal Ray-

leigh scattering in liquids," *Phys. Rev. Lett.*, vol. 19, pp. 824-828, 1967; see also R. W. Hellwarth, "Third order optical susceptibilities of liquids and solids," in *Progress in Quantum Electronics*, vol. 5, J. H. Sanders and S. Stenholm, Eds. New York: Pergamon, 1977, p. 1.

[22] The effect is similar to the so-called "channels effect," observed by V. F. Kitaeva, N. N. Sobolev, A. S. Folot'ko, L. Csillag, and N. Kroo, "Light diffraction by laser beam created "channels" in nematic liquid crystals," *Mol. Cryst. Liq. Cryst.*, vol. 91, pp. 137-143, 1983; in the case of smectic sample, the reorientation upon supercooling is random, leading to permanent grating information; see also I. C. Khoo and R. Normandin, "Nanosecond laser induced ultrasonic waves and erasable permanent gratings in smectic liquid crystal," *J. Appl. Phys.*, vol. 55, pp. 1416-1418, 1984.

Iam-Choon Khoo ([redacted]) He received the B.S. degree in physics with a first class honors from the University of Malaya, Malaysia, in 1971, and the M.A. and Ph.D. degrees in physics from the University of Rochester, Rochester, NY, in 1973 and 1976, respectively.

He has held postdoctoral and research associate positions of Ames Laboratory, Iowa State University of Science and Technology, Ames, IA, the University of Southern California, Los Angeles, CA, and the University of Toronto, Ont., Canada. He then joined the Physics Department at Wayne State University, Detroit, MI, in 1979 as an Assistant Professor, becoming an Associate Professor in 1983. In 1984, he joined the faculty at the Pennsylvania State University, University Park, PA, as an Associate Professor with the Department of Electrical Engineering. His current research interests are in theoretical and experimental nonlinear optical processes, optical wave mixing, wavefront conjugation, optical bistability, and switching in liquid crystalline materials.

Dr. Khoo is a member of the Optical Society of America.

Richard Normandin received the B.Sc. degree in physics from the Universite' de Montreal, Montreal, P.Q., Canada, in 1973. Subsequently, he obtained the M.Sc. degree for work in optical high-speed signal processing by surface acoustic wave interactions, and the Ph.D. degree in 1980 in the field of nonlinear optics in optical planar waveguides, both from the University of Toronto, Toronto, Ont., Canada.

He was previously with the solid-state physics section of the National Research Council of Canada, following a postdoctoral stay at Stanford University, Stanford, CA, with the support of the Natural Sciences and Engineering Research Council and the Rutherford Memorial Scholarship of the Royal Society of Canada. Currently, he is a research scientist with the National Research Council of Canada in the division of physics. His present interests are in the area of nonlinear optical properties of atoms near or at an interface, and their possible applications in quantum electronics.

Dr. Normandin is a member of the Canadian Association of Physicists, the Society of Photo-optical Instrumentation Engineers and the Optical Society of America.

Liquid crystals: nonlinear optical properties and processes

I. C. Khoo
The Pennsylvania State University
Department of Electrical Engineering
University Park, Pennsylvania 16802

Y. R. Shen
University of California
Department of Physics
Berkeley, California 94720

Abstract. Liquid crystals as nonlinear optical materials are reviewed. Potential applications of these materials in wave mixing, phase conjugation, and optical bistability are discussed. The extremely large optical nonlinearity and the slow response time of these materials make them unique for studies of some highly nonlinear optical processes and their dynamic characteristics.

Subject terms: nonlinear optics; liquid crystals; reorientation; director axis; thermal index; wave mixing; phase conjugation; optical switching.

Optical Engineering 24(4), 579-585 (July/August 1985).

CONTENTS

1. INTRODUCTION

Liquid crystalline materials are generally composed of highly anisotropic molecules. Strong correlation in the orientations of such molecules can lead to the mesomorphic phases in which the molecules are orderly aligned and the medium behaves like an anisotropic fluid.[1,2] The degree of molecular alignment as well as the direction can easily be changed by external perturbation.[1,2] As a result, liquid crystals form a unique class of optical materials that have attracted much attention in the past 15 years. They are strongly birefringent and exhibit huge electro- and magneto-optical effects. Therefore, they have been used in practical applications as sensing, display, and memory devices.[3,4]

Liquid crystals are also highly nonlinear.[5,6] Since they differ from ordinary organic liquids only in molecular arrangement, the electronic contribution to the optical nonlinearity in such materials is not expected to be very different from those of ordinary liquids. Optical-field-induced molecular reorientation is, however, much more significant in liquid crystals because of the strong molecular correlation. As far as field-induced reorientation through induced dipoles on molecules is concerned, dc and optical fields are basically equivalent aside from dispersion. In the mesomorphic phases, a dc field of $\sim$100 V/cm is often sufficient to induce a significant reorientation of the molecular alignment, leading to an average refractive index change as large as $\sim$0.01 to 0.1. The corresponding optical beam intensity is only $\sim$100 W/cm^2, which is readily obtainable from a cw argon laser. Such a high optical nonlinearity is not easily found in other materials and renders liquid crystals ideal for studies of nonlinear optical effects resulting from laser-induced refractive index changes. The rather unique features of liquid crystals as nonlinear optical media are that the samples are inexpensive and easy to prepare, the induced refractive indices are highly anisotropic, and the response times are very slow. Laser heating of liquid crystals in the mesophases can also lead to a change in the optical anisotropy. The response times of the laser-induced thermal effect and the laser-induced molecular reorientation are, however, quite different.

Although liquid crystals are birefringent in the mesophases, they are generally centrosymmetric (except in the cholesteric phase, where the helical molecular arrrangement is weakly centroasymmetric.) Therefore, in such a medium, second-order nonlinear optical processes are forbidden and only third-order processes have been studied extensively. Most of the work has concentrated on studying nonlinear optical effects arising from the optical-field-induced refractive indices in liquid crystals. These studies have included self-focusing,[7-10] self-phase modulation,[11,12] degenerate wave mixing,[13-16] phase conjugation,[17] and optical bistability.[18-21] The slow response of liquid crystals, though detrimental from the practical device point of view, makes transient studies of these effects fairly easy and interesting and provides some new features to these otherwise well-known nonlinear optical phenomena.[7-10,18-21]

In the following sections, we first present a general description of the physical mechanisms giving rise to the optical nonlinearity in the various phases of liquid crystals and then briefly discuss a number of nonlinear optical processes that have been observed in liquid crystals and their possible applications.

Invited Paper NO-105 received Jan. 8, 1985; revised manuscript received Feb. 13, 1985; accepted for publication Feb. 13, 1985; received by Managing Editor April 8, 1985.

2. OPTICAL NONLINEARITY OF LIQUID CRYSTALS

The electronic structure of liquid crystals is mainly dominated by that of individual molecules. The electronic contribution to optical nonlinearity in liquid crystals is therefore essentially the same as that in liquids. It is generally not exceptionally large, and so we will not dwell on it here. Instead, we shall discuss only optical nonlinearity arising from molecular motion, namely, molecular reorientation and laser-induced thermal effect.

Consider first a liquid crystal in the isotropic phase in which molecules are randomly oriented. In the presence of a linearly polarized light, the molecules are partially aligned by the optical field. The degree of alignment is usually described by the so-called orientational order parameter Q (with Q = 0 and Q = 1 referring to random distribution and perfect alignment, respectively). We can define Q in terms of the optical susceptibility tensor χ.[22,23] Assuming that the field E is along $\hat{x}$, we have

$$\chi_{xx} = \bar{\chi} + \frac{2}{3}\Delta\chi_o Q ,$$
$$\chi_{yy} = \chi_{zz} = \bar{\chi} - \frac{1}{3}\Delta\chi_o Q , \tag{1}$$

where $\bar{\chi} = (\chi_{xx} + \chi_{yy} + \chi_{zz})/3$ is the average linear susceptibility of the medium and $\Delta\chi_o$ is the anisotropy when the molecules are perfectly aligned (Q = 1). In the isotropic case, the optically induced Q is expected to be much smaller than one and can be shown to be of the form

$$Q \propto \frac{\Delta\chi_o |E|^2}{T - T^*} . \tag{2}$$

Here, T^* is a fictitious second-order phase transition temperature that is somewhat below the actual isotropic-mesomorphic transition temperature T_{NI} ($T_{NI} - T^*$ is often less than 1 K). Thus, Q should diverge with $(T - T^*)^{-1}$ as T approaches T_{NI}. Such a pretransitional behavior is commonly known as critical divergence. Physically, this happens because the molecular correlation begins to set in as T approaches T^*. The changes in the refractive indices, $\Delta n_{xx} = -2\Delta n_{yy} = -2\Delta n_{zz} = (8\pi/3)\Delta\chi_o Q$, are directly proportional to Q and hence to $(T - T^*)^{-1}$.

The above critical characteristic of liquid crystals has been verified experimentally.[22,23] As an example, Fig. 1(a) shows that $\delta n = n_{xx} - n_{yy}$ of p-methoxy-benzylidene p-n butylaniline (MBBA) indeed varies with $(T - T^*)^{-1}$ as T approaches T_{NI}. [In the figure β is defined as $(n/\pi|E|^2)\delta n$ with $n = (n_{xx} + n_{yy} + n_{zz})/3$.] Because of critical divergence, $\delta n/|E|^2$ becomes as large as 10^{-9} esu even at $T - T_{NI} = 5$ K, which is almost 100 times larger than that of CS_2. Generally associated with critical divergence is the critical slowing-down behavior; that is, the response time τ of δn is also proportional to $(T - T^*)^{-1}$, as shown in Fig. 1(b) for MBBA. At $T - T_{NI} = 5$ K, τ becomes as long as 100 ns. We can define a figure of merit $f = \Delta n_{xx}/|E|^2\tau = (2\pi/3n)\beta/\tau$ to describe the strength of a nonlinear medium in practical applications when both the magnitude and the speed of response of Δn are important. For liquid crystals in the isotropic phase, we find

$$f \propto \frac{(\Delta\chi)^2}{\nu} , \tag{3}$$

where ν is a viscosity coefficient. For example, we have from Fig. 1, $f \simeq 6\times10^{-3}$ esu/s.

In the mesophases, molecules are highly correlated. The optical field is no longer strong enough to modify the degree of molecular alignment in any appreciable sense, but it is strong enough to reorient the direction of molecular alignment. This is quite analogous to the reorientation of magnetization of a ferromagnetic domain by an applied magnetic field. Because of the correlated molecular response (or the correlated spin response in the ferromagnetic case), the resulting change in the refractive indices (or effective magnetic susceptibility in the ferromagnetic case) is extremely large but slow. Realizing that the dc and optical fields are equivalent in orienting the molecules if no permanent dipole is present, we know that a laser intensity of ~250 W/cm^2 (E = 300 V/cm) is capable of inducing an average refractive index change of 0.01 to 0.1 in a nematic film,[24-31] but the response time can be more than a few seconds.

Detailed theoretical and experimental studies of optical-field-induced reorientation of molecular alignment have been carried out on homeotropic nematic films (i.e., molecular alignment perpendicular to the film) with extraordinary laser beams.[24-31] The direction of molecular alignment (known by the director) should obey the Euler equation derived from minimization of the free energy of the system. Let $\theta(z)$ be the angle the director makes with the surface normal at the position z in the film. (see Fig. 2). Then, we have[32]

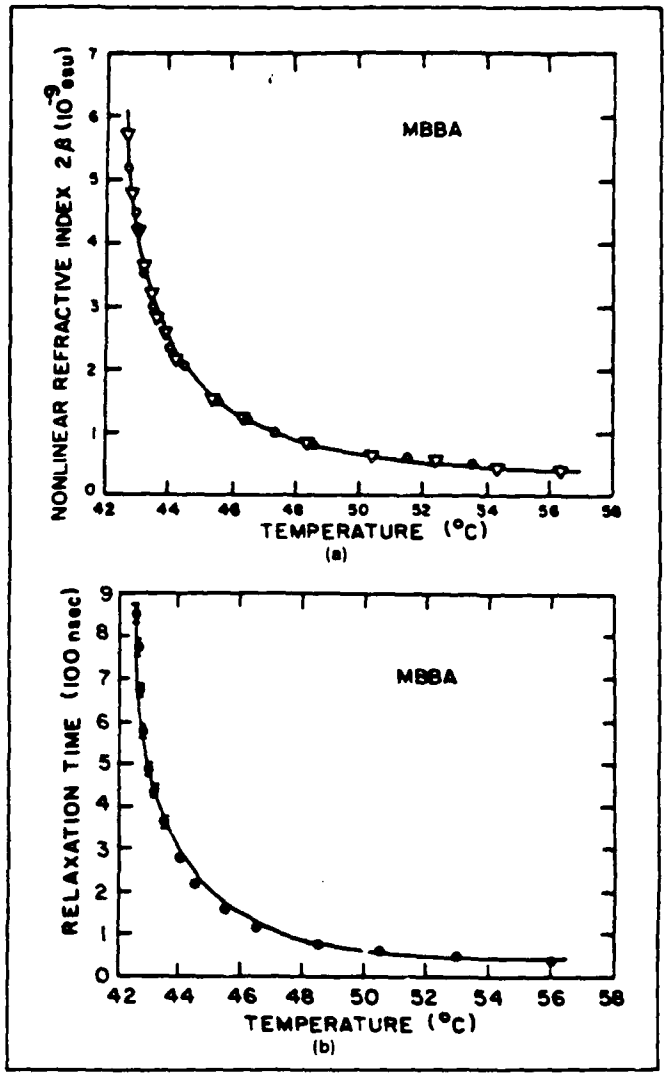

Fig. 1. (a) Nonlinear refractive index as a function of temperature for MBBA. The Δ are experimental data from optical Kerr measurements, and the o are experimental data from ellipse-rotation measurements. The solid curve is given by $5.4\times10^{-9}/(T-T_c)$ with 314.7 K. (b) Relaxation time τ_L of the order parameter as a function of temperature for MBBA. The solid curve is the theoretical curve, and the dots are the experimental data points. (After Refs. 22 and 23.)

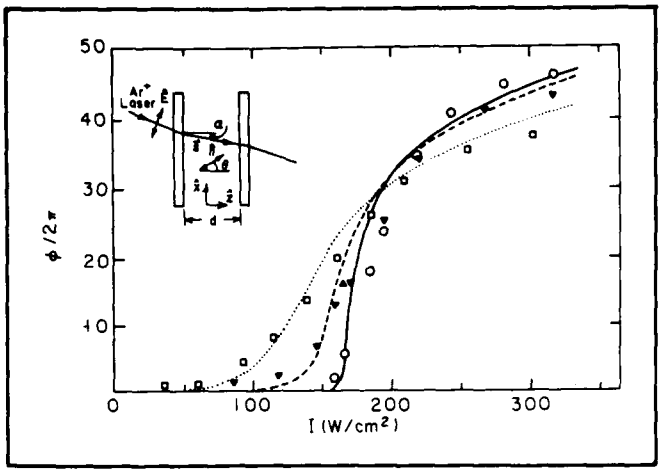

Fig. 2. Experimental data and theoretical curves for the phase shift $\Delta\phi$ induced in a 250 μm, homeotropically aligned, 5CB film by an Ar^+ laser beam at different angles α: circles and solid curve, $\alpha=0°$; solid triangles and dashed curve, $\alpha=3°$; squares and dotted curve, $\alpha=11°$. Inset shows the experimental geometry.

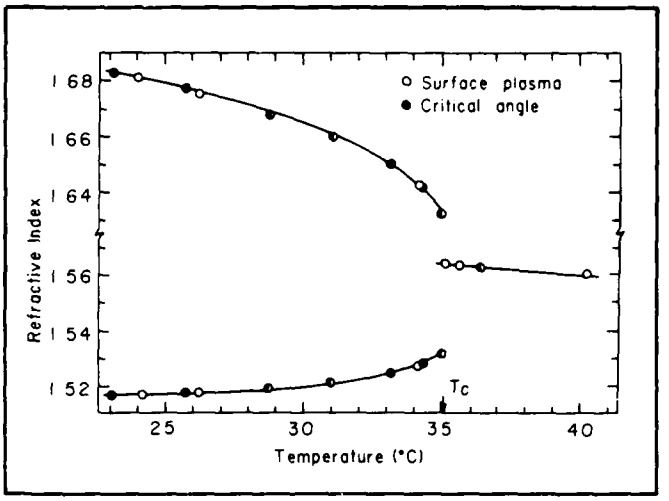

Fig. 3. Refractive indices of 5CB versus temperature, measured by the surface plasmon technique (open circles) and by the critical angle method (solid circles). (After Ref. 39.)

$$\frac{\partial\theta}{\partial z} = \pm\left[\frac{G(\theta)-G(\theta_m)}{H(\theta)}\right]^{1/2}, \tag{4}$$

where

$$G(\theta) = -\left[\frac{\epsilon_{\parallel}(\epsilon_{\parallel}-\epsilon_{\perp}\sin^2\alpha)}{\epsilon_{\parallel}^2-(\epsilon_{\parallel}-\epsilon_{\perp})\epsilon_{\perp}\sin^2\alpha}\right]^{1/2}\frac{I}{c}(1-\epsilon_{\perp}\sin^2\alpha)^{1/2}, \tag{5}$$

$$H(\theta) = \frac{1}{2}(K_{11}\sin^2\theta + K_{33}\cos^2\theta),$$

where $\epsilon_{\parallel}$ and $\epsilon_{\perp}$ are the optical dielectric constants parallel and perpendicular to the director, respectively, I is the incident laser beam intensity, α is the incident beam angle measured in the medium, and K_{11} and K_{33} are the splay and bend elastic coefficients, respectively. The solution of Eq. (4) is subject to the boundary condition $\theta = 0$ at $z = 0$ and $z = d$. If a normally incident probe beam is now used to measure the reorientation, it should experience a local extraordinary refractive index

$$n(z) = \frac{\epsilon_{\parallel}^{1/2}\epsilon_{\perp}^{1/2}}{(\epsilon_{\parallel}\cos^2\theta+\epsilon_{\perp}\sin^2\theta)^{1/2}}. \tag{6}$$

The overall phase shift induced by the optical field across the film is then given by

$$\phi = \frac{2\pi}{\lambda}\int_0^d n(z) - \epsilon_{\perp}^{1/2}dz. \tag{7}$$

Figure 2 shows the calculated ϕ versus I induced in a 250 μm homeotropic 4-cyano-4-pentylbiphenyl (5CB) film at three different incident angles. The theoretical curves are in good agreement with the experimental result. We noticed that in the $\alpha = 0$ case, reorientation occurs only when the pump beam intensity is above a threshold value. Analogous to the dc-field-induced reorientation, such a critical behavior is known as the Freedericksz transition. As seen in Fig. 2, near Freedericksz transition a small change in the pump intensity I can induce a rather appreciable change in the phase shift. One can use a bias field, which can be either optical or dc, to selectively place the initial operating point on the characteristic curve (ϕ versus I). If the operating point on the $\alpha = 0$ curve is set near the transition threshold in Fig. 2, then a pump intensity of a few W/cm^2 is already sufficient to induce a π phase shift. Such an intensity is obtainable even with a focused He-Ne laser beam. The average value of the induced refractive index change across the film in this case is $\Delta n \sim 10^{-3}$, or $\Delta n/|E|^2 \sim 2\times10^{-2}$ esu, which is 2×10^9 times larger than for CS_2.

As one would expect, the very large Δn is generally associated with a very slow response. The dynamic response of director reorientation is quite complex. With some simplifying assumptions, it can be shown that the induced phase shift obeys the following relaxation equation[33]:

$$\left(\frac{\partial}{\partial\tau}+\frac{1}{\tau_\theta}\right)\phi = \frac{\alpha_\theta}{\tau_\theta}I, \tag{8}$$

where α_θ is a constant depending on the initial orientation of the director and $\tau_\theta \simeq \gamma/[\pi^2K/d^2 - G]$ is the relaxation time, where γ is a viscosity coefficient and G is a function of the bias field. Both theory and experiment show that τ_θ is of the order of a few seconds to a few tenths of a second for a 5CB film of $\sim$100 μm. Taking the average $\Delta n/|E|^2$ to be $\sim 2\times10^{-2}$ esu, we have a figure of merit $\beta \simeq \Delta n/(|E|^2\tau_\theta) \simeq 2\times10^{-3}$ esu/s, which is about the same as that for 5CB in the isotropic phase. In comparison, β is $\sim$5 esu/s for CS_2. Thus, in some applications, if both the speed and the magnitude of the nonlinear optical response are important, then nematic liquid crystals are certainly not the best materials to be used in spite of their very high $\Delta n/|E|^2$.

Director reorientation by optical fields can in principle also occur in smectic and cholesteric liquid crystals. The situation is, however, much more complicated because of additional constraints arising from the ordered structures characteristic of such phases. Although theoretical calculations predict the possibility of observing director reorientation in these materials,[34-37] thorough experimental studies of the effect have not yet been carried out.

Aside from laser-induced molecular reorientations, laser heating can also induce a change in the refractive index of the liquid crystal.[38] Even in normally transparent liquid crystalline materials, residual adsorption of a laser beam can lead to a detectable temperature rise. For example, propagation of a 350 W/cm^2 cw Ar^+ laser beam through a 100 μm 5CB film results in a temperature rise of $\sim$2 K on the beam axis. The refractive index change due to heating is

given by

$$\Delta n = \frac{\delta n}{\delta T} \Delta T \ . \tag{9}$$

In the isotropic phase, $\partial n/\partial T$ is not very different from those of other organic liquids and is generally dominated by thermal expansion. Typically, $\partial n/\partial T$ is of the order of 5×10^{-4}/K. In the mesophases, the temperature rises also affect the degree of molecular alignment and hence the refractive indices. Similar to Eq. (1), we can define the order parameter Q of a nematic liquid crystal by the relations

$$\begin{aligned} n_{xx} &= \bar{n} + \frac{2}{3}\Delta n_o Q \ , \\ n_{yy} &= n_{zz} = \bar{n} - \frac{1}{3}\Delta n_o Q \ . \end{aligned} \tag{10}$$

We then have

$$\begin{aligned} \frac{\partial n_{xx}}{\partial T} &= \frac{\partial \bar{n}}{\partial T} + \frac{2}{3} Q \frac{\partial \Delta n_o}{\partial T} + \frac{2}{3}\Delta n_o \frac{\partial Q}{\partial T} \\ &\simeq \frac{\partial \bar{n}}{\partial T} + \frac{2}{3}\Delta n_o \frac{\partial Q}{\partial T} \ , \\ \frac{\partial n_{xx}}{\partial T} &- \frac{\partial n_{yy}}{\partial T} \simeq \Delta n_o \frac{\partial Q}{\partial T} \ . \end{aligned} \tag{11}$$

Figure 3 shows, as an example, how n_{xx} and n_{yy} of 5CB vary with temperature.[39] In the nematic phase, the term $\Delta n_o(\partial Q/\partial T)$ is of the same order of magnitude as $\partial \bar{n}/\partial T$, which is nearly the same as that in the isotropic phase.

The dynamics of the laser-induced thermal effect are also very complex. With simplifying approximations, the induced phase shift ϕ_T across a film can be described by a thermal relaxation equation driven by laser heating[33]:

$$\left(\frac{\partial}{\partial t} + \frac{1}{\tau_T}\right)\phi_T = -\frac{\alpha_T}{\tau_T} I \ . \tag{12}$$

where α_T is proportional to the absorption coefficient, $\tau_T \sim d^2/\pi^2 D$ is the relaxation time, and D is the heat diffusion constant. For a 100 μm film, τ_T is of the order of 0.1 s, which could be two or three orders of magnitude shorter than the orientational relaxation time τ_θ. If we take $\Delta n/|E|^2 \sim 10^{-3}$ esu and $\tau_T \sim 0.1$ s for the laser-induced thermal effect, the corresponding figure of merit $\beta = \Delta n/|E|^2 \tau_T$ is $\sim 10^{-2}$ esu/s. Both laser-induced molecular reorientation and laser-induced thermal effect may influence the observed nonlinear optical effects in liquid crystals, as will be shown in the following sections.

3. NONLINEAR OPTICAL EFFECTS IN LIQUID CRYSTALS

Nonlinear optical effects in liquid crystals are readily observable. Because of the difference in the magnitudes of optical nonlinearities, studies of nonlinear optical processes in the isotropic phase generally require fairly high-power pulsed lasers. On the other hand, for observation of nonlinear optical effects in mesophases, a medium-power cw laser beam would suffice. Here, we briefly describe a variety of nonlinear optical processes in liquid crystals that have been studied quite extensively in the past and also some of the newly observed interesting phenomena.

3.1. Harmonic generation

Bulk liquid crystals are centrosymmetric. Second harmonic generation is allowed only if a dc field is employed to break the centrosymmetry. Phase matching can be achieved by proper choice of the polarization and wave vector of the fundamental beam with respect to the director axis. The observed nonlinearity is comparable to that observed in CS_2. Saha and Wong[40] have shown that the process could be used to study nematic ordering. They pointed out that smectic liquid crystals, because of their relatively lower scattering loss and the possibility of fabricating large crystals, could be developed into useful harmonic generators, but experimental demonstrations remain to be seen.

Third harmonic generation has been observed in cholesteric liquid crystals.[41–44] In this case, phase matching can be achieved via the Umklapp process with the help of the helical structure in cholesteric liquid crystals, as demonstrated by Shelton and Shen. Experimental results agree very well with the theory based on the continuous model proposed by deVries.[44]

3.2. Degenerate wave mixing and phase conjugation

There have been extensive studies of degenerate wave mixing in liquid crystals. The process involves the formation of a refractive index grating in the medium by input laser beams, followed by diffraction of the input beams by the grating. As is well known, phase conjugation is just a special case of degenerate four-wave mixing.

Fekete et al. have successfully employed isotropic liquid crystals for phase conjugation.[45] As was discussed in Sec. 2, liquid crystals in the nematic phase have much larger optical-field-induced refractive index changes than in the isotropic phase. Degenerate wave mixing and phase conjugation can therefore be observed even with low power cw laser beams.[17,19]

Multiple-order diffraction shows up when the laser intensities are of the order of tens of W/cm^2. If the values of the optical-field-induced refractive index changes are known, the diffraction pattern and efficiency in the thin-film case can be quantitatively described by a simple theory of induced phase modulation on the incoming beams.

It is possible to use beams at one frequency to induce a refractive index grating, which subsequently diffracts an incoming beam at another frequency. This has been demonstrated with Nd:YAG and He-Ne lasers in a nematic film. The process could find practical applications in infrared-to-visible image conversions.[46,47]

Phase conjugation (or wavefront reconstruction) using liquid crystals often suffers from speckle noise associated with a coherent beam [Fig. 4(a)]. This can be eliminated[48] if the input beams in the process are made partially incoherent by passing the laser beam through, for example, a rotating ground glass. A typical conjugated beam is shown in Fig. 4(b). The absence of the background speckle noise is also evident from the photo of the partially incoherent beam distorted by the phase aberrator [Fig. 4(c)]. The idea here is to impart sufficient incoherence to the background noise while retaining sufficient coherence for wavefront reconstruction.

3.3. Self-focusing and self-phase modulation

A laser beam with a transverse intensity profile should induce a spatially varying refractive index, which could lead to a spatial self-phase modulation on the beam and possibly to self-focusing of the beam. Similarly, the time variation of a pulsed laser beam could also lead to a time-varying phase modulation on the beam itself.

The study of self-focusing in liquid crystals dates back to the early 1970s, when the self-focusing phenomenon itself was under intensive investigation. In particular, transient self-focusing was difficult to understand. It turns out that the induced refractive index in an isotropic liquid crystal has a response time that can be varied by temperature over a wide range (a few ns to 1 μs) because of the critical slowing-down behavior. Consequently, such a medium is ideal for the study of transient self-focusing. Typically, the experiment uses a laser intensity on the order of 10^2 MW/cm^2 and a beam propagation length of about 10 cm in the medium. In traversing the medium, both the laser intensity and the phase undergo severe distortion.

Self-focusing also occurs in nematic liquid crystal films, but the situation is very different. The typical film thickness is $\sim$100 μm; even so, because of the extremely large nonlinearity in the nematic

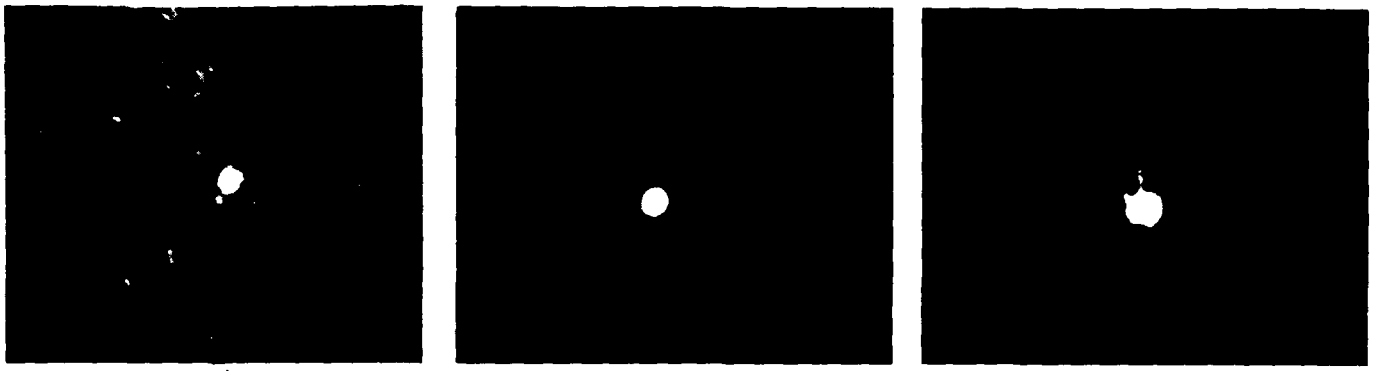

(a) (b) (c)

Fig. 4. (a) Photograph of reconstructed laser beam with coherent lasers. (b) Photograph of reconstructed spatially incoherent laser. (c) Aberrated spatially incoherent laser.

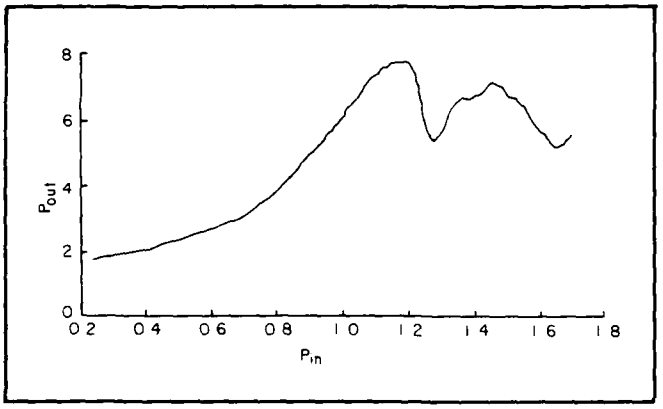

Fig. 5. Plot of the output on-axis power versus the input laser power. (After Ref. 50.)

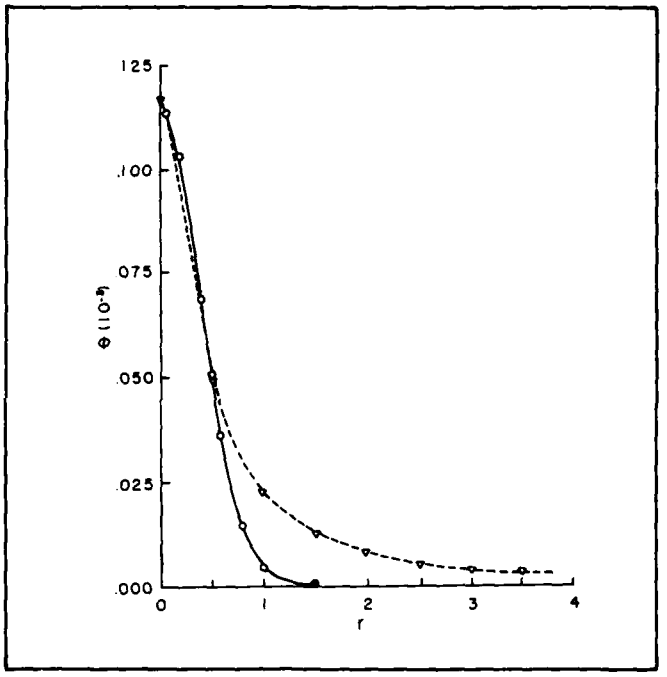

Fig. 6. Dotted curve: theoretical plot of the transverse dependence of the reorientation θ versus r. Solid curve: a Gaussian function for comparison. The width of θ(r) is about 0.5, whereas the input laser beam has a width of 0.14.

phase, a laser intensity of a few W/cm^2 could be sufficient to introduce a large enough wavefront distortion on the beam for self-focusing to occur. However, since the film is very thin, focusing actually appears after the beam passes through the film.

External self-focusing can give rise to a large intensification at the central portion of the beam. Figure 5 is a plot of the on-axis power versus the input. The low-power region is characterized by a linear dependence, while at higher intensity the output is nonlinear and an intensification of at least a factor of four is noted. At higher input, a dip in the on-axis power should appear. These results have been utilized in transverse optical bistability switching and opto-optical modulation experiments.[49-51] The above-mentioned dip in the on-axis power arises because of interference resulting from the relatively large spatial phase modulation ($\sim 2\pi$) on the beam. With increasing input intensity, the spatial phase modulation becomes stronger and stronger and the interference more dramatic, yielding a diffraction pattern with many rings. As many as 100 rings can be observed with an input intensity of a few hundred W/cm^2 in an $\sim$200 μm nematic film.

The spatial self-phase modulation described above can be calculated if the induced local refraction index change is known. In a homeotropic nematic film,[52] the latter can be obtained from the solution of the Euler equation for molecular reorientation, as was mentioned in Sec. 2. The result for an almost normally incident linearly polarized beam with a Gaussian profile is shown in Fig. 6. It shows how the reorientation angle θ of the director varies with the distance from the beam axis. The width of θ(r) depends on the relative magnitudes of the incident beam waist ω_0 and the film thickness d. In general, because of the long-range elastic torque, the width of θ(r) is always larger than the beam width, and θ(r) is not a Gaussian. For $\omega_0 \gg$ d, θ(r) approaches the Gaussian intensity profile of the input beam.

3.4. Optical bistability

Liquid crystals can be used as the nonlinear medium in a Fabry-Perot interferometer for optical bistability experiments. As mentioned earlier, the response times of liquid crystals in the isotropic phase can be varied by temperature over a wide range. Therefore, liquid crystals are ideal materials for investigating the dynamic behavior of a nonlinear Fabry-Perot interferometer. Indeed, such a study, carried out by a pulsed laser,[53,54] did provide us with a basic understanding of the interplay between the cavity round-trip time, the laser pulse length, and the medium response time in the bistable operating characteristics of the interferometer. In order to observe optical bistability, the pulsed laser intensity should be of the order of MW/cm^2.

Optical bistability can also be observed with nematic liquid films. Because of the large nonlinearity, a cw laser beam is often intense

enough for the observation. Two different schemes[18-21] have been used to achieve optical bistability. One is the usual nonlinear Fabry-Perot interferometer with an intracavity nematic film; the other utilizes self-focusing with an external feedback.

In the nonlinear Fabry-Perot interferometer of Khoo et al.,[19-21] a 50 μm homeotropic sample tilted at 45° in a 4 cm long cavity was used. Bistability was observed with an Ar^+ laser at an input intensity of about 600 W/cm^2. Formation of spatial rings and oscillatory behavior in the output were observed at high input intensity. Cheung et al.[18] took a much shorter cavity formed by a 83 μm film sandwiched between two mirrors. A magnetic field was used to move the operation point above the Freedericksz transition in the film (see Sec. 2) in order to increase the optical nonlinearity. As a result, a much smaller laser intensity was needed for bistable switching (~10 W/cm^2). At higher input intensities, the output broke up into periodic oscillations. This was found to be due to the interplay between the laser-induced reorientation, which contributes to a positive phase shift with a slower response time, and laser heating, which contributes to a negative phase shift with a faster response time. The experiemental results were shown to agree well with the theoretical calculation. The same reason probably also explains the oscillatory behavior observed by Khoo et al.

Study of optical bistability resulting from self-focusing with external feedback is a relatively recent endeavor. The experimental situation is schematically depicted in Fig. 7(a). A laser beam with a certain predescribed wavefront is incident on the nematic film, and the transmitted beam is partially reflected onto the film by a mirror to create a feedback in the field-induced refractive index in the film. The variation of the output through a pinhole behind the mirror with the input laser power exhibits optical bistability.

A detailed theory for such a cavityless optical bistability proposed earlier by Kaplan[49] has been worked out.[50,51] Essentially, with a proper arrangement of the lens, mirrors, and the wavefront of the input beam, the feedback can reinforce the self-phase modulation effect, leading to bistability. Figures 7(b) and 7(c) show some examples of the observed bistability curves, with the pinhole at the on-axis and the off-axis locations, respectively.

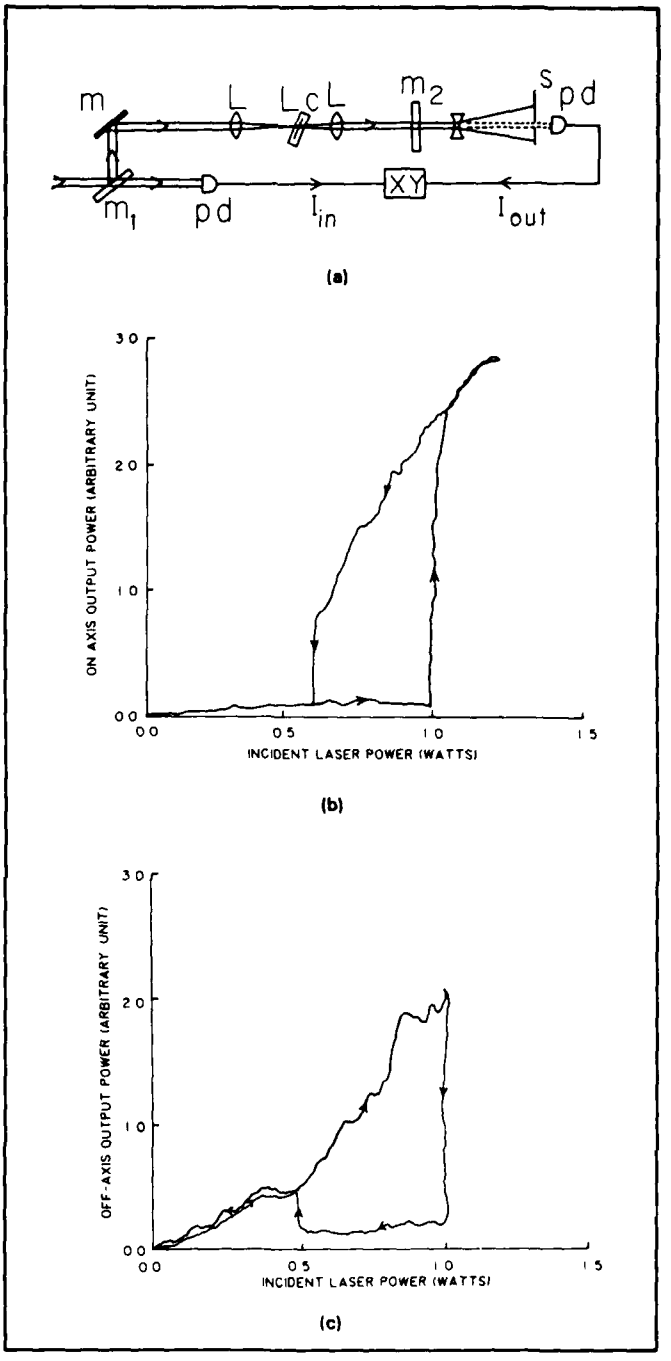

Fig. 7. (a) Experimental setup for observation of transverse intensity bistability. (b) Experimentally observed bistability of the power in the central region of the transmitted beam. (c) Experimentally observed bistability of the power in the off-axis region of the transmitted beam. (After Ref. 51.)

4. CONCLUSION

We have presented a brief summary of the basic nonlinear optical properties of liquid crystals and some observed nonlinear optical processes in liquid crystals. The unique physical and optical characteristics of liquid crystals open up some exciting areas of research that are of fundamental as well as applied interest. There are a number of other experiments in this field that we have not discussed here. Recently, Hsiung et al.[33] have used nanosecond laser pulses to study the dynamics of molecular reorientation as well as the laser-induced thermal effect in a nematic film. Khoo and Normandin have observed the generation of ultrahigh frequency acoustic waves and their effects on the laser-induced thermal gratings by nanosecond laser pulses in nematic[55] as well as smectic liquid crystals.[56] Optical switching at a nonlinear interface formed by nematic liquid crystals and glass[57,58] and nonlinear optical propagation in a planar waveguide cladded by liquid crystals[59] have also been observed. Although there are physical limitations to the use of liquid crystals in optical devices (the most serious of which is the response time), nonlinear optical studies in liquid crystals have continuously provided us with some new insights into the basic understanding of optical phenomena in a nonlinear medium and also into the potential applications of such materials.

5. ACKNOWLEDGMENTS

I. C. Khoo acknowledges the support of the National Science Foundation (ECS8415387) and the Air Force Office of Scientific Research (AFOSR840375). Y. R. Shen's research is supported by a National Science Foundation grant (DMR81-17366).

6. REFERENCES

1. See, for example, E. B. Priestley, P. J. Wojtowicz, and P. Sheng, *Introduction to Liquid Crystals*, Plenum Press, New York (1975).
2. See, for example, P. deGennes, *The Physics of Liquid Crystals*, Oxford University Press, Oxford (1974).
3. See, for example, *Liquid Crystal Devices*, T. Kallard, ed., Optosonic Press, New York (1973).
4. See, for example, M. Tobias, *International Handbook of Liquid Crystal Displays*, Ovum Ltd., London (1975).

5. Y. R. Shen, in *Nonlinear Spectroscopy*, N. Bloembergen, ed., Proc. Int. School of Physics, "Enrico Fermi," Course 64 pp. 201-216, North Holland Publishing Co., Amsterdam (1977).
6. R. M. Herman and R. J. Serinko, Phys. Rev. A19, 1757 (1979).
7. G. K. L. Wong and Y. R. Shen, Phys. Rev. Lett. 32, 527 (1974).
8. D. V. G. L. N. Rao and S. Jayaraman, Appl. Phys. Lett. 23, 539 (1973).
9. E. G. Hanson, G. K. L. Wong, and Y. R. Shen, Opt. Comun. 20, 45 (1977).
10. I. C. Khoo, S. L. Zhuang, and S. Shepard, Appl. Phys. Lett. 39, 937 (1981).
11. S. D. Durbin, S. M. Arakelian, and Y. R. Shen, Opt. Lett. 6, 411 (1981).
12. N. F. Pilipetski, A. V. Sukohov, N. V. Tabiryan, and B. Ya Zel'dovich, Opt. Commun. 37, 280 (1981).
13. S. D Durbin, S. M. Arakelian, and Y. R. Shen, Opt. Lett. 7, 145 (1982).
14. I. C. Khoo, Appl. Phys. Lett. 38, 123 (1981).
15. I. C. Khoo and S. L. Zhuang, Appl. Phys. Lett. 37, 3 (1980).
16. I. C. Khoo, Phys. Rev. A25, 1040 (1982).
17. I. C. Khoo and S. L. Zhuang, IEEE J. Quantum Electron. QE-18, 246 (1982).
18. M. M. Cheung, S. D. Durbin, and Y. R. Shen, Opt. Lett. 8, 39 (1983).
19. I. C. Khoo, Appl. Phys. Lett. 41, 909 (1982).
20. I. C. Khoo, J. Y. Hou, R. Nomandin, and V. C. Y. So, Phys. Rev. A27, 3251 (1983).
21. I. C. Khoo, J. Y. Hou, R. Nomandin, and V. C. Y. So, J. Appl. Phys. 53, 7599 (1982).
22. G. K. L. Wong and Y. R. Shen, Phys. Rev. Lett. 30, 895 (1973).
23. G. K. L. Wong and Y. R. Shen, Phys. Rev. A10, 1277 (1974).
24. B. Y. Zel'dovich, N. F. Pelipetskii, A. V. Sukhov, and N. V. Tabiryan, JETP Lett. 31, 263 (1980).
25. A. S. Zolot'ko, V. F. Kataeva, N. Kroo, N. N. Sobolev, and L. Csillag, JETP Lett. 32, 158 (1980).
26. I. C. Khoo and S. L. Zhuang, Appl. Phys. Lett. 37, 3 (1980).
27. I. C. Khoo, Phys. Rev. A23, 2077 (1981).
28. I. C. Khoo, Phys. Rev. A25, 1636 (1982).
29. I. C. Khoo, Phys. Rev. A27, 2747 (1983).
30. S. D. Durbin, S. M. Arakelian, and Y. R. Shen, Phys. Rev. Lett. 47, 1411 (1981).
31. H. L. Ong, Phys. Rev. A28, 2393 (1983).
32. S. D. Durbin, Ph.D. Thesis, Univ. of California, Berkeley (1984) (unpublished).
33. H. Hsiung, L. P. Shi, and Y. R. Shen, Phys. Rev. A30, 1453 (1984).
34. N. V. Tabiryan and B. Ya. Zel'dovich, Mol. Cryst. Liq. Cryst. 69, 19 (1981).
35. N. V. Tabiryan and B. Ya. Zel'dovich, Mol. Cryst. Liq. Cryst. 69, 31 (1981).
36. H. G. Winful, Phys. Rev. Lett. 49, 1179 (1982).
37. H. L. Ong and C. Y. Young, Phys. Rev. A29, 297 (1984).
38. I. C. Khoo and R. Normandin, IEEE J. Quantum Electron. (1985).
39. K. C. Chu, C. K. Chen, and Y. R. Shen, Mol. Cryst. Liq. Cryst. 59, 97 (1980).
40. S. K. Saha and G. K. Wong, Appl. Phys. Lett. 34, 423 (1979).
41. J. W. Shelton and Y. R. Shen, Phys. Rev. Lett. 25, 23 (1970).
42. J. W. Shelton and Y. R. Shen, Phys. Rev. Lett. 26, 538 (1971).
43. J. W. Shelton and Y. R. Shen, Phys. Rev. A5, 1867 (1972).
44. H. N. deVries, Acta Cryst. 4, 219 (1951).
45. D. Fekete, J. AuYeung, and A. Yariv, Opt. Lett. 5, 51 (1979).
46. G. Martin and R. W. Hellwarth, Appl. Phys. Lett. 34, 371 (1979).
47. I. C. Khoo and R. Normandin, to be published in Technical Digest, Conf. on Lasers and Electro-Optics '85.
48. E. Leith, H. Chen, Y. Cheng, G. Swanson, and I. C. Khoo, Proc. 5th Rochester Conf. on Coherence and Quantum Optics, Rochester, N.Y. (1983).
49. A. E. Kaplan, Opt. Lett. 6, 360 (1981).
50. I. C. Khoo, Appl. Phys. Lett. 41, 909 (1982).
51. I. C. Khoo, T. H. Liu, P. Y. Yan, S. Shepard, and J. Y. Hou, Phys. Rev. A29, 2756 (1984).
52. I. C. Khoo, T. H. Liu, and R. Normandin, to be published in Mol. Cryst. Liq. Cryst.
53. T. Bischoffberger and Y. R. Shen, Appl. Phys. Lett. 28, 731 (1976).
54. T. Bischoffberger and Y. R. Shen, Phys. Rev. A17, 335 (1978).
55. I. C. Khoo and R. Normandin, Opt. Lett. 9, 285 (1984).
56. I. C. Khoo and R. Normandin, J. Appl. Phys. 55, 1416 (1984).
57. I. C. Khoo, Appl. Phys. Lett. 40, 645 (1982).
58. I. C. Khoo and J. Y. Hou, J. Opt. Soc. Am. B. (May 1985).
59. H. Vach, C. T. Seaton, G. I. Stegeman, and I. C. Khoo, Opt. Lett. 9, 238 (1984).

Infrared to visible image conversion capability of a nematic liquid crystal film

I. C. Khoo
Electrical Engineering Department, The Pennsylvania State University, University Park, Pennsylvania 16802
R. Normandin
Division of Microstructural Sciences, National Research Council of Canada, Ottawa, KIA OR6, Canada

(Received 18 April 1985; accepted for publication 3 June 1985)

We present a theoretical evaluation and experimental results of the capability of a nematic liquid crystal film for infrared to visible image conversion using nondegenerate four-wave mixing process.

Degenerate and nondegenerate four-wave mixings have been studied in the context of optical imagings in several materials.[1,2] In particular, Martin and Hellwarth[1] have demonstrated infrared to visible image conversion via Bragg reflections from laser induced thermal gratings in dyed liquids. The basic mechanism is the absorption of the incident ($1R$) light by the dye molecules, which then heat up the solvent via some intermolecular relaxation processes.

Recently, we have demonstrated that nematic liquid crystals possess extraordinarily large optical nonlinearity that can be utilized for wave front conjugation purposes.[3] There are two distinct types of nonlinearities: thermal and orientational. Depending on the thickness of the sample and the interaction geometry between the laser polarization and the liquid crystal axes, one or both of these nonlinearities will dominate the nonlinear optical process under study.[4-6] The thermal nonlinearity, of course, depends on the absorption constant of the liquid crystal, which can be enhanced with traces of dissolved dyes with the appropriate absorption band. A detailed analysis of the thermal nonlinearity of nematics has been performed.[5]

For incident laser polarization parallel to the nematic axis, the "extraordinary" thermal index gradient $dn_{\parallel}/dT$ is given by[5]

$$\frac{dn_{\parallel}}{dT} = 2n^{-1}\left((1.33 + 0.74S)\frac{d\rho}{dT} + 0.74\frac{dS}{dT}\right). \quad (1)$$

And for the incident laser polarization perpendicular to the nematic director axis, the "ordinary" thermal index gradient $dn_{\perp}/dT$ is

$$\frac{dn_{\perp}}{dT} = 2n^{-1}\left((1.33 - 0.37S)\frac{d\rho}{dT} - 0.37\frac{dS}{dT}\right) \quad (2)$$

for PCB (pentyl-cyano-biphenyl), where S is the temperature-dependent order parameter and ρ is the density. A unique characteristic of nematic liquid crystals is the rather large magnitudes of both $dn_{\parallel}/dT$ and $dn_{\perp}/dT$. At temperatures far away from the nematic isotropic transition temperature (e.g., at 22 °C and $T_c = 35$ °C for PCB), both dn/dT's are already comparable to the largest thermal index obtainable in liquids ($\sim 10^{-4}$ K^{-1}). At temperatures closer to T_c, both $dn_{\perp}/dT$ and $dn_{\parallel}/dT$ increase dramatically by more than an order of magnitude. This means that thinner samples and/or low power lasers can be used for optical wave mixing processes, since the diffraction efficiency is proportional to the square of dn/dT, among other factors. In

 0003-6951/85/160350-03$01.00

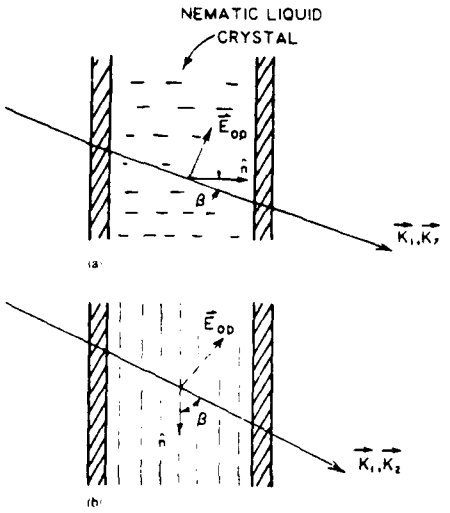

FIG. 1. (a) Homeotropically aligned nematic liquid crystal. (b) Planar nematic liquid crystal. $\mathbf{K}$ and $\mathbf{E}_{op}$ are the wave vector and electric field vector of the laser, respectively. For $\beta = 0$, $\mathbf{E}_{op}$ is parallel to n. For $\beta = 90°$, $\mathbf{E}_{op}$ is perpendicular to $\mathbf{n}$, the director axis of the nematic. $\mathbf{K}_1$ and $\mathbf{K}_2$ are crossed on the sample at 3°.

particular, because of the thinner sample geometry, one expects to get higher resolution element capability in infrared to visible image conversion process as we will explain presently.

Another unique characteristic of liquid crystals is the extraordinarily large optical nonlinearity associated with molecular reorientation. Molecular reorientation of nematic liquid crystal axis is of course wavelength independent which makes it the most versatile and natural mechanism for image conversions (1R to visible, ..., etc.). The optical nonlinearity associated with two lasers (pump-probe) intersecting on the liquid crystals has been calculated before. The induced optical refractive index change is given by[4]

$$\delta n \sim \frac{1}{2}\frac{\delta\epsilon}{n} = \frac{\epsilon_\perp \Delta\epsilon}{2n\epsilon_{\parallel}} \sin 2\beta\,\theta, \tag{3}$$

where θ is the optically induced molecular reorientation. The nonlinearity can be induced in homeotropic or planar aligned nematic liquid crystal films for the optical field-nematic interaction geometries depicted in Figs. 1(a) and 1(b). In general, the molecular reorientational nonlinearity is larger than the thermal nonlinearity. However, it is obvious that for $\beta = 0$, the reorientational nonlinearity is vanishing.

We have experimentally demonstrated the possibility of infrared to visible image conversions in pure nematic films and also in nematic films "doped" with infrared absorbing dyes. The liquid crystal used is PCB (4-cyano-4'-pentyl-biphenyl) and is about 50 μm thick. Both homeotropically aligned and planar nematic films have been shown to give similar results. The sample temperature is 22 °C. Various four-wave mixing (wave vectors) configurations have been attempted. Figure 2(a) shows one of the setups used, with all four waves propagating in the forward direction [cf. Fig. 2(b)]. A 20-ns Nd:YAG laser pulse (λ at 1.06 μm) is split into the reference beam and an object beam (the object is a wire mesh). These two beams recombine on a homeotropically aligned nematic film at an angle of about 3°. The lasers are linearly polarized, with the polarization normal to the director axis. For this geometry, the nonlinearity comes from $dn_\perp/dT$. Traces of Kodak No. 14015 infrared absorbing dyes were dissolved in the liquid crystal to improve the absorption of the PCB at 1.06 μm. A cw 5-mW He-Ne (0.6328 μm) laser is used as a reconstruction beam and is almost collinear with the reference beam. The beam spot sizes on the liquid crystal film are on the order of 0.5 cm^2. Visible diffraction values of the He-Ne were observed for reference beam

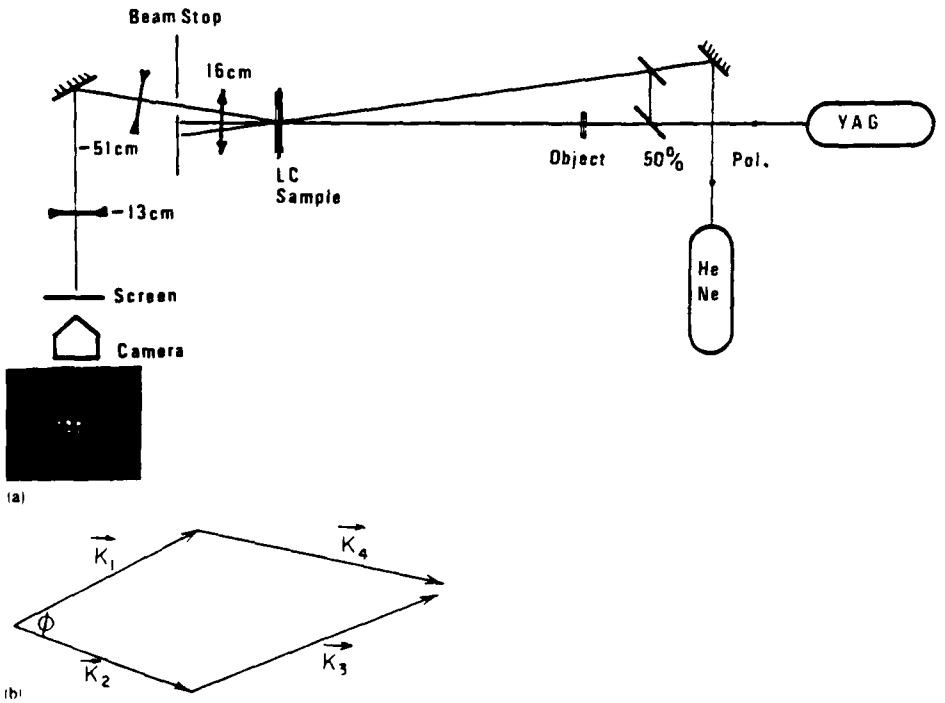

FIG. 2. (a) Schematic of the experimental setup. Photo insert is a sample experimental result. (b) Wave vector configuration of the reference ($\mathbf{K}_1$), the object ($\mathbf{K}_2$), the reconstructing ($\mathbf{K}_3$), and the image beams ($\mathbf{K}_4$).

and object beam energies on the order of 50 and 15 mJ, respectively. The observed diffraction efficiency is on the order of a few percent. The diffracted image beam is imaged via the lens system onto the Polaroid film plate. In general, very good quality image can be reconstructed. The photo insert in Fig. 2 shows a typical reconstructed image of the mesh at the red wavelength (0.6328 μm).

The diffraction efficiency of the 50-μm-thick film is very good, and is on the order of a few percent (as measured from the diffraction from the $1R$ laser pulses with a joulemeter). In Ref. 1, it was reported that similar diffraction efficiency was observed in a 2-mm-thick dye solutions, using pump and probe beam energies on the order of 10 and 1 mJ, respectively, focused on an area of about 0.01 cm^2. In comparison to these liquids, the higher efficiency of the nematic film due to its inherently higher $dn_\perp/dT$ is already evident.

The thickness of the nematic film ($\approx 50\,\mu$m) means that higher resolution elements can be achieved. For the geometry depicted in Fig. 2(b), and using an analysis similar to Martin and Hellwarth, the number of resolution elements, N, can be proven in a straightforward manner to be given by

$$N = \frac{AK_1/l}{1 + K_1/K_3} \tag{4}$$

in the small ϕ limit (i.e., $\phi \ll 1$). This differs from the "folded" geometry used by Martin and Hellwarth by the denominator, where it is replaced by $[1 - K_1/K_3]$. Since $K_1 = 2K_3$, the difference between N here and N in Ref. 1 is a factor of 1/2 to 3/2, i.e., N here is smaller than N in Ref. 1 by a factor of 3. On the other hand, the thickness l in the present case (50 μm) is much smaller than (by a factor of 40) the 2-mm cell thickness. Using thinner cell for higher resolution element is, of course obvious, but the important point here is that one can get comparable diffraction efficiencies even with such thin films. The efficiency obtained here is by no means optimized. We have observed that the diffraction efficiency increased by at least an order of magnitude by raising the temperature of the sample to near T_c (30 °C).

To demonstrate the use of the other type of nonlinearity, namely, orientational nonlinearity, we use a *pure* PCB film (same thickness of 50 μm). The sample does not give visible diffractions even at much higher input laser energies than the ones used in the above experiment involving dyed samples. The sample is tilted such that β, the propagation angle which the wave vector $\mathbf{K}_1$ ($\mathbf{K}_2$) makes with the nematic axis, is 22° (cf. Fig. 1). An almost cw beam of Nd:YAG pulses is obtained by running the laser at 20 pps. This continuous illumination is required simply because the orientational response of the nematic is slow (on the order of milliseconds). In this case, we also observe visible diffraction of the He-Ne beam and images of comparable quality. To check that indeed the mechanism is due to orientational effect, the film is tilted back to the normal position (i.e., $\beta = 0$) and the diffraction vanishes [in accordance to Eq. (3)]. Due to pulse to pulse instabilities, the effects for cw laser are not as large and the quality of the image is not as good as expected. It is clear that better results can be obtained if one uses a cw laser or millisecond $1R$ laser pulses.

The temporal behaviors of the thermal and orientational gratings are quite different. Using an almost identical setup as Fig. 2(a) (with the object removed), we have measured the rise time of the thermal grating by detecting the diffraction from the He-Ne laser. In general, the rise time is on the order of the Nd:YAG pulse width (≈ 20 ns), while the decay time is on the order of 50–100 μs, depending on various parameters but mostly on the grating spacing. On the other hand, the rise time associated with molecular reorientation is much slower. Under cw excitation, the rise time is on the order of 10^2 ms, and becomes shorter at higher incident laser intensity (very similar to liquid crystal reorientation by dc field).[7] The decay time is also on the order of 10^2 ms, and depends primarily on the grating constant and/or film thickness.

In conclusion, we have demonstrated the possibility of infrared to visible image conversion. Without optimization, the results are comparable to those achievable in much thicker high thermal index liquids. We are currently investigating the details of this process with respect to various parameters, e.g., laser pulse length, absorption constants, geometry, etc., and will report the result in a longer article elsewhere.

This research is supported by a grant from the National Science Foundation ECS 8415387 and from the Air Force Office of Scientific Research under AFOSR 840375.

[1] G. Martin and R. W. Hellwarth, Appl. Phys. Lett. **34**, 371 (1979).
[2] J. F. Reintjes, *Nonlinear Optical Parametric Processes in Liquids and Gases* (Academic, Orlando, 1984) and references therein on degenerate four-wave mixings, Chaps. 5, 6.
[3] I. C. Khoo and S. L. Zhuang, IEEE J. Quantum Electron. **QE-18**, 246 (1981); E. N. Leith, H. Chen, Y. Cheng, G. Swanson, and I. C. Khoo, Proceedings of 5th Rochester Conference on Coherence and Quantum Optics, June 1983, Rochester, N.Y.
[4] I. C. Khoo, Phys. Rev. A **25**, 1637 (1982); **27**, 2747 (1983).
[5] I. C. Khoo and R. Normandin, IEEE J. Quantum Electron. **QE-21**, 329 (1985); I. C. Khoo and R. Normandin, Opt. Lett. **9**, 285 (1984).
[6] I. C. Khoo and Y. R. Shen, Opt. Eng. Special Issue, July (1985).
[7] P. G. deGennes, *The Physics of Liquid Crystals* (Oxford University, Oxford, England, 1974).

Nonlinear optical properties of liquid crystals for optical imaging processes

I. C. Khoo, MEMBER SPIE
The Pennsylvania State University
Department of Electrical Engineering
University Park, Pennsylvania 16802

Abstract. We present an account of two recently observed nonlinear optical imaging processes, wavefront conjugation and infrared-to-visible image conversion, in liquid crystal films. We include discussion of dynamics, efficiency, resolution, aberration correction, and noise removal in these two processes.

Subject terms: optical information processing; lasers; thermal indexing; liquid crystals; reorientation; nonlinear imaging.

Optical Engineering 25(2), 198-201 (February 1986).

CONTENTS

1. INTRODUCTION

The theory and practice of liquid crystal director axis reorientations, and the associated electro-optical birefringence, by a dc or low frequency ac field have been established for many years. Various optical imaging, image processing, modulation, switching, and display devices are based on these rather simple physical effects. When integrated with other thin-film materials (semiconductors, photoconductors, metallic films, etc.), liquid crystals become one of the most versatile optical materials that find application in an ever-increasing array of optical information processing systems.[1]

Recently, the feasibility of employing moderate power lasers to induce molecular reorientation in liquid crystals has been demonstrated.[2] All three mesophases (nematics, smectics, and cholesterics) exhibit extraordinarily large optical nonlinearity associated with the director axis reorientation. To date, however, the most conclusive theories and experiments have been performed in nematics, which are also the most used materials for liquid crystal optical devices.[3] There are two basic types of optical nonlinearities in nematics: (1) optically induced refractive index change associated with director axis reorientation and (2) thermal indexing effect. These nonlinearities have been studied in the context of self-focusing,[4] degenerate four-wave mixing,[5] self-phase modulations,[6] bistability,[7] and optical switching[8] and have been reviewed in a recent article by Khoo and Shen.[2]

In this paper, we concentrate on two recently observed nonlinear optical processes that bear on optical imaging applications, namely, wavefront conjugation and IR-to-visible image conversion. We discuss details that are not included in preliminary reports. Specifically, we address the conditions necessary for observing the effects, the diffraction efficiencies, rise and fall times, and other pertinent imaging characteristics.

Invited Paper MD-101 received June 29, 1985; revised manuscript received Oct. 4, 1985; accepted for publication Oct. 7, 1985; received by Managing Editor Nov. 18, 1985.

2. WAVEFRONT CONJUGATION

The theory of wavefront conjugation, an example of degenerate four-wave mixing processes, has been established for many years.[9] An experimental setup for wavefront conjugation is shown schematically in Fig. 1(a). The object beam and the reference beam interfere to induce an index grating (a transient hologram) on the liquid crystal film by means of either the orientational or the thermal nonlinearity. The reconstructing beam is retroreflected from the reference beam, and the image-bearing generated fourth wave traverses back along the object beam path. There are several significant advantages of this type of real-time imaging process, a few of which are high resolution, reflections with gain, and aberration correction capability.

In an earlier wavefront conjugation experiment,[10] we showed that because of the extremely large optical nonlinearity of liquid crystals, cw lasers of a few W/cm^2 intensity suffice for visible phase conjugation results. We have also demonstrated phase-aberrated corrections. More recently, we have succeeded in using a spatially partially coherent cw laser to remove the coherent noise that inevitably accompanies the use of lasers for imaging. In nematic film, the problem is particularly severe owing to extremely high scatterings from director axis fluctuations. Figure 1(b) is an example of an extremely degraded (by the coherent artifacts) reconstructed image beam in a wavefront conjugation experiment using a coherent laser. The photograph is taken at a temperature near T_c, the transition temperature. At temperatures far from T_c, the noise is less overwhelming but still very severe and is compounded by the ever-present noise from random scatterings in the optical system.

Two methods of removing the coherent noise in phase conjugation have been demonstrated to be quite successful. In the method employed by Huignard et al.,[11] a diffuser plate is placed in the path of the object beam (pulsed laser), and multiple exposures are taken for various settings of the diffuser plate. In our collaborative study with Leith et al.,[12] the

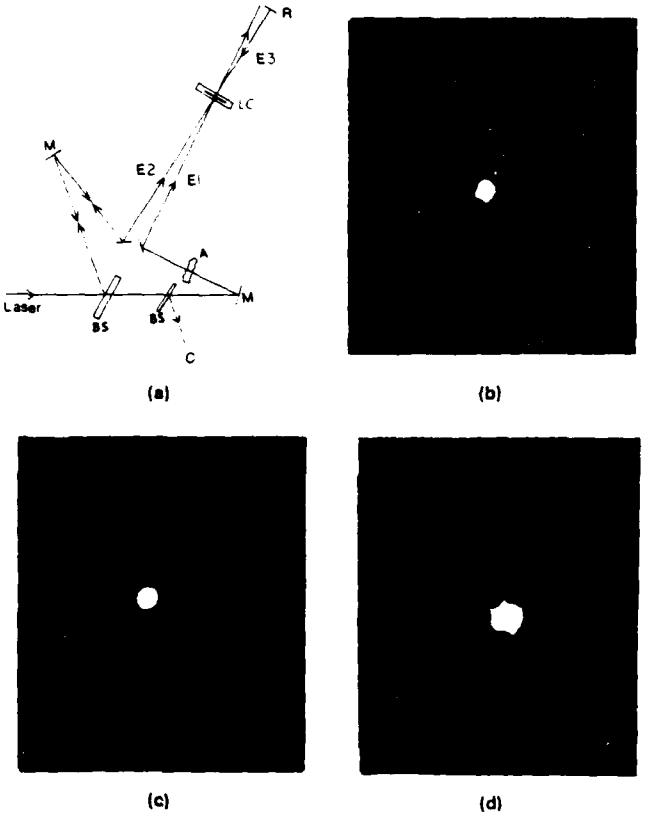

Fig. 1. Wavefront conjugation. (a) Experimental setup. BS: beam splitter. M: mirror. R: total reflector. S: sample. E_2: reference beam. E_1: object beam. E_3: reconstruction beam. A: aberrator. C: image. (b) Image beam reconstructed with coherent laser. (c) Image beam reconstructed with spatially incoherent laser. (d) Aberrated beam.

cw laser was first rendered spatially partially incoherent by collimation through a rotating ground glass. Because the rise time of the conjugation process with cw laser illumination is slow, the incident laser beam is practically averaged over many settings of the rotating ground glass, so that a *single* exposure recording of the image beam will suffice. As shown in Fig. 1(c) of the reconstructed beam and Fig. 1(d) of the aberrated beam, the technique both preserves the aberration correction capability and removes coherent noise.

Recently we demonstrated[13] that wavefront conjugation with a nanosecond pulsed laser is feasible using the thermal nonlinearity. Near T_c, four-wave mixing with moderate laser energy (≤ 1 mJ) is possible, with microsecond response (rise and fall). We are currently investigating various means of achieving coherent-noise-free wavefront conjugation imaging.

The diffraction efficiency for wavefront conjugation and the related infrared-to-visible image conversion at the phase-matched Bragg's condition depend principally on the magnitude of the induced index grating on $(\mathbf{K}_1 - \mathbf{K}_2)$ between the reference beam (at $\mathbf{K}_1$) and the object beam (at $\mathbf{K}_2$). In the absence of loss, the maximum diffraction efficiency R_{max} is given roughly by $R_{max} \simeq (\mathbf{K}^2/4\eta^2)(\Delta\eta)^2 d^2$, where d is the thickness of the film (or interaction length, whichever is shorter), K is the magnitude of $\mathbf{K}_1$ and $\mathbf{K}_2$, and η is the average refractive index. The magnitude of $\Delta\eta$ depends on which nonlinearity is responsible for the wave mixing process.

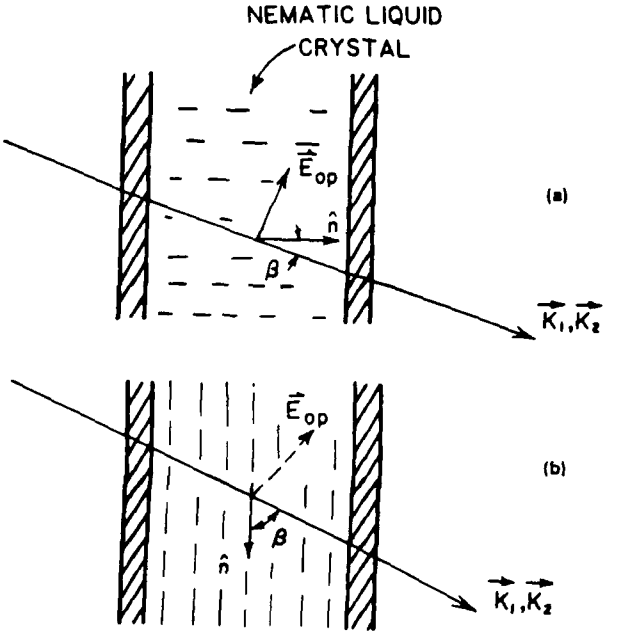

Fig. 2. Schematics of laser propagation in (a) a homeotropic nematic liquid crystal film and (b) a planar nematic film. $\vec{K}_1$ and $\vec{K}_2$ are the propagation wave vectors; $\vec{E}_{op}$ is the optical field vector. The two laser beams lie in a plane perpendicular to the paper and intersect at a wave-mixing angle on the film.

For orientational nonlinearity, $\Delta\eta(\mathbf{K}_1 - \mathbf{K}_2)$ has been calculated[14] for the homeotropic and planar nematic films, as depicted in Fig. 2. A unique characteristic of nematic nonlinearity is that it is a collective phenomenon; it is extremely dependent on the boundary forces or torques. The optical torques at the interference intensity maxima must overcome not only the elastic restoring torque from the boundary plates, where molecules are rigidly anchored, but also torques from molecules situated at the intensity minima.[14] The torque is inversely proportional to the characteristic length; in this case, the two characteristic lengths are the film thickness d and the grating constant $\lambda(\mathbf{K}_1 - \mathbf{K}_2)$. The smaller these lengths, the higher is the optical intensity needed to induce the same amount of $\Delta\eta$, and therefore the lower is the diffraction efficiency. This has been verified in our experiments reported in Ref. 14, where details of the experimental results are also given.

The magnitude of $\Delta\eta$ due to laser heating depends to a large extent on the temporal characteristics of the laser. If cw lasers are used, then the thermal diffusion process during the grating buildup has to be accounted for. This is quite complicated and has hitherto not been addressed. On the other hand, if pulsed lasers (with pulse lengths shorter than the smallest diffusion time constant) are used, the analysis is simpler. In this case, $\Delta\eta$ depends simply on the heat capacity of the nematics, on the absorption constant of the nematics at the laser wavelength used, and to a great extent on the temperature (whether close to or far from T_c). Details of these for the nematic PCB (4-cyano-4-pentylbiphenyl) for pulsed lasers at 5145 Å have been presented.[15] Typical values are $\Delta\eta \simeq 10^{-4}$ for laser energies of approximately 20 mJ/mm^2 at $T_c - T \simeq 14°$. Near T_c, however, laser fluence on the order of 1 mJ will generate the same diffraction efficiency.

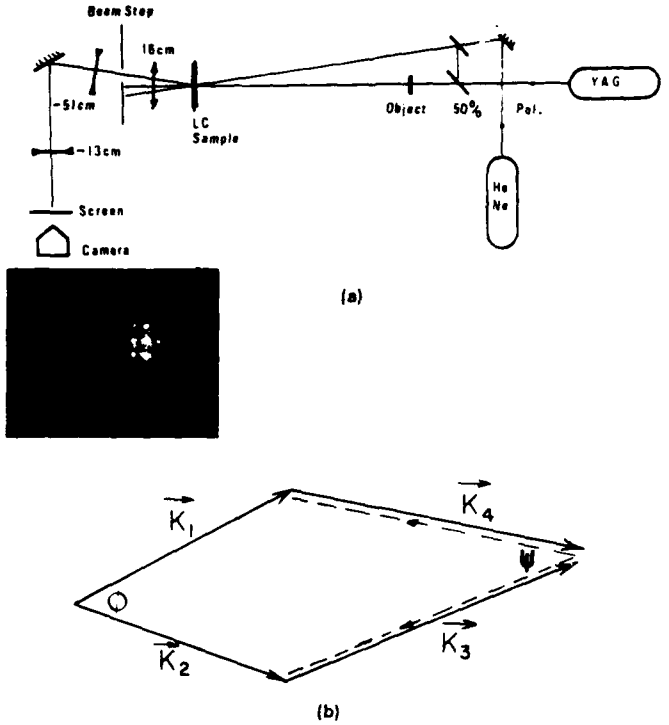

Fig. 3. Infrared-to-visible image conversion. (a) Experimental setup. (b) Phase matching of the four interacting waves. Dotted lines show the configuration used in Ref. 18. $\vec{K}_1$: reference beam. $\vec{K}_2$: object beam. $\vec{K}_3$: reconstruction beam. $\vec{K}_4$: image beam.

The rise and fall times of these nonlinear processes depend on several factors. In the orientational process, the rise time τ_{on} and fall time τ_{off} are given by expressions similar to those involving dc fields, with the optical field E_{op} replacing the dc field E_{dc}, and with the appropriate values for the dielectric anisotropies.[2,16] Because the optical field can make an arbitrary angle with the director axis, depending on the laser propagation direction, the rise time is also dependent on the configuration. In general, the smaller the grating constant (or thickness of the film, whichever is smaller), the faster is the response. τ_{on} and τ_{off} are proportional to λ^2 (or d^2), greater than the viscosity, and inversely proportional to the elastic constant, as we will presently see.

More specifically, consider the four-wave mixing geometry depicted in Fig. 2(a) or 2(b). Because the film is thin (50 μm or so) and the beam sizes in all the wave mixing experiments are much larger (on the order of millimeters), the two beams can be assumed to be plane waves. Their interference, therefore, sets up a grating in the y direction, with grating wave vector $\mathbf{K}_1 - \mathbf{K}_2$ and a grating constant λ ($\lambda = 2\pi/|\mathbf{K}_1 - \mathbf{K}_2|$). The reorientational angle θ thus possesses spatial variation in both the z and y directions (see Ref. 14). Using a simplifying one-elastic constant approximation, the dynamics of the process may be described by[15]

$$\gamma \frac{d\theta}{dt} = K\left(\frac{d^2\theta}{dy^2} + \frac{d^2\theta}{dz^2}\right) + \frac{\Delta\epsilon E_{op}^2}{4\pi}\left[(\cos 2\beta)\theta + \frac{\sin(2\beta)}{2}\right]. \quad (1)$$

If the optical field term is smaller than the elastic term, then since $\theta(y) \simeq \sin[(2\pi/\lambda)y]$ and $\theta(z) \simeq \sin[(\pi/d)z]$, and following the usual analysis,[16] one gets a response time (rise or fall)

$$\tau \simeq \frac{\gamma}{K\left[\left(\frac{2\pi}{\lambda}\right)^2 + \left(\frac{\pi}{d}\right)^2\right]}. \quad (2)$$

On the other hand, if the optical term is much larger than the elastic term

$$\tau_{on} \simeq \frac{4\pi\gamma}{\Delta\epsilon E_{op}^2 \cos(2\beta)}. \quad (3)$$

One interesting possibility is that the rise time can be decreased with the use of high intensity lasers. Nanosecond laser-induced molecular reorientation has been demonstrated by Hsiung et al.[13] The decay time, however, is at best on the order of a few ms for d or λ on the order of a few μm. In the case of thermal grating, the rise time is on the order of the laser pulse length. The fall time depends on the heat diffusion process, the sample thickness, the grating constant, and the diffusion constant.[17] Decay times on the order of 50 to 100 μs were observed in our experiment involving λ on the order of 20 μm.

3. INFRARED-TO-VISIBLE IMAGE CONVERSION

Using a thin-film geometry, or the phase-matched Bragg scattering configuration, it is possible to create a holographic phase grating with reference and object beam at one wavelength and reconstruction and image beam at another wavelength. An example of this special case of four-wave mixing is the so-called infrared-to-visible image conversion, where the object and reference beams are in the infrared, and the reconstruction and the image beams are in the visible [Fig. 3(a)]. There is obvious practical usefulness of such an image conversion process. As detailed by Martin and Hellwarth,[18] this four-wave mixing process can also yield high image resolution capability. Typically, the number of resolution elements is on the order of 10^4 or better.

The resolution of the imaging process obviously depends on the relative configurations between the various interacting beams. The geometry employed by Martin and Hellwarth is of the "folded" or "wavefront conjugation-like" type [see Fig. 3(b)], whereas the geometry we used is the "forward" wave-mixing type. In both cases, the angle ψ is the Bragg scattering angle. In our configuration the amount of variation in ϕ (the angle between K_1 and K_2) that would still allow for phase matching (i.e., $\Delta K\ell < \pi$) is given by $2\pi\phi\delta\phi \simeq 4\pi^2[K_1 d\,|1 + (K_1/K_3)|]^{-1}$. The diffraction solid angle of the object beam, which subtends on area A on the sample, is given by $\phi_D = 4\pi^2/K_1^2 A$. This gives the number of resolution elements $N \simeq \delta\phi/\phi_D$ as

$$N \simeq \frac{AK_1}{\ell|1 + (K_1 \cdot K_3)|}. \quad (4)$$

This differs from N for Fig. 3(b) (dotted line) by the denominator.[18] Since K_1 and K_3 are quite different for infrared-to-visible conversion, this difference in the denominator amounts to a factor of unity in N. For very nonlinear material (e.g., liquid crystals), the use of a thin film (small d) will increase the resolution capability considerably more than this unity factor between the two types of geometry.

Two unique characteristics of nematics make them far superior to the materials (mostly organic liquids doped with

IR-absorbing dyes) employed by Martin and Hellwarth. One is the unusually large $d\eta/dT$ of nematics, especially near T_c, where both the ordinary and extraordinary $d\eta/dT$'s are about two orders of magnitude larger than for most liquids of high thermal index. The other, more important characteristic is the unusually large reorientational nonlinearity, which is non-wavelength-selective; that is, any infrared lasers can be used. The basic mechanism for infrared-to-visible image conversion is the formation of the grating by the IR beams. Therefore, the dynamics and magnitude of the grating formed are the same as discussed in the preceding section.

Using the experimental setup of Fig. 3(a), we have demonstrated the feasibility of employing either kind of nonlinearity for infrared-to-visible image conversion. The infrared laser used is from a Nd:YAG, in single-pulsed (thermal) or high repetition rate pulsed (for quasi cw reorientation process) modes. The photograph inset in the figure is a typical visible reconstructed image of the wire mesh (infrared illuminated object). In general, a very good quality image can be reconstructed, with a diffraction efficiency on the order of a few percent. We found that traces of IR-absorbing dyes (Kodak #14015) dissolved in the liquid crystal help reduce the required laser energies (to approximately 1 mJ/cm^2) for visible diffraction. This is because pure PCB, like most other liquid crystals, does not absorb appreciably at 1.06 μm. For optimal thermal effect, therfore, "doping" with dyes with appropriate spectral absorption characteristics is needed. We are currently employing other infrared light sources to ascertain the general characteristics, and also some spec c details, concerning image conversion in nematic and other mesophases of liquid crystals.

4. CONCLUSION

We have briefly discussed two four-wave-mixing-based imaging applications of nematic liquid crystal films. The underlying thermal and reorientational nonlinearities are uniquely large and versatile. It is obvious that other nonlinear optical processes, such as opto-optical modulations, optical switchings, and many real-time image processings, can also be realized using nematic films. We anticipate reporting the results of these studies in the near future.

5. ACKNOWLEDGMENTS

This research is supported by grants from the National Science Foundation (ECS 8415387) and the Air Force Office of Scientific Research (AFOSR 840375).

6. REFERENCES

1. See, for example, B. Bahadur, Mol. Cryst. Liq. Cryst. 109, 3 (1984); see also U. Efron, S. T. Wu, J. Grinberg, and L. D. Hess, Opt. Eng. 24(1), 111 (1985) and references therein on the use of Hughes liquid crystal light valves.
2. I. C. Khoo and Y. R. Shen, Opt. Eng. 24(4), 579 (1985) and references therein.
3. See, for example, B. Bahadur, Mol. Cryst. Liq. Cryst. 109, 3 (1984).
4. I. C. Khoo, S. L. Zhuang, and S. Shepard, Appl. Phys. Lett. 39, 937 (1981).
5. I. C. Khoo and S. L. Zhuang, Appl. Phys. Lett. 37, 3 (1980); I. C. Khoo, Phys. Rev. A25, 1040 (1982); S. D. Durbin, S. M. Arakelian, and Y. R. Shen, Opt. Lett. 7, 145 (1982).
6. S. D. Durbin, S. M. Arakelian, and Y. R. Shen, Opt. Lett. 6, 411 (1981); N. F. Pilipetski, A. V. Sukhov, N. V. Tabiryan, and B. Ya Zel'dovich, Opt. Commun. 37, 280 (1981).
7. I. C. Khoo, Appl. Phys. Lett. 41, 909 (1982); M. M. Cheung, S. D. Durbin, and Y. R. Shen, Opt. Lett. 8, 39 (1983); I. C. Khoo, J. Y. Hou, R. Normandin, and V. C. Y. So, Phys. Rev. A27, 3251 (1983).
8. I. C. Khoo, Appl. Phys. Lett. 40, 645 (1982); I. C. Khoo and J. Y. Hou, J. Opt. Soc. Am. B2, 761 (1985).
9. See, for example, *Optical Phase Conjugation*, R. Fisher, ed., Academic Press, New York (1983); see also, J. F. Reintjes, *Nonlinear Optical Parametric Processes in Liquids and Gases*, Academic Press, New York (1983).
10. I. C. Khoo and S. L. Zhuang, IEEE J. Quantum Electron. QE18, 246 (1982).
11. J. P. Huignard, J. P. Herrian, P. Aubourg, and E. Spitz, Opt. Lett. 4, 21 (1979).
12. E. N. Leith, H. Chen, Y. S. Cheng, G. J. Swanson, and I. C. Khoo, *Proc. 5th Rochester Conference on Coherence and Quantum Optics* (June 1983). Plenum Press, New York (1984).
13. I. C. Khoo and R. Normandin, presented at the 1983 Annual Meeting of the Optical Society of America, New Orleans; see also H. Hsiung, L. P. Shi, and Y. R. Shen, Phys. Rev. A30, 1453 (1984) for molecular reorientation with ns laser pulses.
14. I. C. Khoo, Phys. Rev. A27, 2747 (1983).
15. I. C. Khoo, Phys. Rev. A25, 1636 (1982); I. C. Khoo, Phys. Rev. A26, 1131 (E) (1982); I. C. Khoo, Phys. Rev. A25, 1040 (1982).
16. See, for example, P. G. deGennes, *The Physics of Liquid Crystals*, Oxford University Press, Oxford (1974).
17. I. C. Khoo and R. Normandin, IEEE J. Quantum Electron. QE21, 329 (1985).
18. G. Martin and R. W. Hellwarth, Appl. Phys. Lett. 34, 371 (1979).

Wave front conjugation with gain and self-oscillation with a nematic liquid-crystal film

I. C. Khoo
Department of Electrical Engineering, The Pennsylvania State University, University Park, Pennsylvania 16802

(Received 15 July 1985; accepted for publication 12 August 1985)

We have observed for the first time wave front conjugation with amplified reflection return using the thermal nonlinearity of a thin film of nematic liquid crystal in conjunction with a low power laser (intensity on the order of 25 W/cm^2). Self-oscillation is also observed.

Wave front conjugation, and the associated phenomena of imaging through aberration, amplified reflections, and other useful adaptive optical processes have been vigorously studied in the last few years.[1] Materials for wave front conjugation include sodium vapor, semiconductor crystals, barium titanate, electro-optic crystals (BSO), various liquids, liquid crystals, and others. The basic mechanism for nonlinearity ranges widely. In some materials the nonlinearity is sufficiently large for amplified reflection of the probe beam, leading to self-oscillations.[2] Such an effect has important applications in image amplification, laser designs, and other adaptive optics processes.

In nematic liquid crystal, there are two basic mechanisms for optical nonlinearities[3-5] that have been used for degenerate four-wave mixing processes: optically induced refractive index change associated with the director axis reorientation, and laser induced thermal index effect. The fundamental mechanisms for these processes have been quantitatively documented. Application of these nonlinearities for wave front conjugation,[6] where the aberration correction and speckle noise reduction (with spatially partially incoherent lasers) have also been demonstrated. In this letter we report the first successful demonstration of wave front conjugation with gain and self-oscillation, using the thermal nonlinearity in a nematic film in conjunction with low power cw (chopped) lasers.

Consider two linearly polarized lasers propagating through a homeotropically aligned nematic liquid crystal as shown in Fig. 1(a). The two beams are crossed at a small wave mixing angle θ in a plane perpendicular to the paper. For this geometry the refractive index as seen by the optical wave is given by

$$n_e = \frac{n_\perp n_\parallel}{(n_\parallel^2 \cos^2\beta + n_\perp^2 \sin^2\beta)^{1/2}} \qquad (1)$$

for $\beta = 0$, $n_e = n_\perp$. On the other hand, if $\beta = 90°$, e.g., using a planar-aligned nematic as shown in Fig. 1(b), $n_e = n_\parallel$. Both $n_\perp$ and $n_\parallel$ are strongly dependent on the temperature. At temperature removed from the nematic–isotropic transition temperature T_c, the magnitudes of $dn_\perp/dT$ (positive) and $dn_\parallel/dT$ (negative) are already as large as most high index liquids ($\simeq 2\times 10^{-4}$ k^{-1}). As the temperature approaches T_c, both increase by more than an order of magnitude. As a consequence of this large nonlinearity, visible diffractions (with efficiency on the order of one percent or more) can be obtained by mixing two milliwatt cw lasers,[5] using the natural absorption of some nematic [e.g., methoxy benzylidine *p-n*-butylaniline (MBBA)] at the laser wavelength (5145 Å).

Another important characteristic of thermal grating formation in nematic is the relatively faster response. If the two incident lasers are chopped, there are two distinct components in the diffraction. (See Khoo and Shepard in Ref. 5.) One component rises instantaneously with the laser corresponding to a local heating at the interference intensity maxima at the sample. The other component, which is much slower, corresponds to an overall heating of the sample due to thermal diffusion from the grating maxima to the minima; the overall heating raises the temperature of the sample, and therefore increases the change in the refractive index. This overall heating of the sample is quite detrimental to the grating diffraction process if it raises the temperature of the sample over T_c, when the grating diffractions practically vanish. In our study, the duty cycles and duration of chopped cw lasers are adjusted such that the diffraction is maximized while minimizing the overall heating, as discussed in Ref. 5.

The process of laser induced thermal index change and the diffusion process (either in the liquid-crystal medium or through the cell walls) is a complicated three-dimensional problem. In ordinary liquids or in crystals, the fundamental parameters are the temperature T and the density ρ. In liquid

FIG. 1. Schematics of laser interaction in (a) a homeotropically aligned and (b) a planar aligned nematic liquid-crystal film. $\mathbf{K}_1$ (probe beam) $\mathbf{K}_2$ (pump beam) are the propagation wave vectors. $\mathbf{E}_1$ and $\mathbf{E}_2$ are the optical field vectors. The two laser beams intersect in a plane perpendicular to the paper.

 0003-6951/85/210908-03$01.00

crystal, one has also to include the order parameter S. If the chopped laser pulse durations are on the order of milliseconds, one would expect the density fluctuations in the sample to equilibrate, and we are thus left with S and T. The interplay between S and T, and the refractive indices $n_{\parallel}$ and $n_{\perp}$ have been dealt with in a recent article. (See Khoo and Normandin in Ref. 5.) For our purpose here one may simplify the consideration by adopting T as the working parameter, described by the usual thermal diffusion equation

$$\rho c_v \frac{\partial T}{\partial t} - k\nabla^2 T = \frac{nc\alpha}{4\pi} E_{\rm op}^2 , \tag{2}$$

where ρ is the density of the nematic, c_v the specific heat, k the diffusion constant, n the refractive index, α the absorption constant, and $E_{\rm op}$ is the amplitude of the optical electric field. Both ρ and c_v are strongly temperature dependent, especially near T_c. However, their influence on the refractive index may be viewed as secondary; the primary effect comes from the change in T.

The total optical electric field $E_{\rm op}$ incident on the sample is made up, of course, of the contribution from the probe (E_1) and the pump beam (E_2). Their interference gives rise to an oscillating term $E_1 E_2 \cos qy$, where q is the grating wave vector ($q = 2\pi/\lambda_q$; $\lambda_q = \lambda{\rm op}/2 \sin(\theta/2)$,$\theta$: wave mixing angle in the nematic), and y is the coordinate perpendicular to $\mathbf{K}_1 - \mathbf{K}_2$. If the incident lasers are pulsed, with pulse lengths shorter than all the thermal diffusion time constants (characteristics of diffusion time between the intensity maxima and the minima, and between the center plane of the liquid-crystal cell and the cell walls etc.), then the change in temperature ΔT [from Eq. (1)] is simply given by

$$\Delta T = \frac{\alpha}{\rho C_v} U(y) , \tag{3}$$

where U is the energy of the laser pulse. On the other hand, if the laser pulses are longer than the diffusion time (which is true for our experiment using chopped cw lasers; laser pulses $\approx$ 100 ms, diffusion time constant $\approx$ 5 ms), then the spatial redistribution of the absorbed energy and the rise in temperature is obviously a complicated three-dimensional problem, a complete solution of which is clearly outside the scope of this letter. Nevertheless, in the steady state ($\partial T/\partial t = 0$) involving chopped cw lasers, one may note that the spatial derivative ($\nabla^2 = \partial^2/\partial y^2 + \nabla_z^2$) imply that the temperature rise ΔT will be inversely proportional to the grating constant (and cell thickness). This point is particularly obvious if we perform a simple one-dimensional calculation, and is expected from physical grounds. This dependence was qualitatively verified in our experiment. The diffraction efficiency increases with increasing grating constant.

The experimental setup used for the observation of amplified reflection and oscillation is depicted in Fig. 2. The laser used is the 5145-Å line from an Ar^+ laser. The path lengths of the beam are adjusted to be very nearly equal to optimize the interference modulation. The two laser beams are crossed at a very small angle θ on the sample (θ ranges from 1/250 to 1/350 rad). The size of the laser beam on the sample is about 2 mm. The sample used is a homeotropically aligned MBBA film with a thickness of 100 μm. The lasers are almost normally ($\beta = 0$) incident on the film, i.e., the

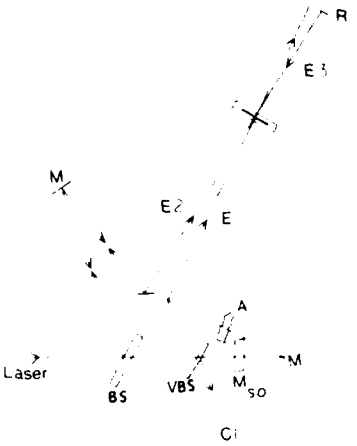

FIG. 2. Schematics of the experimental setup for observing wave front conjugation and self-oscillation. The incident laser is chopped. M: mirrors; S: sample; R: 100% reflector; BS: beam splitter; A: aberrator; VBS: variable beam splitter; M_{50} (in dotted line) is a 99% reflecting mirror to be inserted for self-oscillation effect.

optical electric field is perpendicular to the director axis. The incident probe laser power is adjusted with the variable beam splitter. The mirror M_{50} (in dotted line) when used for self-oscillation experiments, is aligned to exactly reflect the probe beam E_1. The incident laser beam is chopped at a rate of about 4 Hz. At this rate there is an overall heating of the sample. However, this overall heating effect is just sufficient to warm the sample (from room temperature 27 °C) to near T_c (T_c of MBBA is 42 °C) when very large wave-front conjugation efficiency is obtained.

Very strong conjugated signals are observed for a wide range of probe beam powers used. At equal pump and probe power, a reflection efficiency of about 1% is observed for the sample maintained at room temperature (by using very low power pump and probe laser < 100 mW). A dramatic increase in the reflection efficiency (to more than 20 times) is observed if the temperature of the sample is raised (cf. Fig. 3) either by placing the sample in a temperature cell or by an overall heating with an increase in the laser powers to about 1 W. The reflection efficiency increases if the ratio of the pump beam power to the probe beam power is increased. At a beam ratio of about 250, and an external wave mixing angle $\theta = 1/300$ (corresponding to a wave mixing angle of 1/450 within the sample, and a grating constant $\lambda_q = 225$ μm), amplified reflection (> 100%) is observed. This occurs at a pump beam of 1 W, corresponding to a pump laser intensity of about 25 W/cm^2 on the sample.

Because of the amplified reflection capability, self-oscillation starting from noise generated in the film in conjunction with an external feedback is also possible. To observe this effect, the mirror M_{50} (99% reflecting at 5145 Å) is inserted between the variable beam splitter VBS and the mirror M. The probe beam is blocked with an opaque material between the beam splitter (BS) and VBS. With a pump power input of about 1 W, a clearly visible self-oscillation generated beam is observed in the direction along C_1. The exit beam power at C_1 is estimated to be tens of microwatts. The self-oscillation occurs despite a strong scattering loss ($\approx$ 25%) experienced by all the beams in traversing the sample and the

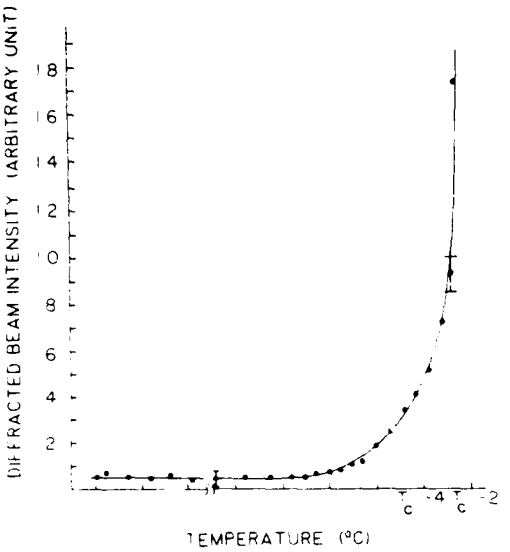

FIG. 3. Plot of the diffraction efficiency R as a function of the temperature at very low pump and probe laser power at temperature far from T_c, the diffraction efficiency is about 1%. Near T_c, it increases by about 20 times.

presence of the aberrator. Because of thermal fluctuations in the path of the lasers, and also in the liquid-crystal film itself, there is considerable instabilities in the observed self-oscillations. The oscillations appear as a highly brightened beam along C_1 (observed on a screen) that lasted several seconds, disappeared temporarily, and appeared again, very much like a cw laser just above threshold and oscillating in an open atmosphere (i.e., no enclosure to minimize the thermal instability in the air). We have also used a much more simplified setup from Fig. 2, consisting of a retroreflecting (for the pump laser) mirror and another mirror oriented to reflect the conjugated beam back to the sample.

Although MBBA possesses a significant absorption at 5145 Å, it tends to deteriorate in quality with age, as often noted by many researchers. We have experimented with the more stable liquid-crystal PCB, in which traces of dyes (R6G) are dissolved to improve the absorption rate of 5145 Å (PCB possesses very little amplified natural absorption at 5145 Å), and observed similar wave front conjugation and self-oscillation effects.

In conclusion, we have demonstrated the possibility of observing amplified reflection in wave front conjugation, and self-oscillation, using the thermal nonlinearity of a nematic liquid-crystal film. The configurations and conditions for these effects have obviously not been optimized, but the results of this and our recent studies clearly provide the basis for optimization. The effect can also be applied in constructing a ring oscillator. It is also obvious that other types of lasers (cw or pulsed) can also be used (e.g., CO_2 laser at 10.6 μm where liquid crystals also possess natural absorption, Nd:YAG laser at 1.06 μm if the liquid crystal is "doped" with traces of IR absorbing dyes, etc.). Works along these lines are currently in progress and will be reported elsewhere.

I am grateful for some technical assistance by R. R. Michael, G. Finn, and T. H. Liu. The support of the National Science Foundation (ECS 8415387) and the Air Force Office of Scientific Research (840375) is also acknowledged.

[1] For a recent review see, for example, *Optical Phase Conjugation*, edited by R. Fisher (Academic, New York, 1983); see also J. F. Reintjes, *Nonlinear Optical Parametric Processes in Liquids and Gases* (Academic, New York, 1983) and all the references therein on nonlinear materials.

[2] See, for example, J. Feinberg and R. W. Hellwarth, Opt. Lett. **5**, 519 (1980); H. Rajbenbach and J. P. Huignard, Opt. Lett. **10**, 137 (1985); B. Fisher, M. Cronin-Golomb, J. P. White, and A. Yariv, Opt. Lett. **6**, 519 (1981); R. Jain and G. Dunning, Opt. Lett. **7**, 420 (1982); R. G. Caro and M. C. Gower, Appl. Phys. Lett. **39**, 855 (1981).

[3] See, for example, I. C. Khoo and Y. R. Shen, Optical Engineering **24**, 579 (1985) which provides an overview of the two types of nonlinearity.

[4] On orientational nonlinearity, see I. C. Khoo and S. L. Zhuang, Appl. Phys. Lett. **37**, 3 (1980); I. C. Khoo, Phys. Rev. A **23**, 2077 (1981); **25**, 1636 (1982); **27**, 2747 (1983); S. D. Durbin, S. M. Arakelian, and Y. R. Shen, Phys. Rev. Lett. **47**, 1411 (1981); H. L. Ong, Phys. Rev. A **28**, 2393 (1983).

[5] On thermal nonlinearity, see I. C. Khoo and S. Shepard, J. Appl. Phys. **54**, 5491 (1983); I. C. Khoo and R. Normandin, IEEE J. Quantum Electron. **QE-21**, 329 (1985); Opt. Lett. **9**, 285 (1984); H. Hsiung, L. P. Shi, and Y. R. Shen, Phys. Rev. A **30**, 1453 (1984).

[6] I. C. Khoo and S. L. Zhuang, IEEE J. Quantum Electron. **QE-18**, 246 (1982); E. N. Leith, H. Chen, Y. S. Cheng, G. J. Swanson, and I. C. Khoo, Proceedings of 5th Rochester Conference on Coherence and Quantum Optics, Rochester, June 1983.

Dynamic Gratings and the Associated Self Diffractions and Wavefront Conjugation Processes in Nematic Liquid Crystals

IAM-CHOON KHOO, MEMBER, IEEE

(Invited Paper)

Abstract—**The origins and the dynamics of optical nonlinearities in nematic liquid crystal films, namely, laser-induced molecular reorientational and thermal refractive index changes, are analyzed in the context of optical wave mixings. Theoretical expressions for the basic nonlinearities, the rise and decay time, diffraction efficiencies, and other pertinent parameters involved in the dynamic grating formation are derived. Experimental results obtained with visible and infrared laser pulses are analyzed. Some newly observed novel nonlinear processes are also reported.**

I. Introduction

LINEAR and nonlinear optical properties of liquid crystals in their mesophases have been studied in several contexts, in both fundamental and application-oriented pursuits. In the context of nonlinear optical processes, they have recently received considerable renewed interests as a result of the newly discovered extraordinarily large optical nonlinearity due to the laser-induced molecular reorientation, and a renewed effort explicitly at the large thermal index effect in liquid crystals. In the last few years, several groups [2]–[10] have looked at the optical nonlinearity in the mesophases of liquid crystals and the associated nonlinear processes. A brief review of some of these nonlinear optical processes and the fundamental mechanisms in both the liquid crystal and the isotropic phases has recently appeared [1]. In this paper, therefore, we will concentrate only on optical wave mixing processes that are relevant to this Special Issue.

Specific effects include optical self diffractions, generation of high-frequency acoustic waves, optical wave front conjugation (with gain) and self oscillations, and infrared-to-visible image conversion. The origin of the optical nonlinearities responsible for these processes is either the optical-induced molecular reorientation or the laser-induced thermal refractive index change. In the next section, we will review these two types of nonlinearities, and especially their dynamical dependences. This is followed by a summary discussion of the aforementioned nonlinear processes.

Manuscript received October 7, 1985; revised March 3, 1986. This work was supported by the National Science Foundation under Grant ECS 8415387 and the U.S. Air Force Office of Scientific Research under Grant AFOSR840375.

The author is with the Department of Electrical Engineering, Pennsylvania State University, University Park, PA 16802.

IEEE Log Number 8609096.

II. Liquid Crystal Nonlinearity and Dynamics

A. Orientational

In theory, all three mesophases (nematics, smectics, and cholesterics) of liquid crystals posses extraordinarily large optical nonlinearity [1]–[3]. To date, the most extensive and conclusive experimental studies have been performed in the nematic phase [1]–[10] where the molecules are directionally correlated but positionally random. The direction is characterized by the director axis n, and the correlation by an order parameter S[11]. Two of the most commonly employed cell alignments are depicted in Fig. 1(a) and (b), termed homeotropic and planar cells, respectively. Homeotropic samples are obtained by coating the glass slides with a surfactant, while planar samples are often made using glass slides that have been rubbed in a unidirectional direction [11]. Nematics are highly birefringent, with $\Delta n = n_1 - n_2 = 0.2$ or larger where n_1 and n_2 are the refractive indexes for the optical field parallel and perpendicular to the director axis, respectively. In analogy to well-known dc field-induced electrooptical effects, the primary effect of an optical field is the dielectric torque exerted by the optical electric field in the liquid crystal. Under suitable conditions, (which we will presently elaborate) the optical torque creates a distortion or reorientation of the director axis and an accompanying self (laser)-induced refractive index change.

Nematic director axis reorientation by an optical field and the associated wave mixing and self-focusing effect were first theoretically quantitatively studied by Tabiryan and Zel'dovich [4], who also discussed similar processes in smectic and cholesteric liquid crystals. Herman and Serinko [5] presented a theory of nematic liquid crystal axis reorientation by an optical field in the presence of a strong bias dc magnetic field and the associated wave mixings and optical diffraction effects. Others [2], [3], [5]–[10] have also considered a similar reorientation process under steady-state or time-dependent optical illumination. A quantitative analysis and experimental study of transient nanosecond laser-induced molecular reorientation and heating have recently been presented by Hsiung

et al. [12] and by Khoo and Normandin [13]. In this paper, we shall therefore provide a brief simplified version of the theories for orientation and thermal effect whereby the physics of the nonlinearity and the nonlinear optical processes in the transient regime can be clearly appreciated. The interested readers could also refer to the lengthy detailed treatments by Tabiryan and Zel'dovich [4] and Ong [7].

Consider two linearly polarized lasers incident on a homeotropic nematic film as shown in Fig. 1(a). The two beams' interference gives rise to an intensity sinusoidal on the film, i.e., the total electric field amplitude E on the film is given by

$$E^2 = E_1^2 + E_2^2 + 2E_1E_2 \cos q \cdot y \tag{1}$$

where E_1 and E_2 are the amplitudes of the two optical fields

$$q = |\vec{q}| = |\vec{K}_1 - \vec{K}_2|.$$

The free-energy density of the system in the one-elastic constant approximation is given by [11]

$$F = \frac{K}{2}\left[\left(\frac{\partial\theta}{\partial y}\right)^2 + \left(\frac{\partial\theta}{\partial z}\right)^2\right] - \frac{\Delta\epsilon}{8\pi}(E_1^2 + E_2^2 + 2E_1E_2 \cos qy) \sin^2(\theta + \beta) \tag{2}$$

where $\Delta\epsilon$ is the optical dielectric constant anisotropy. $\Delta\epsilon = \epsilon_1 - \epsilon_2$ and θ is the reorientation angle of the director axis $\hat{n}$ from the initial alignment.

The time dependence of the molecular reorientation following the usual Ericksen–Leslie approach becomes [11]

$$\gamma\frac{\partial\theta}{\partial t} = K\left(\frac{\partial^2\theta}{\partial y^2} + \frac{\partial^2\theta}{\partial z^2}\right) + \frac{\Delta\epsilon}{8\pi}E^2 \sin 2(\theta + \beta) \tag{3}$$

where γ is the effective viscosity coefficient. In writing (1)–(3), we have neglected several terms associated with flow and inertia (see Hsiung *et al.* [12]) in the medium which have been shown to be negligible in all of the wave-mixing experiments so far.

In the small-angle (θ) limit (which is often the case in actual wave-mixing experiments), (3) becomes

$$\gamma\frac{\partial\theta}{\partial t} = K\left(\frac{\partial^2\theta}{\partial y^2} + \frac{\partial^2\theta}{\partial z^2}\right) + \frac{\Delta\epsilon E^2}{4\pi}\left[(\cos 2\beta)\,\theta + \frac{\sin 2\beta}{2}\right]. \tag{4}$$

An approximate solution of this equation is

$$\theta = \theta(t) \cos qy \sin\frac{\pi z}{d} \tag{5}$$

which satisfies the so-called hard-boundary conditions ($\theta = 0$ at $z = 0$ and at $z = d$).

Substituting (5) into (4) gives

$$\gamma\frac{\partial\theta}{\partial t} = \left[\frac{\Delta\epsilon E^2 \cos 2\beta}{4\pi} - K\left(\frac{\pi^2}{d^2} + q^2\right)\right]\theta + \frac{\Delta\epsilon E_{op}^2}{8\pi}\sin 2\beta \tag{6}$$

or

$$\frac{\partial\theta}{\partial t} + \frac{1}{\tau}\theta = \frac{\Delta\epsilon E^2}{8\pi\gamma}\sin 2\beta \tag{7}$$

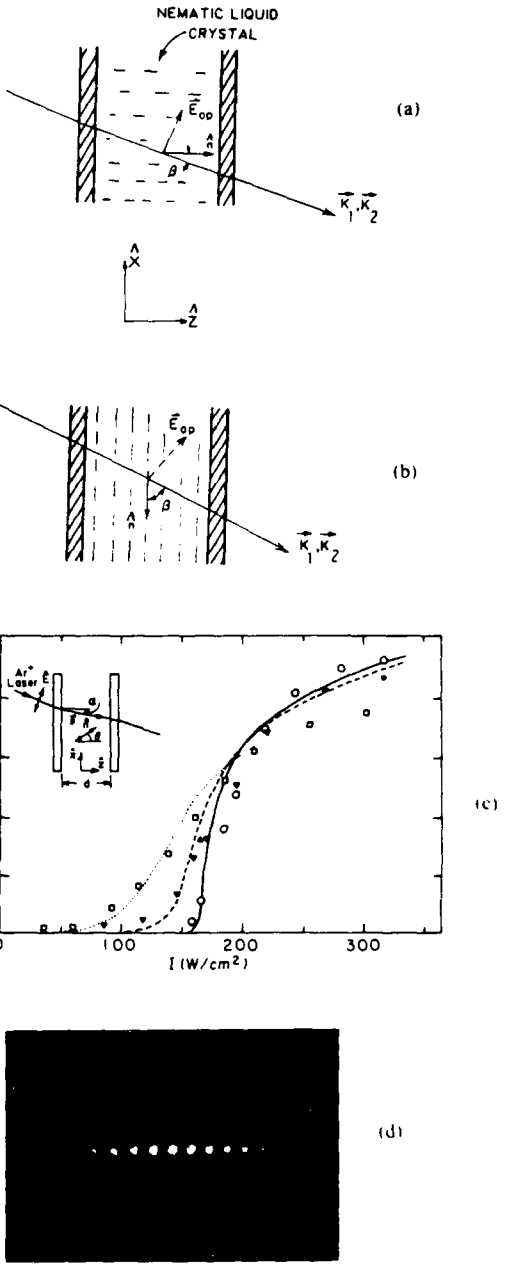

Fig. 1. Schematic of two optical waves propagating in (a) a homeotropic and (b) a planar nematic liquid crystal film. $\vec{K}$'s are the propagation directions, E_{op} is the optical electric field, and $\hat{n}$ is the director axis direction. The two optical beams are crossed at a wave-mixing angle in a plane perpendicular to the plane of the paper. (c) Experimental data and theoretical curves for the phase shift $\Delta\phi$ induced in a 250 μm, homeotropically aligned, 5CB film by an Ar^+ laser beam at different angles α: circles and solid curve, $\alpha = 0°$; solid triangles and dashed curve, $\alpha = 3°$; squares and dotted curve, $\alpha = 11°$. Inset shows the experimental geometry (after [3]). (d) Photograph of the multiorder diffractions via two wave mixings in a nematic liquid crystal film using CW lasers with intensities on the order of a few watts/cm^2. Similar multiorder diffractions are observed via transient wave mixings with nanosecond laser pulses (I. C. Khoo, unpublished).

where

$$\tau = \left[\frac{-\gamma}{\frac{\Delta\epsilon}{4\pi}E^2\cos 2\beta - K(\pi^2/d^2 + q^2)}\right]. \quad (8)$$

τ is the time constant characterizing the buildup of the reorientation process.

Depending on the magnitude of the optical field, the growth of the reorientation process can be slow or fast. If we define an optical Freedericks transition field E_F^1,

$$E_F = \frac{4\pi^3 K}{\Delta\epsilon d^2},$$

in analogy to dc field effect, (8) gives

$$\frac{1}{\tau} = \frac{4\pi}{\Delta\epsilon}d^2\frac{\gamma}{\left|E^2\cos 2\beta - E_F^2\left(1 + \frac{q^2}{\pi^2}d^2\right)\right|}. \quad (9)$$

Most previous studies of molecular reorientation employed an optical field below or just above the Freedericks field E_F, and thus τ is large. It is obvious that if the optical field strength increases, e.g., to 10^4 statvolt/cm^2 or more, τ can be very short (microseconds or tens of nanoseconds), using standard values for d, $\Delta\epsilon$, K, γ, and q ($q = 2\pi/\Lambda$ where Λ is the grating constant) (e.g., $d \approx 50$ μm $\approx \Lambda$, $\Delta\epsilon = 0.6$, $K = 10^{-7}$ dynes, $\gamma = 0.1$ poise). The complication arising from optical reorientation with a high-power pulsed laser is that the liquid crystal will also be heated [12], [13], via some finite absorption. This heating effect and the associated refractive index changes have been characterized by different time scales from the orientational process, as will be discussed in the next section.

The decay time of the process is simply

$$\frac{1}{\tau_{\text{decay}}} = \frac{\gamma}{K(\pi^2/d^2 + q^2)}. \quad (10)$$

For a typical thickness $d \sim 50$ μm and $\Lambda \sim 50$ μm, the decay time is on the order of 1 s. Millisecond decay time is achieved for d or Λ on the order of a few micrometers.

The magnitude of the reorientation angle θ depends obviously on the magnitude as well as the duration of the pulsed optical field, and will saturate when all the molecules are aligned in the direction of the optical field. We note here, however, that for large reorientation angles, (6) is no longer valid and one has to use (3), the solution of which has been discussed in various contexts by several workers [3], [4], [7], [12]. On the other hand, for small θ, the stationary maximum value of θ is roughly given by

$$\theta \sim \frac{\Delta\epsilon E^2 \sin 2\beta \sin \pi Z/d \cos qy}{8\pi\left[K(\pi^2/d^2 + q^2) - \frac{\Delta\epsilon E^2\cos 2\beta}{4\pi}\right]}. \quad (11)$$

For a given reorientation θ, the change in the refractive index Δn associated with the two extraordinary rays (e.g., Fig. 1 where the laser beams propagate as an extraordinary ray) is given by

$$\Delta n = n_e(\beta + \theta) - n_e(\beta)$$

where n_e is given by

$$n_e(\beta + \theta) = \frac{n_1 n_2}{\sqrt{n_1^2\cos^2(\beta + \theta) + n_2^2\sin^2(\beta + \theta)}}. \quad (12)$$

Equation (12) gives, in the small θ limit, an index grating

$$\Delta n(\theta) \sim \theta\frac{n\Delta\epsilon}{2\epsilon_1}\sin 2\beta. \quad (13)$$

In the small θ limit, and for $E_{op}^2 \ll E_F^2$, (11) reduces to a form analogous to those obtained in previous publications [1]–[4]. The significance of $\Delta n(\theta)$ is its magnitude. For $d \sim 100$ μm, $\beta \sim 0.5$ rad, an optical intensity on the order of 100 W/cm^2 will induce a Δn of 10^{-3} ($\theta \sim 10^{-2}$). For example, Fig. 1(c) shows a detailed measurement by Durbin *et al.* [3] of the laser-induced phase shift [due to $\Delta n(\theta)$] in a nematic liquid crystal film for various values of the angle β (denoted as α in [3]). In the context of wave mixings involving two laser beams E_1 and E_2 as described earlier, the theory and experiments were first quantitatively studied by this author [2]. The dependence of the self-diffraction effect on the angle β, the grating spatial frequency, and also the temperature *independence* of the nonlinear diffraction were experimentally verified. In the presence of a strong dc bias field, the optical nonlinearity of a nematic liquid crystal film is enhanced; as may be seen in the photograph of Fig. 1(d). This shows the multiorder diffractions from a 75 μm thick nematic film where an applied bias magnetic field is used to first reorient the director axis. Diffraction efficiencies on the order of more than 10 percent are observed for laser intensities of only a few watts/cm^2. The effect was first confirmed by an observation by Khoo [2] following the prediction of Herman and Serinko [5]. Subsequently, Durbin *et al.* [10] have also studied the problem involving the multiple diffraction orders, and have presented a detailed analysis of the multiple diffraction effects.

II. Thermal Nonlinearity

The dependence of the refractive index of nematic liquid crystal on the temperature has occupied central importance in the study of the fundamental and applied properties of liquid crystals [11]. In this discussion, we will follow the literature [11], [14] and choose as the starting point of our analysis of the thermal nonlinearities the dielectric constants $\epsilon_1 = n_1^2$ and $\epsilon_2 = n_2^2$. Depending on the levels of sophistication one desires, there are several possible forms of ϵ_1 and ϵ_2 in terms of molecular parameters (see, for example, De Jeu, [11]). In the simplest case, they are given by

$$\epsilon_1 = 1 + (N\rho/3\epsilon_0 M)[\alpha_l K_l(2S + 1) + \alpha_t K_t(1 - 2S)] \quad (14)$$

and

$$\epsilon_2 = 1 + (N\rho/3\epsilon_0 M)[\alpha_l K_l(1 - S) + \alpha_t K_t(2 + S)] \quad (15)$$

where $\alpha_{e,l}$ and $K_{e,l}$ are the longitudinal and transverse components of the molecular electronic polarization α and the internal field tensor K; N is the Avagadro number, ρ is the density of the liquid crystal, M is the molecular weight, and S is the order parameter. The degree of sophistication depends on the various models used for evaluating K. To understand the key factor affecting the thermal refractive index change, we shall use a slightly simplified version where the local field correction factors are ignored. In that case, ϵ_1 and ϵ_2 from (14) and (15) can be expressed in the form

$$\epsilon_1 = \epsilon_l + \tfrac{2}{3}\Delta\epsilon \tag{16}$$

$$\epsilon_2 = \epsilon_l - \tfrac{1}{3}\Delta\epsilon \tag{17}$$

where

$$\epsilon_l = 1 + \frac{N\rho}{3\epsilon_0 M}(\alpha_l k_l + 2\alpha_t k_t) \sim 1 + \text{const.}\ \rho \tag{18}$$

and

$$\Delta\epsilon \sim \frac{N\rho S}{\epsilon_0 M}(\alpha_l k_l - \alpha_t k_t) \sim \rho S. \tag{19}$$

On the other hand, the order parameter S (defined in many standard texts) can be shown to be well approximated by the expression

$$S = [1 - 0.98\ TV^2/T_{ni}V_{ni}^2]^{0.22} \tag{20}$$

where T_{ni} is the nematic → isotropic phase transition temperature and V_{ni} is the corresponding volume. The most significant contributions to the refractive index dependence on temperature are from ρ and S. Other parameters are also highly temperature dependent, such as the volume V and the specific heat C_V that is involved in the laser heating of the liquid crystals. One can think of the contributions from ρ and S as being primary, while others are only secondary and may be neglected.

The most significant feature of laser-induced thermal index change is the magnitude of dn_1/dT and dn_2/dT. Fig. 2 is a plot of the thermal index gradients (dn_1/dT and dn_2/dT) of PCB from experimental values of the refractive indexes [14].

Typically, (dn_1/dT) is on the order of 4×10^{-4} K^{-1} while (dne/dT) is about 1.5×10^{-3} K^{-1}, which are already much larger than most other high thermal index materials (e.g., cyclohexane). Near T_c, both dn/dT's increase by more than an order of magnitude.

For transient wave mixings, the detailed calculations for the three-dimensional thermal grating buildup and temperature distribution and dissipation are obviously very complex, and are further complicated by the anisotropic thermal diffusion constants of the liquid crystals, as well as the enclosing glass slides. In the simplest case where the thermal grating is reducible to a one-dimensional problem [14] (e.g., the case of very small grating constant Λ compared to the cell thickness d), the thermal decay time constants for heat dissipation along and perpendicular to the nematic axis are, respectively $\tau_1 = (D_1 q_1^2)^{-1}$ and $\tau_2 = (D_2 q_2^2)^{-1}$. For typical liquid crystals, $D_2 \sim 7.9 \times 10^{-4}$ cm^{2}s^{-1} and $D_1 \sim 1.25 \times 10^{-3}$ cm^{2}s^{-1}. For a grating constant $\Lambda_2 = 2\pi/q_2 \sim 17$ μm, one gets $\tau_2 \sim 110$ μm. On the other hand, $\tau = 11\ (n_2/n_1)^2\tau_2 \approx 50$ μs. These estimated values are in good agreement with the experimental data obtained in a recent study [13].

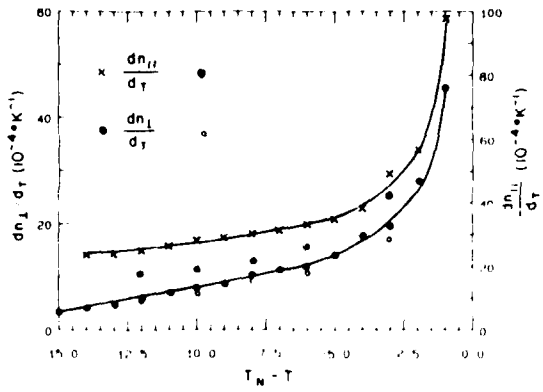

Fig. 2. The dependences of $(dn_{//}/dT)$ $(n_{//} = n_1)$ and $(dn_\perp/dT)$ $(n_\perp = n_2)$ on temperature deduced from data in [14]. T_N is the nematic → isotropic transition temperature. Some theoretical values obtained using (16)–(20) (cf. [13]) are also indicated (0 and 0).

III. Experimentally Observed Dynamic Grating Effects

A. Nonlinear Diffraction and High-Frequency Acoustic Waves

From (15), (16), and (20), it is obvious that the change in the refractive index as a function of a temperature rise is due to a change in the order parameter S and the density ρ. In the transient regime involving very short laser pulses (short compared to the acoustic phonon lifetime), the interference of two laser beams will give rise to an index grating comprising a nonpropagating component associated with S and a propagating component from ρ. These two components, under appropriate conditions (temperature, angle, etc., as detailed in [13]), will interfere and produce modulation in the diffraction of a probe beam from the grating produced by the two incident beams [15], [16]. The frequency of modulation is given by C_s/Λ where C_s is the sound velocity in the bulk liquid crystalline film. Fig. 3(a) shows the dynamics of the defraction of a CW He-Ne probe laser from a grating produced by two linearly polarized nanosecond Nd:YAG second harmonic laser pulses in a nematic film [17]. The initial portion clearly shows the modulation caused by the acoustic interference. A principal requirement for generating these gigahertz acoustic waves is that the bandwidth of the two exciting lasers be large enough to accommodate the acoustic frequency; hence, we have the use of picosecond lasers in some studies [15], [16]. Alternatively, one can employ a two-mode laser and a wave-mixing angle such that the grating constant Λ and therefore the sound frequency C_s/Λ matches the frequency separation of the two modes [17].

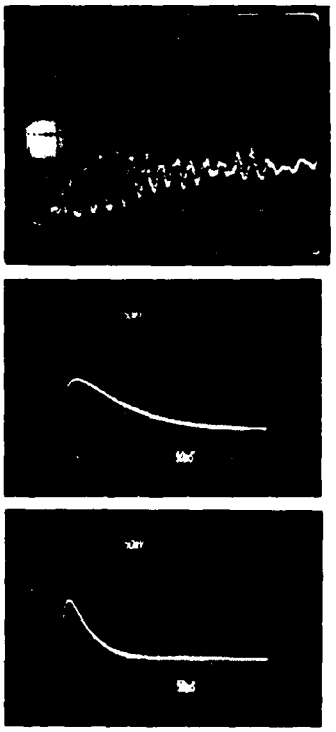

Fig. 3. (a) The temporal dependence of the diffraction of a CW He-Ne laser from a transient grating induced by two nanosecond Nd: YAG second harmonic laser pulses in a nematic film (PCB, 40 μm thick, homeotropically aligned) (after [17]). Time scale is 20 ns/div. Similar ultrasonic wave generation was also observed in a smectic liquid crystal film [17b]. (b) The dynamics of the thermal grating formation and decay in a nematic film as monitored by a CW He-Ne probe laser diffraction. The grating wave vector $K_1 - K_3$ is perpendicular to the director axis. (c) Same as in (b), but for $K_1 - K_3$ along the director axis.

Using the pump probe experiment, and from modulation data similar to Fig. 3(a), both the velocity of sound and the acoustic attenuation constant in the bulk nematic can be measured simultaneously. The sound velocities in the nematic and smectic phase obtained using these transient wave-mixing effects are in excellent agreement with those obtained by other techniques [18], [19]. Obviously, if the incident plane of the laser and the wave-mixing angle are chosen appropriately, and using a planar sample, one could also study the acoustic velocity and attenuation anisotropies. These transient wave-mixing interference effects, therefore, could be developed into very versatile and powerful techniques (cf. work by Nelson *et al.* [16] and Eichler and Stahl [15]) for studying bulk acoustic properties in nematics as well as smectics.

In these experiments, self diffractions from the two incident Nd: YAG lasers are also observed. This shows that the rise time of the thermal grating buildup is therefore on the order of the laser pulse duration, as mentioned earlier. To investigate further the rise and fall dynamics, we again monitor the diffraction from a CW He-Ne beam. Fig. 3(b) and (c) show the typical dynamics of the thermal buildup and decay for the grating wave vector q perpendicular and parallel to the nematic axis, respectively. The rise time is on the order of the incident laser pulses, while the decay time depends on the grating wavevector direction with respect to the director axis, as well as on the grating constant. Obviously, for a much smaller grating constant, the decay time can be considerably shorter than the 50 μs or so observed here.

In some nematics, e.g., PCB (4-cyano-4'-pentylbiphenyl), the natural absorption is quite small at the second harmonics of the Nd: YAG laser. To enhance the absorption constant and thus the nonlinearity, it is possible to dissolve some dyes that absorb at around 0.53 μm, e.g., rhodamine 6G. Experiments have been conducted [13], [17] in nematic films with traces of dissolved dyes which showed that the required laser energies for several nonlinear processes based on the thermal effect were drastically reduced. A detailed study of the rise portion of the He-Ne diffraction also shows that the intramolecular relaxation processes that transfer the excitation from the dye to the liquid crystal take place probably at much shorter time scales than the laser pulse length, as the diffraction from a dyed sample has exactly the *same* rise time as the undyed sample.

IV. Optical Wavefront Conjugation and Multiwave Mixings

Fig. 4 depicts a typical optical configuration for wavefront conjugation studies. The two incident waves E_1 and E_2 generate a grating (via thermal or reorientational effect). E_3 is the retroreflection of E_2, while E_4 is the generated fourth (conjugated or reflected) wave. In liquid crystalline systems, there have been several studies of wavefront conjugation based on different nonlinearity mechanisms. Fekete *et al.* [20] employed nanosecond laser-induced molecular reorientation in the *isotropic* phase, the mechanism and dynamics of which were first studied quantitatively by Wong and Shen [20]. These individual molecular reorientational effects exhibit some enhancement, owing to greater molecular correlation as the liquid is cooled towards the isotropic $\rightarrow$ nematic transition temperature T_c. On the other hand, Garibyan *et al.* [21] employed a liquid crystal light valve for optical wave-mixing processes. The reference and object beam set up an interference intensity grating on the light valve which, acting on the photoconductor material coating, changes the impedance of the (nematic) liquid crystal film. In conjunction with an applied dc field, the intensity grating leads to an orientational (and therefore a phase) grating that optical wavefront conjugation rising purely optical field-induced effect in the nematic phase was first demonstrated by our group where the phase aberration correction capability was also confirmed [22]. In a later study, Leith *et al.* [23] employed thermal nonlinearity to demonstrate the feasibility of speckle-noise removal in wavefront conjugation using a spatially partially coherent laser beam.

For highly nonlinear materials, it is possible to obtain amplified phase conjugation reflections [24]. Moreover, noise originating from the system could also interfere coherently with the pump beams and, with proper feedback

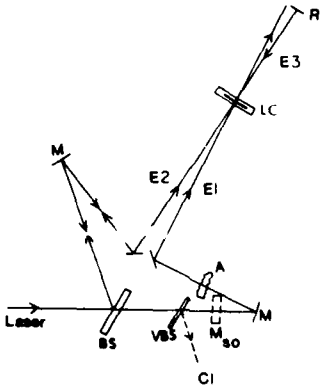

Fig. 4. Schematic of the setup for optical wavefront conjugation using a liquid-crystal (LC) film. E_1: object beam, E_2: reference beam, A: aberrator, M: mirror, M_{so}: mirror to be used for self-oscillation effect, VBS: variable beam splitter to control the intensity of E_1, BS: beam splitter, R: total reflector. For an example of wavefront conjunction result, see Fekete *et al.* [20] (isotropic phase of liquid crystal) or [20] (nematic phase).

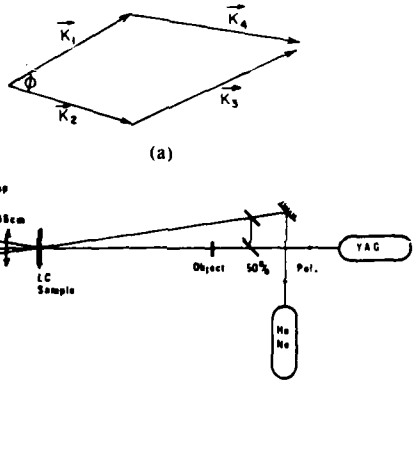

Fig. 5. (a) Phase matching in optical wavelength conversion using K_1 and K_2 to induce the grating and K_3 to generate K_4 via four-wave mixing process. (b) Experimental setup for infrared-to-visible image conversion using the transient grating induced by infrared (1.06 μm) Nd:YAG laser pulses in a dyed nematic liquid crystal film. The reconstructing beam is a CW He-Ne (0.63 μm) laser. The photo insert is a typical observed reconstructed image of the wire mesh object.

from a mirror, lead to self oscillations [25]. A study of amplified reflection based on thermal nonlinearity of nematic has been reported [26]. Another consequence of very strong two-wave mixing is that the probe beam will be amplified by the pump [26]. Herman and Serinko [5] first calculated the efficiency of this process in a nematic film just above a dc magnetic field-induced Freedericks transition. They predicted that amplification of the probe could arise with a very low power laser (with power on the order of a few watts). This was indeed verified (Khoo and Zhuang [2]). There are obviously several possible further studies based on these results, such as image amplification via phase conjugations and ring-laser oscillators. Extension of these studies involving visible lasers to lasers in the infrared regime are also envisioned.

It is possible to use beams at one wavelength to induce a refractive index grating (or hologram), which subsequently diffracts an incoming beam at another wavelength [27]. Fig. 5(a) shows the basic geometry required for phase matching used in our study using a nematic liquid crystal [28]. For a variation of the Bragg diffraction angle ϕ by $\delta\phi$ for which the phase-matched condition is still satisfied, i.e., $\Delta kl < \pi$, one gets

$$\delta\phi = 2\Pi\phi^{-1}(k_1 d(1 + k_1/k_2))^{-1}$$

where k_1 and k_2 are the wavevectors. The diffraction solid

angle of the object beam which sends an area A on the sample is given by $\phi_D = 4\Pi^2/k_1^2 A$. It is therefore possible, in principle, to have the number of resolution elements N, defined as $N \sim \delta\phi/\phi_D$, as

$$N \sim \frac{Ak_1}{l(1 + k_1/k_2)}.$$

For example, if $A \sim 1$ mm^2, $l \sim 100$ μm, and $k_1 = 2\pi/\lambda \sim 2\pi/(1.06\ \mu\text{m})$, we have $N \sim 10^4$. Resolution of this order was reported by Martin and Hellwarth [27] using a slightly different (but basically similar) geometry where both K_3 and K_4 are exactly opposite in directions to those depicted in Fig. 5 here. The point about nematic liquid crystal film is that using liquid crystal "doped" with some infrared absorbing dyes, one could perform these real-time holographic processes with less laser energy (per unit area) because of the unusually high thermal indexes. Fig. 5(b) is a setup used in a recent experiment [28]. The liquid crystal used is a PCB sample with traces of dissolved infrared absorbing dyes. The object used for this real-time holographic imaging process is a wire mesh. The pump and probe beams are from a 20 ns, 1.06 μm Nd:YAG laser pulse, while the probe beam is a CW He–Ne laser (0.6328 μm). Visible images (at 0.6328 μm) are observed at input energies on the order of 50 and 15 mJ on a spot size of 0.5 cm^2. The energy per unit area is considerably less than that used in previous studies [27]. If the sample temperature is raised to near T_c, a decrease in the energy requirement by an order of magnitude is observed. This process of infrared-to-visible image conversion is by no means the only possible or the most desirable one, but it points to the possibility of other applications based on this nonlinear interaction between laser beams of different wavelengths in the transient or steady-state regime. It is also conceivable that one can utilize the orientational effect to achieve infrared-to-visible conversion, as briefly demonstrated also in [28].

V. Conclusion

We have presented a discussion of the theories and experiments on laser-induced optical nonlinearities and some recently observed wave-mixing processes in nematic liquid crystals based on the phase grating induced by two laser pulses. These studies have demonstrated again the unique and interesting physical characteristics of liquid crystals that have attracted the attention of fundamental and applied researchers alike. It is also clear that some practically useful nonlinear optical devices could be constructed. The nematic phase is but one of the several mesophases of liquid crystal that possess these interesting nonlinearities. Cholesterics and smectics [4] and other hybrid forms of nematics [6] also possess large nonlinearities. We anticipate that many more effects will be observed in the near future.

Acknowledgment

The author is grateful to all his co-workers and to Prof. Y. R. Shen of the University of California, Berkeley, for several constructive discussions over the years, and for the use of Fig. 1(c).

References

[1] I. C. Khoo and Y. R. Shen, "Nonlinear optical properties and processes," *Opt. Eng.*, vol. 24, pp. 579–585, 1985.

[2] E. C. Khoo, "Optically induced molecular reorientation and third order nonlinear process in nematic liquid crystals," *Phys. Rev.*, vol. A23, pp. 2077–2081, 1981; see also I. C. Khoo and S. L. Zhuang, "Nonlinear light amplification in a nematic liquid crystal above the Freedericks transition," *Appl. Phys. Lett.*, vol. 37, pp. 3–5, 1980; I. C. Khoo, "Theory of optically induced molecular reorientation and quantitative experiments on wave-mixings and self-focusing of light," *Phys Rev.*, vol. A25, pp. 1636–1644, 1982; I. C. Khoo, "Reexamination of the theory and experimental results of optically induced molecular reorientation and nonlinear diffraction in nematic liquid crystals: spatial frequency and temperature dependence," *Phys. Rev.*, vol. A27, p. 2747, 1983.

[3] S. D. Durbin, S. M. Arakelian, and Y. R. Shen, "Optically induced birefringance and Freedericks transition in nematic liquid crystal," *Phys. Rev. Lett.*, vol. 47, pp. 1411–1415, 1981.

[4] B. Ya Zel'dovich, N. V. Tabiryan, and Yu S. Chilingaryan, *Zh. Eksp. Teor. Fiz.*, vol. 81, p. 72, 1981 (*Sov. Phys. JETP*, vol. 54, pp. 32–36, 1981; N. V. Tabiryan and B. Ya Zel'dovich, "The orientational optical nonlinearity of liquid crystals," *Molec. Cryst. Liq. Cryst.*, vol. 62, pp. 237–250, 1980; N. F. Pilipetskii, A. V. Sukhov, N. V. Tabiryan, and B. Ya Zel'dovich, "The orientational mechanism of nonlinearity and the self-focusing of He–Ne laser radiation in nematic liquid crystal mesophase (theory and experiment)," *Opt. Commun.*, vol. 37, pp. 280–284, 1981; S. R. Galstyan, O. V. Garibyan, N. V. Tabiryan, and Yu S. Chilingaryan, "Light induced Freedericks transition in a liquid crystal," *JETP Lett.*, vol. 33, pp. 437–441, 1981.

[5] R. M. Herman and R. J. Serinko, "Nonlinear optical processes in nematic liquid crystals near a Freedericks transition," *Phys. Rev.*, vol. A19, pp. 1757–1769, 1969.

[6] G. Barbero, F. Simoni, and P. Aiello, "Nonlinear optical reorientation in hybrid aligned nematics," *J. Appl. Phys.*, vol. 55, pp. 304–309, 1984; see also G. Barbero and F. Simoni, *Appl. Phys. Lett.*, vol. 41, p. 504, 1982.

[7] H. L. Ong, "Optically induced Freedericks transition and bistability in a nematic liquid crystal," *Phys. Rev.*, vol. A28, pp. 2393–2407, 1983.

[8] A. S. Zolot'ko, V. F. Kitaeva, N. Kroo, N. N. Sobolev, and L. Chillag, "The effect of an optical field on the nematic phase of the liquid crystal OCBP," *JETP Lett.*, vol. 32, pp. 158–162, 1980; L. Csillag, J. Janossy, V. F. Kitaeva, N. Kroo, and N. N. Sobolev, "The influence of the finite size of the light spot size on the laser induced reorientation of liquid crystals," *Molec. Cryst. Liq. Cryst.*, vol. 84, pp. 125–135, 1982.

[9] Y. G. Fuh, R. F. Code, and G. X. Xu, "Time dependence and diffraction efficiency of optically-induced phase gratings in nematic liquid crystal films," *J. Appl. Phys.*, vol. 54, pp. 6388–6393, 1983.

[10] S. D. Durbin, S. M. Arakelian, and Y. R. Shen, "Strong optical diffraction in a nematic liquid crystal with high nonlinearity," *Opt. Lett.*, vol. 1, pp. 145–149, 1982.

[11] See, for example, E. B. Priestley, P. J. Wojtowicz, and P. Sheng, *Introduction to Liquid Crystals*. New York: Plenum, 1975; see also W. H. de Jeu, *Physical Properties of Liquid Crystalline Materials*. New York: Gordon and Breach, 1980, ch. 4 and references therein.

[12] H. Hsiung, L. P. Shi, and Y. R. Shen, "Transient laser-induced molecular reorientation and laser heating in a nematic liquid crystal," *Phys. Rev.*, vol. A30, pp. 1453–1462, 1984.

[13] I. C. Khoo and R. Normandin, "The mechanism and dynamics of transient thermal grating diffraction in nematic liquid crystal films," *IEEE J. Quantum Electron.*, vol. QE-21, pp. 329–335, 1985; I. C. Khoo and S. Shepard, "Submillisecond grating diffractions in nematic liquid crystal films," *J. Appl. Phys.*, vol. 54, pp. 5491–5494, 1983.

[14] R. G. Horn, "Refractive indices and order parameters of two liquid crystals," *J. Phys.*, vol. 39, pp. 105–109, 1978; W. Urbach, H. Hervet, and F. Rondelez, "Thermal diffusivity measurement in nematic and smectic phases by forced Rayleigh light scattering," *Molec. Cryst. Liq. Cryst.*, vol. 46, pp. 209–221, 1978.

[15] See, for example, H. Eichler and H. Stahl, "Time and frequency behavior of sound waves thermally induced by modulated laser pulses," *J. Appl. Phys.*, vol. 44, pp. 3429–3435, 1973.

[16] K. A. Nelson, R. J. D. Miller, D. R. Lutz, and M. D. Fayer, "Optical generation of tunable ultrasonic waves," *J. Appl. Phys.*, vol. 53, pp. 1144-1149, 1982.

[17] I. C. Khoo and R. Normandin, "Nanosecond laser induced optical wave mixing and ultrasonic wave generation in the nematic phase of liquid crystals," *Opt. Lett.*, vol. 9, pp. 285-287, 1984; see also I. C. Khoo and R. Normandin, "Nanosecond laser induced ultrasonic waves and erasable permanent gratings in smectic liquid crystal," *J. Appl. Phys.*, vol. 55, pp. 1416-1418, 1984.

[18] K. Miyano and J. B. Ketterson, "Ultrasonic study of liquid crystals," *Phys. Rev.*, vol. 12, pp. 615-635, 1975; M. E. Mullen, B. Luthi and M. J. Stephen, "Sound velocity in a nematic liquid crystal," *Phys. Rev. Lett.*, vol. 28, pp. 799-801, 1972.

[19] A. E. Lord, Jr. and M. M. Labes, "Anisotropic ultrasonic properties of a nematic liquid crystal," *Phys. Rev. Lett.*, vol. 25, pp. 570-572, 1970; A. E. Lord, Jr. "Anisotropic ultrasonic properties of a smectic liquid crystal," *Phys. Rev. Lett.*, vol. 29, pp. 1366-1369, 1972.

[20] D. Fekete, J. AuYeung, and A. Yariv, "Phase conjugate reflection by degenerate four-wave mixing in a nematic liquid crystal in the isotropic phase," *Opt. Lett.*, vol. 5, pp. 51-53, 1980; P. Ye, G. Chu, Z. Chang, P. Fu, G. Ji, and X. Lin, "Four-wave mixing and its relaxation effect in liquid crystals," in *Tech. Dig., 11th Int. Quantum Electron. Conf.*, 1980, pp. 638-639; G. K. L. Wong and Y. R. Shen, "Optical-field-induced ordering in the isotropic phase of a nematic liquid crystal," *Phys. Rev. Lett.*, vol. 30, pp. 895-897; see also C. Flytzanis and Y. R. Shen, "Molecular theory of orientational fluctuations and optical Kerr effect in the isotropic phase of a liquid crystal," *Phys. Rev. Lett.*, vol. 33, pp. 14-17, 1974.

[21] O. V. Garikyan, I. N. Kompanets, A. V. Parfyonov, N. F. Pilipetsky, V. V. Sukunov, A. N. Sudarkin, A. V. Sukhov, N. V. Tabiryan, A. A. Vasiliev, and B. Ya Zel'dovich, "Optical phase conjunction by microwatt power of reference waves via liquid crystal light valve," *Opt. Commun.*, vol. 38, pp. 67-70, 1981.

[22] I. C. Khoo and S. L. Zhuang, "Wave front conjugation in nematic liquid crystal films," *IEEE J. Quantum Electron.*, vol. QE-18, pp. 246-248, 1981.

[23] E. N. Leith, H. Chen, Y. Cheng, G. Swanson, and I. C. Khoo, "Phase conjugation with light of reduced spatial coherence," in *Proc. 5th Rochester Conf. Coherence and Quantum Opt.*, Rochester, NY, June 1983.

[24] See, for example, B. Fischer, M. Cronin-Golomb, J. O. White, and A. Yariv, "Amplified reflection, transmission and self-oscillation in real-time holography," *Opt. Lett.*, vol. 6, pp. 519-521, and references therein.

[25] H. Rajbenbach and J. P. Huignard, "Self induced coherent oscillations with photorefractive $Bi_{12}SiO_{20}$ amplifier," *Opt. Lett.*, vol. 10, pp. 137-139, 1985; J. Feinberg and R. W. Hellwarth, "Phase-conjugating mirror with continuous-wave gain," *Opt. Lett.*, vol. 5, pp. 519-521, 1980.

[26] I. C. Khoo, "Wavefront conjugation with gain and self-oscillation with a nematic liquid crystal film," *Appl. Phys. Lett.*, vol. 47, pp. 908-910, 1985; I. C. Khoo and S. L. Zhuang, "Nonlinear light amplification in a nematic liquid crystal above the Freedericks transition," *Appl. Phys. Lett.*, vol. 37, pp. 3-5, 1980.

[27] G. Martin and R. W. Hellwarth, "Infra-red to optical image conversion by Bragg reflection from thermally induced index gratings," *Appl. Phys. Lett.*, vol. 34, pp. 371-373, 1979.

[28] I. C. Khoo and R. Normandin, "Infra-red to visible image conversion capability of nematic liquid crystal film," *Appl. Phys. Lett.*, vol. 47, pp. 350-352, 1985.

Iam-Choon Khoo ([redacted]). He received the B.S. degree in physics with first class honors from the University of Malaya, Malaysia, in 1971, and the M.A. and Ph.D. degrees in physics from the University of Rochester, Rochester, NY, in 1973 and 1976, respectively.

He has held postdoctoral and research associate positions at Ames Laboratory, Iowa State University of Science and Technology, Ames, IA, the University of Southern California, Los Angeles, CA, and the University of Toronto, Ont., Canada. He then joined the Physics Department at Wayne State University, Detroit, MI, in 1979 as an Assistant Professor, becoming an Associate Professor in 1983. In 1984, he joined the faculty at The Pennsylvania State University, University Park, PA, as an Associate Professor with the Department of Electrical Engineering. His current research interests are in theoretical and experimental nonlinear optical processes, optical wave mixing, wavefront conjugation, optical bistability, and switching in liquid crystalline materials. He has published about 100 journal articles and conference proceedings.

Dr. Khoo is a member of the Optical Society of America, the American Physical Society, and the Society for Photo-Optical Instrumentation Engineers.

Reprinted from Optics Letters, Vol. 11, page 227, April, 1986.

Passive optical self-limiter using laser-induced axially asymmetric and symmetric transverse self-phase modulations in nematic liquid crystals

I. C. Khoo, G. M. Finn, R. R. Michael, and T. H. Liu

Department of Electrical Engineering, Pennsylvania State University, University Park, Pennsylvania 16802

Received October 11, 1985; accepted January 15, 1986

Using low-power cw lasers in conjunction with the symmetric and asymmetric nonlinear transverse self-phase modulation imparted by a nematic liquid-crystal film, we have demonstrated two forms of transverse intensity-switching and power-limiting operations. Applications to high-power nanosecond laser are also feasible.

The passage of a laser beam through a nonlinear medium is accompanied by interesting transverse optical intensity-redistribution phenomena, such as self-focusing, defocusing, ring formation, and beam breakup.[1] These processes have found applications in some optical devices,[2–4] among them the so-called passive optical limiter.[5]

We report the experimental observation of two forms of optical intensity-switching processes associated with a transverse self-phase-modulation effect in a nematic liquid crystal first observed by Zolotko *et al.* and Durbin *et al.*[6] In one case, the whole incident beam is involved, creating what we call a transversely symmetric self-phase modulation (SSPM). By imposing an asymmetry on the incident laser beam (e.g., by half blocking it), an asymmetric self-phase-modulation (ASPM) effect is induced.

Figure 1 is a schematic of the experimental setup used. The laser used is a cw linearly polarized Ar^+ laser (0.5145-μm line). The liquid crystal used is a homeotropically aligned (cf. Fig. 2) (pentylcyanobiphenyl) (PCB) film. The configuration of the director axis $\hat{n}$, the optical electric field $\mathbf{E}_{op}$, and the propagation wave vector $\mathbf{k}$ is such that large reorientational nonlinearity is induced.[7] The laser-induced reorientation dielectric-constant change $\delta\epsilon(r)$ is given by[7]

$$\delta\epsilon(r) \sim \frac{\Delta\epsilon\pi^2}{4}\frac{I_{op}(r)}{I_F}\sin^2 2\beta, \qquad (1)$$

where I_F is the optical Freedericksz intensity[7] [$I_F = (nc\pi^2K/2\Delta\epsilon d^2)$]; $\Delta\epsilon$ is the optical dielectric anisotropy ($\Delta\epsilon = \epsilon_{11} - \epsilon_\perp$, where ϵ_{11} and $\epsilon_\perp$ are the optical dielectric constant for field polarization parallel to and perpendicular to the director axis, respectively); K is the elastic constant; and d is the thickness of the sample.

In terms of the refractive-index change δn, we have

$$\delta n(r) = n_2 I(r) = (\Delta\epsilon\pi^2/4nI_F)\sin^2 2\beta I_{op}(r). \qquad (2)$$

If the incident laser beam is half blocked (e.g., beginning in the positive x direction), then, roughly, these two expressions will be multiplied by a step function $\theta(x)$ [$\theta(x) = 0$, $x < 0$; $\theta(x) = 1$, $x > 0$]. The liquid-crystal film has a thickness of 75 μm. In this case, the effect of the transverse nonlinearity is to impart an intensity-dependent phase shift on the laser beam. This phase shift leads to external self-focusing (and the associated change in the laser-beam divergence) in the case of SSPM or to self-deflection in the case of ASPM.

For a given radially symmetric incident optical electric-field distribution at the plane of the nonlinear film, $I_0(r, 0)$, the transmitted field at a distance z, $E(r, z)$, is simply given by the usual diffraction integral,[3]

$$I(r, z) = \left(\frac{2\pi}{\lambda z}\right)^2\left|\int_0^\infty \sqrt{I_0(r)}\,dr r J_0(2\pi r r_0/\lambda z) \times \exp\left\{-ik\left[\frac{r^2}{2z} + \frac{r^2}{2R} + \delta n(r)d\right]\right\}\right|^2;$$

where $\sqrt{I_0(r)}$ is the incident electric-field amplitude, R is the radius of curvature, d is the thickness of the nonlinear thin film, and λ is the wavelength of the laser.

Obviously, the intensity distribution $I(r, z)$ depends on several parameters. Most importantly, if the input laser beam is Gaussian [i.e., if $I_0(r, 0) \sim I_0 \exp -2r^2/w_0^2$, where w_0 is the beam waist], then the far-field intensity distribution in the case of SSPM will yield

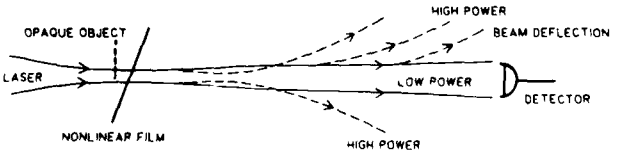

Fig. 1. Schematic of the experimental setup for symmetric and asymmetric (with the use of the opaque object to half block the laser) self-phase-modulation effect. Symmetric self-phase modulation gives rise to self-focusing and divergence of the laser at the detector plane at high power, as shown by the dashed lines. Also shown by dashed lines is the self-bending effect associated with asymmetric self-phase modulation.

0146-9592/86/040227-03$2.00/0

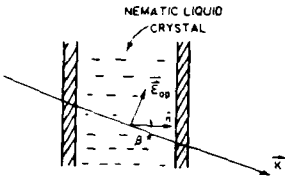

Fig. 2. Optical propagation in a homeotropic nematic crystal film.

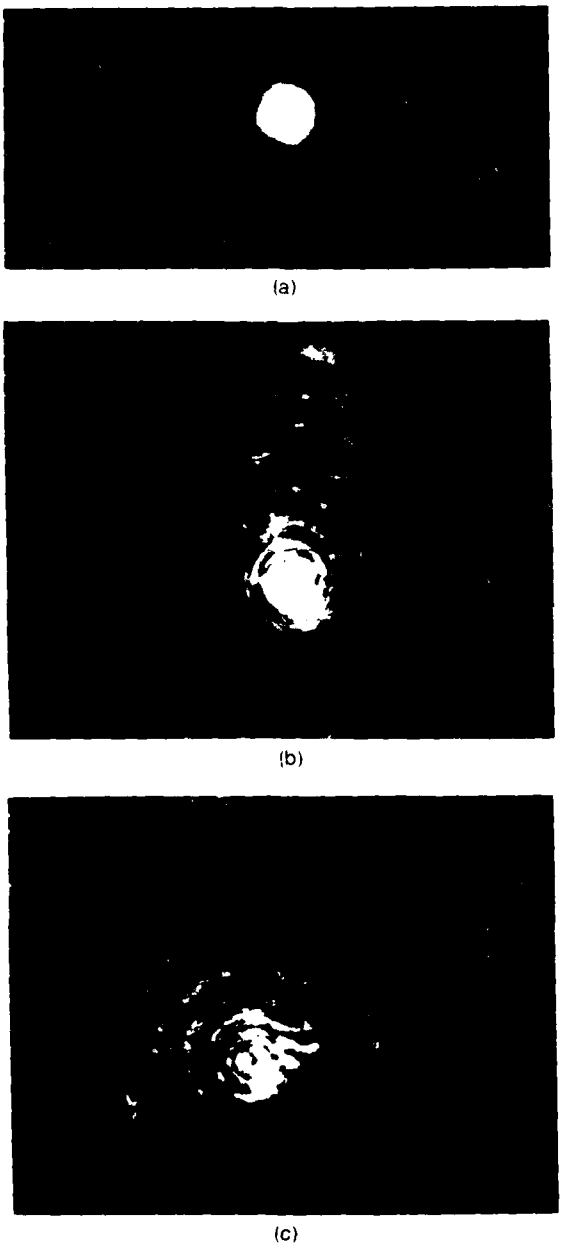

Fig. 3. (a) Photograph of the laser at the detector plane at low power. (b) Photograph of the laser at higher power showing ring formation and increased divergence for the case when the incident laser has a positive radius of curvature. The central portion remains bright for the full laser-power range. (c) Photograph of the laser at the detector plane at high power for the case when the incident laser has a negative radius of curvature. The central portion tends to be dark for the entire power range.

interference rings at high input intensity. Moreover, the divergence of the beam will also change drastically. This is observed in our experiment and in other studies.[3,6] In the case of ASPM, the asymmetry in the self-phase modulation (in the x direction for the present case) gives rise to self-bending of the beam besides the other effects associated with SSPM mentioned above.

The photograph in Fig. 3(a) is that of the laser beam (detected at a plane located 7 m from the sample) at low power, where there is no appreciable self-phase-modulation effect. At high intensity ($\sim$100 W/cm^2), both diffraction rings and a drastic increase in the divergence of the laser are observed [cf. Figs. 3(b) and 3(c)].

As the sample is moved around the focal plane of the lens L_1 (i.e., the radius of curvature R of the wave front changes in sign as well as in magnitude), the intensity distribution at the detector plane varies considerably.[7] Figure 3(b) is typical of the intensity distribution if the sample is located just beyond the focal plane of L_1, i.e., if R is positive.

The central portion, i.e., the on-axis part of the beam, has a small region of brightness that seems to persist at all input intensities. On the other hand, Fig. 3(c) is typical of the intensity distribution if the sample is located before the focal plane of L_1. The central region is dark at high-input laser intensity. These are obviously diffraction effects, coupled with the nonlinear transverse phase shift.

As a result of the drastic increase in the divergence of the beam at the detector plane, the detected power (the so-called output) versus the input laser power will deviate from linear, tending to a so-called "*limiting*" form. This is indeed observed, as is shown in Fig. 4. The detector collects almost all the transmitted laser beam, at low power. But at higher intensity, the output shows limiting behavior even as the input is increased by almost 10 times.

In the case of ASPM, similar ring formation and laser-divergence change are observed, with an additional effect that the whole beam bends toward the negative X direction.[9] Figures 5(a) and 5(b) show such a deflection effect. The beam moves by a displacement of roughly twice the laser-beam waist at the observation plane. The experimentally observed deflection angle is found to be 0.03 rad. Using Eq. (2), one can estimate this deflection angle. For the liquid

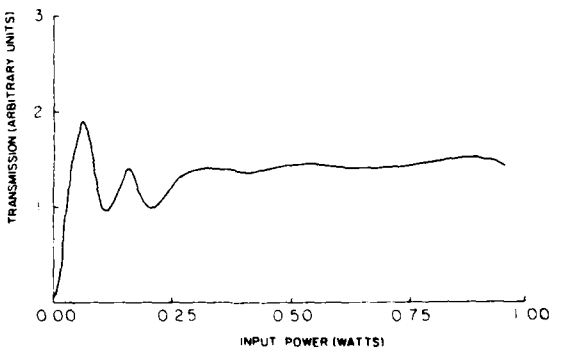

Fig. 4. Plot of the detector power versus the incident laser power showing power-limiting effect.

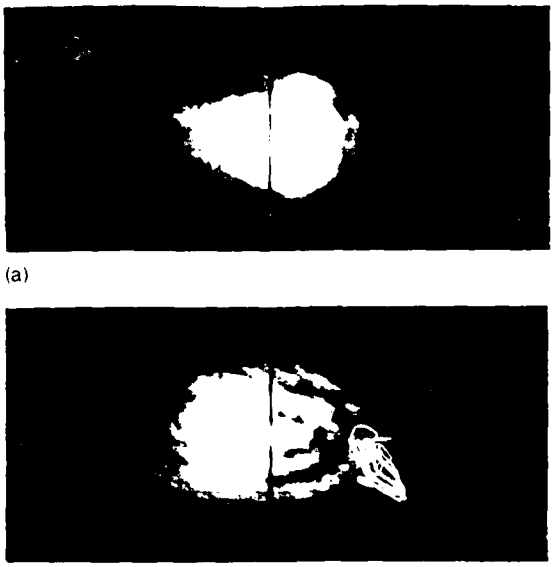

(a)

(b)

Fig. 5. (a) Photograph of the laser spot on the observation plane at low power. Black line at center is for reference purpose. (b) Same as in (a), but at high power. The beam deflects by a displacement of about twice the laser-beam waist.

Fig. 6. Photograph of the increased divergence and ring formation due to nanosecond laser-induced self-phase modulation.

crystal used in the deflection experiment, the thickness $d = 100\ \mu m$ and $\beta = 15°$, I_F is about 500 W/cm^2 (using $\Delta\epsilon = 0.8$, $\epsilon \sim 2.25$, $K = 0.8 \times 10^{-6}$ dyn). The optical intensity used is 100 W/cm^2. From Eq. (2), then, we get $\delta n(r = 0) \simeq 0.06$. The half-block laser has a radius of about 0.05 cm. The refractive-index coefficient is therefore about 0.06–0.05 $\sim$ 1.2 cm^{-1}. The deflection angle θ associated with this index coefficient is therefore given by $\theta \sim 0.07$ rad. This is close to the experimentally observed value in view of several factors of unity overestimation in the theory.

Molecular reorientation in nematics can also be induced by high-power nanosecond lasers. Hsiung *et al.*[10] had shown that a homeotropic nematic liquid crystal will be reoriented by a normally incident nanosecond laser pulse, provided that a strong dc bias magnetic field is present, in analogy to the cw case.[7] In our experiment, the nanosecond laser pulse (Q-switched Nd:YAG second harmonic; 20-nsec duration; 10 mJ; 1-mm^2 beam size) is incident at an nonnormal angle as in Fig. 2. In this case, molecular reorientation will occur *without a bias field*, in analogy again to the cw case.[7] Furthermore, we use a nematic liquid crystal (EM chemicals EK46) at a temperature far below the nematic → isotropic point to minimize the thermal contribution. External self-focusing effect and also the formation of ring structures associated with SSPM are observed. Figure 6 is a photograph of the transmitted (single-shot) laser pulse. A coincident cw He–Ne laser also shows similar far-field diffraction effects that collapse back to the original laser-beam profile in about 4 or 5 sec, which is the orientational relaxation time characteristic of the 75-μm sample used.[7] An output-versus-input plot also shows power-limiting behavior similar to that shown in Fig. 3.

This research is supported in part by grant ECS 8415387 from the National Science Foundation and grant 840375 from the U.S. Air Force Office of Scientific Research. Some helpful discussions with A. E. Kaplan on laser self-bending effect are also acknowledged.

References

1. See, for example, J. F. Reintjes, *Nonlinear Optical Parametric Processes in Liquids and Gases* (Academic, New York, 1984), Chap. 5 and references therein.
2. J. E. Bjorkholm, P. W. Smith, W. J. Tomlinson, and A. E. Kaplan, Opt. Lett. **6**, 345 (1981).
3. I. C. Khoo, Appl. Phys. Lett. **41**, 909 (1982); I. C. Khoo, T. H. Liu, P. Y. Yan, S. Shepard, and J. Y. Hou, Phys. Rev. A **29**, 2756 (1984).
4. K. Tai, H. M. Gibbs, N. Peyghambarian, and A. Mysyrowicz, Opt. Lett. **10**, 220 (1985).
5. M. F. Soileau, W. E. Williams, and E. W. Van Stryland, IEEE J. Quantum Electron. **19**, 731 (1983); T. F. Boggess, Jr., A. L. Smith, S. C. Moss, I. W. Boyd, and E. W. Van Stryland, IEEE J. Quantum Electron. **QE-21**, 488 (1985); J. A. Hermann, J. Opt. Soc. Am. A **1**, 729 (1984), and references therein.
6. A. S. Zolotko, V. F. Kitaeva, N. Kroo, N. N. Sobolev, and L. Chillag, JETP Lett. **32**, 158 (1980); S. D. Durbin, S. M. Arakelian, and Y. R. Shen, Opt. Lett. **6**, 411 (1981).
7. I. C. Khoo, Phys. Rev. A **23**, 1636 (1981); **25**, 1636 (1982); **26**, 1131 (1983); **27**, 2747 (1983); see also I. C. Khoo and Y. R. Shen, Opt. Eng. **24**, 579 (1985), and references therein.
8. E. Santamato and Y. R. Shen, Opt. Lett. **9**, 564 (1984).
9. A. E. Kaplan, JETP Lett. **9**, 33 (1969); Opt. Lett. **6**, 360 (1981).
10. H. Hsiung, L. P. Shi, and Y. R. Shen, Phys. Rev. A **30**, 1453 (1984).

J-QE/23/2/11725

Optically-Induced Molecular Reorientation in Nematic Liquid Crystals and Nonlinear Optical Processes in the Nanoseconds Regime

I. C. Khoo
R. R. Michael
P. Y. Yan

Reprinted from: IEEE JOURNAL OF QUANTUM ELECTRONICS, Vol. QE-23, No. 2, FEB. 1987.

Optically-Induced Molecular Reorientation in Nematic Liquid Crystals and Nonlinear Optical Processes in the Nanoseconds Regime

IAM-CHOON KHOO, SENIOR MEMBER, IEEE, R. R. MICHAEL, AND P. Y. YAN

Abstract—**We present a detailed theoretical analysis and experimental study of purely optically-induced nematic axis reorientation and the associated nonlinear optical processes such as self-phase modulations and optical switching. It is shown that under a sufficiently intense laser field (~ 100 MW/cm^2), nematic liquid crystals will respond in the nanosecond regime. Single nanosecond laser pulse self-phase modulation and intensity switching effects are observed. The magnitude and dynamics of the response are in agreement with theoretical expectations. Optical power limiting and switching effects associated with self-phase modulations are also demonstrated.**

I. Introduction

IN ANALOGY to dc field induced effects, optical field induced director axis reorientations in nematic liquid crystal films have given rise to many interesting optical and electro- or magneto-optical effects [1]. The dynamics of the optical process are analogous to the dc (or low frequency ac) field effect [2]; under low optical fields (up to or just above the optical Freedericksz field strength), the response times of the orientation process depends on the characteristic length (e.g., thickness and grating constant) that influences the molecular torque, which in turn affects the rise or fall time. These response times are typically in the range of milliseconds to seconds. Recently, Hsiung *et al.* [3] have investigated these reorientation processes under the combined influence of a strong dc magnetic field and nanosecond lasers. It was demonstrated that the liquid crystals will respond to nanosecond laser pulses. The process is very much in analogy to studies where CW lasers are employed, in conjunction with a strong dc magnetic field (that caused a dc Freedericksz transition in the nematic film [4]).

In this paper, we present a detailed study of the problem where only the optical field is present. In analogy to the CW laser case [5], it is shown that director axis reorientation will occur only under appropriate geometrical conditions. Furthermore, we have calculated explicitly the magnitude of the reorientation and their contribution to the self-phase modulation of a single nanosecond laser pulse through the medium. We have observed very strong self-phase modulation effects induced by nanosecond laser pulses, leading to external self-focusing and far-field diffraction ring formation [6], and the related optical switching and interesting off-axis switching and intensity modulation effects.

Manuscript received May 30, 1986; revised October 3, 1986. This work was supported in part by the National Science Foundation under Grant ECS8415387 and by the Air Force Office of Scientific Research under Contract AFOSR840375.

The authors are with the Department of Electrical Engineering, The Pennsylvania State University, University Park, PA 16802.

IEEE Log Number 8611725.

II. Theoretical Consideration

A. Dynamics

The dynamics of the reorientation of the nematic director axis is described by the torque balance between the torques created by the optical field on the liquid crystal and the elastic forces between the molecules. Consider a plane polarized beam incident on a homeotropically aligned nematic liquid crystal film, as shown in Fig. 1. Ignoring flow and the inertia effect, the equation of motion following the Ericksen-Leslie approach [7] is given by

$$\gamma \frac{\partial \theta}{\partial t} = K \frac{\partial^2 \theta}{\partial z^2} + \frac{\Delta \epsilon E_{op}^2}{8\pi} \sin (2\beta + 2\theta). \qquad (1)$$

In deriving (1), we have made the one-constant approximation (i.e., the three elastic constants for bend, splay, and twist are assumed to be given by K). This assumption is even better when β and θ are small, which is usually the case in the nonlinear optical processes we are considering. Because of the large birefringence of the liquid crystal, a small change θ (-10^{-2} to 10^{-3}) is sufficient to cause a very large nonlinear effect. In (1), γ is the viscosity constant, $\Delta\epsilon$ the optical dielectric anisotropy, and E_{op} the optical electric field.

Under the so-called hard boundary condition $\theta_{Z=0} = \theta_{Z=d} = 0$, $\theta(Z, t)$ to the first approximation is a simple sine wave

$$\theta(Z, t) = T(t) \sin \left(\frac{\pi}{d} Z \right) \qquad (2)$$

where the initial condition on $T(t)$ is $T(t)/_{t=0} = 0$.

Substituting (2) into (1) and integrating both sides of the equation with respect to z from $z = 0$ to $z = d$ yields

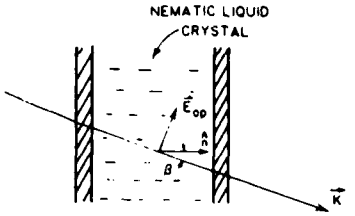

Fig. 1. Schematic of a linearly polarized laser beam propagating through a homeotropically aligned nematic liqud crystal film.

$$\frac{dT}{dt} = \left(\frac{2bK}{\gamma}\cos 2\beta - \frac{\pi^2 K}{d^2\gamma}\right) T - \left(\frac{16Kb}{3\pi\gamma}\sin 2\beta\right) \cdot T^2 + \frac{4bK}{\pi\gamma}\sin 2\beta \tag{3}$$

where we have used the expansion $\sin(2\beta + 2\theta) \simeq \sin 2\beta - 2(\sin 2\beta)\theta^2 + 2(\cos 2\beta)\theta$ for small θ.

In (3), $b = \Delta\epsilon E_{op}^2/8\pi K$. Using the following definitions

$$A = \frac{2bK}{\gamma}\cos 2\beta - \frac{\pi^2 K}{d^2\gamma}$$

$$B = \frac{16Kb}{3\pi\gamma}\sin 2\beta$$

$$C = \frac{4bK}{\pi\gamma}\sin 2\beta. \tag{4}$$

Equation (3) can be integrated to give

$$\int \frac{dT}{T - \frac{B}{A}T^2 + \frac{C}{A}} = \int A\,dt = \frac{\Delta\epsilon}{4\pi\gamma}\cos^2\beta \int_{-\infty}^{t} E_{op}^2(t')\,dt'. \tag{5}$$

For simplicity, we shall assume that the laser pulse is a square pulse described by: $E_{op} = 0$, $t < 0$; $E_{op}(t) = E_{op}$, $0 \le t \le T_p$ where T_p is the pulse duration. In that case, we obtain that

(i) $0 \le t \le T_p$

$$T(t) = \frac{A}{B}\left[\frac{\frac{1}{2} + D\left[\left((D - \frac{1}{2})/(D + \frac{1}{2})\right) e^{2ADt} - 1\right]}{\left[1 + \left((D - \frac{1}{2})/(D + \frac{1}{2})\right) e^{2ADt}\right]}\right] \tag{6}$$

where

$$D = \sqrt{\tfrac{1}{4} + BC/A^2}. \tag{7}$$

For our calculation of $T(t)$ [and therefore $\theta(t)$] to be valid, we require that e^{2ADt} be much smaller than unity, i.e., the growth of $T(t)$ in the small-signal regime is linear in t. This allows us to identify a so-called risetime τ_{rise} given by

$$\tau_{rise} = (2AD)^{-1}. \tag{8}$$

In explicit form, using (7) and (4), τ_{rise} becomes

$$\tau_{rise} = \frac{\gamma/k}{\left(f(E_{op}, \beta) - \frac{\pi^2}{d^2}\right)\sqrt{1 + g(E_{op}, \beta)/\left(f^2(E_{op}, \beta) - \frac{\pi^2}{d^2}\right)^2}} \tag{9}$$

where

$$f(E_{op}, \beta) = \frac{\Delta\epsilon E_{op}^2}{4\pi K}\cos 2\beta \tag{10}$$

and

$$g(E_{op}, \beta) = \frac{4\Delta^2\epsilon E_{op}^4}{3\pi^4 K^2}\sin^2 2\beta. \tag{11}$$

Notice that this expression for τ_{rise} yields a risetime for normal incidence

$$(\beta = 0),\ \tau_{rise}(\beta = 0) = \frac{\gamma/K}{\frac{\Delta\epsilon E_{op}^2}{4\pi K} - \pi^2/d^2}$$

that is in agreement with previous calculations.

The magnitude of θ, and the risetime τ_{rise}, depends on the optical field intensity (E_{op}^2) besides other parameters ($\Delta\epsilon$, K, d and γ). We can separate the response into two distinct cases:

1) $E_{op}^2 << E_{th}^2$, and 2) $E_{op}^2 >> E_{th}^2$, where E_{th} is the optical Freedericksz transition field ($E_{th}^2 = 4\pi^3 K \cdot \Delta\epsilon^{-1} d^{-2}$).

Case 1): For $E_{op}^2 << E_{th}^2$

$$\tau_{rise} = -\frac{1}{2AD} \cong -\frac{1}{2A} \approx \frac{\gamma}{K\left(\frac{\pi^2}{d^2} - \frac{\Delta\epsilon E_{op}^2\cos^2\beta}{4\pi K}\right)} \cong \frac{\gamma d^2}{K\pi^2}. \tag{12}$$

For typical nematic parameters, $\gamma \sim 0.1$ poise, $d \sim 100$ μm and $K \sim 10^{-7}$ dynes, one gets $\tau_{rise} \approx 7$ s.

In order to have significant nematic reorientation in a short time scale (e.g., as induced by a nanosecond laser pulse) it is obvious that an optical field much larger than the Freedericksz threshold is needed. Consider therefore the other case:

Case 2): In this case, $E_{op}^2 >> E_{th}^2$,

$$\tau_{rise} = \frac{1}{2AD} \approx \frac{\gamma}{\frac{\Delta\epsilon E_{op}^2}{4\pi}\cos 2\beta}. \tag{13}$$

The disappearance of the elastic constant K from this

expression reflects the fact that in this high-field regime, the dynamics of the reorientation is decided by the torque balance between the viscous force (characterized by the viscosity coefficient γ) and the optical field; the torque from the boundary plates (characterized by K and d) is negligible in comparison to the optical field.

For typical values of $\gamma \sim 0.1$ poise, $\Delta\epsilon \sim 0.6$ (in the case of PCB (pentyl-cyano-biphenyl)), an optical field $E_{op} = 10^4$ statV/cm will give a response time $\tau_{rise} \approx 20$ ns.

In the short pulse regime, even though the optical electric field is much larger than the Freedericksz field, the induced reorientation angle θ (for typical value of E_{op} used in the experiment) is quite small. This may be seen from (7). Using the expansion $e^{2ADT} \approx 1 + 2ADt$, and $D \sim \frac{1}{2}(1 + 2BC/S^2)$ for $4BC/A^2 << 1$ (i.e., $\beta < 1$), we obtain

$$T(t) \sim \frac{3\Delta\epsilon}{4\pi^2\gamma} \sin 2\beta \int_{-\infty}^{t} E_{op}^2(t')\, dt'. \tag{14}$$

The maximum reorientation angle (at $z = d/2$ and for $t = T_p$), is therefore

$$\theta_{max} = \frac{3}{4}\frac{\delta\epsilon}{\pi^2\gamma} \sin 2\beta\, E_{op}^2 T_p. \tag{15}$$

An interesting point about θ_{max} is that it is independent of the elastic constant K and the film thickness d, but depends on the angle β between the director axis and the optical propagation vector. In this sense, one may say that nematics under the nanosecond laser pulse excitation have lost some of their liquid crystal characteristics [i.e., no dependence on K or d in (15)], yet they still retain the correlated nature as reflected in the dependence on the angle β characterized by the director axis direction. For an optical intensity of 10^2 MW/cm^2 ($E_{op} = 10^3$ statV/cm), $T_p = 20$ ns, $\Delta\epsilon = 0.6$, and $\gamma \sim 0.1$ poise, $\theta_{max} \approx 1.2 \times 10^{-2}$ rad.

The fall of the reorientation process is obtainable in a trivial way from (1) by setting $E_{op} = 0$ and using θ from (2). One gets

$$\tau_{fall} = \frac{\gamma}{K(\pi^2/d^2)} \tag{16}$$

which is on the order of 10^2 ms as we estimated earlier (see (12) and the discussion that follows).

B. Transverse Self-Phase Modulation

In the preceding discussion, the optical field is assumed to be an infinite plane wave. We now consider a more realistic case where the laser transverse profile is Gaussian, i.e.,

$$E_{op}^2 \to E_{op}^2(r) = E_o\, e^{-2r^2/w_0^2}$$

where w_0 is the beam waist.

For a given reorientation $\theta(t)$, there is an accompanying change in the refractive index $\Delta n(\theta)$ given by

$$\Delta n(t, z; r) = n(\beta + \theta(t, z; r)) - n(\beta) \tag{17}$$

where the refractive index for the extraordinary ray is given by

$$n(\beta + \theta) = \frac{n_\perp n_{11}}{\sqrt{n_\perp^2 \sin^2(\beta + \theta) + n_{11}^2 \cos^2(\beta + \theta)}}. \tag{18}$$

For $\theta << 1$, we get

$$\Delta n(t, z, r) = \frac{\Delta\epsilon n_\perp^3}{2\epsilon_{11}\epsilon_\perp} \sin 2\beta \cdot \theta(t, z, r). \tag{19}$$

Correspondingly, the laser acquires a transverse phase shift $\Delta\phi(r, t)$ given by

$$\Delta\phi(r, t) = \frac{2\pi}{\lambda} \int_0^d \Delta n(t, z, r)\, dz. \tag{20}$$

Using (19) and (14), we get

$$\Delta\phi(r, t) = \frac{3d}{4\gamma}\frac{\Delta\epsilon^2 n_0^3}{\epsilon_{11}\epsilon_\perp \pi^2\gamma} \sin^2 2\beta \int_{-\infty}^{t} E_{op}^2(r, t')\, dt'. \tag{21}$$

Given the phase shift in (21), the intensity distribution of the transmitted laser at a distance z from the thin film is given by [8]

$$I(r', z, t) = \left(\frac{2\pi}{\lambda z}\right)^2 I_0 \left| \int_0^\infty e^{-r^2/w_0^2} r\, dr\, J_0(2\pi r r'/\lambda z) \cdot \exp\left[-ik\left(\frac{r^2}{2z} + \frac{r^2}{2R}\right) + i\Delta\phi(r, t)\right]\right|^2 \tag{22}$$

where w_0 is the spot size and R the radius of curvature of the wave front of the incident laser. r' is the transverse coordinate at z from the film.

In the case of CW laser illuminations, as has been shown by various groups [6], the resultant steady-state intensity distribution will exhibit interference rings, self-focusing, and divergence changes, etc. In the time-dependent case, the transmitted laser pulse will experience a time-dependent divergence change, progressively forming larger numbers of interference rings. The intensity distribution is obviously a function of several parameters, the most important of which are the incident laser beam waist w_0, the radius of curvature of the wavefront and the nonlinear time dependent phase shift. These detailed dependences have been analyzed before [9] in conjunction with our study of transverse bistability and in a recent detailed time-dependent calculation of the transmitted intensity distribution using (22) above [10]. The calculations for various ranges in values of these parameters are too detailed to be included here. As an example, we note here a specific case where the film is situated just beyond the focal spot of the incident laser beam (i.e., the radius of curvature of the incident laser is positive). As shown in Fig. 2, the transmitted intensity distribution as a func-

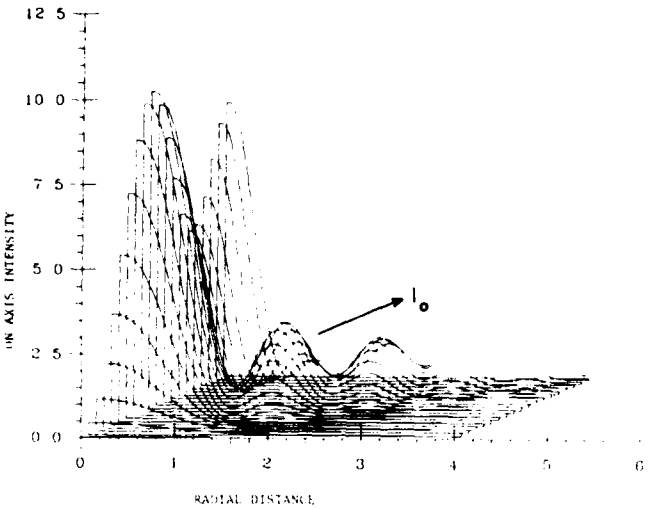

Fig. 2. The theoretically calculated radial dependence of the transmitted beam intensities as a function of the input intensities. As the input intensity is increased the laser beam diverges and interference sideband rings occur.

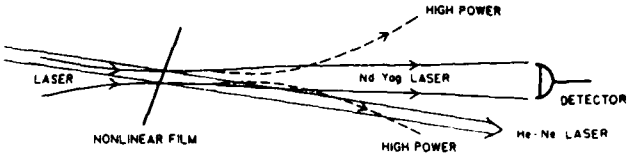

Fig. 3. Schematic of the experimental setup to observe self-phase modulation effect associated with molecular reorientation in a nematic film. The He-Ne laser is almost collinear with the Nd:Yag laser and both lasers are linearly polarized.

Fig. 4. Photograph of the transmitted far-field intensity of the Nd:Yag laser at high power showing an increase in divergence and the formation of sideband rings. The asymmetry in the ring system is due to input laser azimuthal asymmetry.

tion of time (or laser intensity) evolves from a single Gaussian to a much diverged beam with interference sideband rings. This is indeed observed experimentally.

III. Experiment and Results

Fig. 3 schematically depicts our experimental setup. A Q-switched linearly polarized 20 ns Nd:Yag second harmonic pulse (0.53 μm) is lightly focused (spot size = [0.5 mm]^2) on the nematic film. We have experimented with two kinds of nematic liquid crystals, PCB and EM chemicals E46 (which has a nematic range from -9.5 to 88°C, and has a small thermal effect). The liquid crystals are homeotropically aligned and 75 μm in thickness and kept at 22°C. The angle β between the laser propagation and the director axis (c.f., Fig. 1) is varied from 0 to about 22°. A pinhole is situated about 4 m downstream, and in conjunction with a fast photodiode, monitors either the on-axis or the off-axis intensity. An almost coincident linearly polarized He-Ne is used to monitor the Nd:Yag laser pulse-induced lensing effect. The energies in the laser pulses are varied up to about 6 mj, at which point the sample shows signs of permanent damage (decomposition).

For both samples, the observed self-phase modulation effect as a function of β, dynamics, etc. are very similar. The discussion that follows pertains to our experiment with PCB cells.

Reorientational effects are not observable for $\beta = 0$, but are easily observable for $\beta > 0$ ($\beta \approx 22°$). The reorientation effect is manifested in the increased divergence of the transmitted laser beam as well as the formation of rings (c.f., Fig. 4), and is easily monitored with the He-Ne laser after each Nd:Yag pulse. Typically, the He-Ne laser will exhibit an "instantaneous" divergence change and rings (similar to Fig. 4), which collapse back to the original beam in about 4 s. For the experimental geometries ($w_0 \approx 0.5$ mm, $d = 75$ μm), the orientational relaxation time is estimated to be about 4 s, which is in excellent agreement with the experimental observation.

As β is decreased from a value of 22° towards 0; the divergence effects gradually disappeared. This dependence on β is in accordance with the theory and is similar to the reorientational effect induced by low-power lasers. For $\beta = 0$, and at a *much higher laser intensity* (laser pulse energy $\gtrsim 5$ mj), thermal effect associated with the change in the ordinary refractive index n_0 with laser heating (i.e., dn/dt) sets in, and is manifested also in a divergence change. The dynamics of such effect, as monitored by the He-Ne laser, is very different from the reorientational case (as has been noted in recent studies [3], [11]). The He-Ne laser exhibits a relaxation time (the collapsing back of the diverged beam to the original beam profile) in a few milliseconds. From our previous study [11] of thermal diffusion in PCB, the characteristic thermal decay time is in our present case governed by the thickness of the film (75 μm) which is much smaller than the laser beam waist (0.5 mm). Hence, the thermal diffusion process is predominantly a one-dimensional process towards the cell walls from the nematics. The characteristic time is therefore given by

$$\tau \sim (d^2/4\pi^2 D)$$

where D is the diffusion constant [12]. Using $D \sim 7.9 \times 10^{-4}$ cm^2/s^{-1}, $d = 7.5 \times 10^{-3}$ cm, we get $\tau \sim 1.8$ ms, which is in accordance with the experimental observation.

The increase in divergence due to the thermal effect (at $\beta = 0$) is also observed to be much less than the diver-

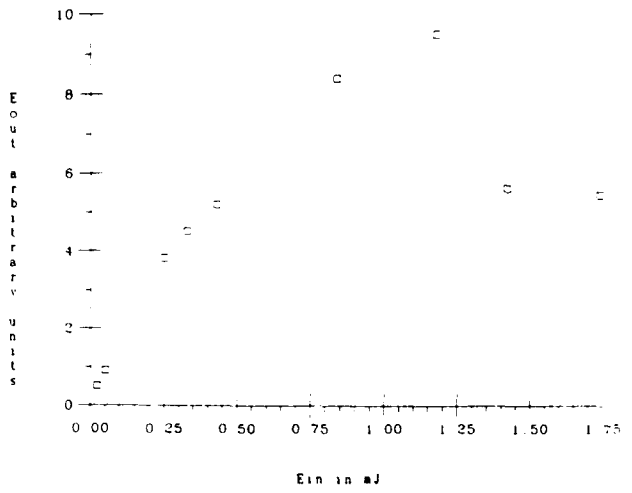

(a)

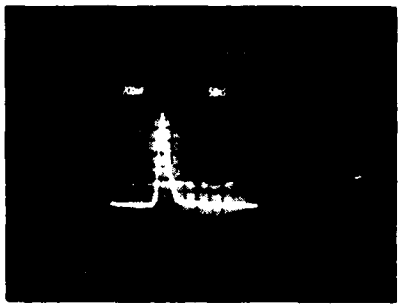

(b)

(c)

Fig. 5. (a) Experimentally observed on-axis detected laser energy as a function of input laser energy showing enhancement of the on-axis power due to external self-focusing effect, the occurrence of a dip in the intensity and power-limiting behavior at higher input powers. (b) Oscilloscope trace of the transmitted laser pulse at $\beta = 0$ (laser pulse energy ~ 1 mJ). (c) Oscilloscope trace of the transmitted laser pulse at $\beta = 22°$ (laser pulse energy ~ 1 mJ).

gence associated with the reorientational effect at $\beta = 22°$. In the former case, the divergence change is about two to three times the laser original divergence (with hardly any ring). On the other hand, in the latter case, the induced divergence (even at a smaller laser intensity) is about ten times larger, accompanied by many side interference rings (typically more than four or five rings are observed, c.f., Fig. 4 of the transmitted Nd:Yag pulse). A corresponding number of rings are observed in the transmitted He–Ne laser.

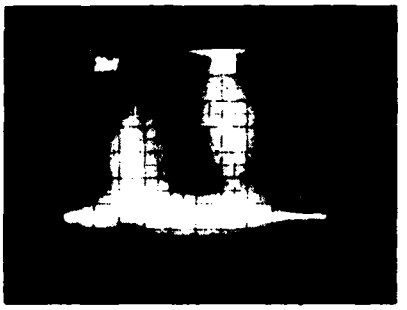

Fig. 6. Oscilloscope trace of the power detected on an off-axis location showing an initial switch on (due to the increased divergence of the laser) followed by oscillations due to the interference rings moving out from the central region. The total detected power includes some (side-scattering) background contribution from the input laser, which explains why the oscillation modulation is not unity. (Horizontal time scale is 50 ns/division.)

Fig. 5 is the on-axis power (versus the input laser power) as monitored by the detector. It shows a remarkable resemblance (which is expected) to that observed with CW laser. As the self-focusing effect intensifies, the transmitted beam experiences a secondary focusing effect, leading to enhanced divergence at the detector plane, and a corresponding decrease in the on-axis power. This effect has found applications in the construction of passive/optical power limiters [13]. Fig. 5(b) and (c) are oscilloscope traces of the on-axis detected power for two different angles β. For $\beta = 0$, where there is no orientational effect, the output detected pulse is similar to the input laser pulse. On the other hand, when reorientational effect sets in (e.g., for $\beta = 22°$), the detected on-axis pulse is much smaller in amplitude. This region of diminished output versus input behavior occurs at an incident laser energy of > 1 mJ (c.f., Fig. 5).

The switching of the on-axis power to the off-axis location can be more directly monitored with the detector situated at about $3w_0$ from the beam axis. Fig. 6 shows a typical detected pulse when self-focusing and diverging interference rings occur. The small detected nonoscillatory signal comes from background scattering from the nematic films whose time evolution resembles the incident laser pulse.

The later part (after about 10 ns) of the detected off-axis laser pulse, however, shows that the power switched up to a high value, followed by oscillations associated with the diverging rings. About 5 rings are observed, corresponding to about the same number of spatial rings observed on the detector plane. The occurrence of these oscillations is the temporal equivalence of the spectral broadening effects observed in other self-phase modulation studies [14]. In an approximate way [6], one can ascribe a maximum phase shift difference of $2\pi(N)$ between the central maximum intensity point ($r = 0$, $I = I_0$) and the radial wing ($r >> w_0$, $I \sim 0$), where N is an integer. From expression (20), the maximum phase shift can be calculated using the data: E_{op} (1 mJ pulse in 20 ns on (0.5 mm)^2 area) $\approx 3 \times 10^3$ statV/cm (intensity of 2×10^8 W/cm^2). This gives $\theta \simeq 2.4 \times 10^{-1}$ rad, and therefore

a $\Delta n \sim 0.48 \times 10^{-1}$. The corresponding phase shift is 2π (7), i.e., about 7 rings are expected. This is in good agreement with the experiment.

IV. Conclusion

We have presented a study of the theory of purely optical field induced molecular reorientation in a nematic film in the nanosecond regime, as well as experimental results of the self-phase modulation effects associated with the reorientational nonlinearity. In the 10^8 W/cm^2 regime, it is shown that the nematics could respond to nanosecond laser pulses for nonvanishing angle between the laser beam propagation and the director axis. The boundary torques from the cell walls play an insignificant role in the turn on process although the overall highly correlated nature of the nematic phase (as characterized by the director axis direction and the dependence of the nonlinearity on β) still does. We have also experimentally observed self-focusing (in the form of an increased divergence of the far-field transmitted intensity), optical switching, and other self-phase modulation effects. The experimentally observed divergence, spatial rings, response times, and magnitude of the reorientation, etc. are in good agreement with theoretical expectations.

References

[1] See, for example, I. C. Khoo and Y. R. Shen, "Liquid crystals—Nonlinear optical properties and processes," *Opt. Eng.*, vol. 24, pp. 579–785, 1985.

[2] E. B. Priestley, P. J. Wojtowicz, and P. Sheng, *Introduction to Liquid Crystals*. New York: Plenum, 1975.

[3] H. Hsiung, L. P. Shi, and Y. R. Shen, "Transient laser induced molecular reorientation and laser heating in a nematic liquid crystal," *Phys. Rev.*, vol. A30, pp. 1453–1462, 1984.

[4] I. C. Khoo and S. L. Zhuang, "Nonlinear light amplification in a nematic liquid crystal above the Freedericksz transition," *Appl. Phys. Lett.*, vol. 37, pp. 3–5, 1980.

[5] S. D. Durbin, S. M. Arakelian, and Y. R. Shen, "Optically induced birefringence and Freedericksz transition in nematic liquid crystal," *Phys. Rev. Lett.*, vol. 47, pp. 1411–1415, 1981; I. C. Khoo, "Optical induced molecular reorientation and third order nonlinear processes in nematic liquid crystals," *Phys. Rev.*, vol. 23, pp. 2077–2081, 1981; H. L. Ong, "Optically induced Freedericksz transition and bistability in a nematic liquid crystal," *Phys. Rev.*, vol. A28, pp. 2393–2407, 1983.

[6] See, for example, A. S. Zolot'ko, V. F. Kitaeva, N. Kroo, N. N. Sobolev, and L. Chillag, "The effect of an optical field on the nematic phase of the liquid crystal OCBP," *Sov. Phys.-JETP*, vol. 32, pp. 158–162, 1980; E. Santamato and Y. R. Shen, "Field curvature effect on the diffraction ring pattern of a laser beam dressed by spatial self-phase modulation in a nematic film," *Opt. Lett.*, vol. 9, p. 564, 1984 and references therein; N. F. Pilipetski, A. V. Sukhov, N. V. Tabiryan, and B. Y. Zel'dovich, "The orientational mechanism of nonlinearity and the self-focusing of He-Ne laser radiation in nematic liquid crystal mesophase (theory and experiment)," *Opt. Commun.*, vol. 37, pp. 280–284, 1981. See also [9].

[7] P. G. DeGennes, *The Physics of Liquid Crystals*. Oxford, England: Clarendon, 1974.

[8] See, for example, M. Born and E. Wolf, *Principles of Optics*. New York: Pergamon, 1959.

[9] I. C. Khoo, P. Y. Yan, T. H. Liu, S. Shepard, and J. Y. Hou, "Theory and experiment on optical transverse intensity bistability in the transmission through a nonlinear thin (nematic liquid crystal) film," *Phys. Rev.*, vol. A29, p. 2756, 1984; see also P. Y. Yan, M.S. thesis, Wayne State Univ., Detroit, MI, 1983, where the dependence of the spatial rings, self-focusing, etc., are analyzed using (22).

[10] I. C. Khoo, "Laser spot size dependence, nonlocality, and saturation effect in transverse optical bistability," in *Proc. Quebec SPIE Conf. Optic. Chaos*, Invited Paper, 1986, p. 220.

[11] I.-C. Khoo and R. Normandin, "The mechanism and dynamics of transient thermal grating diffraction in nematic liquid crystal films," *IEEE J. Quantum Electron.*, vol. QE-21, pp. 329–335, Apr. 1985; I. C. Khoo and S. Shepard, "Submillisecond grating diffractions in nematic liquid crystal films," *J. Appl. Phys.*, vol. 54, pp. 5491–5494, 1983.

[12] See, for example, W. Urbach, H. Hervet, and F. Rondelez, "Thermal diffusivity measurement in nematic and smectic phases by forced Rayleigh light scattering," *Mol. Cryst. Liq. Cryst.*, vol. 46, pp. 209–221, 1978.

[13] See, for example, M. J. Soileau, W. E. Williams, and E. W. Van Stryland, "Optical power limiter with picosecond response time," *IEEE J. Quantum Electron.*, vol. QE-19, pp. 731–735, Apr. 1983; J. A. Hermann and M. E. Grigg, "Optical power limiting with nonlinear media," *Opt. Commun.*, vol. 49, pp. 367–370, 1984.

[14] See, for example, J. F. Rentjes, *Nonlinear Optical Parametric Processes in Liquids and Gases*. New York: Academic, 1984, ch. 5 and the numerous references therein.

Iam-Choon Khoo ([redacted]). He received the B.S. degree in physics with first class honors from the University of Malaya, Malaysia, in 1971, and the M. A. and Ph.D. degrees in physics from the University of Rochester, Rochester, NY, in 1973 and 1976, respectively.

He has held postdoctoral and research associate positions at Ames Laboratory, Iowa State University of Science and Technology, Ames, IA, the University of Southern California, Los Angeles, CA, and the University of Toronto, Ont., Canada. He then joined the Physics Department at Wayne State University, Detroit, MI, in 1979 as an Assistant Professor, becoming an Associate Professor in 1983. In 1984, he joined the faculty at The Pennsylvania State University, University Park, PA, as an Associate Professor with the Department of Electrical Engineering. His current research interests are in theoretical and experimental nonlinear optical processes, optical wave mixing, wavefront conjugation, optical bistability, and switching in liquid crystalline materials. He has published about 100 journal articles and conference proceedings.

Dr. Khoo is a member of the Optical Society of America, the American Physical Society, and the Society for Photo-Optical Instrumentation Engineers.

R. R. Michael, photograph and biography not available at the time of publication.

P. Y. Yan, photograph and biography not available at the time of publication.

Reprinted from Journal of the Optical Society of America B, Vol. 4, page 115, February 1987

Nonlocal radial dependence of laser-induced molecular reorientation in a nematic liquid crystal: theory and experiment

I. C. Khoo, T. H. Liu, and P. Y. Yan

Department of Electrical Engineering, The Pennsylvania State University, University Park, Pennsylvania 16802

Received June 2, 1986; accepted October 6, 1986

We present a detailed theoretical calculation, with experimental verification, of the nonlocal molecular reorientation of the nematic-liquid-crystal director axis induced by a cw Gaussian laser beam. The natures of the torque balance equations and the solutions are significantly different for normally and nonnormally incident laser beams. The nonlocal effects resulting from molecular correlation effects are particularly important for laser spot sizes that are different (smaller or larger) from the sample thickness. Experimental measurements for the transverse dependence of the molecules and the dependence of the Freedericksz threshold as a function of the laser beam sizes are in excellent agreement with theoretical results. We also comment on the effect of these nonlocal effects on transverse optical bistability.

INTRODUCTION

Studies of optical-field-induced molecular reorientations in the nematic phase of liquid crystals have revealed interesting nonlinear effects of both fundamental and applied significance.[1] Earlier studies by several groups have revealed the extraordinarily large optical nonlinearity that can be induced with relatively modest-power lasers,[2] and recent studies have shown the possibilities of utilizing these nonlinear effects in optical bistabilities and wave-mixing processes.[3] A particularly salient point of nematic response to an optical field is the strong correlation among the molecules. This correlation is manifested in the existence of molecular elastic torques within the bulk nematics and from cell boundaries. This results in a so-called nonlocal response of the nematics to a laser of finite beam size, i.e., the transverse dependence of the molecular reorientation angle exhibits a width that is in general different from the width of the laser beam. This problem has been treated briefly by several workers in various contexts.[4,5]

In these studies, however, either physically unrealistic assumptions (such as assuming that the laser transverse beam profile is a rect function) are made or the treatments are too qualitative (they apply to only one particular geometry). In some nonlinear optical processes, e.g., transverse self-phase modulations, self-focusing effects, and bistability,[6,7] a more exact description of the transverse spatial dependences of both the laser beam and the nematic reorientation are required.

In a recent study[8] we presented a calculation for the case of a linearly polarized laser incident obliquely upon a nematic film (i.e., where the laser propagation wave vector makes a finite angle with the director axis). We showed that, under physically reasonable assumptions (e.g., all the angles involved are small), the torque balance equations lend themselves to analytical solutions. Some transverse dependences of the reorientation as a function of cell geometry and optical director-axis configurations were discussed.

In this paper we present several new aspects of this problem. They include an experimental confirmation of the theoretical results for the oblique-incidence case as well as the theory for the reorientation of normally incident lasers (i.e., when the laser polarization is orthogonal to the director axis of the nematic film) and experimental results for the observed Freedericksz transition field and broadened (or narrowed) radial dependence.

THEORY

Consider the problem of a linearity polarized laser incident upon a homeotropically aligned nematic film, as shown in Fig. 1. We shall limit our discussion to the case in which $\theta < \beta < 1$, for the sake of simplicity as well as for practical considerations (because in general a small reorientation θ will contribute to a rather large change in the optical refractive index for nonlinear effects to manifest). Since the theoretical results for the $\beta \neq 0$ case have been discussed before, we will discuss here the theoretical calculation for the case $\beta = 0$.

In general, the free-energy density of the system consists of the terms from the three elastic torques (bend, splay, and twist) and the optional torque. The free-energy density term F_1 associated with the bending distortion is given by

$$F_1 = \frac{k_1}{2}(\nabla \cdot \mathbf{n})^2$$

$$= \frac{k_1}{2}(\cos^2\theta\cos^2\phi\theta_r^2 - 2\sin\theta\cos\theta\cos\phi\theta_r\theta_z + \sin^2\theta\theta_z^2), \quad (1)$$

where k_1 is the elastic constant for bending, ϕ is the azimuthal angle, z the direction of propagation of the laser that coincides with the unperturbed director axis, and θ_r and θ_z are the derivatives of θ with respect to r and to z, respectively.

0740-3224/87/020115-06$02.00

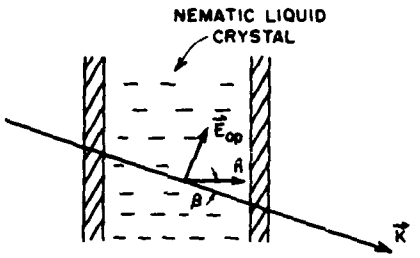

Fig. 1. A linearly polarized laser beam incident upon a homeotropically aligned nematic-liquid-crystal film.

The free-energy density term associated with twist is given by

$$F_2 = \frac{k_2}{2}(\nabla \cdot \nabla \times \mathbf{n})^2 = \frac{k_2}{2}\sin^2\phi\theta_r^2, \tag{2}$$

and that associated with splay is

$$\begin{aligned} F_3 &= \frac{k_3}{2}(\nabla \times \nabla \times \mathbf{n})^2 \\ &= (\sin\theta\sin\phi\cos\theta\cos\phi\theta_r - \cos^2\theta\cos\phi\theta_z \\ &\quad - \sin\theta\cos\theta\theta_r)^2 + (\cos\phi\sin\theta\cos\theta\cos\phi\theta_z \\ &\quad + \cos\phi\sin^2\theta\theta_r + \sin\theta\sin\phi\cos\theta\sin\phi\theta_Z)^2 \\ &\quad + (\cos^2\theta\sin\phi\theta_Z + \sin\theta\cos\phi\cos\theta\sin\phi\theta_r)^2, \end{aligned} \tag{3}$$

where k_2 and k_3 are the elastic constants for twist and splay, respectively.

The total free energy of the system associated with the elastic forces is therefore given by

$$\begin{aligned} F_e &= \iint r\mathrm{d}r\mathrm{d}Z\int_0^{2\pi}(F_1 + F_2 + F_3)\mathrm{d}\phi \\ &= \iint r\mathrm{d}r\mathrm{d}Z[F_1(r) + F_2(r) + F_3(r)], \end{aligned} \tag{4}$$

where $F_1(r)$, $F_2(r)$, and $F_3(r)$ are given by

$$F_1(r) = \frac{k_1}{2}(\cos^2\theta\theta_r^2 + 2\sin^2\theta\theta_Z^2), \tag{5}$$

$$F_2(r) = \frac{k_2}{2}\theta_r^2, \tag{6}$$

$$F_3(r) = \frac{k_3}{2}(2\cos^2\theta\theta_Z^2 + \sin^2\theta\theta_r^2). \tag{7}$$

On the other hand, the free-energy term arising from the optical torque is given by

$$F_4(r) = \frac{-\Delta\epsilon}{8\pi}\epsilon_\perp/\epsilon_\parallel E_{op}^2(r)\sin^2\theta. \tag{8}$$

The significance of the factor $(\epsilon_\perp/\epsilon_\parallel)$ in Eq. (8) was first pointed out by Csillag *et al.*[4] and arises simply from taking into account carefully the electrodynamics of laser propagation in a birefringent medium.[4,5,9] In Eq. (8), $\epsilon_\perp$ and $\epsilon_\parallel$ are the optical dielectric constants for fields perpendicular and parallel to the director axis, respectively:

$$\Delta\epsilon = \epsilon_\parallel - \epsilon_\perp.$$

The total free energy of the system is given by

$$f = \iint r\mathrm{d}r\mathrm{d}z[F_1(r) + F_2(r) + F_3(r) + F_4(r)]. \tag{9}$$

A minimization of the free energy of the system with respect to θ gives

$$\frac{\partial}{\partial r}\left(\frac{\partial f}{\partial\theta_r}\right) + \frac{\partial}{\partial Z}\left(\frac{\partial f}{\partial\theta_Z}\right) - \frac{\partial f}{\partial\theta} = 0, \tag{10}$$

where

$$f = r[F_1(r) + F_2(r) + F_3(r) + F_4(r)]. \tag{11}$$

This gives, finally, after some lengthy and straightforward calculation, the torque balance equation

$$\begin{aligned} &[(K_1 - K_3)\sin^2\theta + K_3]\theta_{zz} + \tfrac{1}{2}(K_1 - K_3)\sin 2\theta(\theta_z)^2 \\ &\quad + \frac{\Delta\epsilon}{8\pi}E_{op}^2(r)\sin 2\theta + \frac{1}{2}[(K_1 - K_3)\cos^2\theta + K_3 + K_2]\theta_{rr} \\ &\quad + \tfrac{1}{4}(K_3 - K_1)\sin 2\theta(\theta_r)^2 + (K_1 - K_3)\cos^2\theta \\ &\quad + K_2 + K_3)\theta_r/2r = 0. \end{aligned} \tag{12}$$

Even for the case of an infinite plane optical wave, Eq. (12) is extremely difficult to solve. A more meaningful and physically more insightful approach is to make a so-called one-constant approximation (i.e., $K_1 \approx K_2 \approx K_3 \approx K$). Second, in the first-order approximation, the dependence of θ on z is a simple sine wave, i.e., we assume that $\theta(r, z)$ is of the form[10]

$$\theta(r, z) = R(r)\sin\left(\frac{\pi z}{d}\right), \tag{13}$$

which obeys the hard-boundary condition $\theta(r, z) = 0$ at $z = 0$ and at $z = d$. In that case, F_1, F_2, and F_3 from Eqs. (1), (2), and (3) add up and contribute to the total elastic free energy

$$F_e^1 = 2\pi k\int_0^d \mathrm{d}z\int_0^\infty r\mathrm{d}r\left[\frac{K}{2}(\theta_r^2 + \theta_Z^2)\right], \tag{14}$$

while the optical free-energy density term remains unchanged. The total free energy is therefore

$$F^1 = 2\pi\int_0^d \mathrm{d}z\int_0^\infty r\mathrm{d}r\left[\frac{K}{2}(\theta_r^2 + \theta_Z^2) - \frac{\Delta\epsilon}{8\pi}E_{op}^2(r)\sin^2\theta\right]. \tag{15}$$

In the case of a Gaussian laser beam, $E_{op}^2(r)$ is given by

$$E_{op}^2(r) = E_{op}^2 e^{-ar^2}, \tag{16}$$

where $a = 2/w_0^2$ and w_0 is the beam waist. Using Eqs. (16) and (13) in Eq. (15), and using $\sin^2\theta \sim \theta^2 - \theta^4/3$, we get, finally,

$$\begin{aligned} F^1 = \pi k\frac{d}{2}\int_0^\infty r\mathrm{d}r\Bigg[&(\mathrm{d}R/_{\mathrm{d}r})^2 + \left(\frac{\pi}{d}\right)^2 R^2 \\ &- \frac{\Delta\epsilon}{4\pi k}E_{op}^2 e^{-ar^2}R^2 + \frac{\Delta\epsilon E_{op}^2}{16\pi K}e^{-ar^2}R^3\Bigg]. \end{aligned} \tag{17}$$

The minimization of the integrand in Eq. (17), denoted as $I(R', R)$, gives

$$\frac{\mathrm{d}}{\mathrm{d}r}\left[\frac{\partial I(R', R)}{\partial R'} - \frac{\partial I(R, R')}{\partial R}\right] = 0, \tag{18}$$

$$R'' + \frac{R'}{r} + \left[be^{-ar^2} - \left(\frac{\pi}{d}\right)^2 \right] R - \frac{b}{2} e^{-ar^2} R^3 = 0, \qquad (19)$$

where $b = (\Delta\epsilon/4\pi k)E_{op}^2$ and the boundary conditions on R are

$$R'(0) = 0,$$
$$R(\infty) = 0. \qquad (20)$$

In Eqs. (17)–(19), $R' = \partial R/\partial r$ and $R'' = \partial^2 R/\partial r^2$.

Equation (19) is an interesting nonlinear equation in $R(r)$. The occurrence of the cubic term (αR^3) is due to our expansion of sin θ to third order in θ [see the sentence just before Eq. (17)], and its inclusion is necessary for a nonvanishing solution of R. In analogy to the infinite plane-wave case, a nonvanishing value of R occurs only if the optical field exceeds a threshold value. In the infinite plane wave, approximately ($a = 0$), the threshold field is well defined by the relation

$$b_{th} = \pi^2/d^2 (E_{th}^2 = 4\pi^3 K \Delta\epsilon^{-1} d^{-2}).$$

However, in the present case, because of the Gaussian function e^{-ar^2} attached to the optical-field square amplitude E_{op}^2, the equation for $R(r)$ clearly breaks up into two distinct regions: one region (region I) corresponds to the square-bracketed term in Eq. (19) being positive, while the other (region II) corresponds to the term being negative. Furthermore, since the molecules outside the laser beam exert torques on those in the central region of the beam, in competition or conjunction with the torque from the cell walls, the so-called threshold field also obviously depends on the laser beam waist.

It is instructive to compare Eq. (19), derived under the condition that $\beta = 0$, with the equation governing the radial function for $\beta \neq 0$ derived previously. We denote the reorientation angle $\theta(r, Z)$ for the case $\beta \neq 0$ as $\theta(r, Z) = R_1(r)\sin(\pi Z/d)$; then $R_1(r)$ obeys the equation

$$R_1''(r) + \frac{\dot{R}_1}{r} + \left[b \cos 2\beta e^{-ar^2} - \left(\frac{\pi}{d}\right)^2 \right] R_1 + \frac{b}{2} e^{-ar^2} \sin 2\beta = 0. \qquad (21)$$

Equation (21) contains a so-called "bias" term $b/2e^{-ar^2} \sin 2\beta$, i.e., there is a nonvanishing torque exerted initially by the optical field on the director axis. Optically induced reorientation is therefore possible for any finite value of E_{op}. As a result of this difference between the $\beta = 0$ case and the $\beta \neq 0$ case, the nonlocal dependences, which are manifested in the form of differences between the width of the laser beam and the width of $\theta(r)$, are quite different for the two cases. In the case of $\beta \neq 0$, the width of $\theta(r)$ is always larger than w_0, but for the $\beta = 0$ case the width can be greater or less than w_0, depending on the laser beam waist compared with the thickness of the film.

As was shown previously,[8] there is a closed-form solution to Eq. (21). Equation (20), however, does not yield any meaningful closed-form solution, but it can be readily solved numerically. In the next two sections, we discuss some of the salient points of the nonlocal dependence for the $\beta = 0$ case. We then also recall the counterpart results for the $\beta \neq 0$ case and compare these results with our experimental observations.

NUMERICAL RESULTS

Numerical results for $R(r)$ are obtained for a large range of values of w_0 (measured with respect to the thickness of the sample d).

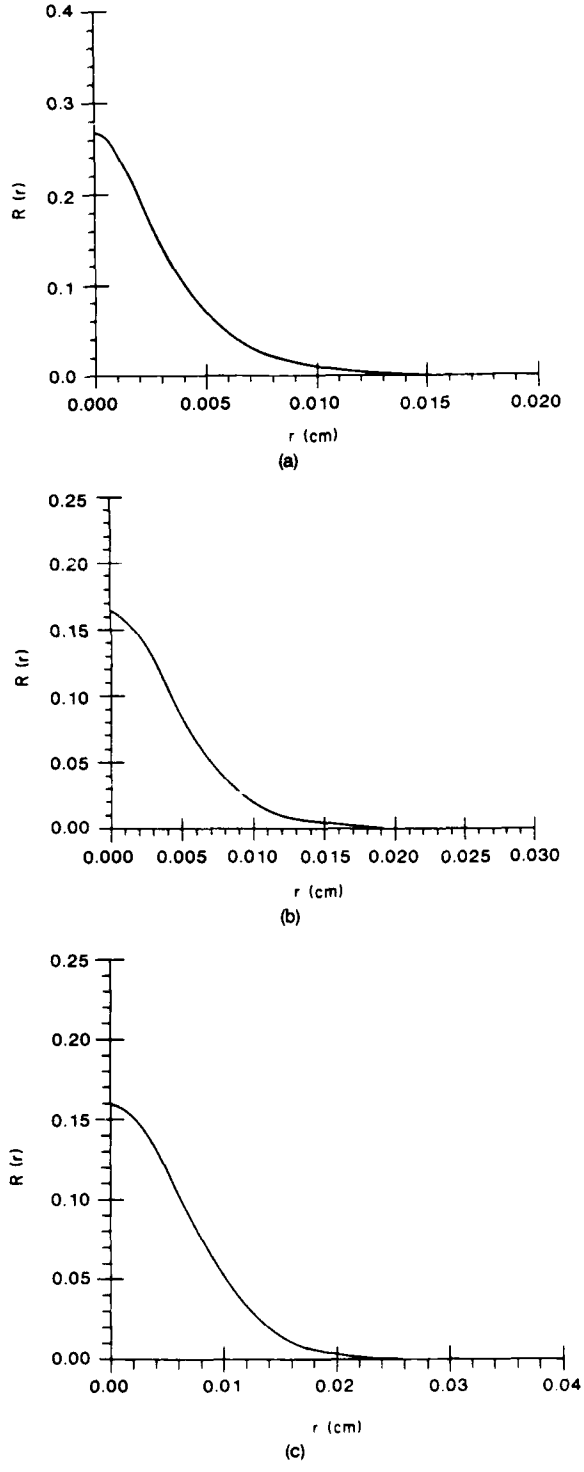

Fig. 2. (a) Solution of the reorientation transverse profile $R(r)$ for the case $w_0/d = 0.4$ [$w_0 = 40$ μm, $d = 100$ μm]; (b) $R(r)$ for $w_0/d = 1$; (c) $R(r)$ for $w_0/d = 2$. For all $\beta = 0$, $d = 0.01$ cm.

In the $\beta = 0$ case, director-axis reorientations do not occur until the central maximum intensity $I(0) = (nc/4\pi)E_{op}^2$ is greater than the Freedericksz threshold intensity [i.e., for $b > b_{th}^{(0)}$, where $b_{th}^{(0)} = (\Delta\epsilon/8\pi k)E_{th}^2$]. The values of b for which $\theta \neq 0$ occurs depend on w_0.

Figures 2(a), 2(b), and 2(c) show the typical dependence of $R(r)$ for $w_0/d = 0.4$, $w_0/d = 1$, and $w_0/d = 2$, respectively. In general, the director reorientations occur only after the incident optical electric field is well above the threshold field (which we shall discuss presently). The important point about Figs. 2(a)–2(c) is that the width of $R(r)$ (which is measured by the e^{-2} point; even though the curve is not a Gaussian this somewhat arbitrary approach gives us a measure of the width of the curve) with respect to the incident laser beam width is clearly dependent on the laser beam width relative to the thickness of the sample. As shown in Fig. 2(a), where $w_0/d = 0.4$, the width of $R(r)$ (denoted as w_θ) is larger than the incident laser beam width w_0. On the other hand, Fig. 2(c) shows that for $w_0/d = 2$, one finds w_θ to be less than w_0

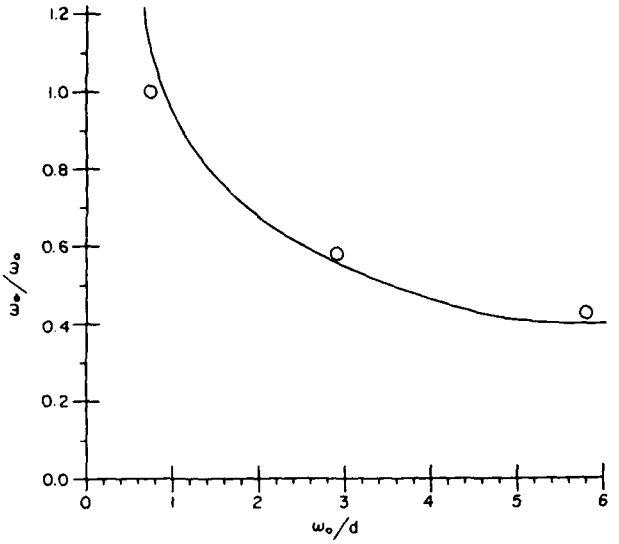

Fig. 3. Plot of the width w_θ of $R(r)$ as a function of the ratio of incident laser beam waist to the thickness of the film (w_0/d). Circles are experimentally observed points. ($\beta = 0$.)

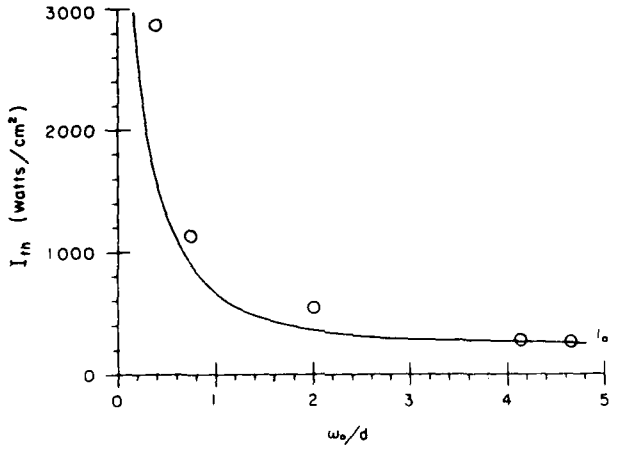

Fig. 4. Plot of the theoretically predicted threshold intensity I_{th} at which reorientation occurs versus w_0/d. The value $I^{(0)}$ corresponds to the case involving an infinite plane wave ($\beta = 0$). Circles are experimentally observed points.

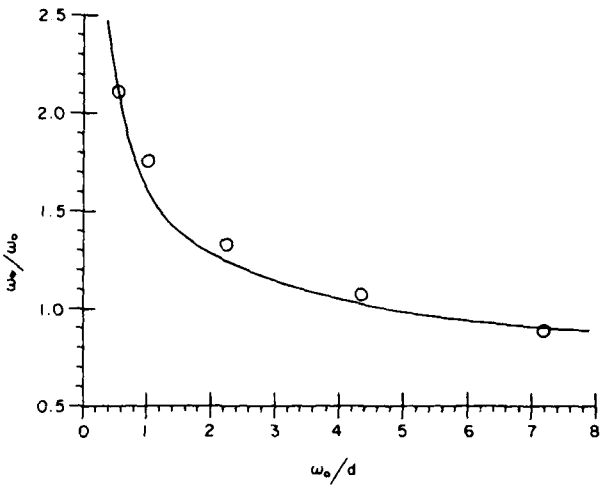

Fig. 5. Plot of the width of the reorientation transverse profile w_θ/w_0 versus w_0/d for the case $\beta \neq 0$ (from previous calculations in Ref. 6). Circles are experimentally observed points.

This variation of w_θ/w_0 with w_0/d is plotted in Fig. 3, which shows this trend, i.e., the value of w_θ/w_0 drops off monotonically from being larger than unity (for $w_0/d < 1$) to smaller than unity (for $w_0/d > 1$). At $w_0/d \sim 1$, we have $w_\theta/w_0 \sim 1$.

As we mentioned earlier, as a result of the significant elastic torque from molecules surrounding the laser beam (besides the boundary elastic torque), the field required to create finite molecular reorientation (which we shall denote b_{th}) is, in general, larger than that associated with infinite-beam-size lasers. Figure 4 shows a plot of the value of b_{th} for which nonzero reorientation $\theta(r)$ occurred. As a function of w_0/d, we note that $b_{th} \to b_{th}^{(0)}$ for $w_0 \gg d$.

For the case $\beta \neq 0$, there is no threshold field; the solution of Eq. (21) shows one other main difference, namely, that the width of the response $R_1(r)$ is *always larger than the laser* beam width. Figure 5 is a plot of w_θ/w_0 versus w_0/d from the numerical results obtained from our previous study. For $w_0/d = 2$, for example, one gets $w_\theta/w_0 \sim 1.5$ for the $\beta \neq$ case. On the other hand, for the $\beta = 0$ case, we get $w_\theta/w_0 \sim 0.7$.

EXPERIMENTS

The transverse dependence of the molecular reorientation and the associated transverse dependence of optical refractive-index change on the laser spot size play a crucial role in nonlinear processes involving the nonlinear (intensity-dependent) transverse phase shift. In self-phase modulation, and in transverse optical bistability, the observed effect depends both on the size of the laser beam and on the detailed index profile change. These concerns motivate our experimental verifications of the preceding theoretical results.

Figure 6 is a schematic of the experimental setup to measure the reorientation profile. The nematic liquid crystal used is a homeotropically aligned 100-μm-thick EM chemi-

cal E46 sample at 22°C. E46 has a $\Delta\epsilon$ of 0.7, a nematic range from −9.5 to 88°C, and little (negligible) thermal effect at the Ar laser 5145-Å line. The Ar laser is linearly polarized and focused onto the liquid crystal. The beam waist of the Ar laser on the liquid crystal is monitored with a knife edge mounted on another translator (not shown). The translator shown in the figure, with a 0.5-μm resolution, translates the He–Ne probe beam. Both the He–Ne and the Ar lasers experience a self-phase modulation effect associated with the transverse phase shift caused by the molecular reorientation (induced by the Ar^+ laser). These self-phase modulation effects are manifested in the form of an increased divergence and appearance of interference rings of the laser beams at the screen (placed 5 m away from the sample).

The liquid-crystal film is oriented such that β assumes a value of either 0° or 22° with respect to the Ar laser beam direction.

The results, as shown by the experimental data points in Figs. 3–5, show a remarkable agreement with theoretical calculation. The measured widths of the radial reorientation profile w_θ (relative to w_0) versus the waist (relative to the thickness d) are of the order of unity for $w_0/d \sim 1$ and decrease as w_0 increases (cf. Fig. 3) in the case of $\beta = 0$. On the other hand, for $\beta \neq 0$, as shown in Fig. 4, the experimental measured width w_θ is always greater than the laser beam waist w_0 for all values of w_0; w_θ approaches w_0 for large values of w_0.

As is shown in Fig. 5, the experimentally observed threshold field dependence on w_0/d also follows the theoretical prediction. For E46, a 100-μm sample has a Freedericksz transition field intensity of 200 W/cm^2 (using the values $\Delta\epsilon = 0.3$, $K \sim 10^{-7}$, $d = 0.01$ cm, and $n \approx n_0 \approx 1.5$). For large values of w_0/d (for example, $w_0/d \geq 5$), the observed threshold field approaches this value. However, as the incident laser beam size decreases to a value comparable with the thickness d or less, the threshold optical intensities increase dramatically. At $w_0 \sim d$, the threshold intensity increases by almost an order of magnitude. In general, the experimentally observed relative increase of the threshold field is slightly larger than the theoretical value, probably because of a systematic difference between the experimental observation of the onset of reorientation (by the appearance of the self-focusing effect on the exit Ar^+ laser beam) and also because of an error in the spot-size measurement. Nevertheless, the overall dramatic dependence of the threshold intensities on the beam waist is conclusively demonstrated in Fig. 5.

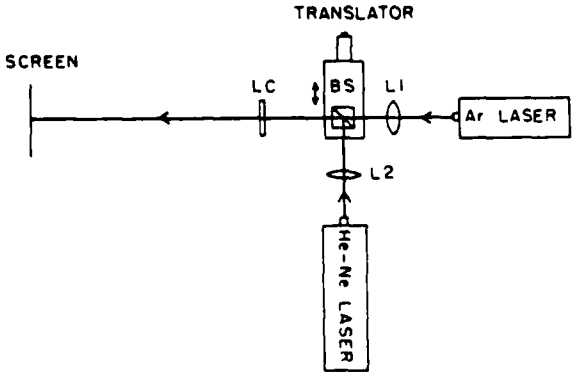

Fig. 6. Experimental setup for measuring the width of the director axis reorientation induced by a Gaussian laser beam. BS, beam splitter; L, lens; LC, liquid-crystal film.

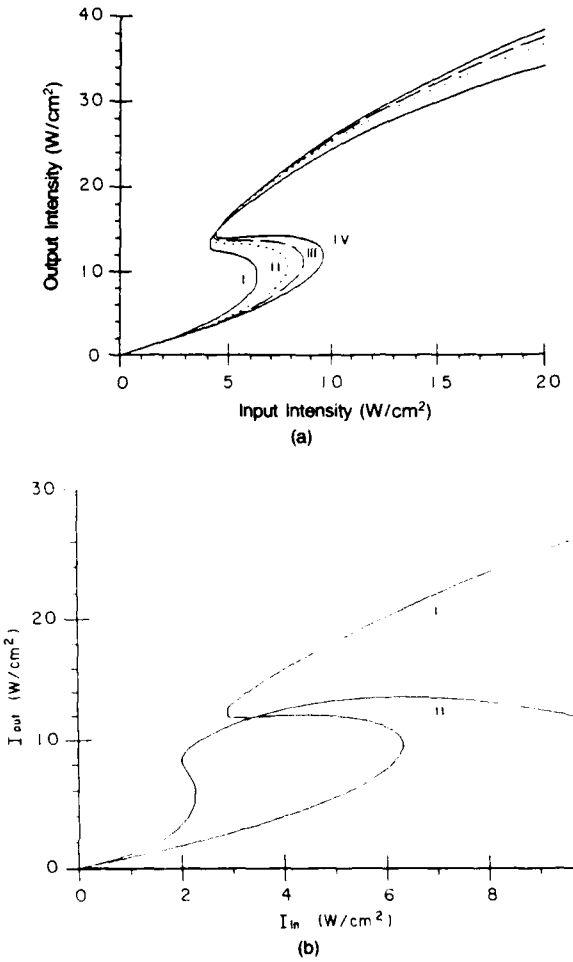

Fig. 7. (a) Transverse optical bistability for the case $\beta = 22°$, showing how the switching changes as the width of the reorientation profile is varied. Curve I: width of $\theta(r)$ = laser width, i.e., local response; curve II: width of $\theta(r)$ = 1.5-laser width; curve III: width of $\theta(r)$ = 2-laser width; curve IV: width of $\theta(r)$ = 4-laser width. (b) Transverse optical bistability for the case $\beta = 0°$. Curve I: local response, width of $\theta(r)$ = laser width; curve II: width of $\theta(r)$ = 1/3 laser width showing markedly different switching characteristics.

FURTHER REMARKS

The observed (experimentally and theoretically) broadening or narrowing of the response of the nematic reorientation could, and should, be taken into account in the study of nonlinear transverse optical effects involving a focused beam. We end this section with reference to transverse optical bistability, which recently has received considerable attention.

Figure 7(a) (calculated using the technique developed in Ref. 7) shows what would happen to the output versus input bistability (of the transmitted on-axis laser intensity) for various laser beam sizes in comparison with the thickness of the film for the case $\beta = 22°$. Although the switch-down

intensities do not seem to vary much, the switch-up intensity increases by about 60% as the laser spot size is decreased from d to $d/4$. The point to note about this exercise is that in extrapolating the observed switching intensities for a large-sized beam to smaller beams (presumably for some integrated-optics consideration) these nonlocal effects should be properly accounted for. For $\beta = 0$, the fact that the observed width of $R(r)$ is in general smaller than the laser beam waist is also interesting. Figure 7(b) shows a comparison of the switching characteristics for the case when the induced index profile is smaller than the incident laser beam's waist with the case when the nonlocality is ignored. Both the switching intensities and the bistability loops are dramatically different. A detailed account of this case is clearly outside the context of this paper and is reserved for a lengthy future publication on transverse bistability.

CONCLUSION

We have presented a quantitative theoretical and experimental study of the transverse dependence of the nematic axis reorientation induced by an optical field. For most geometrical configurations, there are significant nonlocal effects, which are experimentally confirmed. Similar effects are expected in any diffusive type of optically induced nonlinearities (e.g., thermal and solid-state electronics) and are particularly pronounced when the laser beam sizes are smaller than the characteristic lengths (sample thickness, thermal diffusion length, electron–hole recombination length, etc.). In studies of transverse nonlinear optical effects, such as self-phase modulation, self-focusing, and optical switching (passive optical limiting or optical bistability), these nonlocal effects must be accounted for appropriately.

ACKNOWLEDGMENT

This research is supported by grant ECS8415387 from the National Science Foundation and by grant AFOSR-840375 from the U.S. Air Force Office of Scientific Research.

REFERENCES

1. See, for example, the review paper by I. C. Khoo and Y. R. Shen, Opt. Eng. **24,** 579 (1985).
2. N. F. Pilipetski, A. V. Sukhov, N. V. Tabiryan, and B. Ya Zel'dovich, Opt. Commun. **37,** 280 (1981); S. R. Galstyan, O. V. Garibyan, N. V. Tabiryan, and Yu. S. Chilingaryan, JETP Lett. **33,** 437 (1981); A. S. Zolot'ko, V. F. Kitaeva, N. Kroo, N. N. Sobolev, and L. Chillag, JETP Lett. **32,** 158 (1980); I. C. Khoo and S. L. Zhuang, Appl. Phys. Lett. **37,** 3 (1980); S. D. Durbin, S. M. Arakelian, and Y. R. Shen, Phys. Rev. Lett. **47,** 1411 (1981).
3. B. Ya. Zel'dovich, N. V. Tabiryan, and Yu. S. Chilingaryan, Sov. Phys. JETP **54,** 32 (1981); I. C. Khoo, Appl. Phys. Lett. **41,** 909 (1982); I. C. Khoo and S. L. Zhuang, IEEE J. Quantum Electron. **QE-18,** 246 (1981).
4. L. Csillag, J. Janossy, V. F. Kitaeva, N. Kroo, and N. N. Sobolev, Mol. Cryst. Liq. Cryst. **84,** 125 (1982).
5. E. Santamato and Y. R. Shen, Opt. Lett. **9,** 564 (1984).
6. A. E. Kaplan, Opt. Lett. **6,** 360 (1981); M. LeBerre, E. Ressayre, A. Tallet, K. Tai, and H. M. Gibbs, IEEE J. Quantum Electron. **QE-21,** 1404 (1985); J. E. Bjorkholm, P. W. Smith, W. J. Tomlinson, and A. E. Kaplan, Opt. Lett. **6,** 345 (1981); J. E. Bjorkholm, P. W. Smith, and W. J. Tomlinson, IEEE J. Quantum. Electron. **QE-18,** 2016 (1982).
7. I. C. Khoo, P. Y. Yan, T. H. Liu, S. Shepard, and J. Y. Hou, Phys. Rev. A **29,** 2756 (1984).
8. I. C. Khoo, T. H. Liu, and R. Normandin, Mol. Cryst. Liq. Cryst. **131,** 315 (1985).
9. See, for example, H. L. Ong, Phys. Rev. A **28,** 2393 (1983); B. Ya. Zel'dovich, N. V. Tabiryan, and Yu. S. Chilingaryan, Sov. Phys. JETP **54,** 32 (1981).
10. See, for example, P. G. deGennes, *The Physics of Liquid Crystals* (Clarendon, Oxford, 1984).

TRANSVERSE SELF-PHASE MODULATION OPTICAL BISTABILITY

I. C. Khoo

pp. 196–201

REPRINTED FROM

PROCEEDINGS
OF THE
INTERNATIONAL CONFERENCE
ON

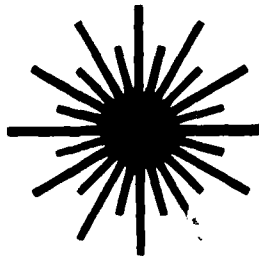

LASERS '84

TRANSVERSE SELF-PHASE MODULATION OPTICAL BISTABILITY

I. C. Khoo
Electrical Engineering Department
University Park, PA 16802

Abstract

We present here further analytical results for the fundamental mechanisms of bistable transverse intensity distribution of a Gaussian laser beam after its passage through a thin nonlinear medium. We have derived explicit analytical expressions for the transmitted intensity distribution in the case where the beam undergoes only self-phase modulation effects and where a single reflection feedback is present. The geometrical conditions for bistable optical switching, the dependences on various geometrical and laser parameters for both positive and negative nonlinearities, and the effect of saturation, are discussed.

Introduction

Recently, a new class of so-called cavity-less optical bistability phenomenon has received considerable attention. In particular, Kaplan[1] has proposed several schemes for optical bistability utilizing the self-focusing process, in conjunction with a single reflection feedback. A detailed theory[2] with experimental observations for the case of "weak" or "external" self focusing involving a nonlinear thin film has recently been described.

In this paper, we present further new analytical results for this type of optical bistability, which originates from the transversely dependent nonlinear phase shift experienced by a Gaussian laser beam in traversing the nonlinear thin film. We generalize the theoretical consideration to both positive and negative nonlinearities (i.e. for $n_2 > 0$ and for $n_2 < 0$) and derive explicit expressions for the conditions for bistable operation. The theory presented here should be applicable to all nonlinear thin film, and in particular, solid-state thin films which appear to be the best candidate for optical processing applications.

Theory

The configuration for the observation of transverse intensity bistability is schematically depicted in Figure 1. A cw laser with a curvature R, incident on the nonlinear thin film (where the laser beam waist is ω_0) is reflected after passage through the film and a lens back onto itself. The transmission through the mirror is monitored by a pin-hole placed at various radial positions from the axis of the beam. The refractive index change induced on the film is of the form

$$\Delta n = n_2 I(r) \tag{1}$$

where I (r) is the optical intensity at the film and n_2 is the nonlinearity coefficient. Typically, $n_2 \sim 10^{-7}$ for a liquid crystal film, and of the same magnitude or larger for solid-state thin film.

This refractive index change imparts a transverse phase shift on the optical field

$$\delta\phi(r) = \frac{2\pi}{\lambda} \int_0^d n_2(Z) I(r) dZ = \frac{2\pi}{\lambda} n_2 \, dI(r) \tag{2}$$

where d is the thickness of the nonlinear film
The total optical intensity on the sample is given by the sum of the forward propagating and backward propagating (reflected) beam

$$I = I_0 + I_R \tag{3}$$

Without loss of generality, and for the sake of clarity, we will ignore the presence of the lens. (The effect of including the lens is to introduce a geometrical factor and will be discussed in a later section). In this case, the exit beam electric field at a distance z from the nematic field is given by

$$E(r_0,z) = \frac{2\pi}{i\lambda z} \exp(ikz) \exp\frac{-ikr_0^2}{2z} \int_0^\infty E_0(r,0) \exp\frac{-ikr^2}{2z} J_0\left|\frac{2\pi r r_0}{\lambda z}\right| \exp[-i\delta\phi(r)] r \, dr \tag{4}$$

where $r_o = (x_o + v_o)^{\frac{1}{2}}$ and $r = (x^2 + y^2)^{\frac{1}{2}}$ and J_o is the zeroth-order Bessel Function. The incident laser beam is assumed to be a Gaussian, and its electric field is given by

$$E_0(r,0) = \sqrt{I_0}\exp\left[-\frac{r^2}{\omega^2} - \frac{ikr^2}{2R}\right] \tag{5}$$

The output intensity at z is given by squaring both sides of equation (4) to give

$$I(r_0,z) = \left|\frac{2\pi}{\lambda z}\right|^2 I_0 \left| \int_0^\infty dr\, rJ_0(2\pi r r_0/\lambda z)\exp(-r^2/\omega_0^2) \times \exp\left\{-ik\left[\frac{r^2}{2z} + \frac{r^2}{2R} + \bar{n}_2 I_0 d\exp\left[-\frac{2r^2}{\omega^2}\right] + \bar{n}_2 R_m dI(r,z)\right]\right\}\right|^2 \tag{6}$$

Notice from (6) that it is an integral equation for the intensity distribution I(r,z). The possibility of bistable or multistable intensity distribution is therefore obvious It is not possible to get a closed-form solution for (I(r,z) from (6). We found that, however, by making very reasonable approximations, we can convert equation (6) to a set of very simple transcendental algebraic equations from which much insight about the bistable operation can be gained. The approximation employed can be shown to be equivalent to the lens approximation, and consist of the simple procedure of expanding $I(r_o,z)$ as well as I_o and I_b in the form

$$I(r_0,z) = \sum_{n=0}^{\infty} (-1)^n A_{2n} r_0^{2n} \tag{7}$$

and retaining only the first two terms. [We have shown in previous work that it is possible to redo the problem by including all the terms for the forward propagating field (corresponding to I_o), but the result for the bistable switching is not appreciably changed]. Following reference 2, we get,

$$A_0 = \frac{I_0}{4z^2\left|\left(\frac{1}{\omega^2 k}\right)^2 + \left(\frac{1}{2z} + \frac{1}{2R} - \frac{2n_2 I_0 d}{\omega^2} - n_2 d R_m A_2\right)^2\right|} \tag{8}$$

and, by introducing a unitless parameter u

$$u = \omega^2 k(1/2z+1/2R-2n_2 I_0 d/\omega^2 - n_2 d R_m A_2) \tag{8a}$$

the solutions for A_o and A_2 are given by the solution for u in the equation

$$B_1 - B_2 u = \frac{1}{(1+u^2)^2} \tag{9}$$

where

$$B_1 = \frac{8z^4(1/2z+1/2R-2n_2 I_0 d/\omega^2)}{R_m n_2 I_0 d\omega^6 k^4} \tag{10}$$

and

$$B_2 = \frac{8z^4}{R_m n_2 I_0 d\, \omega^6 k^5} \tag{11}$$

Figure (2) is a plot of the function $B_1 - B_2 u$ (L.H.S. of (9)), and $(1 + u^2)^{-2}$ (R.H.S. of (9)). Where there are triple intersection points correspond to the bistable switching region.

Discussion

Before we proceed to discuss the geometrical significance and conditions deducible from Figure (2), it is instructive to note here that aside from the expected dependence of B_1 and B_2 on z, and the radius of curvature R, both B_1 and B_2 are extremely sensitive to the beam waist ω of the incoming laser beam. $B_1 \sim \omega^{-6}$ while $B_2 \sim \omega^{-8}$ On the other hand, the existence of the triple-value solutions from Figure 2 is clearly dependant on the value of B_1 and B_2. This implies of course that transverse optical bistability is extremely sensitive to the incoming laser beam waist Such a dependence is actually experimentally verified in our study of transverse optical bistability involving a nematic

liquid crystal film, and is expected to hold true too for other thin film with nonlinearity of the form given in (1).

There is a similarity between Figure (2) and the usual Fabry-Perot optical bistability treatment. Both involve solving for triple valued quantity from the intersection of a straight line and a bell-shaped function. The slope of the straight line is inversely proportional to the optical intensity of the incoming beam. The difference in the present case is that only one (as opposed to the usual Fabry-Perot, which involves infinite, periodic) bell-shaped function is involved. Also, the intercept of the straight line with the "u" axis also changes with the beam intensity.

Figure (2) allows one to deduce the geometrical conditions for observing bistability. When $I_o = 0$, slope $-B_2$ (denoted as m) is infinite, while the intercept (denoted as $B_x = B_1/B_2$) is given by

$$B_x = \omega^2 k \quad \left(\frac{1}{2z} + \frac{1}{2R} - 2n_2 I_o d/\omega^2 \right) \tag{12}$$

Consider the case $n_2 > 0$. If I_o is increased, then B_x will move towards $u = 0$, i.e. decreases, as shown in Figure 2. At the same time, the slope m will decrease in magnitude (m is still negative). In order for triple-valued solution to occur, a sufficient condition is that the magnitude of the slope must be less than the maximum magnitude of the tangent to the bell-shaped function on the positive u side. Let the corresponding optical intensity be denoted I_c i.e.

$$m\ (I_c) > -1.04 \tag{13}$$

where 1.04 is the maximum magnitude of the tangent to the bell-shaped function.

Correspondingly, the intercept is given by

$$b_{xc}\ (I_c) = 1.12 \tag{14}$$

A necessary condition for bistability is that $b_x\ (I=0) \geq 1.12$
From (14), we get

$$I_c = \frac{i}{2n_2 dk} \left[\frac{\omega^2 k}{2} \left(\frac{1}{z} + \frac{1}{R} \right) - 1.12 \right] \tag{15}$$

And from (13), we get the sufficient condition for bistability as

$$\frac{8z^4}{R_m n_2 d\ \omega^8 k^5 \frac{(-1)}{2n_2 dk} \left[\frac{\omega^2 k}{2} \left(\frac{1}{z} + \frac{1}{R} \right) - 1.12 \right]} \tag{16}$$

The square-bracket term in the denominator of (16) is positive by virtue of the fact that $b_x\ (I=0) > 1.12$. From (16), we have

$$\frac{1}{R} > \frac{30.8\ z^4}{R_m (\omega^2 k)^5} + \frac{2.24}{\omega^2 k} - \frac{1}{z} \tag{17}$$

where R_m is the reflectivity of the feedback mirror.
Notice that n_2 cancels out exactly in the denominator of (16). The condition for optical bistability is independent of the magnitude of n_2! From (17), we see that transverse optical bistability is clearly a geometrical effect, depending only on the geometrical parameter like z and R. Equally noteworthy is the extreme sensitivity of the condition on the ω.

For the case of negative nonlinearity ($n_2 > 0$), the same argument can be pursued in an almost mirror-image fashion of Figure 3, leading to the conditions

$$b_x^-\ (I_c) = -1.12 \tag{18}$$

$$m^-\ (I_c) < 1.04 \tag{19}$$

This gives

$$I_c = -\frac{1}{2|n_2|dk}\left[\frac{\omega^2 k}{2}\left(\frac{1}{z}+\frac{1}{R}\right)+1.12\right]$$

and, finally, the sufficient condition for bistability is

$$\frac{1}{R} < -\left[\frac{30.8z^4}{Rm(\omega^2 k)^5}+\frac{2.24}{\omega^2 k}+\frac{1}{z}\right] \qquad (20)$$

Again, the condition is independent of the magnitude of n_2, although it does reflect the sign of the n_2 by imposing the requirement that the radius of curvature of the incoming laser beam be negative.

In the presence of a lens between the thin film and the mirror, the analysis is straightforward though lengthy. Following Reference 2, the solutions for the output intensity (A_o and A_2) can again be obtained by solving an equation of the form[2]

$$B_1 - B_2 V = (1+V^2)^{-2} \qquad (21)$$

where

$$B_1 = \frac{D_1^4}{2b_1^2 b^4 I_0 \omega^6 n_2 dR_m}\left[\frac{1}{2z}+\frac{1}{2R}-\frac{2n_2 I_0 d}{\omega^2}+\frac{ab}{kD_1}\right] \qquad (22)$$

and

$$B_2 = \frac{D_1^4}{2b_1^2 b^4 I_0 \omega^8 n_2 dR_m k} \qquad (23)$$

and $a = k/2z - k/2R$, $b = (k/2z)^2$ and $D_1 = b_1 - a_1 a$ ($b_1 = (k/2z_1)^2$ and $a_1 = k/2z_2 - k/2f$). Obviously ab/kD, appearing in B_1 is a purely geometrical quantity. The similarity between the set of equation (21)-(23), and the set (9)-(11), not surprisingly, again leads to conditions for bistability that are independent of the magnitude of n_2, and are dependent only on the various geometrical factors. For $n_2 > 0$, we have, for example

$$\frac{D_1^4}{-b_1^2 b^4 \omega^8\left[\frac{\omega^2 k}{2}\left(\frac{1}{z}+\frac{1}{R}+\frac{ab}{kD_1}\right)-1.12\right]} < 1.04 \qquad (24)$$

Although we have not conducted a thorough experimental investigation of how these conditions are obeyed, the geometric parameters used in our experimental observation of transverse bistability are within the prescribed conditions. We have deliberately experimented with set-ups that fall outside the condition for bistability and have not observed any switching. The preceding discussion also brings forth a hitherto neglected consideration, namely, the nonlinear response of the thin film does not necessarily have the same shape and/or width as the transverse dependence of the incident laser. Under cw illumination, diffusion processes (in solid state material) or nonlocal long-range interaction (e.g. in liquid crystal) will in general broaden the response. It becomes critical in view of the extreme dependence of the transverse bistability on the laser beam width, and the width of the response, therefore, to calculate exactly the transverse response of the material when these diffusive types of processes are present. Work is currently underway in this direction.

The theory as outlined above, and detailed in Reference 2, can be applied in the study of the effect of saturation, which has hitherto not been addressed to in the case of external or "weak" self focusing bistability. Saturation of the optical nonlinearity can assume many forms, depending on the corresponding physical processes involved. It is concommitant with the extraordinary large optical nonlinearity observed in materials like nematic liquid crystal films (molecular reorientational nonlinearity), solid state multi-quantum well structures (excitronic absorption) and sodium vapors (electronic resonances).

We have investigated several forms of saturation behaviour and how they affect the transverse bistability switching process. One of the most commonly occurring form is such

that the optically induced refractive index change is given as in Equation (1), but with n_2 replaced by an intensity dependent coefficient $n_2(I)$.

$$n_2(I) = \frac{n_2}{1 + I(r)/I_s} \tag{25}$$

where I_s is the saturation intensity. Details of our calculation are clearly outside the scope of the present paper. It suffices to note here that one could proceed with the same expansion procedure as outlined here and Reference 2 to obtain again two algebraic equations for A_0 and A_2 (c.f. Equation (8). However, it is no longer possible to derive simple explicit analytical expressions for the conditions for bistability operations. Nevertheless, these algebraic equations can be very easily solved numerically. An interesting theoretical result, which occurs at a small range of saturation intensity, is depicted in Figure 3. The calculation uses the geometrical parameters similar to the set used in the experimental observation described in Reference 2, with an assumed saturation intensity I_s value near the switch-up point. As clearly depicted in Figure 3, two very closely bistability loops appear. The first loop occurs at a lower intensity, and is almost identical to one obtained with ($I_s=\infty$). The second loop occurs right after the switch-up point in the first loop, and the direction of switching is opposite to the initial loop. As we emphasized earlier, the occurrence of these two closeby loop holds true only for a small range of I_s. At other values of I_s, the two bistability loops either merge into one, or break up into one bistability loop and a unidirection "dip" at the higher intensity point.

Acknowledgement

I am indebted to T. H. Liu and R. Normandin for some assistance in the numerical computation. This research is supported by a grant from the National Science Foundation under grant number ECS8415387 and the Air Force Office of Scientific Research AFOSR 840375.

References

1. A. E. Kaplan, Opt. Letts. 6, 360 (1981)
2. I. C. Khoo, P. Y. Yan, T. H. Liu, S. Shepard and J. Y. Hou, Phys. Rev. A29, 2756 1984; see also references therein for a more complete list of references on similar work.

Figure Captions

Figure 1. Schematic of the experimental set up for observing transverse intensity bistability. m: mirror; p: pinhole; NF: nonlinear thin film; $Z = 2(Z_1 + Z_2)$.

Figure 2. Plot of the functions B_1-B_2 u and $(1+u^2)^{-2}$. B_x and B_{xc} are intercepts of B_1-B_2 u with the u-axis. m is the tangent to the bell-shaped function $(1+u^2)^{-2}$.

Figure 3. Theoretical bistability output versus input plot for the on-axis region.

Fig.1

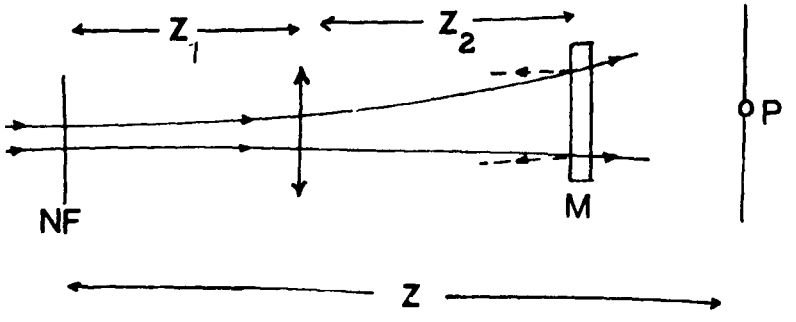

Fig.2

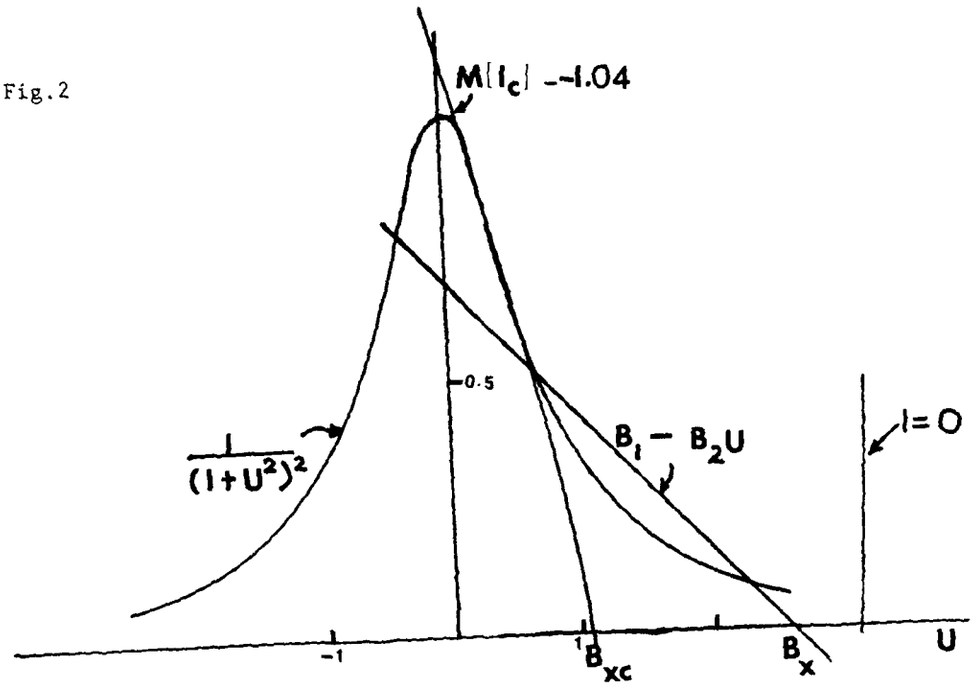
M(I_c) --1.04
0.5
1/(1+U²)²
B₁ − B₂U
I=O
-1
1
B_xc
B_x
U

Fig.3

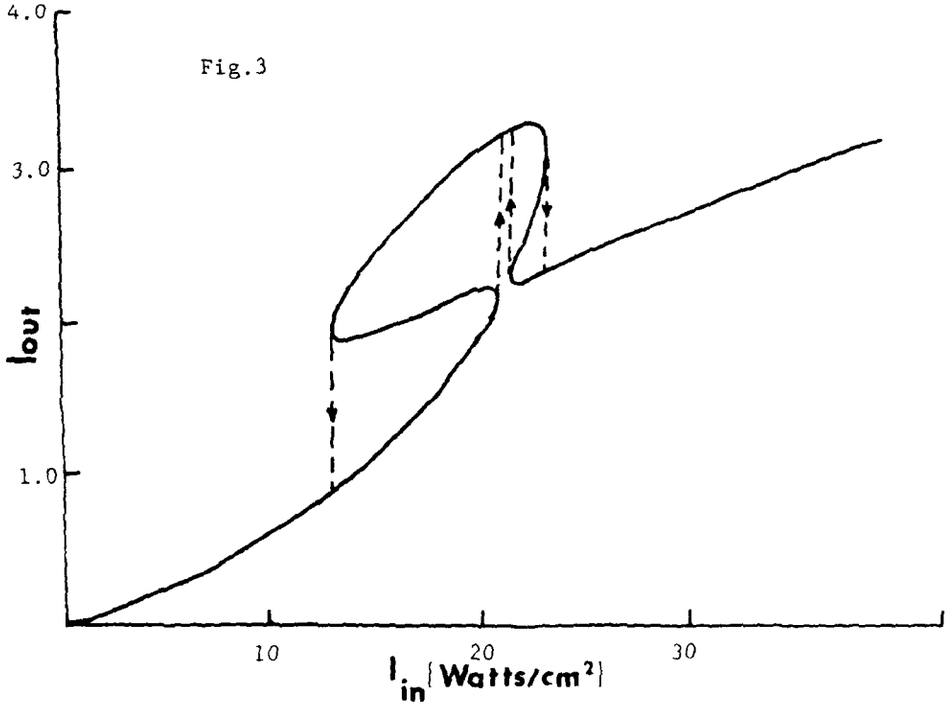
4.0
3.0
1.0
I_out
10
20
30
I_in (Watts/cm²)

J-QE/23/2/11726

Probe Beam Amplification via Two- and Four-Wave Mixings in a Nematic Liquid Crystal Film

I. C. Khoo
T. H. Liu

Reprinted from: IEEE JOURNAL OF QUANTUM ELECTRONICS, Vol. QE-23, No. 2, FEB. 1987.

Probe Beam Amplification Via Two- and Four-Wave Mixings in a Nematic Liquid Crystal Film

IAM-CHOON KHOO AND T. H. LIU

Abstract—**We have observed very large probe beam gain (up to 600 percent) in a thin film (100 μm) of nematic liquid crystal, for a low pump beam intensity on the order of 2 W/cm². The effect is nonlinearly dependent on the pump intensity and the wave mixing angle.**

INTRODUCTION

THE EXTRAORDINARILY large orientational optical nonlinearity of nematic liquid crystal has been well-documented in the studies of several nonlinear optical processes [1]. Optical wave mixing effects, such as wavefront conjugations (with coherent and partially coherent light) and optical self-diffractions have been studied by several workers. These studies are centered on the index grating induced by a pump (or reference) and a probe (or image) beam. Wavefront conjugation is obtained if the pump beam is retroreflected, and the generated fourth wave transverses back along the probe beam. On the other hand, the two incident beams can "self-diffract" from the grating into beam 2 and 3 directions [as shown in Fig. 1(a)]. An interesting effect arises in these mixing effects when probe beam 1 is much weaker in intensity than pump beam 0. In that case, beam 1 can be amplified (or diminished), depending on the beam coupling between them.

In similar studies in other materials [2], such as BSO and $BaTiO_3$, a $\pi/2$ phase shift between the refractive index grating and the optical intensity grating is induced. This gives rise to a strong coupling between the two beams, and amplifies beam 2 at the expense of beam 1. If the phase shift is vanishing, this coupling disappears.

In this letter, we report the observation of very large probe beam amplification *even under a zero phase shift condition*. The effect is attributed to a multiwave mixing effect. By frequency shifting one of the beams, thereby creating a phase shift between the gratings, a two-wave mixing effect is observed. The two-wave coupling enhances (or diminish) the multiwave mixing produced probe gain depending on the sign of the phase shift.

Before we describe our experimental results we shall briefly go through the basic theories. Nematic films are Kerr-like media. The optical dielectric constant may be written in the form

Manuscript received July 7, 1986; revised October 3, 1986. This work was supported in part by the National Science Foundation under Grant ECS8415387 and by the Air Force Office of Scientific Research under Contract AFOSR840375.

The authors are with the Department of Electrical Engineering, The Pennsylvania State University, University Park, PA 16802.

IEEE Log Number 8611726.

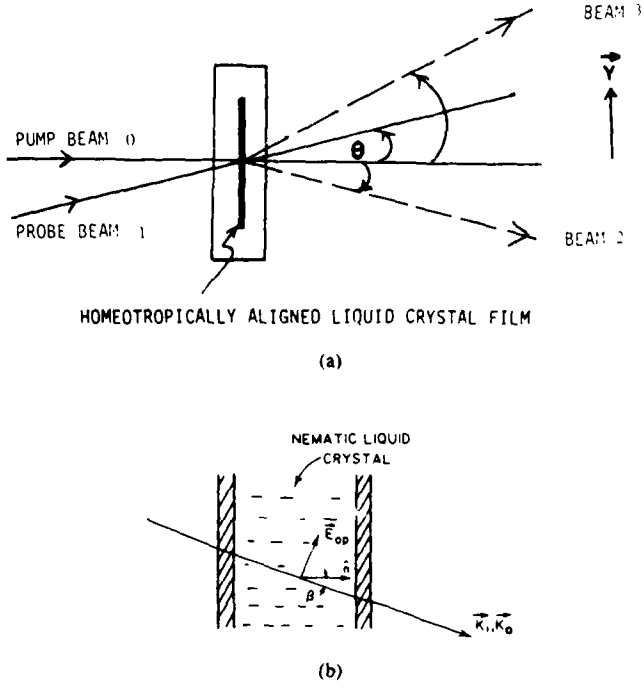

Fig. 1. (a) Schematic of optical self-diffractions in a nonlinear film induced by the pump 0 and the probe 1 beams. (b) Schematic of lasers propagating through a homeotropically aligned nematic liquid crystal film.

$$\epsilon_e = \epsilon_{eo} + \epsilon_1 E^2 \tag{1}$$

where ϵ_e is the extraordinary ray dielectric constant, ϵ_{eo} is the unperturbed value, ϵ_1 the nonlinearity coefficient, and E^2 is the square of the optical electric field. We had used Fig. 1(b) as the interaction geometry; hence the use of the extraordinary refractive index.

In general, E^2 contains dc, low-frequency ac, and high (optical) frequency components if the film is subjected to a combination of several optical fields. However, since nematic responses are slow, only the dc and low-frequency components produce nonvanishing reorientation responses. Consider the case where E is made up of the pump and probe beam and the first diffracted beam on the side of the pump. The other diffracted beam is generally very weak and plays a negligible role in these wave mixing processes, i.e.,

$$E = E_0 + E_1 + E_2 \tag{2}$$

where E_i's are given by

0018-9197/87/0200-0171$01.00

$$E_j = \tfrac{1}{2}\left(A_j(z)\, e^{i(\vec{k}_j \cdot \vec{r} - \omega_j t)} + \text{c.c.}\right), \quad j = 0, 1, 2 \quad (3)$$

and the A's are the amplitudes of the plane optical waves.

The intensity of the pump beam is much larger than that of the probe beam. In our experiment, the beam ratios used range from 10:1 to 10^2:1

Putting (3) and (2) into (1), we get

$$\begin{aligned}\epsilon_i = \epsilon_{eo} &+ \Delta\epsilon_e(\text{due to dc terms in } E^2) \\ &+ \frac{\epsilon_1}{2}\left[(A_0 A_1^* + A_2 A_0^*)e^{i(\vec{k}\cdot\vec{r}+\phi)}\right. \\ &\left. + (A_0^* A_1 + A_2^* A_0)e^{-i(\vec{k}\cdot\vec{r}+\phi)}\right] \\ &+ \text{higher order grating terms} \end{aligned} \quad (4)$$

where $\vec{k} = \vec{k}_0 - \vec{k}_1$, and ϕ is the phase shift between the refractive index grating and the intensity grating. For a Kerr medium like nematic liquid crystal film, ϕ is zero.

Following the usual coupled wave approach, we get the following equations for the amplitudes $A_j s'$, we get

$$\frac{\partial A_0}{\partial z} = \frac{i\epsilon_1\omega^2}{4c^2 k_0}\left(|A_1|^2 A_0 e^{i\phi} + 4A_0^* A_1 A_2 \cos\phi\right) \quad (5)$$

$$\frac{\partial A_1}{\partial z} = \frac{i\epsilon_1\omega^2}{4c^2 k_1}\left(|A_0|^2 A_1 + A_0^2 A_2^*\right)e^{-i\phi} \quad (6)$$

$$\frac{\partial A_2}{\partial z} = \frac{i\epsilon_1\omega^2}{4c^2 k_2}\left(|A_0|^2 A_2 + A_0^2 A_1^*\right)e^{i\phi} \quad (7)$$

where terms that are negligibly small are omitted. We have also ignored the phase-mismatch because we are considering very thin cells (200 μm) and large grating constant (grating $\sim$ 200 μm). In the usual treatment of two-wave mixing [3], the second terms on the RHS of (5)–(6) and the diffracted beam A_2 are neglected because of phase mismatch (in a thick sample, for example). The theory then shows that the coupling of A_0 and A_1 (i.e., exchange of their intensities) is vanishing if $\phi = 0$. In medium where ϕ is known to be vanishing, nonvanishing contribution to the energy exchanges between the beams is via the multiwave mixing effects that properly include the second terms of the RHS of (5)–(7) and the role played by A_2.

These equations are readily solved using numerical methods. However, one can readily show that in the small gain regime (and ignoring pump depletion) the gain in the intensity of beam 1 (via the grating term $A_0^2 A_2^*$), is proportional to the square of the intensity of the pump beam. This square dependence of the four-wave mixing term is different from the (small-signal) linear dependence of the two-wave mixing effect [via the first term on the RHS of (5)–(7)] on the pump intensity. We shall discuss our experimental results and our analysis.

Experiments and Analysis

Fig. 1(a) shows a schematic of the experimental setup. A strong pump beam and a relatively much weaker beam are crossed at the nematic film, creating an intensity grating in the y direction. The laser used is a linearly polarized Ar^+ laser (5145A) and the pump and probe beams are obtained with the use of a beam splitter and attenuators (placed on the probe beam). The liquid crystal used is a homeotropically aligned PCB (Pentyl-cyano-biphenyl) nematic film of thickness $\sim$200 μm. The two laser beams propagate in a plane that makes an angle β with the director axis of the film [c.f. Fig. 1(b)]. The film is maintained at room temperature (22°C). The crossing angles θ between the two beams are varied from about 10^{-3} to about 10^{-2} rad. The pump beam is about 240 times intense than the probe beam. Other pump/probe beam ratios have also been used.

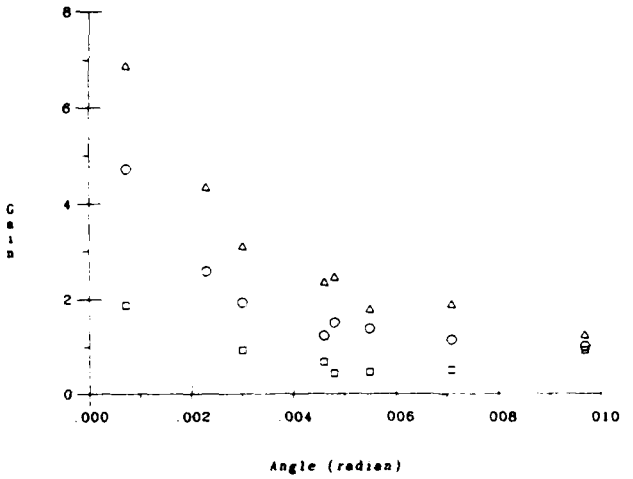

Fig. 2. (a) Circles: experimentally observed probed beam gain as a function of the crossing angle of the pump and probe beams when there is no frequency shift between the beams. (b) Triangles: probe beam gain when it is frequency down-shifted with respect to the pump beam frequency showing an enhancement. (c) Squares: probe beam frequency upshifted, the gain is reduced.

In nematic films a previous study has shown that the magnitude of the optically induced reorientations depend on the grating spacing as well as the film thickness [4] (d). Indeed, the reorientation is inversely proportional to $(k^2 d^2 + 1)$, where $k = |\vec{k}_0 - \vec{k}| = 2\pi/\lambda g$ (λg: the grating spacing) is the magnitude of the grating wave vector. For optimum wave mixing efficiency, λg should be at least as large as d. This is experimentally observed before in our previous study of self-diffraction [3]. In the present case, the probe beam gain is also sensitively dependent on the grating spacing (which is related to the crossing angle θ by

$$\lambda g = \frac{\lambda_{op} \sin^{-1}\theta/2}{2}$$

where λ_{op} is the optical wavelength). Fig. 2(a) is a plot of the probe beam gain as a function of the wave mixing angle θ. At $\theta = 10^{-1}$ rad, there is hardly any gain. On the other hand, a gain (I_{out}/I_{in}) of 600 percent is observed for $\theta = 10^{-3}$ rad. The gain is observed at a pump beam intensity of about 2 W/cm^2, and a probe beam intensity that is 1/200 of the pump beam.

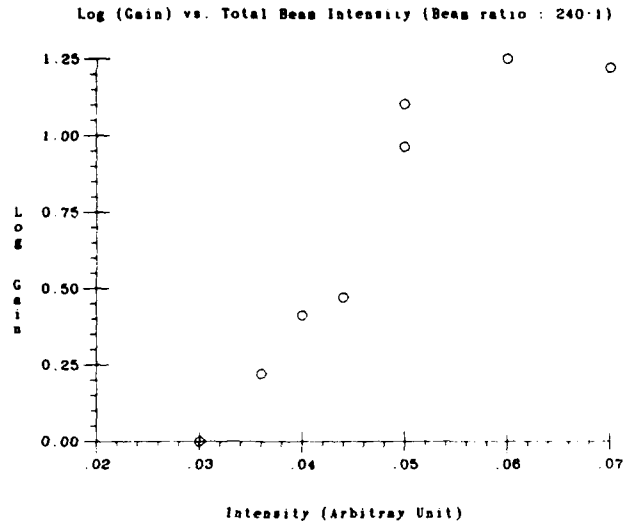

Fig. 3. Observed dependence of the probe beam gain as a function of the pump beam intensity (pump : probe beam ratio is 240 : 1).

Following the theory of optical field-induced nematic axis reorientation, we expect the refractive and the intensity gratings to coincide, i.e., no phase shifts between the two grating [3]. The amplification of the probe beam can therefore be explained in terms of four-wave couplings. There are two possible routes (which we term four-wave mixing processes) that scatter the pump beam into the probe beam directions: one is via a grating formed by beam 1 and the diffracted beam 3, and the other is via a grating formed by 0 and 2. The second one is predominant since beam 0 intensity is much larger than beam 1, while beam 2 intensity is much larger than that of beam 3.

In our experiment, both beams 2 and 3 are observed, and their intensities ratio (beam 2 : 3) is roughly the same as beam 0 : 1 ratio. As a result of these four-wave coupling processes the gain of beam 1 [defined as ln (transmitted probe intensity / input probe)] is a highly nonlinear function of the input pump intensities, cf., Fig. 3. Beam 1 grows almost as fast as the I_0^2 pump initially, which is typical of the four-wave coupling gain. Amplification is not observed under conditions (e.g., low pump beam intensity and/or large wave mixing angle) where beam 2 and 3 are not generated.

To create a phase shift between the refractive index grating and the intensity grating, we employed the technique used successfully by Huignard *et al.* in their studies involving BSO crystal, i.e., the probe beam is imparted a frequency shift ($\Omega = w_1 - w_2$) with respect to the pump beam. Following the usual two-wave coupling theory, we expect a positive gain contribution for $-\Omega$ and a negative gain for $+\Omega$. Fig. 2(b) and (c), obtained for negative and positive frequency shifts, respectively, confirm this theoretical expectation. The frequency shift Ω imparted on the probe beam is obtained by translating the mirror guiding the probe beam onto the film at a rate approximating one optical wavelength per one relaxation time constant τ. (Typical relaxation time of a 100 μm thick film is about a few seconds.) From Fig. 2(b) and 2(c), we note that as much as 40 percent gain (3*b*) or loss (3*c*) from the nonshifted value is created by this moving grating induced two-wave coupling process.

In conclusion, we have observed for the first time interesting two- and multiwave mixings induced probe beam amplification process. There are obvious details concerning these two processes such as theoretical solutions of the multiwave mixing equations, couplings between these processes, effects of sample thickness, etc., that remain to be thoroughly investigated. These problems, as well as the possibility of applying this beam amplification process to ring oscillations [5] and image amplifications [6] with visible and other type of laser sources (e.g., we have initiated studies with CO_2 lasers) are currently being investigated and will be reported elsewhere.

Acknowledgment

The technical assistance of R. R. Michael is appreciated.

References

[1] See, for example, I. C. Khoo and Y. R. Shen, "Liquid crystals: Nonlinear optical properties and processes," *Opt. Eng.*, vol. 24, pp. 579-585, 1985, and references therein; I.-C. Khoo, "Dynamic gratings and the associated self diffractions and wavefront conjugation processes in nematic liquid crystals," *IEEE J. Quantum Electron.*, vol. QE-22, pp. 1268-1275, Aug. 1986.

[2] J. F. Huignard, H. Rajbenbach, P. Refregier, and L. Solymar, "Wave mixing in photorefractive bismuth silicon oxide crystals and its applications," *Opt. Eng.*, vol. 24, pp. 586-592, 1985; J. Feinberg, "Optical phase conjugation in photorefractive materials," in *Optical Phase Conjugation*, R. A. Fisher, Ed. New York: Academic, 1983, ch. 11.

[3] See, for example, P. Yeh, "Exact solution of a nonlinear model of two-wave mixing in Kerr Media," *J. Opt. Soc. Amer.*, vol. B3, pp. 747-750, 1986, for an interesting theoretical discussion.

[4] I. C. Khoo, "Reexamination of the theory and experimental results of optically induced molecular reorientation and nonlinear diffractions in nematic liquid crystals: Spatial frequency and temperature dependence," *Phys. Rev.*, vol. A27, pp. 2747-2749, 1983.

[5] See, for example, J. O. White, M. Cronin-Golomb, B. Fisher, and A. Yario, "Coherent oscillation by self-induced gratings in the photorefractive crystal $BaTiO_3$," in *Optical Phase Conjugation*, R. A. Fisher, Ed. New York: Academic, 1983. J. Feinberg and G. D. Bacher, "Self-scanning of a continuous-wave dye laser having a phase-conjugating resonator cavity," *Opt. Lett.*, vol. 9, pp. 420-422, 1984; H. Raybenback and J. P. Huignard, "Self-induced coherent oscillations with photorefractive $Bi_{12}SiO_{20}$ amplifier," *Opt. Lett.*, vol. 10, pp. 137-139, 1985.

[6] F. Laert, T. Tschudi, and J. Albers, "Coherent CW image amplifier and oscillator using two-wave interaction in $BaTiO_3$ crystal," *Opt. Commun.*, vol. 47, pp. 387-390, 1983; J. Feinberg and R. W. Hellwarth, "Phase-conjugating mirror with continuous-wave gain," *Opt. Lett.*, vol. 5, pp. 519-521, 1980.

J-QE/23/8/15386

Simultaneous Occurrence of Phase Conjugation and Pulse Shortening in Stimulated Scattering in Liquid Crystal Mesophases

I.-C. Khoo
R. R. Michael, Jr.
P.-Y. Yan

Reprinted from: IEEE JOURNAL OF QUANTUM ELECTRONICS, Vol. QE-23, No. 8, AUG. 1987.

Simultaneous Occurrence of Phase Conjugation and Pulse Shortening in Stimulated Scattering in Liquid Crystal Mesophases

IAM-CHOON KHOO, SENIOR MEMBER, IEEE, ROBERT R. MICHAEL, JR., AND PEI-YANG YAN

Abstract—**We have observed for the first time simultaneous occurrence of phase conjugation and pulse shortening in stimulated back scattering of nanosecond laser pulses from thin film of smectic and nematic liquid crystals, and from thick samples of isotropic cholesterics. Aberration correction capability and high compression ratio are obtained.**

STIMULATED backward scattering (Brillouin, Raman, Rayleigh Wing, etc.) as an efficient single-input-wave phase conjugation process has received considerable interest recently [1]. As first studied by Zel'dovich *et al.* [2] in 1972, the effect took on a remarkable development in 1980 in the study by Hon [3], who demonstrated that the phase conjugated laser pulse is also highly compressed. Recently, Rao *et al.* [4] have shown that similar pulse compression can be achieved by stimulated Brillouin scattering in the isotropic phase of cholesteric liquid crystals. In their experiment, the sample was placed very far from the laser oscillator so that multiple or regenerative scattering and amplification of the backward scattered pulses (which account for the highly compressed pulses in Hon's study) were avoided.

In this paper, we report the observation of stimulated Brillouin scattering from thin films of nematic and smectics or bulk samples of isotropic liquid crystals (cholesterics) *where both phase conjugation and pulse shortening occur simultaneously*. Compression ratios as high as 20 and correction of severe distortions by the phase conjugation effect are observed. We have conducted experiments with several liquid crystals. In some cases, there is evidence of interference effects from stimulated Raman component. In the experimental results to be described below, the fundamental mechanism is attributed to stimulated Brillouin scattering.

For experiments involving the mesophases (i.e., nematic and smectic), the liquid crystal (4,4'-n-octyl-cyano-biphenyl, OCB) is used. OCB is smectic (*A*) in the temperature range 21.5–33.5°C and nematic in the range 33.5–40.5°C. A thick (250 μm) hometropically aligned film is fabricated with surfactant treatment on the glass slides and by applying an aligning dc field on the sample when it is cooling from the nematic to the smectic phase. The incident laser pulse is focused by a positive lens (focal length = 20.5 cm) into the film from one of the open side ends between the slides [as shown in Fig. 1(a)].

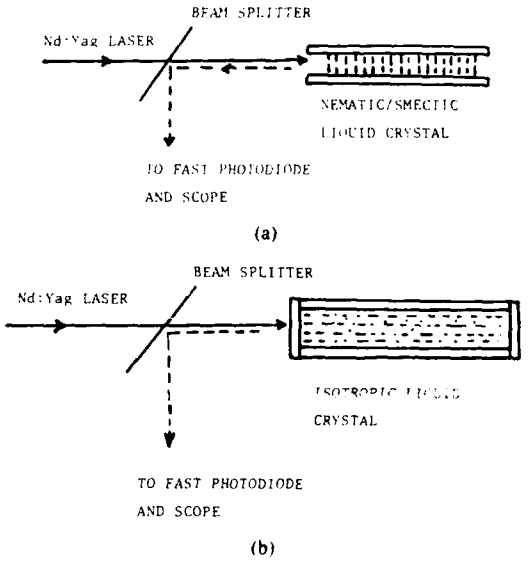

Fig. 1. (a) Schematic of the experimental set up for studying stimulated laser backscattering from smectic and nematic liquid crystal film. (b) Schematic for laser backscattering from isotropic liquid crystal sample.

For experiments involving the isotropic phase, we obtained very well defined phase conjugation and compressed pulses from bulk samples of the cholesteric (EM chemicals, TM74-A), which has a cholesteric → isotropic transition temperature 15.9°C. The liquid is placed in a 2.5 cm long area and maintained at a room temperature of 22°C. The laser pulse is focused by a 50 cm focal length lens into the cholesteric sample [Fig. 1(b)].

The laser pulses are from a *Q*-switched, frequency-doubled Molectron Nd:YAG laser that is nearly Gaussian in transverse profile. The laser pulse in general contains one strong mode and a much weaker second mode, but occasionally may contain two equally strong modes. Fig. 2(a) is a typical laser pulse, measuring about 20 ns FWHM. The laser pulse energy is measured with a joulemeter and

Manuscript received March 30, 1987; revised April 20, 1987. This work was supported in part by the National Science Foundation under Grant ECS8415387 and in part by the U.S. Air Force Office of Scientific Research under Contract AFOSR840375.

The authors are with the Department of Electrical Engineering, Pennsylvania State University, University Park, PA 16802.

IEEE Log Number 8715386.

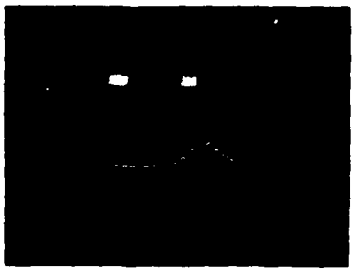

Fig. 2. Oscilloscope trace of a typical input laser pulse. Scale: 10 ns/div.

the backscattered light is monitored with a fast photodiode and a 400 MHz Tektronix storage scope. The laser is linearly polarized and is focused onto the nematic or smectic film with the polarization parallel to the director axis of the sample.

For the nematic and smectic film, a visible backscattered pulse (with an energy equal to about 1 percent of the input energy) is observed at an incident laser energy of 0.8 mJ (corresponding to a power of 40 kW). The estimated focal spot size of the laser at the entrance face of the film is 4×10^{-4} cm^2 (i.e., the laser pulse peak intensity is about 100 MW/cm^2). In spite of the severe aberration created at the irregular entrance surface of the smectic and nematic films, the backscattered laser appears nice and round and closely resembles the unaberrated laser. Fig. 3(a) is the reflection of the laser from the film surface showing the distortion imposed on the laser upon its entrance to the film. On the other hand, Fig. 3(b) shows the phase conjugation beam (for nematic and smectic film, the phase conjugated beam is surrounded with considerable noisy background, but for cholesteric isotropic phase, the phase conjugated signal is much clearer). The temporal dependence of the reflected pulse is depicted in Fig. 3(c), which shows that the laser is highly compressed. The phase conjugated pulse has an FWHM of about 2 ns. At higher input energy (>6 mJ), the stimulated Brillouin process is so strong that the liquid crystal at the entrance face is "pitted" away with a clearly audible click. At this point, the back-reflected signal disappears. Almost identical observations (i.e., threshold power, phase conjugation and shortening, etc.) are made in both the smectic and the nematic phase (obtained by warming the smectic film). We do not observe any "discontinuity" or unusual features as the smectic → nematic transition is passed. This is consistent with our previous studies of high-frequency acoustic waves in nematic and smectic phase [5], [6]. The sound velocities and attenuation constants (or lifetimes) are essentially the same in both phases. Since the acoustic lifetimes in these films (nematic and smectic) are on the order of 100 ns, the preceding observed phase conjugation and pulse shortening process is in a high gain transient regime. Because of the large attenuation (due to spurious orientational fluctuation scatterings) of the nematic and smectic film (typically about 25 dB/cm for nematic and 10 dB/cm for smectic), the so-called gain length in these films is not expected to be more than a few

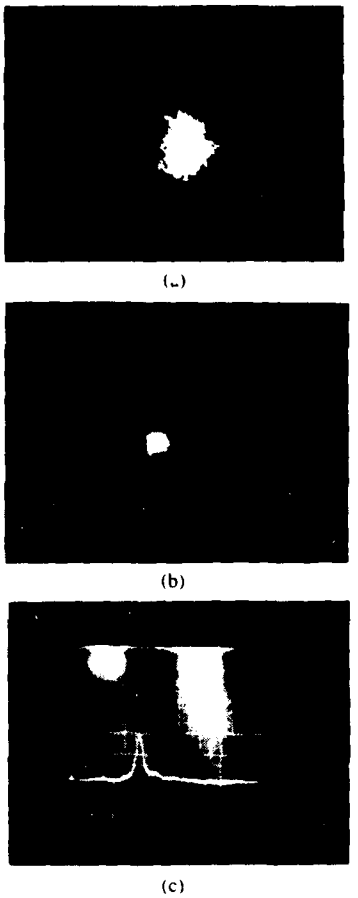

Fig. 3. (a) Photograph of the reflected beam from the entrance face of the smectic film (detected at a distance of 2 m from the entrance face). (b) Phase conjugated reflected beam detected at the image plane. (c) Oscilloscope trace of the reflected phase conjugated pulse. Time scale is 10 ns/div.

mm. That one could observe simultaneous phase conjugation and pulse shortening in these liquid crystal films is simply due to the high gain arising from the high electrostrictive constants of liquid crystals.

Before we proceed any further to discuss the effects observed in the isotropic phase, it is important to point out here that the type of "compression" observed in these studies is different from the so-called "true compression" observed in other studies involving very long interaction length (meters) [7], [8]. In our studies involving nematic and smectic films, the gain length is estimated to be a few mm's, and the experiment in the isotropic phase to be described below involves a gain length of about 2 cm or less. These "compressed" pulses may therefore be more properly called "spikes" associated with transient stimulated Brillouin scattering. At these input intensities (≈ 100 MW/cm^2), our previous studies of the same nematic and smectic films showed that there is considerable thermal buildup which may very well terminate these stimulated Brillouin scattering processes. What is interesting in these studies is that even under these adverse almost uncontrollable conditions, the back-reflected beam is very nicely phase conjugated.

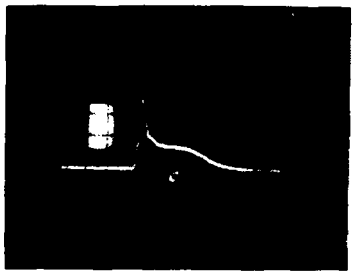

Fig. 4. Oscilloscope trace of the backscattered stimulated beams from isotropic MBBA and PCB samples, showing the presence of both Brillouin and Raman contribution. Scale: 10 ns/div.

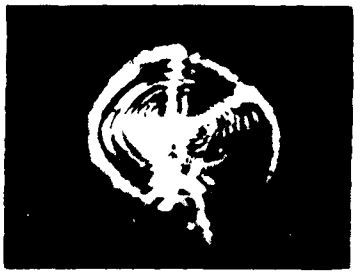

Fig. 5. Highly distorted laser beam after its passage through an aberrator before the cholesteric sample.

In the case of bulk isotropic liquid crystal, the observed results depend on the particular liquid crystal used. We have conducted experiments with isotropic nematic PCB (pentyl-cyano-biphenyl), nematic MBBA (methoxy-benzylidene-p-n-butylaniline), and cholesteric (EM chemicals, TM74A). In PCB and MBBA, we tend to observe a backscattered pulse of temporal behavior depicted in Fig. 4. Such temporal behavior is due to a combination of stimulated Raman and Brillouin scatterings [4], and in general, we do not observe good phase conjugation. On the other hand, the isotropic cholesteric (TM74A) consistently gives a very good phase conjugated beam (with aberration correction capability) and a nicely compressed temporal form similar to Fig. 3(c). Fig. 5(a), for example, shows how the beam is distorted after its passage through an aberrator placed before the sample. On the other hand, the stimulated reflected beam is practically distortion free [cf. Fig. 3(b)]. In the experiment on cholesteric, visible backscattered light is observed at an input energy of 1 mJ. The beam size on the sample is on the order 1.3×10^{-1} cm^2. (This corresponds to a threshold power of ≈ 50 kW or an intensity of 4 MW/cm^2.) The pulse energy needs to generate a similarly observable backscattered beam scale with the sample length (within the confocal length of the focused laser beam), i.e., for a sample length of 1 cm, we observe a two-fold increase in the threshold power.

At higher input energy (≈ 10 mJ), one notices multiple (two short) pulse formations, which are evidently caused by the multimode nature of the input pulse. The reflected pulses are compressed to an FWHM of about 2 ns [cf. Fig. 3(c)] and contain large "noisy" background besides an on-axis phase conjugated component. At this input energy, an almost permanent structural distortion is created along the path of the laser beam as evident by the high aberrated pattern of the transmitted beam that persists even as the input laser beam is reduced to very low energy. The origin of these structural changes is not clear, but they are probably due to bubbles formed within the laser path; they disappear when the sample is left alone for a day or so or momentarily warmed up. At room temperature, which is 6°C above the liquid crystal → isotropic transition point, the cholesteric is extremely viscous and highly correlated; the observed laser-induced index change effects could be due to a phase-transition form of critical expansion (or melting) as well as the electrostrictive mechanism. Molecular reorientations, which occur readily at these temperatures just above the transition point, are ruled out by results obtained with the use of circularly polarized light; we have observed similar pulse shortening and phase conjugation effects at similar laser energies for linearly and circularly polarized input beams.

In conclusion, we have observed for the first time the simultaneous occurrence of phase conjugation and pulse shortening in thin films of nematic and smectic films and in bulk isotropic cholesteric liquid crystals. In the latter case, we obtained a very good phase conjugated signal. Since it is possible to fill a long hollow tubing with such isotropic materials, a much longer interaction length can be achieved, thus requiring lower power and enabling true pulse compression. Work along this line is currently underway.

REFERENCES

[1] See, for example, *Optical Phase Conjugation*, R. A. Fisher, Ed. New York: Academic, 1983, ch. 6 by B. Ya. Zel'dovich *et al.* and ch. 7 by R. W. Hellwarth, and references therein, also, B. Ya. Zel'dovich *et al.*, *Principles of Phase Conjugation*. New York: Springer, 1985.

[2] B. Ya. Zel'dovich, V. I. Popovichev, V. V. Ragul'skii, and F. S. Faizullov, "Connection between the wave fronts of the reflected and exciting light in stimulated Mandel'shtam-Brillouin scattering," *Sov. Phys. JETP*, vol. 15, pp. 109-112, 1972.

[3] D. T. Hon, "Pulse compression by stimulated Brillouin scattering," *Opt. Lett.*, vol. 5, pp. 516-518, 1980.

[4] D. N. Ghosh Roy, D. V. G. L. N. Rao, and H. Bronk, "Optical pulse compression in a cholesteric liquid crystal," *Appl. Phys. Lett.*, vol. 39, p. 474, 1981. D. V. G. L. N. Rao and D. K. Agrawal, "Stimulated Raman scattering in a nematic liquid crystal," *Phys. Lett.*, pp. 383-384, 1971. *J. Appl. Phys.*, vol. 59, p. 332, 1986.

[5] I. C. Khoo and R. Normandin, "Nanosecond laser induced transient and erasable permanent grating diffractions and ultrasonic waves in a smectic film," *J. Appl. Phys.*, vol. 55, pp. 1416-418, 1984.

[6] —, "Nanosecond degenerate optical wave mixing and ultrasonic wave generation in the nematic phase of liquid crystals," *Opt. Lett.*, vol. 9, pp. 285-287, 1985.

[7] V. A. Gorbunov, *Sov. Phys. Tech. Phys.*, vol. 27, p. 1418, 1982; vol. 29, p. 1081, 1984.

[8] M. J. Damzen and H. Hutchinson, *IEEE J. Quantum Electron.*, vol. QE-19, p. 7, 1983. *Opt. Lett.*, vol. 8, p. 313, 1983. *IEEE J. Quantum Electron.*, vol. QE-21, p. 1558, 1985.

Iam-Choon Khoo (M'85-SM'86), for a photograph and biography, see p. 272 of the February 1987 issue of this JOURNAL.

Robert R. Michael, [redacted]. He received the B.S. (with distinction) and M.S. degrees in electrical engineering from The Pennsylvania State University, University Park, in 1984 and 1987, respectively.

Currently, he is a Ph.D. degree candidate, a research and teaching assistant, and a Dean's Fellow with the Department of Electrical Engineering, The Pennsylvania State University. His research interests include nonlinear optical properties and processes in liquid crystal films, as well as electrooptic and optooptic devices using liquid films and other nonlinear materials.

Pei-yang Yan [redacted]. She received the B.S. degree in physics from Nankai University, Tianjin, in 1981, and the M.S. degree in physics from Wayne State University, Detroit, MI, in 1983.

She is currently completing work towards the Ph.D degree in electrical engineering at The Pennsylvania State University, University Park.

Ms. Yan is a student member of the American Physical Society and IEEE Laser and Electro-Optics Society.

Reprinted from Journal of the Optical Society of America B, Vol. 4, page 886, June 1987

Transverse self-phase modulation and bistability in the transmission of a laser beam through a nonlinear thin film

I. C. Khoo, J. Y. Hou, T. H. Liu, P. Y. Yan, R. R. Michael, and G. M. Finn

Department of Electrical Engineering, The Pennsylvania State University, University Park, Pennsylvania 16802

Received October 13, 1986; accepted February 11, 1987

We present a theoretical study, with reference to experimental results, of transverse self-phase modulation effects in the transmission of a laser beam through a nonlinear thin film. The occurrence of interference rings, intensification or dimming of the on-axis beam intensity, and transverse optical bistability in the presence of a feedback can all be systematically documented in terms of geometrical/optical parameter classifications. These studies provide further insights and useful guides for experimental studies.

INTRODUCTION

The distortions of a laser beam after its passage through a nonlinear medium, in the form of self-focusing, self-defocusing, self-trapping, beam breakups, spatial ring formations, etc., have been studied ever since lasers were invented. In thick media, the laser experiences severe amplitude and phase distortions, and detailed analyses of the transmitted intensity have been rather complex and mostly numerical in nature.[1] Recently, with the discovery of highly nonlinear materials in the form of thin films, the problem of calculating the transmitted beam intensity takes on a much less complicated but nevertheless instructive form. In this case, the laser beam does not experience any appreciable loss or intensity modulation through the nonlinear film, and the transmitted intensity at the exit side of the nonlinear film can be accurately calculated by assuming that the laser simply acquires a nonlinear (i.e., intensity-dependent) transverse spatial phase shift. This problem has been studied by various researchers in various contexts.[2-5]

The writing of this paper is motivated by our (and others') recent work on optical switching[2] and limiting effects[6] due to the transverse nonlinear phase shift, the formation of spatial rings,[3] and the relationship between these effects and transverse optical bistability.[2-4] The last-named phenomenon occurs if part of the transmitted beam is reflected back onto the nonlinear film to provide a feedback. We start by analytically examining Kirchhoff's diffraction integral[7] and identifying the key parameters governing the nonlinear diffraction process. This examination leads to some natural and physically meaningful grouping or classification of the phases involved in the process. We will show that this reexamination enables us to classify the transmitted intensities into distinct characteristics and to make direct connections with observed self-phase modulation effects (focusing, defocusing, rings, etc.) and transverse optical bistability. Some experimental results are also presented in support of the theoretical analysis.

THEORY

Consider the transmission of a laser beam through a nonlinear thin film depicted schematically in Fig. 1. The film imparts an intensity-dependent and transversely varying phase shift to the beam. The intensity at a distance Z from the film, i.e., at the observation plane, may be calculated by using Kirchhoff's diffraction integral. Assuming that the incident laser beam is Gaussian, i.e., that it is at the entrance plane of the nonlinear film, we have

$$I(\text{laser}) = I_0 \exp\left(-\frac{2r^2}{\omega^2}\right),$$

where ω is the beam waist and I_0 is the on-axis intensity. A straightforward application of Kirchhoff's diffraction integral yields the intensity distribution at the observation plane:

$$I(r_1, Z) = \left(\frac{2\pi}{\lambda Z}\right)^2 I_0 \left| \int_0^\infty r\,dr J_0(2\pi r r_1/\lambda Z) \times \exp\left(\frac{-2r^2}{\omega^2}\right) \exp[-i(\phi_D + \phi_{NL})] \right|^2, \quad (1)$$

where the diffractive phase ϕ_D and the nonlinear- (intensity-) dependent phase ϕ_{NL} are given, respectively, by

$$\phi_D = k\left(\frac{r^2}{2Z} + \frac{r^2}{2R}\right), \quad (2)$$

$$\phi_{NL} = k\bar{n}_2 d I_0 \exp\left(-\frac{2r^2}{\omega^2}\right). \quad (3)$$

where $\bar{n}_2$ is the nonlinear refractive-index coefficient, $k = 2\pi/\lambda$, λ is the optical wavelength, and d is the thickness of the nonlinear film.

Using the following definitions:

$$v = r/\omega_0, \quad (4a)$$

$$C_1 = \frac{4\pi}{(\lambda z)^2}\omega_0^2, \quad (4b)$$

$$C_2 = \frac{2\pi}{\lambda}\omega_0 \tan\theta_m, \quad \tan\theta_m = \frac{\lambda}{\pi\omega_0}, \quad (4c)$$

$$C_3 = \frac{2\pi}{\lambda} n_2 I_0, \quad (4d)$$

0740-3224/87/060886-06$02.00

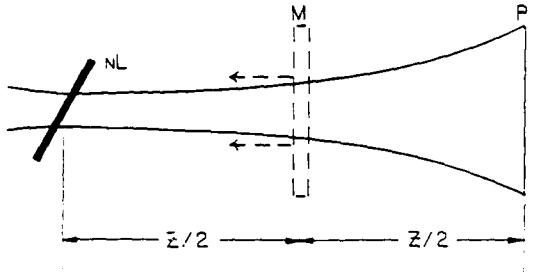

Fig. 1. Schematic of a laser beam passing through a nonlinear thin film (NL). P is the observation plane. A photodetector (not shown) monitors the intensity at various locations. M is a partially reflecting mirror to be used for providing feedback in transverse optical bistability study.

$$C_b = \frac{\pi}{\lambda}\omega^2\left(\frac{1}{Z}+\frac{1}{R}\right), \tag{4e}$$

and

$$\theta = \frac{r_1}{Z\tan\alpha_0}, \tag{4f}$$

we can rewrite Eq. (1) as

$$I(r_1, Z) = C_1 I_0 \left|\int_0^\infty \exp(-2y^2)y\exp\{-i[C_a\exp(-2y^2) + C_b y^2]\}J_0(C_2\theta y)\mathrm{d}y\right|^2. \tag{5}$$

ON-AXIS INTENSITY DISTRIBUTION (CURVATURE AND GEOMETRIC DISTANCE EFFECT)

There are a few important features that we can note here before we proceed with a numerical solution of Eq. (5). Because of the appearance of $f(y) = y\exp(-y^2)$ in the integrand, the integration rapidly converges for $y \gtrsim 2.5$ or so. The single most important factor in the integral value is the phase factor

$$\phi(y) = C_a\exp(-2y^2) + C_b y^2 \tag{6}$$

in the range of integration ($y = 0$ to $y \gtrsim 2.5$).

Consider, for example, the on-axis intensity [i.e., $\theta = 0$, $J(\theta) = 1$]. If the value of $\phi(y)$ remains fairly constant (i.e., if $\mathrm{d}\phi/\mathrm{d}y$ is small in the region $y \simeq 0.25$–1.5), then the integral for $I(r_1 = 0, Z)$ will give a large value.

The essence of our observations after several numerical computations and analyses lead us to discuss the problem (and, in a way, to classify the intensity distributions) in terms of the *relative* and absolute magnitudes of C_a and C_b.

Since C_a depends on $\bar{n}_2$ and on a postive variable I_0, it can assume either positive ($\bar{n}_2 > 0$) or negative ($\bar{n}_2 < 0$) values. We shall discuss the ($\bar{n}_2 > 0$) case in detail; the corresponding ($\bar{n}_2 < 0$) case will be obvious.

For ($\bar{n}_2 > 0$), consider the following three cases corresponding to typical values of I_0 at which diffraction rings are observed:

$$\text{(case a)} \quad C_a = 15, \qquad C_b = -4, \tag{7a}$$

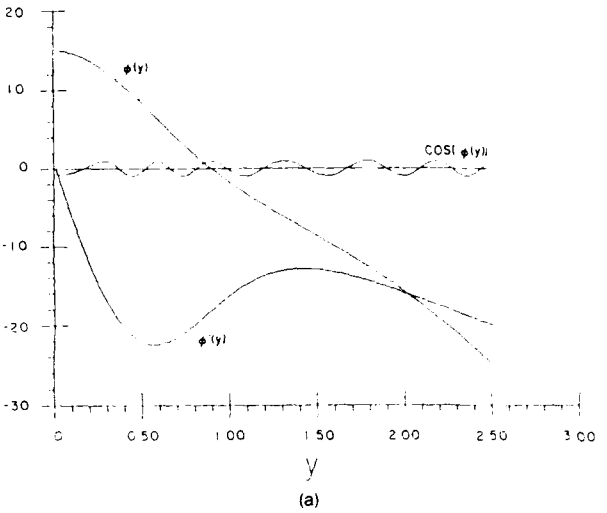

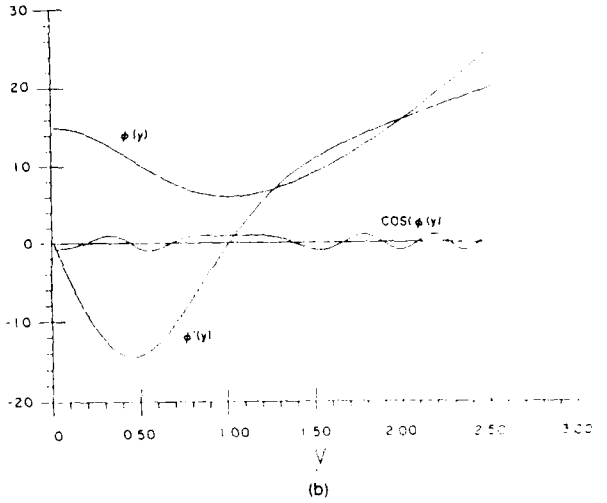

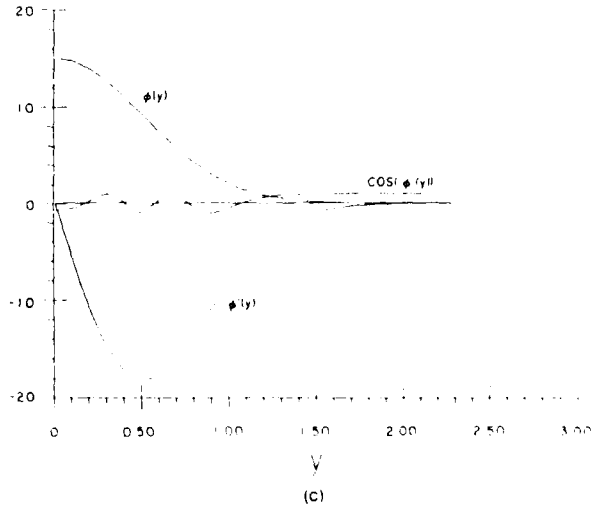

Fig. 2. (a) Plot of ϕ, $\phi' = \mathrm{d}\phi/\mathrm{d}y$, and $\cos\phi$ as a function of y [for y ranging from 0 to 3.00 for $C_a = 15$, $C_b = -4$, where C_a and C_b are defined in Eqs. (7)]. (b) Plot of ϕ, ϕ', and $\cos\phi$ as a function of y for case (b) in Eqs. (7). (c) Plot of ϕ, ϕ', and $\cos\phi$ for case (c) in Eqs. (7).

(case b) $C_a = 15, \quad C_b = 4,$ (7b)

(case c) $C_a = 15, \quad C_b = 0.$ (7c)

The parameters used in Eqs. (7) are $\omega = 0.03$ cm, $Z = 42.2$ cm, $R = 17.5$ cm, and $\lambda = 0.51$ μm. Figure 2(a) [corresponding to case (a)] shows that throughout the integration range that matters, $\cos\phi$ is an oscillatory function and the integrand gives a very small value for $I(0, Z)$.

Figure 2(b) [corresponding to case (b)] shows a plot of the phase factor ϕ as a function of y from 0 to 3.00. In the region $y \approx 0.7$–1.4 [which also corresponds to the region where the function $f(y)$ in the integrand assumes large values], $\cos\phi$ remains fairly constant (no oscillation). The integrand thus gives a large value for $I(0, Z)$.

A so-called intermediate region is the case described by Eqs. (7c). In this case, one notes that for $y \gtrsim 1.0$, $\cos\phi$ is almost constant. Thus the integrand will also give a large value for the on-axis intensity $I(0, Z)$.

In setting $C_a = 15$, we have, of course, chosen a value for $\bar{n}_2 d$, I_0 (i.e., the intensity I_0). Obviously, the intensity I_0 varies from 0 to some finite value. However, the above conclusions regarding the behavior of the on-axis intensity $I(r_1 = 0, Z)$ as a function of the *sign* and the *magnitude* of C_b remain valid for general values of I_0 [where the intensity-dependent $\phi(y)$ is significant]. In other words, for $n_2 > 0$, in general, under conditions when C_b is positive, one gets a bright central region in the far-field intensity distribution. If C_b is negative, then the on-axis region will be darkened.

From Eq. (4e) for C_b, we note that since ω and λ are fixed, the *sign and the magnitude* of C_b obviously depend on the *sign and the magnitude* of R, and on the magnitude of Z, through their *combined* effect in the factor $(1/Z + 1/R)$. These curvature (R) and distance (Z) effects have also been recognized in previous work, although we emphasize here the fact that Z and R must be considered together. In other words, it is incomplete and could be misleading to classify the transmitted intensity distribution due to *positive* or *negative* radii of curvature, since for either position or for negative values of R there exists a range of physically accessible values of Z that will make the factor $(1/Z + 1/R)$ positive.

The conclusions to be drawn in the case of negative $\bar{n}_2$ are almost the mirror image of the cases described in Eqs. (7). Concisely stated, we have the following:

$\bar{n}_2 < 0,$

$C_a = -15, \quad C_b = -4$ (bright on-axis intensity), (7a′)

$C_a = -15, \quad C_b = 4$ (dark on-axis intensity), (7b′)

$C_a = -15, \quad C_b \approx 0$ (transition region). (7c′)

RADIAL INTENSITY DISTRIBUTION

The profound effects of the phase factor $\phi(y)$ on the on-axis intensity are also reflected in the radial intensity distribution. The effects become apparent when C_a (which depends on the incident intensity I_0) assumes a value of the order of or greater than 2π. In that case, there is a phase shift of more than 2π experienced by the central portion of the beam compared with the wing portion. Since these two portions could have the same propagation constant, they could there-

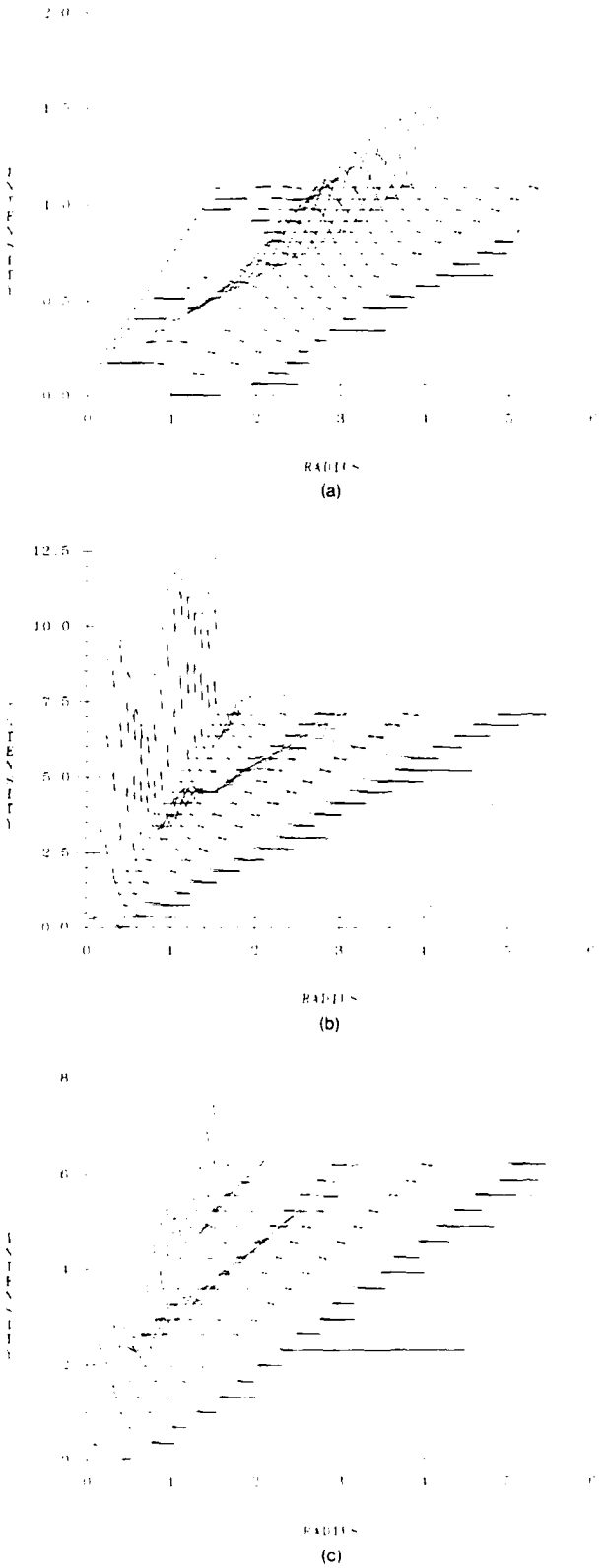

Fig. 3. (a) Plot of the radial intensity distribution (in units of ω) as a function of increasing input intensity corresponding to case (a) in Eqs. (7). (b) Plot of the radial intensity distribution as a function of increasing input intensity for case (b) in Eqs. (7). (c) Plot of the radial intensity distribution as a function of increasing input intensity for case (c) in Eqs. (7).

fore produce interference effects in the transmitted radial intensity pattern. Following the analysis in the preceding sections, we expect that these radial dependences will be quite different for various combinations of the values of C_a and C_b. Again, we can classify the intensity distributions in accordance with the three cases defined in Eqs. (7) [or in Eqs. (7') if we deal with negative $\bar{n}_2$].

For case (a), the intensity distribution is Gaussian at low incident intensity, as depicted in Fig. 3(a). As the incident intensity is increased, the power from the central region appears to be pushed out into the wing region; the whole distribution assumes a doughnut form, with the central intensity progressively suppressed. A further increase in the incident intensity shows that the central intensity begins to rise slightly and a second ring is pushed out. Relative to the value of the first peak, the central intensity is always lower, and thus one may say that, for this case, the intensity distribution is characterized (at high incident intensity I_0) by a dark central region surrounded by rings.

For case (b), the intensity distribution (at high incident intensity I_0) is characterized by a bright central region (which oscillates as a function of the incident intensity, but the oscillation minima are relatively *bright*). More and more rings appear on the wing as I_0 is increased.

Case (c) (for $C_b = 0$) appears to be a mixture of cases (a) and (b), and we can thus classify it as a transition region. The central spot appears bright or *dark* (i.e., the minimum is quite pronounced) as I_0 is increased. For $C_b \lesssim 0$, the overall pattern (not shown) tends to be more like that of case (a), and for $C_b \gtrsim 0$, the overall pattern tends to be more like that of case (b).

With the use of highly nonlinear thin films such as nematic liquid-crystal films, these theoretical results can be experimentally verified. For a nematic film and a laser-beam interaction geometry as depicted in the insert in Fig. 4, the nonlinearity $\bar{n}_2$ arises from the reorientation of the liquid-crystal director axis by the optical field. For a laser-beam size (ω) much greater than the film thickness, the response of the medium to a Gaussian laser beam is approximately Gaussian.[8] For typical values of the film used ($d \sim 100\ \mu$m, $\beta \simeq 22°$, $\Delta\epsilon \sim 0.8$), $\bar{n}_2 \sim 10^{-4}$ cm^2 W^{-1}. Figures 4(a) and 4(b) are the transmitted intensity distribution corresponding to cases (a) and (b) [as defined in Eqs. (7)], respectively.

For Fig. 4(a), the radius of curvature of the laser (Ar^+ 5145-Å line, $\omega = 0.3$ mm) R is -100 cm and $Z = 200$ cm (i.e., $1/Z + 1/R = -1/200$ cm^{-1}). The intensity pattern coincides with the theoretical one discussed in the preceding section. On the other hand, Fig. 4(b) [obtained by translating the sample to a plane where the radius of curvature $R = 400$ cm, and $Z = 400$ cm (i.e., $1/Z + 1/R = 1/200$ cm^{-1})] depicts the intensity distribution typical of case (b) described above.

We have not included here a detailed analysis of the number of rings appearing as a function of intensity in view of the work by Santamato and Shen.[5] These authors discuss the problem (for $\beta = 0$ in a nematic film) of these ring formations on the basis of the *curvature* (R) effect alone. As our preceding discussion shows, it is more appropriate to consider the problem by considering Z and R together through the

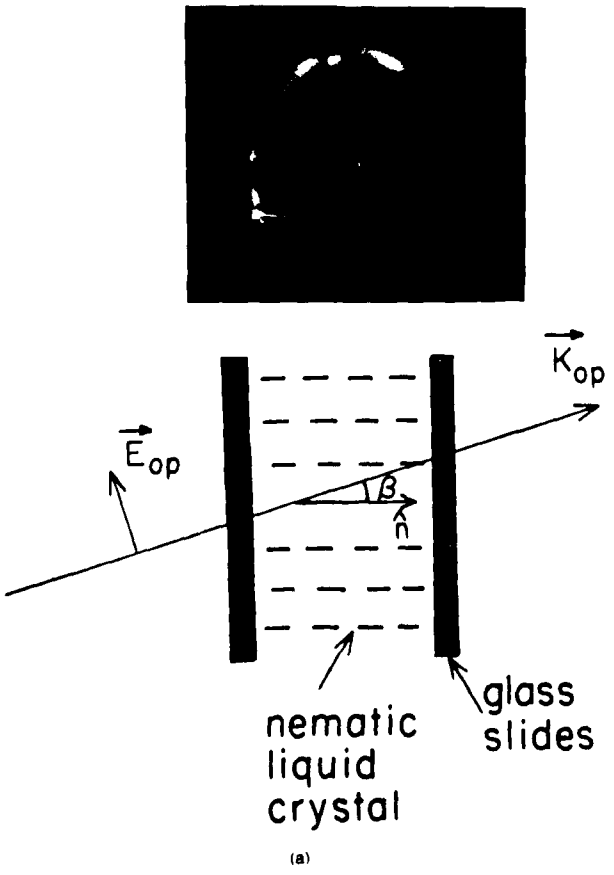

(a)

(b)

Fig. 4. (a) Experimentally observed far-field intensity distribution of a laser beam after its passage through a nonlinear thin film for case (a) defined in Eqs. (7), i.e., for $1/Z + 1/R < 0$. The insert shows the geometry of the laser polarization with respect to the nematic-film director axis in a homeotropically aligned nematic film. (b) Experimentally observed far-field intensity for conditions corresponding to that defined in case (b) in Eqs. (7), i.e., $1/Z + 1/R > 0$.

factor $1/Z + 1/R$ in C_b. For the radius of curvature $R = -200$ cm used in Fig. 4(a), one can move the observation plan to $Z = 200/3$ cm. In that case, even though R is negative, $1/Z + 1/R$ gives 1/100, and we observed an intensity distribution resembling that of Fig. 4(b) rather than Fig. 4(a).

RELATION TO TRANSVERSE BISTABILITY

The major role that the diffraction geometrical factor C_b plays in the transverse self-phase modulation processes is also manifested in transverse optical bistability, which occurs if part of the transmitted intensity is reflected back onto the nonlinear film.[3] In that case, the nonlinear phase ϕ_{NL} in Eq. (3) contains an additional term that depends on the reflectivity R_m of the mirror, i.e., we have $\phi_{NL} \rightarrow \phi_{NL}'$, where ϕ_{NL}' is given by

$$\phi_{NL}' = k\bar{n}_2 d\left[I_0 \exp\left(\frac{-2r^2}{\omega^2}\right) + R_m I(r_1, Z)\right], \tag{8}$$

where, for convenience, we have assumed that the mirror is placed halfway between the film and the observation plane. Given Eqs. (1) and (8), one can see that $I(r_1, Z)$ is a function of an integral involving itself and may therefore contain multiple solutions. From a more physical point of view, the mirror partially images (for $R \neq 1$) the transmitted intensity distribution $I(r_1, Z)$ onto the film. For the reflected part to reinforce the phase shift caused by the Gaussian laser beam on the film, the intensity must also be of a similar type of distribution, i.e., the central portion must be bright and remain bright at higher intensity. This would occur if the geometrical condition described by C_b were such that C_b were positive, i.e.,

$$\frac{\pi}{\lambda}\omega^2\left(\frac{1}{Z} + \frac{1}{R}\right) > 0. \tag{9}$$

To get a quantitative expression for the geometrical relationship, we shall reexamine here the switching conditions for transverse bistability. Following the theoretical development of Ref. 3, the transmitted intensity distribution $I(r_1, Z)$, as well as the incident intensity, is expanded in a series form:

$$I(r_1, Z) = \sum_{n=0} (-1)^n A_{2n} r_1^{2n}. \tag{10}$$

We will consider only the first two terms in the expansion. Our previous study has shown that one can include *all* the terms in the incident intensity, i.e., a complete Gaussian function, but the results for switching behavior and condition are not appreciably different. We make this two-term approximation here for simplicity of presentation. The solutions for A_0 and A_2 are found by solving the equations

$$B_1 - B_2 U = (1 + U^2)^{-2}, \tag{11}$$

where

$$B_1 = \frac{8Z^4(1/2Z + 1/2R - 2\bar{n}_2 I_0 d/\omega^2)}{R_m \bar{n}_2 I_0 d\omega^6 k^4}, \tag{12}$$

$$B_2 = \frac{8Z^4}{R_m \bar{n}_2 I_0 d^2 k^2}, \tag{13}$$

$$U = \omega^2 k(1/2Z + 1/2R - 2\bar{n}_2 I_0 d/\omega^2 - \bar{n}_2 d R_m A_2), \tag{14}$$

and

$$A_0 = \frac{I_0}{4Z^2\left[(\omega^2 k)^{-2} + \left(1/2Z + 1/2R - \dfrac{2\bar{n}_2 I_0 d}{\omega^2} - \bar{n}_2 d R_m A_2\right)^2\right]}. \tag{15}$$

The analysis for the switching condition is most easily done by solving for U in Eq. (11) by graphic means. Figure 5 shows a plot of the functions $B_1 - B_2 U$ and $(1 + U^2)^{-2}$. It is obvious that, starting with $I_0 = 0$, the straight-line function will begin to acquire a smaller negative slope, while its intercept will move toward the left. In order for triple-valued solutions for U (and therefore for A_0 and A_2) to occur, a sufficient condition is that the magnitude of the slope of $B_1 - B_2 U$ (which is negative) be less than the maximum magnitude of the tangent (m) to the bell-shaped function on the positive-U side. Suppose that this occurs at an optical intensity I_c, i.e., that the sufficient condition is

$$m(I_c) > -1.04, \tag{16}$$

where 1.04 is the maximum magnitude of the tangent to the function $(1 + U^2)^{-2}$. Correspondingly, the intercept $b_x(I_c)$ of $B_1 - B_2 U$ with the U axis is given by

$$b_x(I_c) = 1.12. \tag{17}$$

From Eq. (17) we get

$$I_c = \frac{1}{2\bar{n}_2 d k}\left[\frac{\omega^2 k}{2}\left(\frac{1}{Z} + \frac{1}{R}\right) - 1.12\right]. \tag{18}$$

Note that, at $I = 0$, $b_x(I = 0) \geq 1.12$ for Eq. (17) to be obeyed. This means that the term inside the square brackets on the right-hand side of Eq. (18) must be positive. Inequality (16) states this more precisely.

From inequality (16) we get the sufficient condition for bistability as

$$\left[\left(\frac{1}{R} + \frac{1}{Z}\right)\right]\omega^2 k > \frac{30.8Z^4}{R_m(\omega^2 k)^4} + 2.24 \tag{19}$$

or

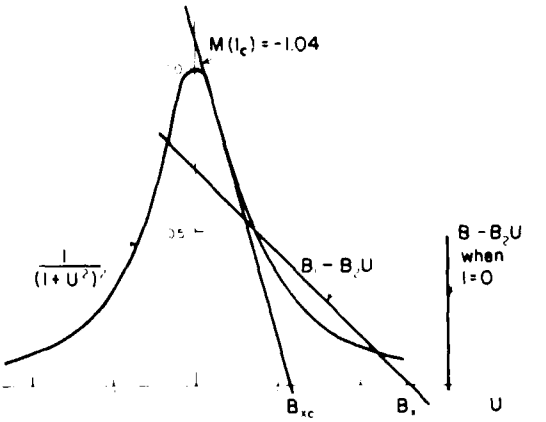

Fig. 5. Plot of the functions $B_1 - B_2 U$ and $(1 + U^2)^{-2}$ for solving U.

$$\frac{\pi\omega^2}{\lambda}\left(\frac{1}{R}+\frac{1}{Z}\right) > \frac{15.4Z^4}{R_m(\omega^2 k)^4} + 1.12$$

$$> 0. \tag{20}$$

Comparing condition (20) with condition (19), which is obtained by our self-phase modulation diffraction theory, we see that inequality (20) confirms our assertions exactly. Furthermore, the right-hand side of inequality (20) (for a given Z, λ, ω, and R_m) provides us with a numerical value (positive) for the geometry whereby transverse bistability is expected.

We mention that, for the negative $\bar{n}_2$ case, the conditions for the intensity distribution are almost mirror images of the positive $\bar{n}_2$ case. One can proceed in an analogous fashion and derive the condition for transverse bistability to occur and obtain the condition ($\bar{n}_2 < 0$)

$$\frac{\pi\omega^2}{\lambda}\left(\frac{1}{R}+\frac{1}{Z}\right) < -\left[\frac{15.4Z^4}{R_m(\omega^2 k)^4} + 1.12\right]$$

$$< 0. \tag{21}$$

Since Z, ω, and λ are all positive quantities, this condition means that, for negative $\bar{n}_2$, the incident laser beam must be of negative radius of curvature, and the mirror displacement $|Z|/2$ from the sample must not be larger than $|R|/2$. Notice here, of course, that for $\bar{n}_2 < 0$ the condition in inequality (21) would ensure that the feedback onto the sample consists of an intensity distribution that is bright in the on-axis region, i.e., a positive feedback.

Relations (20) and (21) can be put into an even more lucid form if we define a so-called confocal parameter $Z' = \pi\omega^2/\lambda$. They become, respectively,

$$\frac{\pi\omega^2}{\lambda}\left(\frac{1}{R}+\frac{1}{Z}\right) > \left[\frac{0.96}{Rm}\left(\frac{Z}{Z'}\right)^4 + 1.12\right] \qquad (\text{for } \bar{n}_2 > 0)$$

and

$$\frac{\pi\omega^2}{\lambda}\left(\frac{1}{R}+\frac{1}{Z}\right) < -\left[\frac{0.96}{Rm}\left(\frac{Z}{Z'}\right)^4 + 1.12\right] \qquad (\text{for } \bar{n}_2 < 0). \tag{22}$$

Notice here that these conditions for bistability are strictly geometrical and are independent of the value for $\bar{n}_2$. Bistability does depend on the mirror reflectivity R_m.

CONCLUSION

We have studied the problem of the transmitted transverse intensity distribution of a Gaussian laser beam after its passage through a nonlinear thin film. We found that, for both positive and negative nonlinearities, one can group together the geometrical/optical parameters involved into three distinct classes. These classifications allow us to gain further insights into the conditions for transverse optical bistability. Most of these conclusions are quite general in nature and may provide a good guide for experimental studies.

ACKNOWLEDGMENT

This research is supported by grant ECS8415387 from the National Science Foundation.

REFERENCES

1. See, for example, Y. R. Shen, *The Principles of Nonlinear Optics* (Wiley, New York, 1984), Chap. 17 and references therein; J. R. Reintjes, *Nonlinear Optical Parametric Processes in Liquids and Gases* (Academic, New York, 1984).
2. A. E. Kaplan, Opt. Lett. **6**, 360 (1981).
3. I. C. Khoo, P. Y. Yan, T. H. Liu, S. Shepard, and J. Y. Hou, Phys. Rev. A **29**, 2756 (1984).
4. M. Leberre, E. Ressayre, A. Tallet, K. Tai, and H. M. Gibbs, IEEE J. Quantum Electron. **QE-21**, 1404 (1986).
5. E. Santamato and Y. R. Shen, Opt. Lett. **9**, 564 (1984).
6. I. C. Khoo, G. M. Finn, R. R. Michael, and T. H. Liu, Opt. Lett. **11**, 227 (1986); J. A. Hermann, J. Opt. Soc. Am. A **1**, 729 (1984).
7. M. Born and E. Wolf, *Principles of Optics* (Macmillan, New York, 1964).
8. I. C. Khoo, Phys. Rev. A **25**, 1637 (1982); I. C. Khoo and T. H. Liu, Mol. Cryst. Liq. Cryst. **131**, 315 (1985).

Mol. Cryst. Liq. Cryst., 1987, Vol. 143, pp. 57-60
Photocopying permitted by license only

Printed in the United States of America

PROBE BEAM AMPLIFICATION VIA TWO AND FOUR WAVE MIXING IN A KERR-LIKE (LIQUID CRYSTAL) MEDIUM

I. C. Khoo and T. H. Liu

The Pennsylvania State University
Department of Electrical Engineering
University Park, PA 16802

Abstract

Probe beam amplification in a Kerr-like medium, e.g. a nematic liquid crystal film via 2-wave mixing is possible if it is stoke shifted relative to the pump beam. We report experiment observation of this effect and contribution from other multi-wave mixing effects.

Introduction

Two wave mixings, which were observed as early as the 60's by several workers, have received considerable renewed interests recently. In particular, for photorefractive materials where the medium responses are nonlocal (i.e. the refractive index grating is shifted relative to the intensity grating formed by the two incident light), these weak beam amplification effects have led to several interesting applications. For Kerr-like medium, i.e. where there is no phase shift between these two gratings, the gain of the weak beam via two wave mixing process can be achieved if a small frequency shift is imparted on the weak beam relative to the strong pump beam. As analyzed by Yeh[1] recently, for a Kerr medium, the complex phase shift imparted on the refractive index grating is related to the frequency shift Ω by

$$\phi = -\tan^{-1} \Omega\tau \qquad (1)$$

where τ is the relaxation time of the medium. The frequency shift ϕ appears in the coupled wave equations for the amplitudes A_1 and A_2 of two laser beams in a typical pump probe experiment set up.

$$\frac{\partial A_1}{\partial z} = \frac{-i\omega^2 n_o n_2 e^{-ix}}{2k\ c^2} \left| A_2 \right|^2 A_1 \qquad (2)$$

$$\frac{\partial A_2}{\partial z} = \frac{-i\omega^2 n_o n_2 e^{-i\phi}}{2kc^2} \left| A_1 \right|^2 A_2 \qquad (3)$$

where z is the direction of propagation of the wave, k is the propagation constant along z, ω is the frequency of the light, n_o is refractive index of the medium in the absence of optical field interactions, and n_2 is the nonlinearity coefficient. An exact solution of equation (2) and (3) shows that for ϕ=0, no gain or loss mechanism is possible.

In our experiment, the strong and a much weaker probe beams are derived from a linearly polarized A_r^+ laser (5145 A line). The liquid crystal used is a hometropically aligned PCB (Pentyl-cyano-biphenyl) nematic film of 200μm thick. The lasers propagate at an angle β relative to the nematic axis. The film is maintained at room temperature (22°C). The crossing angle between the two lasers are varied from about 1/300 to 10^{-2} radians. Frequency shifting of the probe beam is achieved by translating a mirror that directs the beam to the sample at a rate of one optical wavelength/sec^2.

Figures 1a-c summarize some of the experimental results, obtained for a pump to probe beam ratio of about 200:1. The laser beam size is about 3mm^2, and the pump power is about 35mWatt.

At a crossing angle of 0.007 radian, for example, one notes that the probe beam experiences no gain (circle). When the probe frequency is downshifted, there is a gain (triangle). On the other hand, if the probe beam is frequency upshifted, it experiences a loss (square). A measurement of the probe gain at this crossing angle also shows that the gain is an increasing function of the pump: probe beam ratio m, reaching a "saturated" value at m≈100.

What is interesting about figures 1b is that at smaller crossing angle, the probe beam experiences a large gain even without the frequency shift. We attribute this gain as arising from four wave mixing process involving the

scattering of the pump beam (into the probe beam direction) from a grating formed by the pump beam with the diffracted beam on the side of the pump beam. Our experimental result shows that imparting a negative frequency shift to the probe further enhances this gain while a positive frequency shift causes loss.

The overall dependence of the gain on the wave mixing angle is also consistent with our earlier theory and observation that increasing the wave mixing angle, i.e. smaller grating constant, will diminish the molecular reorientational response[3]. This is due to the fact that molecules situated at the intensity minima will create torques on molecules at the intensity maxima that reorient with respect to the field. Maximal response is obtained for grating constant on the order of, or larger than the nematic film thickness.

A complete detailed account of the theory and experiments will be presented in a longer article elsewhere.

This research is supported by a grant from the National Science Foundation ECS8415387 and in part by the Air Force Office of Scientific Research AFOSR840375.

References

1. P. Yeh, JOSA B3, 747 (1986).

2. J. P. Huignard, H. Rajbenbach, Ph. Refregier and L. Solymar, Opt. Eng. 24, 586 (1985).

3. I. C. Khoo, Phys. Rev. A27, 2747 (1983).

Figures

Figure 1a Triangles: observed probe beam gain as a function of the wave mixing angle when frequency downshifted.

Figure 1b Same as 1a, but no frequency shift.

Figure 1c With positive probe beam frequency shift.

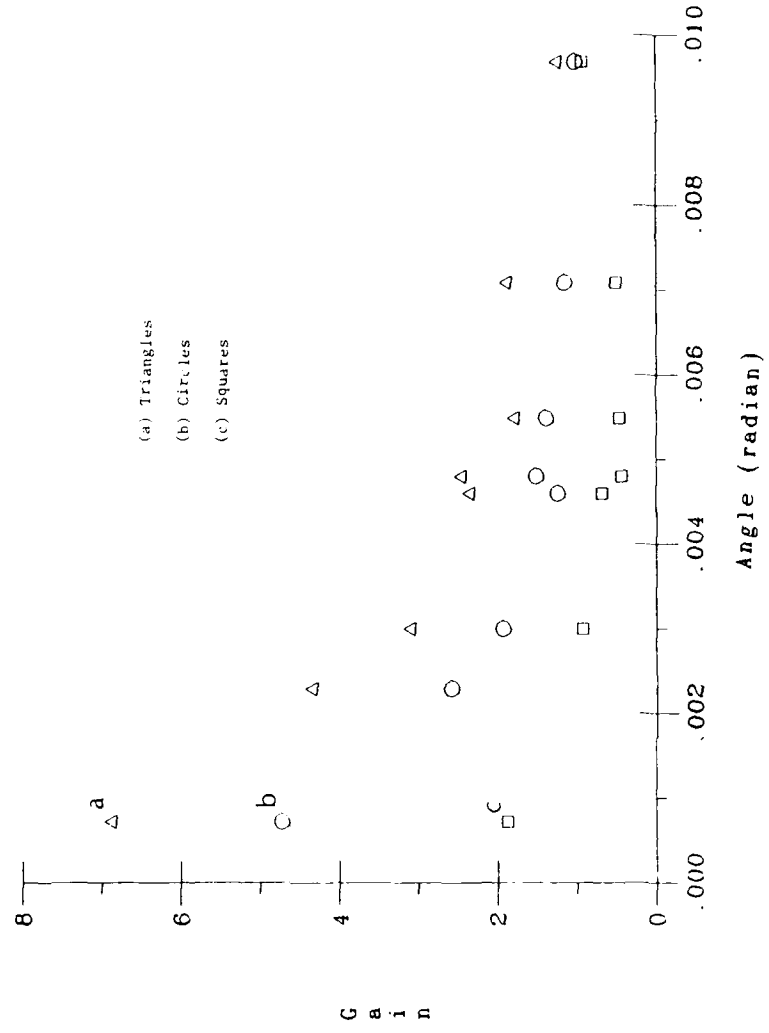
(a) Triangles
(b) Circles
(c) Squares
a
b
c
8
6
4
2
0
Gain
.000
.002
.004
.006
.008
.010
Angle (radian)

Nanosecond laser amplification via degenerate multiwave mixing in silicon

I. C. Khoo
Electrical Engineering Department, Pennsylvania State University, University Park, Pennsylvania 16802

R. Normandin
Division of Physics, National Research Council of Canada, Ohawa K1A OR6, Canada

(Received 27 July 1987; accepted for publication 9 December 1987)

We present the results of a detailed study of degenerate multiwave mixing mediated nanosecond 1.06 μm pulse amplification in silicon, taking into account higher order diffracted beams, self-phase modulation, pump depletions, intensity-dependent absorption losses, electron-hole plasma attenuation, and other geometrical optical parameters. Excellent agreements between theory and experiment are obtained.

Degenerate optical wave mixings in highly nonlinear media such as photorefractive crystals, semiconductors, liquid crystals, and organic materials have been vigorously studied in the past few years.[1-7] Among the various optical processes that are of fundamental and applied importance, phase conjugation and amplification of a probe beam have been well studied. Recently, we have shown that in highly nonlinear materials, the coupling between the pump and the diffracted beams could give rise to substantial amplification of the probe beam,[8,9] using liquid crystal as the nonlinear material.

In this letter, we apply our multiwave mixing theory to the nanosecond time scale in the semiconductor, where a fairly large Kerr-like nonlinearity can be induced by near-band-gap excitation with 1.06 μm laser pulses. Our theory explicitly and self-consistently accounts for several physical processes that have hitherto been overlooked or unaccounted for in other theories.[10,11] As a result, new theoretical perspectives on the wave mixing process are gained, and better agreements with theory are obtained.

Figure 1 is a schematic of the wave mixing geometry. A pump (E_1) and a probe (E_2) beam, coherent with respect to each other, are crossed on the nonlinear material, creating an intensity grating. For simplicity, both beams are linearly polarized, with their polarizations parallel to each other. In silicon, the nonlinearity is isotropic and Kerr-like, so that degenerate wave mixing mediated probe amplification will occur predominantly via the pump-diffracted (E_3) beam coupling. For crossing angles that are small (i.e., the phase mismatch is small), and using a relatively thin sample (in our case a 500-μm Si wafer), higher order diffracted beams (two orders or more) are generated. In the limit when the probe beam is weak compared to the pump (pump to probe ratio >20), the diffracted beams can be substantial compared to the probe, leading to substantial probe beam amplification, and higher order diffracted beams that are of comparable intensity to the probe.

As a first-order approximation toward a more accurate description of the process, therefore, one has to account for all these diffracted beams and their interplays. A theory[9] taking into account up to second-order diffracted beams has been developed for a general nonlinear medium, which takes into account these multiwave coupling effects, the intensity-dependent phase shifts experienced by all the beams, the phase mismatches, and interaction lengths.

The second-order degree of accuracy may be achieved by accurately accounting for the dominant processes under 1.06-μm nanosecond laser pulses in Si. For laser pulses shorter than the diffusion and recombination times of the photogenerated carriers (via indirect valence- to conduction-band transitions by the 1.06 μm radiation), the carrier concentration $N(t)$ is related to the optical intensity $I(t)$ by

$$\frac{\partial N(t)}{\partial t} = \frac{\alpha(T)}{\hbar\omega} I(t), \tag{1}$$

where $\alpha(T)$ is the linear absorption constant (which is temperature dependent). From the Drude model,[12,13] the change in refractive index is then given by

$$\Delta n = \frac{-e^2\tau\alpha(t)\sqrt{\pi}}{4nm_{eh}\omega^2\epsilon_0\hbar\omega} I(t). \tag{2}$$

One refinement that can be made to this estimate for Δn is to account for the temperature rise and the free-carrier absorption σ_{eh}. The temperature T is described by the equation (for short pulse)

$$C\frac{\partial T}{\partial t} = \sigma_{eh}(T)N(t)I(t), \tag{3}$$

where C is the heat capacity per unit volume. As a result of these temperature dependences of the various parameters, and the dependence of the temperature on the optical intensity, which in turn depends on these parameters, Eqs. (1)–(3) must be solved in a self-consistent manner, together with the coupled multiwave mixing equations (of Ref. 9). Details of this rather lengthy and involved computation will be presented in a longer article elsewhere. In this letter, we will report some of the important theoretical results pertaining to our experimental results.

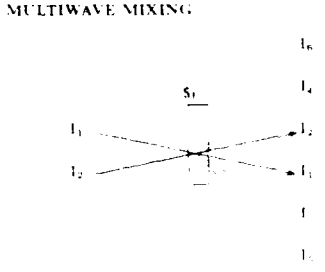

FIG. 1. Schematic of pump-probe generated multiwave mixings in a nonlinear medium.

 0003-6951/88/070525-03$01.00

In our study of pulse amplification, we found that the free-carrier absorption is particularly detrimental to the amplification process at the high end of the range of pump intensity used in the experiment (up to 8 MW/cm^2). Figures 2(a)–2(c) show the theoretically calculated attenuations of the pump beam in traversing a 500-μm-thick Si wafer for the experimental conditions: (pulse length $\tau = 20$ ns; $\lambda = 1.06$ μm; initial temperature $T = 300$ K). The linear absorption constant α is 10 cm^{-1}. Figure 2(a) shows the transmitted beam intensity if only the linear absorption is taken into account—a constant 80% loss for any input pump power. On the other hand, by accounting for the temperature dependences in both $\alpha(T)$ and $\sigma_{eh}(T)$, we obtain Figs. 2(b) and 2(c). Figure 2(b) shows the dependence of the transmitted *peak intensity* $I(t)$ on the input intensity. It shows that beyond an input intensity of about 3 MW/cm^2, the transmitted intensity actually begins to drop quite dramatically due to the free-carrier absorption. A less dramatic effect is seen if the *total* transmitted power is monitored [cf. Fig. 2(c)] (integrated over the laser beam width). This is understandable since the central portion of the laser suffers greater plasma attenuation.[14] Nevertheless, the transmission curve in Fig. 2(c) also shows "saturation" behavior at about 8 MW/cm^2 input beyond which the transmission begins to drop off. Experimentally, this intensity dependence manifests itself in the appearance of a darkened central spot in the transmitted laser pulse at high intensity (around 3 MW/cm^2).[14] In Ref. 14, the transmitted integrated and peak intensity dependences on the input intensity were also experimentally verified.

We have studied several effects associated with the multiwave mixing effects, and the experimentally observed data are in good agreement with the theory outlined above. Specifically, we have studied the probe amplification in a Si wafer under the following experimental conditions [Si thickness = 500 μm; incident lasers are p polarized and incident at the Brewster angle (about 60°) of the Si wafer; refractive index of Si = 3.56; crossing angles between the probe and pump beams are varied from 15×10^{-3} to 45×10^{-3} rad; pulse duration $\tau = 20$ ns; pump to probe beam ratio of 4500]. The laser pulses are obtained from a passively Q-switched single longitudinal mode (SLM) Nd-YAG laser. Data are recorded with a Tektronix R7912 transient waveform digitizer and analyzed only for good SLM operation. The nearly Gaussian in space and time laser pulses are detected by monitoring both the pulse energies and peak intensity. For comparison with theories, we use the data for the peak intensity.

Figures 3(a) and 3(b) are typical transient waveform digitizer traces. The upper trace [3(a)] is the probe pulse in the absence of pump, while the lower trace [3(b)] is when the pump is present. An amplification of the peak intensity by a factor of 6 is obtained. Figure 4 (circles) depicts a typical observed probe beam gain dependence on the input pump intensity, where the gain as defined by probe (presence of pump) − probe (no pump)]/probe (no pump)]. The crossing angle (in air) between the pump and the probe is 0.024 rad; this translates to a grating constant Λ of 44 μm. Using the value of diffusion constant $D \sim 19$ cm^2/s,[12] the grating diffusion time constant τ_g ($\tau_g = \Lambda^2/D$) is 25 ns. Using these values, as well as the parameters ($m_{eh} = 0.16\, m_e$; $n = 3.56$; heat capacity $C = 0.7$ J/g K, initial temperature $T = 300$ K), the theoretical curve [Figure 4(b) solid line] based on the theory outlined above is obtained. It shows a very good agreement with the experimental results. From the theoretical curve [4(b)], a value of $n_2 = 2\times10^{-12}$ SI units is extracted. Converting to the usual CGS units quoted in the literature, we obtained a $\chi^{(3)}_{CGS} = 4.4\times10^{-7}$ esu, which is very close to values obtained by other studies.[14] Figure 4(b) also shows that the "saturation" in the multiwave mixing gain occurs at an input intensity of about

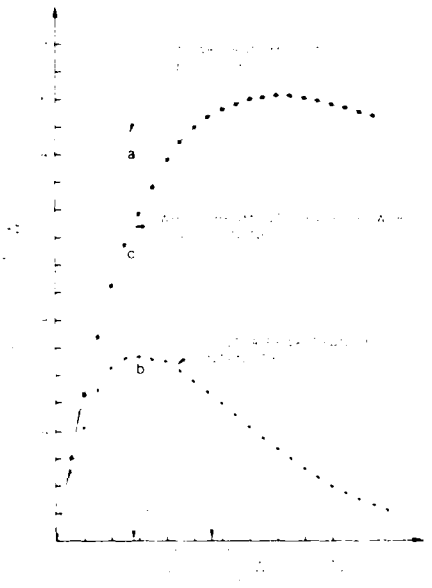

FIG. 2. (a) Plot of transmitted intensity vs input intensity assuming linear absorption, showing a constant transmission of 60%. (b) Plot of the integrated transmission vs the input intensity. (c) Plot of the peak central transmission vs the input intensity.

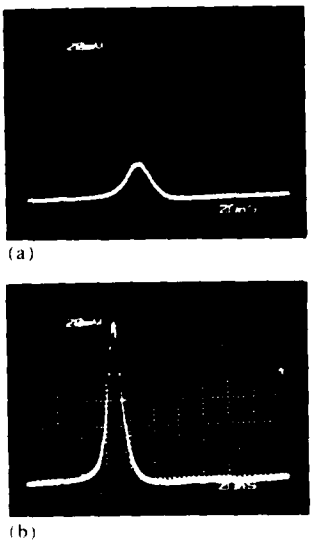

FIG. 3. (a) Oscilloscope trace of the transmitted probe beam in the absence of the pump beam. (b) Oscilloscope trace of the transmitted probe beam in the presence of the pump beam.

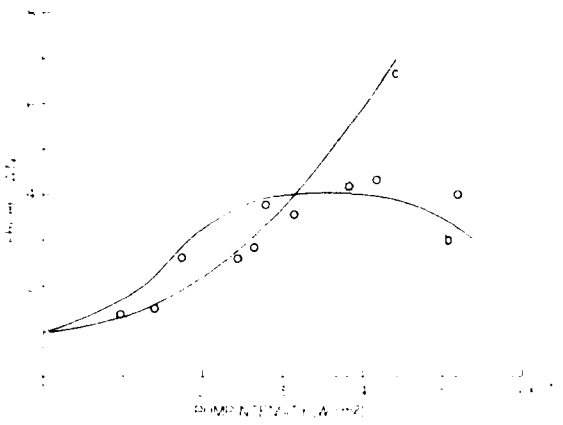

FIG. 4. (circles) Experimentally observed probe beam peak intensity gain as a function of the input beam intensity. (b) Theoretical fit using the multiwave mixing theory described in the text. (c) Theoretical curve based on usual degenerate four-wave mixing theory alone.

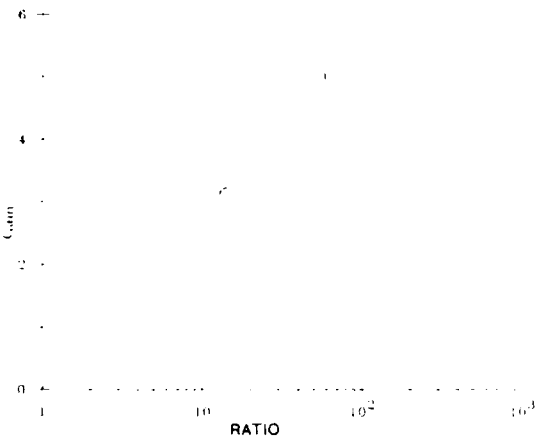

FIG. 5. Circles are experimentally observed probe gain as a function of the pump to probe beam ratio. Solid line is the theoretical fit.

6 MW/cm^2. On the other hand, Fig. 4(c) is a theoretical curve calculated *without* accounting for the free-carrier absorption, and it shows large deviation from the experimental results at high pump intensities. Saturation behavior in degenerate four-wave mixings in other semiconductors has also been observed by others.[15] However, in these studies, the effects of the diffracted beams in the multiwave mixings leading to probe beam gain were not included. In our study, the probe beam gain is due mainly to the pump-diffracted beam coupling and saturation behavior can come from the pump laser induced electron-hole plasma formation, and/or the multiwave coupling effects (cf. Ref. 9).

These multiwave mixing mediated probe amplification processes are very sensitive to the pump to probe beam ratio. Obviously for a pump:probe ratio of unity, there will be no gain. Figure 5 (circles) shows the experimentally observed probe gain as a function of the pump to probe beam ratio (for a fixed input pump energy of 5.5 mJ). The laser beam width is 4 mm in diameter at the location of the Si wafer, and thus the energy per unit area is 41 mJ/cm^2 (or intensity of about 1 MW/cm^2, where the free-carrier absorption effect is not too large). For this lower intensity pump beam we have to use a larger grating constant (i.e., smaller crossing angle θ). In our experiment, we use $\theta_{air} = 16\times10^{-3}$ rad, corresponding to a grating constant of about 100 μm, and a diffusion time constant $\tau_g = 54$ ns. The solid line is the theoretical curve calculated using the multiwave mixing theory as outlined in Eqs. (1)–(5). The theory fits the experimentally observed dependence very well, and gives a value of $n_2 = 3.5\times10^{-12}$ SI units ($\chi^{(3)}$ of 7.7×10^{-7} esu). The higher nonlinear coefficient is due to the larger grating constant used, which allows the buildup of higher refractive index modulation.

We have also studied the probe beam amplification dependence on the wave mixing angle (i.e., grating constant), the thickness of the silicon wafer, and the diffracted beam intensities as a function of the input. In general, we note that for samples of thickness ≤ 1 mm under the range of wave mixing angle used, *multiorder diffractions* are observed. These diffractions play a central role in the amplification of the probe beam and must be properly accounted for in the theory. Details of these experimental results and their corresponding theoretical analysis will be reported in a longer article elsewhere. In this letter, we have shown that it is possible to obtain substantial probe beam gain via this pump-diffracted beam coupling, and good agreement with our detailed multiwave mixing theory. Extension of our theory and experiment to the picosecond time scale and other nonlinear semiconductor materials is also possible.

This research is supported in part by the National Science Foundation ECS 8415387 and the Air Force Office of Scientific Research AFOSR 840375. We acknowledge the help of T. H. Liu in some computational assistance.

[1] B. Fischer, J. O. White, M. Gronin-Golomb, and A. Yariv, Opt. Lett. **11**, 239 (1986) and references therein.
[2] J. P. Huignard, H. Rajbenbach, Ph. Refregier, and L. Solymar, Opt. Eng. **24**, 588 (1985) and references therein on photorefractive crystals; A. E. Chiou and Pochi Yeh, Opt. Lett. **11**, 461 (1986).
[3] I. C. Khoo, IEEE J. Quantum Electron. **QE-22**, 1268 (1986), I. C. Khoo and Y. R. Shen, Opt. Eng. **24**, 579 (1985).
[4] M. T. Tsao, L. Wang, R. Jin, R. W. Sprague, G. Gigioli, H. M. Kuleke, Y. D. Li, H. M. Chou, H. M. Gibbs, and N. Peyghambarian, Opt. Eng. **26**, 41 (1987) and references therein on semiconductors.
[5] D. S. Chemla and J. Zyss, eds. *Nonlinear Optical Properties of Organic Molecules and Crystals* (Academic, New York, 1987).
[6] J. Kumar, G. Albanese, W. H. Steier, and M. Fiari, Opt. Lett. **12**, 120 (1987); M. B. Klein, Opt. Lett. **9**, 350 (1984); N. V. Kukhtarev, V. B. Markov, S. G. Odulov, M. S. Soskin, and V. L. Vinetskii, Ferroelectrics **22**, 949 (1979).
[7] D. S. Chemla, D. A. B. Miller, and P. W. Smith, Opt. Eng. **24**, 556 (1985).
[8] I. C. Khoo and T. H. Liu, IEEE J. Quantum Electron. **QE-23**, 171 (1987).
[9] T. H. Liu and I. C. Khoo, IEEE J. Quantum Electron. **QE-23**, 2020 (1987).
[10] R. Y. Chiao, P. L. Kelley, and E. Garmire, Phys. Rev. Lett. **17**, 1158 (1966); A. Maruani, IEEE J. Quantum Electron. **QE-16**, 558 (1980); P. Yeh, J. Opt. Soc. Am. B **3**, 747 (1986).
[11] R. K. Jain and M. B. Klein, Appl. Phys. Lett. **35**, 454 (1979); H. J. Eichler and M. Glotz, 1987 International Quantum Electronics Conference Technical Digest, pp. 12–13.
[12] H. J. Eichler, Opt. Commun. **45**, 62 (1983); J. P. Heritage and F. A. Beisser, IEEE J. Quantum Electron. **QE-17**, 2351 (1981).
[13] K. G. Svantesson and N. G. Nilsson, J. Phys. C **12**, 3837 (1979).
[14] R. Normandin, Can. J. Phys., Dec. issue (1987); see also R. Normandin, Opt. Lett. **11**, 751 (1986).
[15] See, for example, R. K. Jain and R. C. Lind, J. Opt. Soc. Am. **73**, 647 (1983); also R. K. Jain, M. B. Klein, and R. C. Lind, Opt. Lett. **4**, 328 (1979).

From: NONLINEAR OPTICAL AND ELECTROACTIVE POLYMERS
Edited by Paras N. Prasad and Donald R. Ulrich
(Plenum Publishing Corporation, 1988)

NONLINEAR OPTICAL PROCESSES AND APPLICATIONS IN THE INFRARED WITH NEMATIC LIQUID CRYSTALS

I. C. Khoo

Department of Electrical Engineering
The Pennsylvania State University
University Park, PA 16802

ABSTRACT

Nematic liquid crystal films possess several unique characteristics for applications in optical wave mixings and beam amplifications in the infrared spectral region. We present new theoretical understandings of optical multiwave mixing and beam amplifications in nematic liquid crystal films. Low power laser beams, with intensities of the order of a few Watts/cm^2, are found to be sufficient to generate large useful effects, in conjunction with the director axis reorientational and thermal nonlinearities.

INTRODUCTION

The unique characteristics of nematic liquid crystals[1] and nematic-cholesteric[2] mixtures for infrared applications have been recognized and applied in several electro-optical switching and modulation devices. They are relatively transparent in the infrared; they possess large birefringence ($\Delta n \approx 0.2$), and large operating temperature range (-20°C to 110°C) nematics are readily available commercially, and larger temperature ranges can be achieved with suitable mixtures. This is in addition to their well established fabrication technique, stability and low cost.

Nematic liquid crystals are also potentially excellent candidates for nonlinear optical processes. In addition to the characteristics mentioned above, they naturally possess two mechanisms for strong optical nonlinearities, namely, the director axis reorientational nonlinearity[3] and their large thermal index gradients near the phase transition temperature T_c[4]. In conjunction with visible lasers, these nonlinearities have been successfully utilized in a myriad of optical processes including bistability, switching, phase conjugation, stimulated scatterings, etc.[5] In some of these processes, for example, self-diffraction and beam amplifications[7], it was theoretically and experimentally shown that the efficiency of the process (via orientational nonlinearity) is critically dependent on the grating spacing; the efficiency increased tremendously with the increase in grating constant. With visible lasers, larger grating constants require correspondingly smaller crossing angles between the interference beams;

large grating constants ($\gtrsim$200μm) require that the visible laser be crossed at very small angles ($\lesssim 2 \times 10^{-3}$ rad), making any practical applications very cumbersome. As we will presently see, thermal grating mediated nonlinear effects are also critically dependent on the grating constant in a similar fashion. This special requirement on the grating constant is easily fulfilled with long wavelength (e.g., CO_2) lasers.

The underlying mechanism for phase conjugation, bistability, and other processes mentioned above are quite well known. In this paper, therefore, we will discuss in detail a new wave mixing processes that have recently been demonstrated using nematic liquid crystal films, namely, thermal grating mediated beam amplification via four wave mixing. As we will presently see, the process is particularly relevant to infrared application because of its requirement for a large grating constant for efficient wave mixing.

THERMAL GRATING MEDIATED MULTIWAVE MIXING

Consider the geometry of the laser-nematic interaction as depicted schematically in Fig. 1. The two lasers (pump and probe) produce an intensity grating in the x-direction (on the plane of the paper). We shall consider the case where the pump beam is much stronger than the probe beam in intensity. The physics of the multibeam couplings and heat diffusion in this system are described by the heat diffusion equation and the Maxwell wave equation, respectively.

$$-D_{\perp} \frac{\partial^2 T}{\partial x^2} - D_{//} \frac{\partial^2 T}{\partial z^2} = \frac{c\alpha |E|^2}{4\pi} \tag{1}$$

and

$$\nabla^2 E - \frac{n^2}{c^2} \frac{\partial^2 E}{\partial t^2} = \frac{4\pi w^2}{c^2} P_{NL} \tag{2}$$

where $\vec{E}$ is the optical electric field, $\vec{P}_{NL}$ the nonlinear polarization, T the temperature, α the absorption loss coefficent, and $D_{\perp}$ and $D_{//}$ are the thermal diffusion constant for direction perpendicular and parallel to the director axis, respectively.

In the plane wave approximation, the pump (E_0), probe (E_1) and diffracted beams (E_2) may be expressed as follows:

$$\begin{aligned} E_0(z) &= \varepsilon_0(z)\, e^{i\vec{k}_0 \cdot \vec{r}} = \varepsilon_0\, e^{ikz} \\ E_1(z) &= \varepsilon_1(z)\, e^{i\vec{k}_1 \cdot \vec{r}} = \varepsilon_1\, e^{ikz\cos\theta + ikx\sin\theta} \\ E_3(z) &= \varepsilon_3(z)\, e^{i\vec{k}_2 \cdot \vec{r}} = \varepsilon_2\, e^{ikz\cos\theta + ikx\sin\theta} \end{aligned} \tag{3}$$

where $k = n\omega/c$. Note that k_0 is along the $\hat{z}$-direction.

The generated polarization P^{NL} is given by

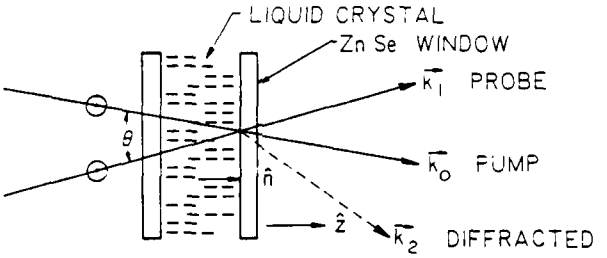

Fig. 1 Schematic of the pump-probe beam interaction in a nematic liquid crystal film. Both beams are linearly polarized in the direction of the plane of the paper.

$$P^{NL} = \frac{2n}{4\pi}\left(\frac{\partial n}{\partial T}\right)_{T_0}(E_1 + E_2 + E_3)\,\Delta T \tag{4}$$

where T_0 is the initial equilibrium temperature, and ΔT is the temperature rise.

Consider the $|E|^2$ term on the right hand side of (2). Using (3), we have

$$\begin{aligned}|E|^2 &= \{|E_0|^2 + |E_1|^2 + |E_2|^2 + E_0E_1^* + E_1E_2^* + E_0E_2^*\} + [c.c]\\ &= \{|\varepsilon_0|^2 + |\varepsilon_1|^2 + |\varepsilon_2|^2 + \varepsilon_0\varepsilon_1^* e^{ikx\sin\theta} + \varepsilon_0\varepsilon_2^* e^{ikx\sin\theta}\\ &\quad + \varepsilon_1\varepsilon_2^* e^{2ikx\sin\theta}\} + c.c.\end{aligned} \tag{5}$$

where for small θ, we have approximated $1-\cos\theta \approx 0$, i.e., we shall include effects coming from the first order in θ. Furthermore, in view of the fact that ε_1 and ε_2 are much smaller than ε_0 (usually ε_0 is about 10^2 times ε_1 or ε_2), we have

$$\begin{aligned}|E|^2 &= |E_0|^2 + |E_1|^2 + |E_2|^2 + (E_0E_1^* + E_2E_0^*)\,e^{-i\beta_0 x}\\ &\quad + (\varepsilon_1\varepsilon_0^* + \varepsilon_0\varepsilon_2^*)\,e^{i\beta_0 x} + \text{negligibly small terms}\end{aligned} \tag{6}$$

where $\beta_0 = k\sin\theta$.

If the laser beam sizes are much larger than the grating constant and the film thickness, then the solution for the temperature rise ΔT may be expressed in the form

$$\Delta T(x,z) = f_0(z) + f_1(z)\,e^{-i\beta_0 x} + f_2(z)\,e^{i\beta_0 x} \tag{7}$$

Substituting (6) and (7) into (2) gives

$$-D_{//}f_0'' = \bar{\alpha}\,(|\varepsilon_0|^2 + |\varepsilon_1|^2 + |\varepsilon_2|^2) \tag{8}$$

$$D_{\perp}\beta_0^2 f_1 - D_{//}f_1'' = \bar{\alpha}\,(\varepsilon_0\varepsilon_1^* + \varepsilon_0\varepsilon_2^*) \tag{9}$$

and

$$D_{\perp}\beta_0^2 f_2 - D_{//}f_2'' = \bar{\alpha}\,(\varepsilon_1\varepsilon_0^* + \varepsilon_0\varepsilon_2^*) \tag{10}$$

In standard differential equation forms, (8) - (10) become

$$f_0'' = -\frac{\bar{\alpha}}{D_{//}}\,(|\varepsilon_0|^2 + |\varepsilon_1|^2 + |\varepsilon_2|^2)$$

$$f_1'' = -\frac{D_{\perp}}{D_{//}}\beta_0^2 f_1 - \frac{\bar{\alpha}}{D_{//}}\,(\varepsilon_0\varepsilon_1^* + \varepsilon_2\varepsilon_0^*) \tag{12}$$

and

$$f_2'' = -\frac{D_\perp \beta_0^2}{D_{//}} f_2 - \frac{\bar{\alpha}}{D_{//}} (\varepsilon_1 \varepsilon_0^* + \varepsilon_0 \varepsilon_2^*) \tag{13}$$

From (4) and (7), we get

$$P_0^{NL} = \frac{2n}{4\pi} \left(\frac{2n}{\partial T}\right)_{T_0} (\varepsilon_0 f_0 + \varepsilon_1 f_1 + \varepsilon_2 f_2)\, e^{ikz} \tag{14}$$

$$P_1^{NL} = \frac{2n}{4\pi} \left(\frac{2n}{\partial T}\right)_{T_0} (\varepsilon_1 f_0 + \varepsilon_0 f_1)\, e^{ikz + ik\beta_0} \tag{15}$$

$$P_2^{NL} = \frac{2n}{4\pi} \left(\frac{2n}{0T}\right)_{T_0} (\varepsilon_2 f_0 + \varepsilon_0 f_1)\, e^{ikz - ik\beta_0} \tag{16}$$

Substituting these polarization terms into the corresponding Maxwell equations for ε_0, ε_1 and ε_2 and using the usual slowly varying envelope approximation[8] yields

$$\frac{\partial \varepsilon_0}{\partial z} = -i \frac{2n\omega^2}{c^2 k} \left(\frac{\partial n}{\partial T}\right)_{T_0} (\varepsilon_0 f_0 + \varepsilon_1 f_1 + \varepsilon_2 f_2) - \frac{\alpha}{2} \varepsilon_0 \tag{17}$$

$$\frac{\partial \varepsilon_1}{\partial z} = -i \frac{2n\omega^2}{c^2 k} \left(\frac{\partial n}{\partial T}\right)_{T_0} (\varepsilon_1 f_0 + \varepsilon_0 f_2) - \frac{\alpha}{2} \varepsilon_1 \tag{18}$$

$$\frac{\partial \varepsilon_2}{\partial z} = -i \frac{2n\omega^2}{c^2 k} \left(\frac{\partial n}{\partial T}\right)_{T_0} (\varepsilon_2 f_0 + \varepsilon_0 f_1) - \frac{\alpha}{2} \varepsilon_2 \tag{19}$$

where we have included the effect of the absorption loss in the last term on the R.H.S. of (17) - (19).

The coupled equations for the temperature distribution (11) - (13) and the Maxwell equations for the pump, probe and diffracted beams (17) - (19) form the basis for our theoretical and experimental studies of the various wave mixing processes (such as diffraction, beam amplification) that are mediated by the thermal grating. In this paper, we shall limit our discussion to the possiblity of probe beam amplification via the pump-diffracted beam coupling, and some experimental confirmation.

In analogy to similar wave mixing effects in a Kerr medium[7], the optical intensity grating terms on the R.H.S. of (11) - (13) may be classified into two distinct types. One arises from the interference between the pump and the probe beam (e.g., $\varepsilon_0 \varepsilon_1^*$ and $\varepsilon_1 \varepsilon_0^*$), which can give rise to probe beam gain only if the resulting refractive index is appropriately phase shifted to the intensity grating. The other arise from the interference between the pump and the diffracted beam ($\varepsilon_0 \varepsilon_2^*$ and $\varepsilon_2 \varepsilon_0^*$), which can give rise to probe beam gain without the phase shift requirement. This observation is borne out in the numerical solutions of equations (17) - (19).

Figure 2 shows a plot of the probe beam intensity as a function of the reduced distance z/d, for the parameters $I_0 = 80$ watt/cm^2, $I_1 = 0.8$

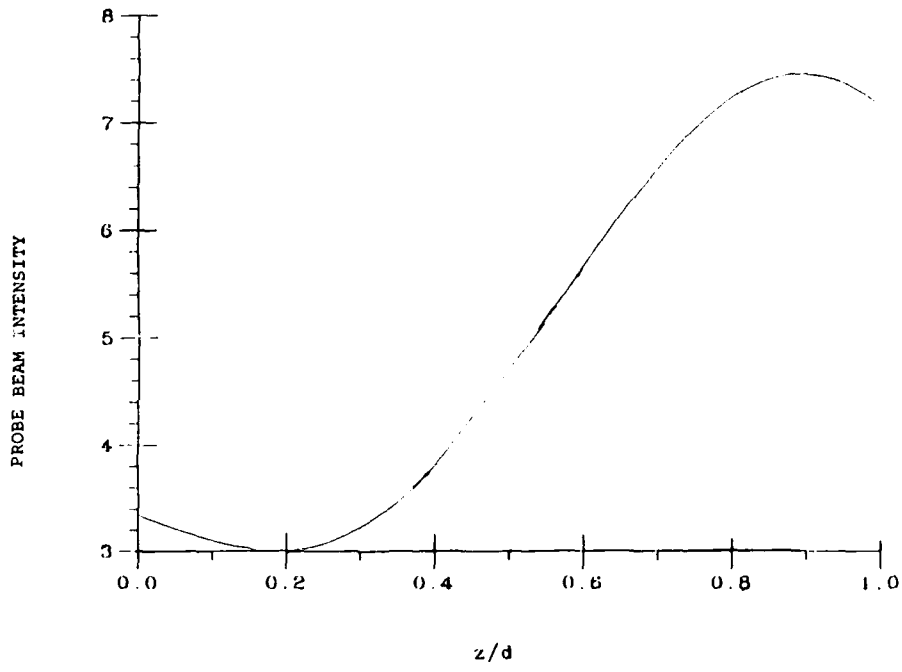

Fig. 2 Plot of the probe beam intensity as a function of the reduced distance z/d, showing amplification effect.

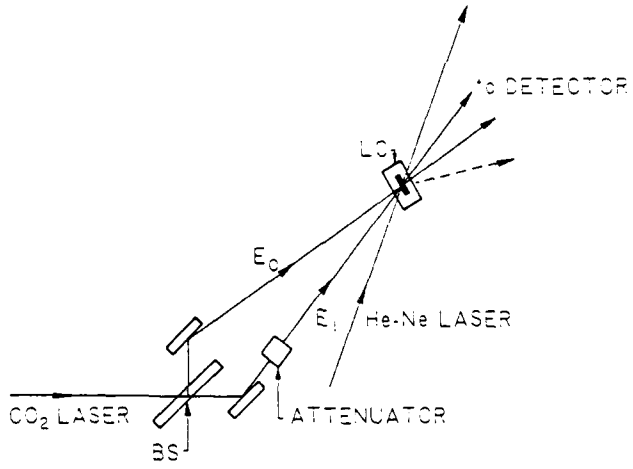

Fig. 3 Plot of the probe beam gain as a function of the grating constant.

watt/cm^2 (i.e, a pump/probe ratio of 100 to 1), a grating constant of

$$\Lambda = \frac{\lambda}{2 \sin(\theta/2)} = 300\mu m,$$

$d = 100\mu m$, $\alpha = 80\ cm^{-1}$ and $dn/dT = dn_0/dT = 10^{-3} K^{-1}$.

It shows a rather interesting result, i.e., that the probe beam intensity can be amplified by more than 200% in traversing this high-loss, but also highly nonlinear medium. For a different value for $\alpha[\alpha = 20\ cm^{-1}]$, we have also studied the dependence of the probe gain as a function of the grating constant (c.f., Fig. 3, which shows that larger gain can be achieved at larger grating constant). The physical reason is that larger grating constant can sustain larger temperature modulation, and therefore, a higher refractive index grating modulation.

Figure 4 is a schematic of the experimental setup. A TEM_{00} CO_2 laser beam (Advanced Kinetic Power-Lase 50) operating at very modest powers is split into a strong pump and a weak probe beam (Pump/probe intensity ratio is 60) and is overlapped on the sample at an (external) crossing angle of 2.3° (corresponding to a grating constant of about 500μm). The beam diameter on the sample is 4mm. The pump power is varied from 1.7 to 3.3 watt, and the power of the transmitted probe beam is monitored. The film is fabricated using ZnSe plates coated with surfactant for homeotropic alignment. The liquid crystal used is PCB (Pentyl-cyano-biphenyl) and the film is 120μm thick, maintained at a room temperature of 22°C. PCB has been shown in a previous study[2] to have good transmission characteristics at 10.6μm. However, it does absorb appreciably at 10.6μm (for d=100μm, $\alpha = 80\ cm^{-1}$) for thermal grating effects to occur readily.

At an input pump power of 1.7 watt (which amounts to 0.8 watt on the liquid crystal because of the 50% reflection loss at the air-(uncoated) ZnSe window interface), an increase of the transmitted probe beam of about 10% is observed. The probe beam gain is observed to be rather nonlinear with respect to the pump power (Fig. 5). At a pump power of 3 watt (intensity on the order of 25 watts/cm^2), a gain of 40%, is observed. Higher probe gain (>100%, not shown in Fig. 5) can be easily obtained by simply increasing the pump intensity. The magnitude of these probe gains for the parameters used in the experiment are in good agreement with the numerical solutions.

The beam amplification effect as described and demonstrated above can be applied in the construction of a ring oscillator[9] (c.f. Fig. 6). The liquid crystal is placed within a ring cavity. Noise originating from scattering from the pump laser (by the liquid crystal film) traveling along the direction of the axis of the ring cavity will form a grating with the pump beam and get amplified. When the amplification is greater than the loss (e.g., by increasing the pump laser power), a ring laser will be created, reaching a steady state value. The steady state corresponds to a probe beam intensity such that at that pump/probe ratio, the gain is just equal to the loss. In some preliminary study, we have observed such self-oscillation effects. Currently, efforts are underway to study this effect in greater details.

One other interesting application of these thermal grating (formed by the pump and the probe beam) is that it can be easily probed with a

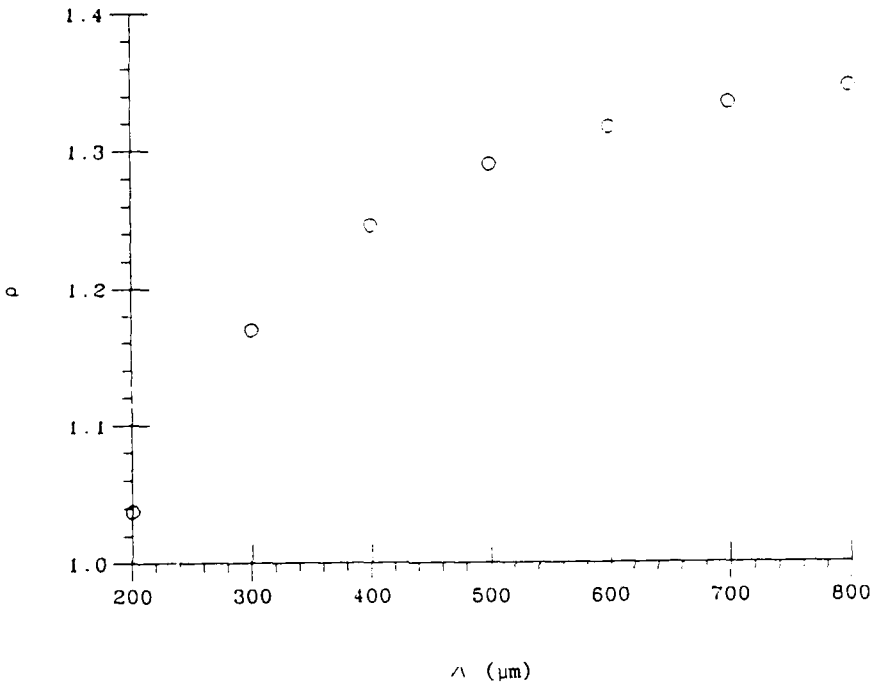

Fig. 4 Schematic of the experimental setup for CO_2 beam amplification. The He-Ne laser is for probing the grating formed by the CO_2 pump and probe beams.

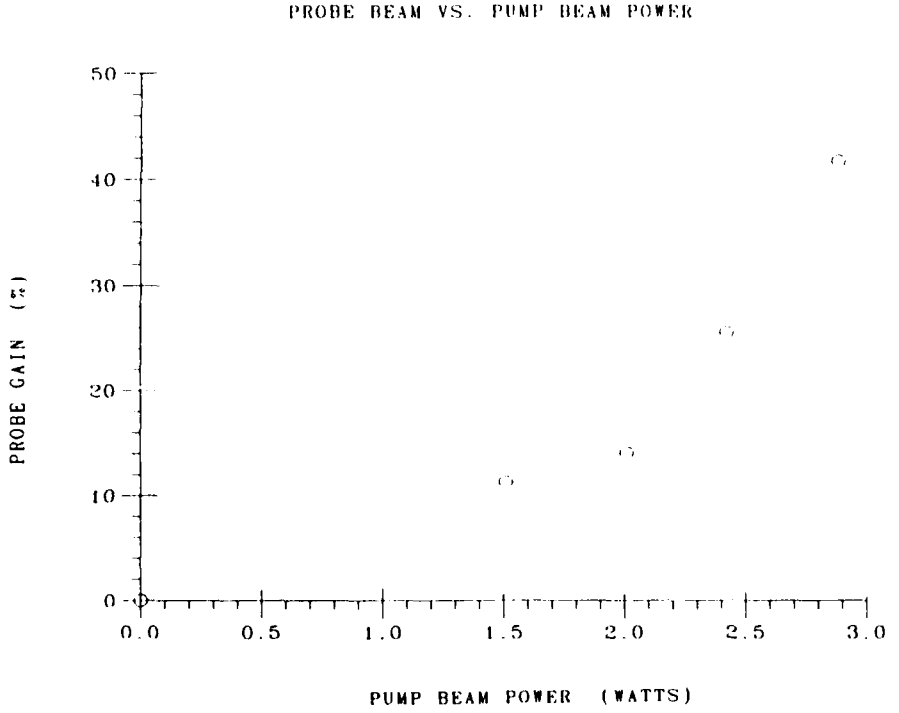

Fig. 5 Observed probe beam amplification dependence on pump beam power.

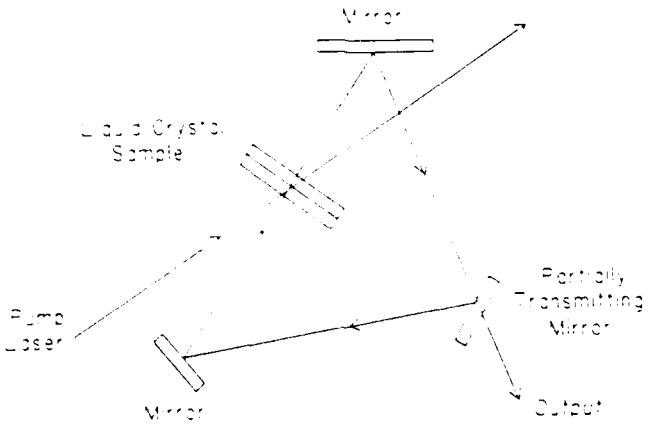

Fig. 6 One of several possible ring oscillators that can be constructed using the beam amplification effect.

visible laser. If the infrared probe beam is a image-bearing beam, obviously one can perform infrared to visible image conversion in a manner analogous to what has previously been observed with near-infrared (1.06μm) laser.[10] A preliminary experiment using this wavelength conversion process has been successfully tested with simple objects (lines, square aperture) and reconstruction with He-Ne. Currently, we are investigating imaging processes involving higher resolution objects.

The response time for all these processes depend inversely on the square of the characteristic thermal diffusion length (either the film thickness, or the grating constant, whichever is smaller). Our previous study has shown that typically for a 17μm grating constant, the decay time constant is 50μs. For a grating constant of 170μm, for example, the (decay) time is about 5ms, which is fairly fast for image processing or laser self-oscillations (compared to photorefractive crystals, for example). The build-up time, of course, depends on the type of laser used. With pulsed laser, it is possible to have a build-up time on the order of a few nanoseconds.[4]

This research is supported by the Air Force Office of Scientific Research under grant no. AFOSR 840375.

REFERENCES

1. See, for example, U. Efron, S. T. Wu and T. D. Bates, J. Opt. Soc. Am. B3, 247 (1986) and references therein.

2. See, for example, J. G. Pasko, J. Tracy and W. Elser, SPIE Proceedings on Active Optical Devices, Vol. 202, 82 (1979).

3. I. C. Khoo, Phys. Rev. A 25, 1637 (1982).

4. I. C. Khoo and R. Normandin, IEEE J. Quant. Electron. QE-21, 329 (1985).

5. See, for example, I. C. Khoo, IEEE J. Quant. Electron. JQE22, 1268 (1986).

6. I. C. Khoo, Phys. Rev. A 27, 2747, 1983.

7. I. C. Khoo and T. H. Liu, IEEE J. Quant. Electron. JQE23, 171 (1987).

8. J. F. Reintjes, "Nonlinear Optical Parametric Processes in Liquids and Gases," Academic Press, NY, 1984.

9. J. P. Huignard, H. Rajbenbach, Ph. Refregier and L. Solymar, Opt. Eng. 24, 586 (1985).

10. I. C. Khoo and R. Normandin, Appl. Phys. Letts. 47, 350 (1985).

Reprinted from Journal of the Optical Society of America B, Vol. 5, page 202, February 1988

Low-power (10.6-μm) laser-beam amplification by thermal-grating-mediated degenerate four-wave mixing in a nematic liquid-crystal film

I. C. Khoo, P. Y. Yan, G. M. Finn, T. H. Liu, and R. R. Michael

Department of Electrical Engineering, The Pennsylvania State University, University Park, Pennsylvania 16802

Received March 2, 1987; accepted September 28, 1987

We present a detailed theoretical analysis of degenerate four-wave mixing by a laser-induced thermal grating in a nematic liquid-crystal film. In particular, we show that the coupling of the (strong) pump beam to the first-order diffracted beam can give rise to substantial amplification of a (weak) probe beam. Experimental verification of this effect with a CO_2 laser beam is also made. A probe-beam gain of greater than 20 can easily be observed in a 120-μm film with a pump intensity of the order of a few watts per square centimeter.

1. INTRODUCTION

Degenerate optical wave mixing in highly nonlinear materials has been the subject of intensive research in the past few years. Various useful and novel processes have been experimentally demonstrated and are beginning to find application.[1] One of the phenomena associated with optical wave mixing is the amplification of one beam by another.[1-9] These two beams form an intensity grating on the medium that in turn creates a refractive-index grating through the underlying nonlinear mechanism. In the case of photorefractive materials,[3-5] the intensity grating is phase shifted with respect to the resultant index grating, thereby creating an energy-coupling mechanism between the two beams. In a Kerr-like medium, the phase shift is zero, and amplification of one beam by the other is possible, provided that the two input beams are appropriately frequency shifted.[6-8]

We recently showed that it is indeed possible to have amplification of a weak beam by a strong beam of the same frequency, even in a Kerr medium, provided that the mixing conditions favor the generation of the diffracted beam.[7] In that study, the nonlinearity is due to director axis reorientation, and the laser-induced refractive-index change (Δn) is proportional to the square modulus of the optical electric field, i.e., $\Delta n = n_2|E|^2$, where n_2 is the nonlinear coefficient and E is the optical electric field. In this paper we extend the study to another class of nonlinearity, namely, thermal nonlinearity that is induced by cw lasers. Because of heat diffusion within the liquid crystals and to the cell walls, the laser-induced refractive-index change Δn is, in general, a nonlocal function of the optical field, i.e., Δn is not simply dependent on the square modulus of the optical intensity at a particular point; for a given applied optical field, Δn must be solved subject to the boundary conditions. This change in refractive index, in turn, will affect the optical field distribution in the medium, and a correct solution of the temperature distribution, the refractive index, and the optical field within the nonlinear medium can be obtained only by self-consistent calculations, subject to the boundary conditions. Nevertheless, in Section 2, by identifying the various wave mixing terms in the basic coupled equations, we show that the basic mechanism for probe-beam amplification is similar to the four-wave mixing effect observed in Kerr media, i.e., the weak probe beam is amplified through the diffractions from the pump beam from a grating formed by the pump beam and the diffracted beam; cf. Fig. 1. For quantitative determination of the effect, a detailed numerical calculation is needed; it is presented in Section 2. Some preliminary experimental results are also presented.

We have conducted a beam-amplification experiment that uses a CO_2 laser for several reasons. One is to demonstrate explicitly that the extraordinarily large optical nonlinearity of liquid crystals can be applied to this spectral region, where few room-temperature, highly nonlinear materials exist. Second, because of the rather long wavelength of the CO_2 laser (compared with the usual ~0.5-μm wavelength of visible light), optical wave mixing involving large grating constants (>200 μm) presents no practical problems. Large grating constants permit efficient thermal-grating-mediated wave mixing in liquid crystals. There are other equally important reasons for extending the success of optical wave mixing effects in the visible and near-infrared regimes to the far-infrared regime. One is the possibility of constructing a ring oscillator and a self-pumped phase conjugator in the infrared (10.6-μm) region.

Figure 1 shows the geometry of the laser-nematic interaction. A strong pump beam ($\mathbf{k}_0$) intersects with a much weaker probe beam ($\mathbf{k}_1$), forming a thermal index grating in the liquid crystals. The first-order diffraction ($\mathbf{k}_2$) occurs on the side of the pump beam. (Because of the weakness of the probe beam, the diffraction on the probe-beam side is negligible.) The physics of the multibeam coupling and heat diffusion in this system is described by the Maxwell wave equation and the diffusion equation, respectively:

$$\nabla^2\mathbf{E} - \frac{n^2}{c^2}\frac{\partial^2\mathbf{E}}{\partial t^2} = \frac{4\pi\omega^2}{c^2}\mathbf{P}^{NL}, \tag{1}$$

and, at steady state,

$$-D_\perp\frac{d^2T}{\partial x^2} - D_\parallel\frac{\partial^2T}{\partial x^2} = \frac{\alpha|E|^2}{4\pi}. \tag{2}$$

0740-3224/88/020202-05$02.00

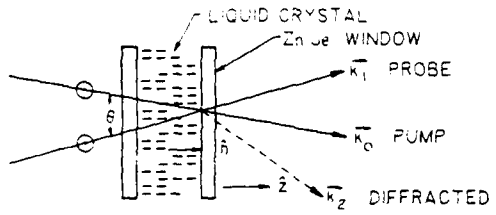

Fig. 1. Schematic of the amplification of a weak probe beam (E_1, $\mathbf{k}_1$) by a strong pump beam (E_0, $\mathbf{k}_0$) and the simultaneous generation of the principal diffracted beam (E_2). The laser is polarized in a direction perpendicular to the plane of the paper.

In Eqs. (1) and (2), $\mathbf{E}$ is the optical electric field, $\mathbf{P}^{\mathrm{NL}}$ the nonlinear polarization, T the temperature, α the absorption loss coefficient, and $D_\perp$ and $D_\parallel$ the thermal diffusion constants for directions perpendicular and parallel, respectively, to the director axis.

In the plane-wave approximation, the pump (E_0), probe (E_1), and diffracted beams (E_2) may be expressed as follows:

$$E_0(z) = \epsilon_0(z)\exp(i\mathbf{k}_0\cdot\mathbf{r}) = \epsilon_0\exp(ikz),$$

$$E_1(z) = \epsilon_1(z)\exp(i\mathbf{k}_1\cdot\mathbf{r}) = \epsilon_1\exp(ikz\cos\theta + ikx\sin\theta),$$

$$E_2(z) = \epsilon_2(z)\exp(i\mathbf{k}_2\cdot\mathbf{r}) = \epsilon_2\exp(ikz\cos\theta - ikx\sin\theta), \quad (3)$$

where $k = n\omega/c$. Note that $\mathbf{k}_0$ is along the $\hat{z}$ direction.

The generated polarization P^{NL} is given by

$$P^{\mathrm{NL}} = \frac{2n}{4\pi}\left(\frac{\partial n}{\partial T}\right)_{T_0}(E_0 + E_1 + E_2)\Delta T, \quad (4)$$

where T_0 is the initial equilibrium temperature and ΔT is the temperature rise.

Consider the $|E|^2$ term on the right-hand side of Eq. (2). Using Eq. (3), we have

$$\begin{aligned}|E|^2 &= [|E_0|^2 + |E_1|^2 + |E_2|^2 + E_0E_1^* \\ &\quad + E_1E_2^* + E_0E_2^* + \text{c.c.}] \\ &= [|\epsilon_0|^2 + |\epsilon_1|^2 + |\epsilon_2|^2 + \epsilon_0\epsilon_1^*\exp(ikx\sin\theta) + \epsilon_0\epsilon_2^* \\ &\quad \times \exp(ikx\sin\theta) + \epsilon_1\epsilon_2^*\exp(2ikx\sin\theta) + \text{c.c}], \end{aligned} \quad (5)$$

where, for small θ, we have approximated $1 - \cos\theta \approx 0$, i.e., we include effects coming from the first order in θ. Furthermore, in view of the fact that ϵ_1 and ϵ_2 are much smaller than ϵ_0 (usually ϵ_0 is about 10^2 times ϵ_1 or ϵ_2), we have

$$\begin{aligned}|E|^2 &= |\epsilon_0|^2 + |\epsilon_1|^2 + |\epsilon_2|^2 + (\epsilon_0\epsilon_1^* + \epsilon_2\epsilon_0^*)\exp(-i\beta_0x) \\ &\quad + (\epsilon_1\epsilon_0^* + \epsilon_0\epsilon_2^*)\exp(i\beta_0x), \end{aligned} \quad (6)$$

where $\beta_0 \equiv k\sin\theta$.

For the geometry depicted in Fig. 1, the temperature distribution may be assumed to be independent of the y dimension for laser-beam sizes that are much larger than the grating constant and the film thickness. (This is true in practice.) The solution for the temperature rise ΔT may thus be expressed in the form

$$\Delta T(x, z) = f_0(z) + f_1(z)\exp(-i\beta_0x) + f_2(z)\exp(i\beta_0x). \quad (7)$$

Substituting Eqs. (6) and (7) into Eq. (2) gives

$$-D\,f_0'' = \bar{\alpha}(|\epsilon_0|^2 + |\epsilon_1|^2 + |\epsilon_2|^2), \quad (8)$$

$$D_\perp\beta_0^2 f_1 - D\,f_1'' = \bar{\alpha}(\epsilon_0\epsilon_1^* + \epsilon_0\epsilon_2^*), \quad (9)$$

and

$$D_\perp\beta_0^2 f_2 - D\,f_2'' = \bar{\alpha}(\epsilon_1\epsilon_0^* + \epsilon_0\epsilon_2^*), \quad (10)$$

where $\bar{\alpha} = c\alpha/4\pi$ and double primes mean $\partial^2/\partial z^2$.

In standard differential-equation form, Eqs. (8)–(10) become

$$f_0'' = -\frac{\bar{\alpha}}{D}(|\epsilon_0|^2 + |\epsilon_1|^2 + \epsilon_2|^2), \quad (11)$$

$$f_1'' = -\frac{D_\perp}{D}\beta_0^2 f_1 + \frac{\bar{\alpha}}{D}(\epsilon_0\epsilon_1^* + \epsilon_2\epsilon_0^*), \quad (12)$$

and

$$f_2'' = -\frac{D_\perp\beta_0^2}{D}f_2 - \frac{\bar{\alpha}}{D}(\epsilon_1\epsilon_0^* + \epsilon_0\epsilon_2^*). \quad (13)$$

From Eqs. (4) and (7), we get

$$P_0^{\mathrm{NL}} = \frac{2n}{4\pi}\left(\frac{\partial n}{\partial T}\right)_{T_0}(\epsilon_0f_0 + \epsilon_1f_1 + \epsilon_2f_2)\exp(ikz), \quad (14)$$

$$P_1^{\mathrm{NL}} = \frac{2n}{4\pi}\left(\frac{\partial n}{\partial T}\right)_{T_0}(\epsilon_0f_0 + \epsilon_0f_2)\exp(ikz + ik\beta_0), \quad (15)$$

$$P_2^{\mathrm{NL}} = \frac{2n}{4\pi}\left(\frac{\partial n}{\partial T}\right)_{T_0}(\epsilon_0f_0 + \epsilon_0f_1)\exp(ikz - ik\beta_0). \quad (16)$$

Substituting these polarization terms into the corresponding Maxwell equations for ϵ_0, ϵ_1, and ϵ_2 yields

$$\frac{\partial\epsilon_0}{\partial z} = -i\frac{2n\omega^2}{c^2k}\left(\frac{\partial n}{\partial T}\right)_{T_0}(\epsilon_0f_0 + \epsilon_1f_1 + \epsilon_2f_2) - \frac{\alpha}{2}\epsilon_0, \quad (17)$$

$$\frac{\partial\epsilon_1}{\partial z} = -i\frac{2n\omega^2}{c^2k}\left(\frac{\partial n}{\partial T}\right)_{T_0}(\epsilon_1f_0 + \epsilon_0f_2) - \frac{\alpha}{2}\epsilon_1, \quad (18)$$

$$\frac{\partial\epsilon_2}{\partial z} = -i\frac{2n\omega^2}{c^2k}\left(\frac{\partial n}{\partial T}\right)_{T_0}(\epsilon_2f_0 + \epsilon_0f_1) - \frac{\alpha}{2}\epsilon_2, \quad (19)$$

where we have included the effect of the absorption loss in the last terms on the right-hand sides of Eqs. (17)–(19).

The coupled equations for the temperature distribution [Eqs. (11)–(13)] and the Maxwell equations for the pump, probe, and diffracted beams [Eqs. (17)–(19)] form the basis for our theoretical and experimental studies of the various wave mixing processes (such as diffraction and beam amplification) that are mediated by the thermal grating. In this paper we shall limit our discussion to the possibility of probe-beam amplification by the pump–diffracted-beam coupling and to some experimental confirmation.

2. DISCUSSION

The special problem associated with thermal nonlinearity is its nonlocal diffusive nature: the equilibrium temperature rise (and therefore the refractive-index change) at a point (x, z) is dependent on the boundary conditions imposed at various other points. Since f_2 involves ϵ_2, and since the magnitude of ϵ_2, the diffracted beam, grows from 0 at $z = 0$ to some finite value at $z = d$, f_2 is therefore an asymmetric function in reference to the midplane $z = d/2$. This asymmetry will be reflected in the grating term $f_2\epsilon_0$, which is responsible for the amplification of the probe beam (as we will see presently).

This asymmetry, in addition to the great variations of the probe beam (it can increase in magnitude by severalfold from $z = 0$ to $z = d$) and the pump beam (owing to losses), renders analytical solutions of these equations impossible. On the other hand, numerical iterative techniques can be employed to solve the problem from which various new insights into the multiwave coupling can be gained.

In analogy to similar wave mixing effects in a Kerr medium[10,11] the optical intensity grating terms on the right-hand sides of Eqs. (11)–(13) may be classified into two distinct types. One arises from the interference between the pump and the probe beams (e.g., $\epsilon_0\epsilon_1^*$ and $\epsilon_1\epsilon_0^*$), which can give rise to probe-beam gain only if the resulting refractive index is appropriately phase shifted to the intensity grating. The other arises from the interference between the pump and the diffracted beams ($\epsilon_0\epsilon_2^*$ and $\epsilon_2\epsilon_0^*$), which can give rise to probe-beam gain without the phase-shift requirement. This observation is borne out in the numerical solutions of Eqs. (17)–(19). Without accounting for the pump–diffracted-beam coupling, the pump- and probe-beam intensities are found to be monotonic decreasing functions of distance, and the main effect of the pump–probe interference is the generation of the diffracted beam. The formalism developed here, however, permits several detailed insights into the problem and the generalization of this diffraction effect to phase conjugation (which involves another strong beam). Optical phase conjugation with gain using thermal effects has been observed in several studies[12] with high-power nanosecond lasers. It is important to point out that the fundamental mechanism for gain in those four-wave mixing processes is different from the one under study here, which the phase-conjugated signal arises from four-wave mixing involving a retroreflected pump beam; i.e., the conjugated (reflected) probe beam and the amplification of the forward probe beam is due to the diffraction of the retroreflected pump beam from the grating set up by the pump and the probe beams. The effect of the diffracted beam was ignored in the previous studies.

Inclusion of the diffracted beam and the numerous gratings that can be formed among the pump, the probe, and the diffracted beams leads to numerous interesting theoretical conclusions. In this paper, we concentrate on some of the salient aspects of this pump–probe–diffracted-beam coupling pertaining to the probe-beam amplification process and the nonlocal nature of the thermal effect on the intensity distribution within the nonlocal media.

Figure 2a shows a plot of the diffracted-beam intensity as a function of the normalized distance z/d, for the parameters $I_0 = 80$ W/cm^2, $I_1 = 0.8$ W/cm^2 (i.e., a pump/probe ratio of 100/1), a grating constant $\Lambda = \lambda/[2\sin(\theta/2)] = 300$ μm, $d = 100$ μm, $\alpha = 80$ cm^{-1}, and $dn/dT = dn_0/dT = 10^{-3}$ K^{-1}. It shows the expected growth of the diffracted beam with distance. Owing to loss (from α), the dependence on z/d shows signs of saturation for $z = d$. For the same parameters, Fig. 2b shows that the corresponding pump-beam intensity decays monotonically by a considerable amount. Figure 2c shows a rather interesting result, i.e., that the probe-beam intensity can be amplified by more than 200% in traversing this high-loss, but also highly nonlinear, medium. Even higher amplification can be obtained at a higher pump intensity, and/or at a larger grating constant, or by using higher nonlinearity. (For a liquid crystal, higher thermal nonlinearity can be obtained either by bringing the sample temperature closer to the nematic → isotropic phase-transition temperature or by using $dn_\parallel/dT$ rather than $dn_\perp/dT$ at a given temperature.) Our detailed theoretical study has generalized this theory to include the interplay among various parameters and physical characteristics, such as intensity, losses, grating constant, thickness, phase mismatch, temperature, presence of other diffracted beams, frequency difference between the incident beams, anisotropies ($\Delta\epsilon$, $D_\parallel - D_\perp$), and pump–probe beams, and will be reported elsewhere.

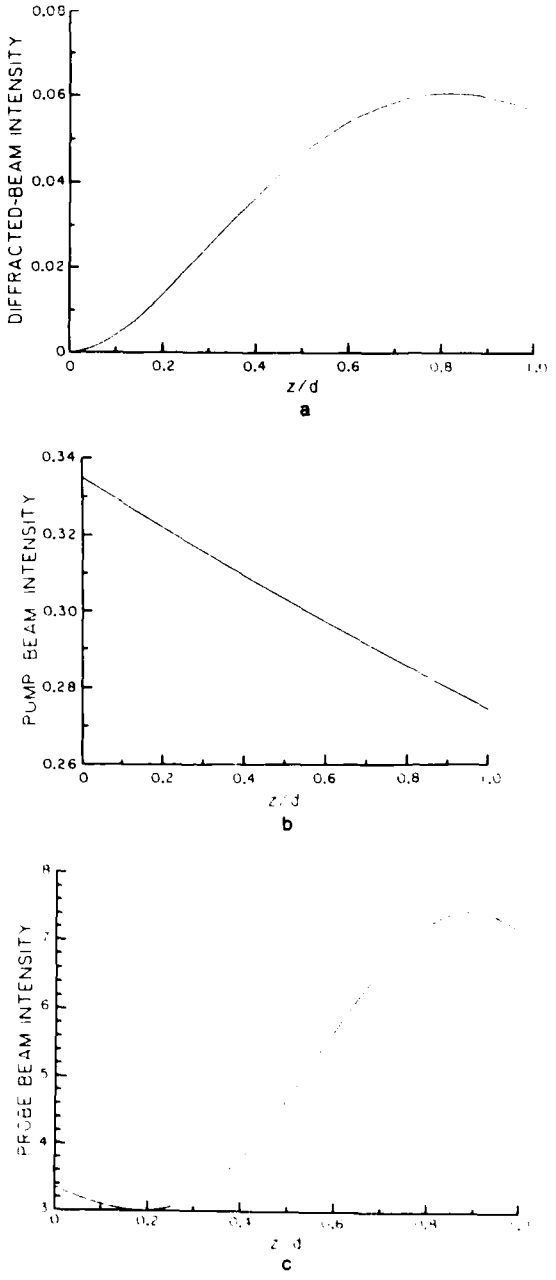

Fig. 2. a, Plot of the diffracted-beam intensity dependence on the reduced distance z/d. b, Plot of the pump-beam intensity as a function of propagation distance into the sample. c, Plot of the probe-beam intensity as a function of the distance z into the sample, showing gain at the exit plane.

In Section 3 we present what we deem to be more important information, i.e., some experimental confirmation.

3. EXPERIMENT

Figure 3 is a schematic of the experimental setup. A TEM_{00} CO_2 laser beam (Advanced Kinetic Power-Laser 50) operating in a cw or pulsed (msec) mode is split into a strong pump and a weak probe beam (the pump/probe intensity ratio is 60) and is overlapped on the sample at an (external) crossing angle of 2.3° (corresponding to a grating constant inside the liquid crystal of about 260 μm). The beam diameter at the sample is 4 mm. The pump power is varied from 1.7 to 3.3 W, and the power of the transmitted probe beam is monitored. The geometry of interaction of the laser polarization and propagation vectors with the liquid-crystal axis is shown in Fig. 1. The polarization is perpendicular to $\hat{n}$, the director axis of the nematic liquid-crystal film. The thermal index gradient is therefore given by dn_0/dT, where n_0 is the refractive index for ordinary rays.[13] The film is fabricated using ZnSe plates coated with a surfactant for homeotropic alignment. The liquid crystal used is pentylcyanobiphenyl (PCB), and the film is 120 μm thick, maintained at a room temperature of 22°C. PCB was shown in a previous study[13] to have good transmission charcteristics at 10.6 μm and does absorb appreciably at 10.6 μm ($\alpha = 80\ cm^{-1}$).

At an input pump power of 1.7 W [which is reduced to 0.8 W on the liquid crystal because of the 50% reflection loss at the air–(uncoated) ZnSe window interface], an increase of the transmitted probe beam of about 10% is observed. The probe-beam gain is observed to be rather nonlinear with respect to the pump power (cf Fig. 4), obeying close to an I^2 pump dependence. At a pump power of 3 W (intensity of the order of 25 W/cm^2), a gain of 40% is observed. The magnitude of these probe gains for the parameters used in the experiment is in good agreement with the numerical solutions (solid line in Fig. 4). The numerical solution is obtained using the parameters $\alpha = 80\ cm^{-1}$, thickness $d = 120\ \mu m$, $\theta = 2.3°$, and $dn_0/dT = 1 \times 10^{-3}\ K^{-1}$.

The basic mechanism responsible for the probe-beam gain is the scattering of the *much stronger* pump beam from the pump–diffracted-beam grating in the direction of the probe. Obviously, at an equal pump–probe-beam ratio, the probe gain will be zero. A higher pump–probe-beam intensity ratio will lead to a higher probe-beam amplification. This was verified experimentally. Figure 5 shows the experimentally observed probe-beam gain as a function of the pump-to-probe-beam ratio for the following parameters: pump power, 1.8 W; $\theta_{air} = 2.6°$; laser-beam size, 0.3 cm^2; initial sample temperature, 29°C. It shows that the probe gain saturates at a value of about 70% for a ratio >100. The experimentally observed dependence is in agreement with the theoretical prediction (Fig. 6). The thermal grating, owing to diffusion, is also highly sensitive to the grating constant. Smaller grating constants can sustain a smaller temperature difference and therefore a smaller refractive-index modulation. Using the same parameters as those used for Fig. 4, we observe that the gain drops from 40% at $\theta = 2.3°$ (i.e., $\Lambda \equiv 260\ \mu m$) to a vanishing value at $\theta > 10°$. This requirement of a large grating constant for appreciable amplification, incidentally, is (in practice) easily met by using infrared lasers (such as CO_2 and CO lasers). Although it is

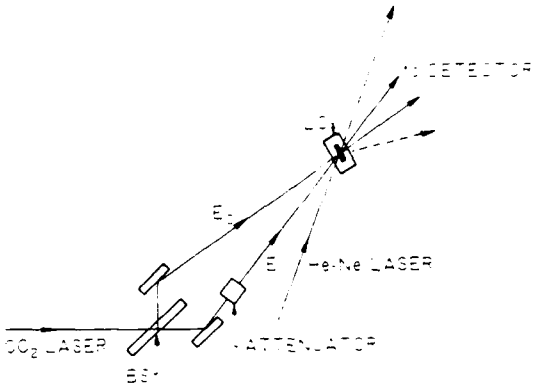

Fig. 3. Schematic of the experimental setup for CO_2 probe-laser amplification. The ratio of the pump-beam to the probe-beam intensity is 60 to 1. The He-Ne laser is for probing the grating. Diffractions from the He-Ne laser are easily visible with the eye. BS, beam splitter; LC, liquid crystal.

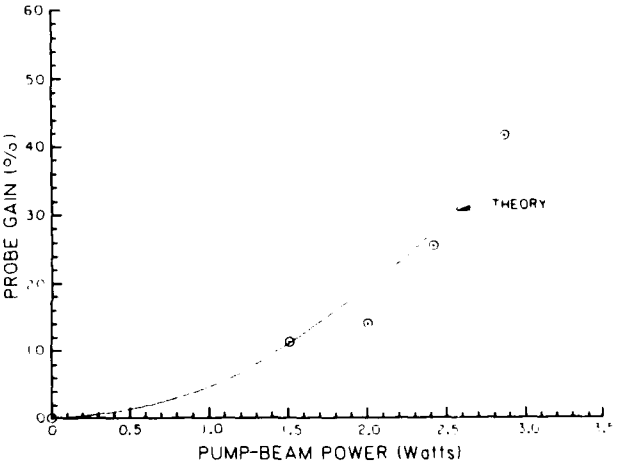

Fig. 4. Plot of the observed probe-beam gain as a function of the pump-beam power, showing nonlinear dependence on the pump-beam intensity. The solid line is a theoretical fit, with $\alpha = 80\ cm^{-1}$, $\theta = 2.3°$, $d = 120\ \mu m$, and $dn_0/dT = 1 \times 10^{-3}\ K^{-1}$.

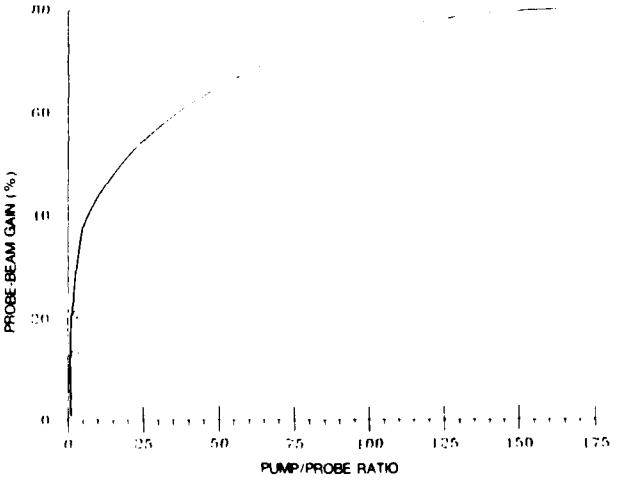

Fig. 5. Experimentally observed probe-beam gain as a function of pump-probe-beam ratio for the experimental parameters stated in the text. The curve shows the theoretically predicted dependence.

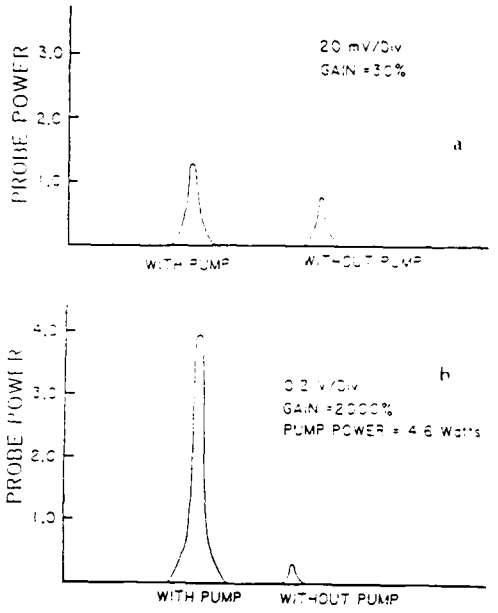

Fig. 6. a, Oscilloscope traces of probe-beam power with and without pump for a pump power of 1 W. The laser pulses used are of 40-msec duration. b, Same as a but for a pump power of 4.6 W. A gain of 20 is observed.

true that, in general, a larger grating constant will produce a higher probe-beam gain, the choice of the input probe beam (much weaker than the pump beam, of course) is important. In general, one should choose it to be as small as possible, so that only *one* diffracted order is observed. If the probe beam, in combination with the high index modulation obtained at a large grating constant, is strong enough to produce many high-order diffractions, we have observed that the probe-beam gain will be quenched at a low value, as a result of the loss through these multiorder diffractions.

For a given pump-probe-beam ratio and grating constant, the probe gain can be increased (>100%) by simply increasing the pump intensity. However, because of absorption, the operating temperature of the liquid crystal under cw laser illumination will rise, eventually exceeding the transition temperature. We observe that at an input cw power exceeding 6 W the sample becomes isotropic (the T_C of PCB is 35.3°C). This ambient overheating problem can be eliminated by simply pulsing the input laser. Typically, we find that laser pulses of tens of milliseconds' duration are ideal for these thermal wave mixing processes (similar to our previous work[11] with a visible laser).

With a pulsed laser, it is possible to utilize the much higher thermal index near T_C without overheating the sample. Figure 6 shows oscilloscope traces of the probe-beam pulse amplitude with and without the pump beam, when the sample is maintained at 32°C, i.e., close to T_C, where dn/dT is large. The pulse duration is 40 msec, chosen because the thermal-grating decay time is of this order. In Fig. 6a, the pump power is 1 W (40 mJ in 40 msec), and a gain of 30% is observed. Figure 6b shows the large gain (20 times) observed at an input pump power of 4.6 W. This large gain is due to the large dn/dT near T_c as well as to more efficient buildup of the thermal refractive-index grating by pulsed lasers.

In conclusion, we have demonstrated, for the first time to our knowledge, how a probe beam can be amplified by a pump beam in a diffusive medium involving a thermal grating. Also, we have experimentally demonstrated the effect and how it may be applied to CO_2 lasers of moderate power. Since the thermal-index gradient for the extraordinary ray dn_e/dT is larger, and also, since these thermal gradients increase greatly near T_C, considerably lower power and/or higher gain of the probe beam can be achieved. By using this high-gain wave mixing effect, processes such as image amplification, ring oscillation, and self-pumped phase conjugation are clearly feasible, and they are currently under study.

ACKNOWLEDGMENT

This research is supported by National Science Foundation grant ECS8415387.

REFERENCES

1. See, for example, R. J. F. Reintjes, *Nonlinear Optical Parametric Processes in Liquid and Gases* (Academic, New York, 1984).
2. R. Y. Chiao, P. L. Kelley, and E. Garmire, Phys. Rev. Lett. **17**, 1158 (1966).
3. J. P. Huignard, H. Rajbenbach, Ph. Refrégier, and L. Solymar, Opt. Eng. **24**, 586 (1985), and references therein.
4. S. J. Stepanov, V. V. Kulikov, and M. P. Petrov, Opt. Commun. **44**, 19 (1982).
5. V. L. Vinetskii and N. V. Kukhtarev, Sov. J. Quantum Electron. **8**, 231 (1978).
6. P. Yeh, J. Opt. Soc. Am. B **3**, 747 (1986).
7. S. Chang and T. Sato, Appl. Opt. **25**, 1635 (1986).
8. Y. Silberg and I. Bar-Joseph, J. Opt. Soc. Am. B **1**, 622 (1984).
9. E. S. Bliss, D. R. Speck, J. F. Holzrichter, J. H. Erkkila, and A. J. Glass, Appl. Phys. Lett. **25**, 448 (1974).
10. I. C. Khoo and S. L. Zhuang, Appl. Phys. Lett. **37**, 3 (1980); I. C. Khoo and T. H. Liu, IEEE J. Quantum Electron. **23**, 171 (1987).
11. I. C. Khoo and S. Shepard, J. Appl. Phys. **54**, 5491 (1983).
12. See, for example, H. Hoffman, J. Opt. Soc. Am B **3**, 253 (1986), and references therein.
13. I. C. Khoo and R. Normandin, IEEE J. Quantum Electron. **QE-21**, 329 (1985); see also Ref. 11.
14. J. G. Pasko, J. Tracy, and W. Elser, Proc. Soc. Photo-Opt. Instrum. Eng. **202**, 82 (1979).

Laser spot size dependence, nonlocality and saturation effects in transverse optical bistability

I.C. Khoo, T.H. Liu, P.Y. Yan and J.Y Hou

Electrical Engineering Department, The Pennsylvania State University
University Park, PA 16802

Abstract

We present here a theoretical discussion of the effect of nonlocality and saturation in transverse optical bistability. It is found that the switching conditions, switching power and characteristics are considerably different from the situation where these effects are not accounted for. We also include an analytical study of the transverse self-phase modulation effect and relate the key parameters explicitly to the transverse bistability switching condition and bistability.

Introduction

Optical bistability in the intensity of a laser beam after its passage through a thin nonlinear film was first experimentally observed by Khoo in 1982[1], following a theoretical discussion by Kaplan[2] in 1981. For such optically thin nonlinear medium, the effect of the nonlinear medium essentially impart a transverse intensity dependent nonlinear phase shift on the incident beam. The process of intensity redistribution and switching was quantitatively analytically analyzed by Khoo[3] et. al. and the theoretical predictions and the experimental results are in good agreement. In reference 3, it is to be noted here that we have actually employed an analysis that is beyond the usual lens approximation (c.f. Appendix in Ref. 3) where the gaussian intensity profile of the incident wave is expanded up to the r^2 term (where r is dimension transverse to the propagation axis z). However, much insights into the process (and little loss of the actual physics) can be gained by employing this approximation. In this paper, we reexamine the process of transverse bistability in lights of an exact theoretical analysis of transverse self phase modulation (without a feedback) and demonstrate the relationship between this process and the bistability switch conditions (when a feedback is present). We will then also discuss the effect of nonlocality (which depends critically on the laser spot size) and saturation effect.

Theory

Figure 1 depicts schematically a typical transverse self phase modulation experiment. A gaussian laser beam is incident from the left on a nonlinear film with a beam radius of curvature R and a beam waist on the film. The intensity of the laser has a transverse dependence given by

$$I_{laser} = I_0 \exp - \frac{2r^2}{w^2} \tag{1}$$

A mirror at a distance $z/2$ is placed behind the film and a pin-hole at a distance z is used to monitor the intensity at various radial displacement r_1 from the axis. The radial intensity distribution at z is given by $I(r_1,z)$. From Kirchoff's diffraction integral, $I(r_1,z)$ can be shown to be given by

$$I(r_1,z) = \left(\frac{2\pi}{\lambda z}\right)^2 I_0 \left| \int_0^\infty r dr\, J_0(2\pi r r_1/\lambda z) \exp(-2r^2/w^2) \exp -i(\phi_D + \phi_{NL}) \right|^2 \tag{2}$$

where the "diffractive" phase ϕ_D and the nonlinear intensity dependent phase ϕ_{NL} are given by

$$\phi_D = k\left(\frac{r^2}{2z} + \frac{r^2}{2R}\right) \tag{3}$$

$$\phi_{NL} = kn_2 d\,[I_0 \exp - 2r^2/w^2 + R_m I(r_1,z)] \tag{4}$$

Where n_2 is the nonlinear refractive index coefficient, $k = \frac{2\pi}{\lambda}$ is the vacuum wave vector wave vector of the light, R_m is the reflectivity of the mirror and d the thickness of the nonlinear film.

We shall discuss here first the case of zero feedback (i.e., R_m=0) to illustrate some interesting important observations. Defining:

$$y = r/w^2$$

$$C_1 = \frac{4\pi^2}{(\lambda z)^2} w^4$$

$$C_a = \frac{2\pi}{\lambda} \bar{n}_2 \, dI_0 \qquad (5)$$

$$C_b = \frac{\pi}{\lambda} w^2 \left(\frac{1}{z} + \frac{1}{R}\right)$$

$$C_2 = 2w/w_0$$

$$\theta = \frac{\pi w_0 r}{\lambda z} \text{ , where } w_0 \text{ is the focused laser beam waist.}$$

equation (2) becomes

$$I(r_1,z) = C_1 I_0 \left| \int_0^\infty e^{-y^2} y \, dy \, J_0(C_2 \theta y) \exp i(C_a e^{-2y^2} + C_b y^2) \right|^2 \qquad (6)$$

It is clear from equation (6) that C_1 affects only the magnitude of the intensity and C_2 the relative scale of the intensity distribution pattern.

The key parameters are C_a and C_b which decide the phases ϕ_{NL} and ϕ_D, respectively, which in conjunction with the integrand $(e^{-y^2} y)$, dictate the intensity distribution $I(r_1,z)$. A detailed numerical analysis of $I(r_1,z)$ as C_a and C_b are varied show that there are three fairly distinct general characteristics for $I(r_1,z)$ depending on the sign and magnitude of C_b relative to C_a.

For N_2>0, i.e., C_a>0 and increasing with I_0, these three regions correspond to

I. C_b>0 .

In this case, the overall intensity distribution $I(r_1,z)$ develops from a gaussian at low intensity to one where the on axis intensity is enhanced, with side band rings at high intensity. The on-axis intensity at higher intensity shows some oscillatory behavior but remain "bright". (c.f. figure 2a)

II. C_b<0 .

In this case, $I(r_1,z)$ acquires side-band rings at high intensity, while the center spot tends to be dark. (c.f. figure 2b)

III. $C_b \lesssim 0$

This situation represents a transition or mixture of cases (I) and (II). There are side rings, but the center spot assume alternatively brighten and darken appearance (c.f. figure 2c). These intensity dependences, as a function of C_b, have been observed recently[4,5].

In the case of transverse bistability, where portion of the transmitted intensity $I(r_1,z)$ is "imaged" back into the nonlinear film, clearly one can expect a so-called "positive feedback" or "reinforcement" to definitely to occur only for case (I) if n_2 is positive. This is indeed the case as demonstrated in a recent analysis of the switching condition[6], where, for positive n_2, the condition for bistability to occur is shown to be given by

$$\frac{\tau}{\lambda} w^2 \left(\frac{1}{R} + \frac{1}{z}\right) > \frac{15.4 z^4}{R_m (w^2 k)^4} + 1.12 \qquad (7)$$

For negative n_2, the situation is exactly reversed, i.e., for C_b>0, the center spot darkens at high intensity; for C_b<0, the central spot intensifies and for $C_b \gtrsim 0$, the central spot alternatively brightens and darkens. The bistability switching condition is

now given by

$$\frac{\pi}{\lambda} w^2 \left(\frac{1}{R} + \frac{1}{z}\right) < -\left[\frac{15.4z^4}{R_m(w^2k)^4} + 1.12\right] \tag{8}$$

This preceding exercise further brings out the importance of the spot size dependence as well as nonlocality of the nonlinearity, since they affect C_a and C_b considerably. As demonstrated explicitly in reference 3, all the switching characteristics depend critically on the incident spot size of the laser beam (to power of six or eight). In this paper, we will examine how the nonlocality of the nonlinearity (associated with diffusion or molecular correlation), which is highly dependent on w, affects the phase factor C_a which in turn affects the overall switching characteristics. To illustrate the point, we will quote results[7] we have calculated for the nonlocal dependence of liquid crystal axis reorientation. For the case where the linearly polarized laser beam is normal to the plane of the liquid crystal (i.e., the optical electric field is normal to the liquid crystal axis) as well as for the non-normally incident case, the transverse widths of the liquid crystal response are, in general, different from (smaller or larger depending on several factors) the laser beam widths. One of the consequences of this is shown in Figure 3a and Figure 3b.

Figure 3a compares two switching curves, one (I) is obtained for the case of local nonlinearity (i.e., laser beam width = response width) and (II) is obtained for the case where the width of the induced response is smaller than the laser beam width. It clearly shows that both the switching power and the switching characteristics (size of the loop, switched intensities, etc.) are drastically changed. The lowering of the switching powers is attributed to the fact that a "narrower" nonlinear response is equivalent to a higher power lens.

Figure 3b shows how the switching behavior differs for the local (I) and the nonlocal (II) (where the width of the response is greater than the laser width). Because of the increase width of the response, i.e., the induced "lens" is equivalently lower-powered, the switching intensities are up. There are, of course, other equally interesting effects due to the nonlocality of the nonlinearity but the preceding discussion brings out the most salient points.

Finally, we shall address the question of saturation effect in transverse bistability. This was briefly alluded to in a previous publication. We have recently performed a detailed calculation based on the form of saturation described by an n_2 of the form

$$n_2 = \frac{n_2}{1 + I(r)/I_S} \tag{9}$$

where n_2 is the non-saturated result. Figure 4 summarizes most of the results calculated using the technique developed in reference 3. For a small region of I_S, widely varying characteristics are obtained. There are multiple switching (loops), single switching loops, and so-called isolas corresponding to isolated region of solutions. There have yet to be experimental confirmation of these results.

Acknowledgement

This research is supported by a grant from the National Science Foundation ECS8415387 and by the Air Force Office of Scientific Research AFOSR840375.

References

1. I. C. Khoo, Appl. Phys. Letts. 41, 909 (1982).

2. A. E. Kaplan, Opt. Lett. 6, 360 (1981); J. E. Bjorkholm, P. W. Smith, W. J. Tomlinson and A. E. Kaplan, Opt. Lett 6, 345 (1981).

3. I. C. Khoo, P. Y. Yan, T. H. Liu, S. Shepard and J. Y. Hou, Phys. Rev. A29, 2756 (1984).

4. E. Santamato and Y. R. Shen, Optic Letters 9, 564 (1984).

5. I. C. Khoo, G. M. Finn, R. R. Michael and T. H. Liu, Opt. Letts 11, 229 (1986).

6. I. C. Khoo, Proceedings of the International Conference on Lasers 1984, p. 86, (1984).

7. I. C. Khoo, T. H. Liu and R. Normandin, Mol. Cryst. Liq. Cryst. 131, p. 315, (1985), for obliquely incident laser. I. C. Khoo et. al. (to be published) for normally incident laser.

Figure Captions

1. Schmeatic of transverse optical bistability setup. F is the nonlinear film, M the mirror.

2a. The on-axis laser intensity as a function of the transverse dimension for various input intensities ($C_b>0$; $n_2>0$ case).

2b. The on-axis laser intensity as a function of the transverse dimension for various input intensity ($C_b<0$; $n_2>0$ case).

2c. The on-axis laser intensity as a function of the transverse dimension for various input intensity ($C_b\lesssim 0$; $n_2>0$ case).

3a. Typical switching curve for (I) local and (II) nonlocal nonlinearity (where the induced nonlinear phase shift profile is narrower than the laser profile).

3b. Comparison of (I) local and (II) nonlocal nonlinearity switching curves. Curve II is obtained for a nonlinear phase shift profile that is wider than the input laser profile.

4. Multiple stable solutions of the output (on-axis intensity) as a function of the input intensity for various values of the saturation intensity I_s.

Optical limiting using self-focusing and self-bending of light by a nematic liquid crystal film

I.C. Khoo, R.R. Michael, T.H. Liu and G. Finn, Electrical Engineering Department
The Pennsylvania State University, University Park, PA 16802
and
A.E. Kaplan, School of Electrical Engineering, Purdue University, West Lafayette
Indiana 47907

Abstract

Optimal power limiting effects associated with self-focusing and self-bending of light in nematic liquid crystal films are studied using low power cw lasers and high power nanosecond pulse lasers.

Introduction

Transverse self phase modulation associated with the transverse intensity profile of a laser beam, and the related self focusing, optical switching and bistability phenomena have received considerable attention recently.[1-3] In conjunction with highly nonlinear materials, these effects have shown promises for applications in optical processings and logic element fabrications. One possible application of transverse self phase modulation is in the fabrication of passive optical limiters, in which the devices possess high transmission at low optical intensity, and, via the nonlinear refractive effect, switch over to a low transmission mode at high input intensity.[3] The process is basically a spatial redistribution of the laser power in the transmitted observation plane. It follows naturally that if the transverse nonlinear (intensity dependent) phase shift is "tailored" appropriately, the intensity at the observation plane will redistribute accordingly. In particular, if the incident laser beam is asymmetric, or if the nonlinear medium itself imparts an asymmetric phase shift, the exit beam will change its propagation direction in a unidirectional pattern[4], which results in self bending of the laser beam.

Discussion

In this paper, we report an experimental demonstration of optical limiting due to self-focusing and bending of a laser beam via transverse phase shift in a nematic liquid crystal film. Figure 1 depicts schematically the experimental set up. For self-focusing experiments, the whole laser beam is incident on the sample. The laser beam is half-blocked by an opaque object placed just before the liquid crystal film for self-bending effect. This creates an asymmetry in the laser intensity in the x-direction. If the medium possesses a positive nonlinearity (i.e. the refractive index n is given by $n = n_0 + n_2 I$; $n_2 > 0$, I = the optical intensity), then the beam will bend in the positive x-direction as shown. A detector located downstream that collects the light along the underated direction will obviously detect an intensity switching effect.

For nematic liquid crystals, there are two principal contributions to the nonlinearity n_2, namely, the refractive index change associated with laser induced director axis reorientation, and the refractive index change associated with laser induced heating.[5,6] Both are extraordinarily large, characterized by widely varying rise and fall times. The magnitude (and sign) of n_2 depends on the interaction geometry. Consider the configuration depicted in Figure 2, involving a linearly polarized laser and a homeotropically aligned nematic liquid crystal film. For molecular reorientation, β must be = 0 or 90°. The change in the dielectric constant $\varepsilon = n^2$ is given by[5]

$$\delta\varepsilon(r) \sim -\frac{\Delta\varepsilon\ \varepsilon_{\perp}}{4\ \varepsilon\ \xi^2}\ \frac{\sin^2 2\beta}{d}\int_0^d (dz - z^2)\,dz \qquad (1)$$

$$-\frac{\Delta\varepsilon\pi^2}{4}\ \frac{I_{op}(r)}{I_F}\ \sin^2 2\beta$$

in the case where the laser beam width is much larger than the sample thickness d, and $E_{op}^2 \ll E_F^2$ where E_F is the optical Freedericksz field ($E_F^2 = 4\pi^3 k \Delta\varepsilon^{-1} d^{-2}$) as detailed in reference 5.

In equation (1), $\Delta\varepsilon$ is the dielectric anisotropy, $\varepsilon_{\parallel}$ and $\varepsilon_{\perp}$ are the optical dielectric constant associated with optical field polarization parallel and perpendicular to the director axis, respectively; $\xi^2 = 4\pi K(\Delta\varepsilon)^{-1} E_{op}^{-2}$ and K the elastic constant.

This gives, in terms of the refractive index

$$\delta n(r) = n_2 I(r) = \frac{\Delta\varepsilon\pi^2}{4n I_F} \sin^2 2\beta\, I(r) \qquad (2)$$

If the incident laser beam is half-blocked, then, roughly, these two expressions will be multiplied by a step function $\theta(x)$ [$\theta(x) = 1$ $x<0$; $\theta(x) = 0$ $x > 0$].

On the other hand, the change in the refractive index associates with laser heating is quite complicated, and has been discussed in details in recent publications.[6] It suffices to note here that for the geometry depicted in Figure 2, at $\beta = 0$, the ordinary refractive index n_0 is probed. The change in n_0 is highly nonlinear (and is positive) near the nematic → isotropic transition temperature Tc. Depending on the absorption rate of the liquid crystal, the magnitude of n_2 varies. For MBBA, for example, laser intensities on the order of tens of watts/cm^2 are sufficient for inducing large (>2π) phase shift (transverse or longitudinal) leading to transverse self-focusing and logitudinal bistability switching effects[1].

We have conducted experiments on laser self-deflection effect using both kinds of nonlinearity. The laser used is a linearly polarized Ar^+ laser operating at the 5145 A line. The liquid crystal used is PCB (Pentyl-cyano-biphenyl) for molecular-reorientation effect, while MBBA (p-methoxybenzylidene - p-n - butylaniline) is used for thermal effect studies. The samples are 100μm thick and are homeotropically aligned. The incident angle (β) is set at $\beta = 15°$ for PCB sample, and at $\beta = 0°$ for MBBA. The laser is half-blocked at the entrance plane of the sample. The transmitted laser beam is monitored on a screen at a distance of 7m from the sample.

For PCB sample, a well-defined bending of the laser beam in the expected direction is observed at an input intensity of 100 watts/cm^2 (laser power = 1 watt, laser spot size, lightly focused is 1mm^2). The beam moves by a displacement (about 2 cms) of roughly 2 beam sizes at the observation plane. This corresponds to a deflection angle θ of 1/350.

For PCB, the relevant parameters are $\Delta\varepsilon = 0.8$, $\varepsilon_{\parallel} \sim 2.25$; $k = 0.8\times10^{-6}$ dynes; $d = 100\mu m$. This gives $I_F = 480$ watts/cm^2. The maximum refractive index change at $r = 0$ is therefore $\delta n(0) = 0.05$ while δn at r about one beam waist (1mm) from $r = 0$ will be vanishing. One can approximate this spatially varying refractive index by an index coefficient $\frac{dn}{dx}$ of about $0.05/0.05 \sim 1cm^{-1}$. The deflection angle θ associated with this index coefficient is given by $\theta \sim \frac{d}{n}\frac{dn}{dx} \sim \frac{0.01}{1.5} \sim 0.06$ radian. This is in good agreement with the experimental observed deflection angle of 0.03, considering there are several factors of unity associated with the various approximations made in the theoretical estimate.

The switching of the laser direction obviously gives rise to a whole beam intensity switching (from ~ 1 watt to vanishing value) for a detector located at position A on the screen. Under low laser power illumination, the switching is quite slow (~ 1 second). However, it is well-known that the molecular reorientation process in liquid crystal will speed up with the increase in the applied field. Very fast[6] (nanosecond) turn-on is possible at laser powers on the order of 10^2 MWatts/cm^2, which is being currently investigated.

Similar beam deflection effects are observed if one employs the thermal effect in MBBA sample (Tc = 42.5°C). The sample is maintained at room temperature (22°C). It is observed that a laser power on the order of 0.5 Watt (unfocused beam intensity of 1 watt/cm^2) will lead to self-bending effect.

In the case of self-phase modulation involving the whole beam, a drastic increase in the divergence of the exit beam is observed at a laser power of about 0.2 Watt.

As the sample is moved around the focal plane of the lense (i.e., the radius of curvature R changes in sign as well as in magnitude), the intensity distribution at the detector plane varies considerably.

In the case where the radius of curvature R of the wavefront is positive, the central portion, i.e., the on-axis part of the beam has a small region of brightness that seems to persist at all input intensities. On the other hand, if the sample is located before the focal plane , i.e., R is negative, the central region is dark at high input laser intensity. These are obviously diffraction effects, coupled with the nonlinear transverse phase shift. The detected intensity distribution is obviously also dependent on the parameter Z. It is probably useful, (but is time consuming and too detailed to be dealt with in this short communication), to identify and somehow classify the region of Z or R

whereby the intensity distributions are classifiable into typical forms. As a result of the drastic increase in the divergence of the beam at the detector plane, the detected power (the so-called output) versus the input laser power will deviate from linear, tending to a so-called "limiting" form. This is indeed observed (as shown in Figure 3). The detector collects almost all the transmitted laser beam, at low power. But at higher intensity, the "output" shows limiting behavior even as the input is increased by almost 10 times. There are some oscillations in the output, reflecting the diffractive interference effects that were also observed in our earlier experiment on transverse bistability.[1]

The configuration, as depicted in Figure 1 and adopted in our experiment demonstration is but one of the several possible set up that will create the required asymmetry in the transverse intensity dependent phase shift for laser deflection. One simple alternative whereby the whole incident laser beam is used would be to use a sample whose thickness varies from one beam edge to the other. For both reorientational and thermal nonlinearly, this variation in the thickness introduce a nonlinear "bias" (and thus asymmetry) on the transverse phase shift. Details of laser deflections using this kind of set up and the dynamics of the process will be presented in a longer article elsewhere.

In conclusion, we have demonstrated laser self-bending and intensity switching effects based on transverse self-phase modulation effects. The effects can be applicable to fairly high speed optical switching and power limiting applications for various types of lasers (the molecular reorientational effect is non-wavelength selective), and are currently being studied in that context.

Acknowledgement

This research is supported by the Air Force Office of Scientific Research AFOSR840375 and a grant from the National Science Foundation ECS 8415387.

References

1. I.C. Khoo, Appl. Phys. Lett. 41, 909 (1982); I.C. Khoo, T.H. Liu, P.Y. Yan, S. Shepard and J.Y. Hou, Phys. Rev. A29, 2756 (1984); J.E. Bjorkholm, P.W. Smith, W.J. Tomlinson and A.E. Kaplan, Opt. Lett. 6, 345 (1981); K. Tai, H.M. Gibbs, N. Peyghambarian and A. Mysyrowicz, Opt. Lett. 10, 220 (1985); M.M. Cheung, S.D. Durbin and Y.R. Shen, Opt. Lett. 8, 39 (1983); I.C. Khoo, J.Y. Hou, R. Normandin and V.C. So, Phys. Rev. A27, 3251 (1983).

2. A.E. Kaplan, Optic Letters, 6, 360 (1981).

3. See, for example, M.F. Soilean, W.E. Williams and E.W. Van Stryland, IEEE J. Quant. Electron. 19, 731 (1983); J.A. Hermann, J. Opt. Soc. Am. B1, 729 (1984); T.F. Boggess, Jr., A.L. Smirl, S.C. Moss, I.W. Boyd and E.W. Van Stryland, IEEE J. Quant. Electron. QE21, 488 (1985).

4. A.E. Kaplan, JETP Lett. 9, 33 (1969), see also reference 2.

5. See, for example, I.C. Khoo and Y.R. Shen, Opt. Eng. 24, 579 (1985) and references therein; for the equation (1) derivation, see I.C. Khoo, Phys. Rev. A25, (1982).

6. I.C. Khoo and R. Normandin, IEEE J. Quant. Electron. QE21, 329 (1985); Opt. Lett. 9, 285 (1984); I.C. Khoo and R. Normandin, J. Appl. Phys. 55, 1416 (1984); H. Hsiung, L.P. Shi, and Y.R. Shen, PRA 30, 1453 (1984).

Figure Captions

Fig. 1 Schematics of the set up for laser self-focusing and self-bending effect.

Fig. 2 Laser propagation in a homeotropically aligned nematic liquid crystal film.

Fig. 3 Optical power limiting associated with the external self-focusing effect.

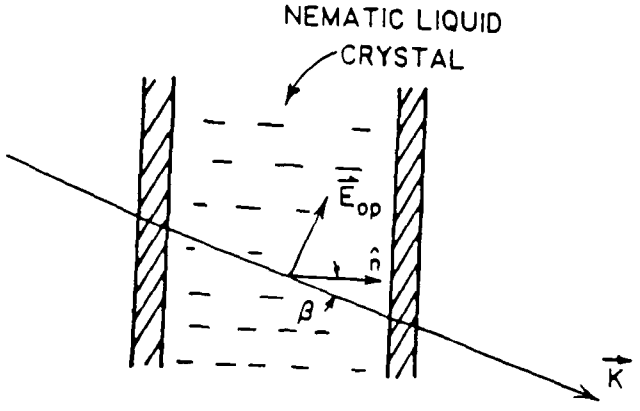

FIGURE 2

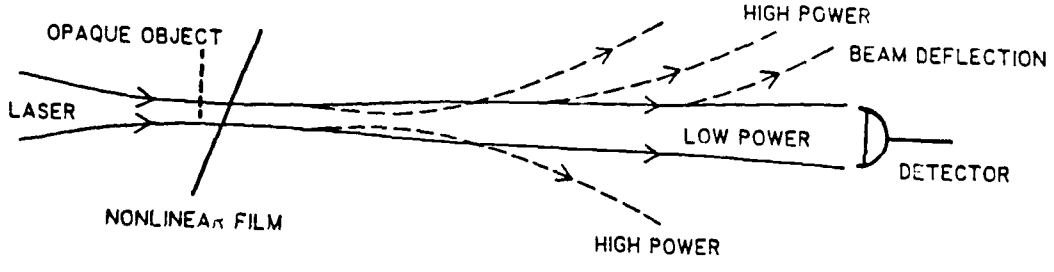

FIGURE 1

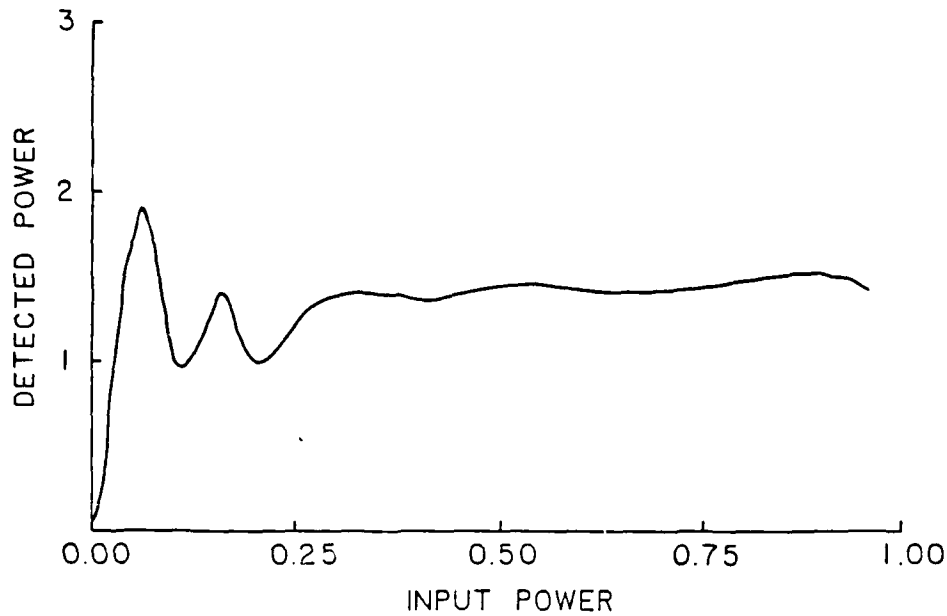

FIGURE 3

Probe Beam Amplification via Degenerate Optical Wave Mixing in a Kerr Medium

TSUEN-HSI LIU, STUDENT MEMBER, IEEE, AND IAM-CHOON KHOO, SENIOR MEMBER, IEEE

Abstract—**The theory of probe beam amplification via degenerate optical wave mixing in a Kerr medium is presented. This theory includes consideration of the self-phase modulation, two-wave mixing, and multiwave mixing terms in the coupled-wave equations. Both analytical solutions, under the assumptions of a nondepleted pump beam and a transparent Kerr medium, and numerical solutions with these assumptions removed are presented. Our solutions show that under certain conditions, phase matching can be satisfied and a high probe beam gain is possible, even for a zero phase shift between the refractive index and the intensity gratings.**

I. Introduction

BEAM amplification via two-wave mixing in photorefractive crystals has been extensively studied over the past few years [1]–[6]. Two major reasons photorefractive crystals are good candidates for two-wave mixing applications are: 1) photorefractive crystals are highly sensitive to light, and 2) in photorefractive crystals, a natural 90° phase shift exists between the refractive index and the intensity gratings formed by the input beams. Normally, this 90° phase shift, a condition for obtaining the optimum two-wave mixing effect, is not present in other nonlinear optical materials. Beam amplification or four-wave parametric amplification in a Kerr medium was considered by Chiao *et al.* [7]. Beam amplification or transformation of light beams by dynamic holograms in a general nonlinear medium was considered by Sidorovich and Stesel'ko [8]. Recently, an exact solution for two-wave mixing in Kerr media was considered by Yeh [9]. In his theory, the required phase shift is induced by the nondegenerate wave mixing (or moving grating) technique [7]–[12].

In this paper, we present a theory of the probe beam amplification via a wave mixing process different from the two-wave mixing mentioned above. This process is due to the simultaneous consideration of all the degenerate third-order wave mixing terms, namely, the forward degenerate four-wave mixing (DFWM), two-wave mixing, and the self-phase modulation terms in the coupled-wave equations derived in Section II. One of the attractive features of this process is that it does *not* need an additionally induced phase shift (between the index and the intensity gratings) to yield the probe beam amplification. Similar study was considered in [13]. However, the emphasis and approximations made in [13] are different from this paper.

Both analytical solutions, under the assumptions of a nondepleted pump beam and a transparent Kerr medium, and numerical solutions without these assumptions are presented in this paper. While more accurate predictions are provided by the numerical solutions, the important insight into this process is well illustrated by the analytical solutions. For example, we show that when the phase matching condition is satisfied, the probe beam gain can grow *exponentially* with the interaction length. The more detailed and exact numerical solutions bring out further insights not found in other simpler approaches involving only two or three beams.

In Section II, the basic coupled-wave equations are derived. In Section III, all the wave mixing terms in these equations are classified and discussed. In Section IV, the analytical solutions are derived. Finally, in Section V, some numerical results are presented.

II. Basic Equations

In this section, we derive the first-order coupled wave equations resulting from the intersecting of two beams in a Kerr medium (see Fig. 1). These first-order equations are deduced from the exact second-order wave equation and the third-order nonlinear polarization. Beside the two input beams, these equations also include four diffracted beams inside the medium (see Fig. 1). In principle, more beams can be included, but in the actual experiments, they are negligibly small. An additionally induced phase shift between the refractive index grating and the input intensity grating is also included.

The well-known second-order wave equation and the multiple expansion of the medium polarization in terms of the optical electric fields are given by [14]–[15]

$$\nabla^2 \boldsymbol{E} - \mu_0 \epsilon \frac{\partial^2 \boldsymbol{E}}{\partial t^2} = \mu_0 \frac{\partial^2 \boldsymbol{P}_{NL}}{\partial t^2} \tag{1}$$

and

$$P^i = \epsilon_0 \chi_{ij} E^j + 2 d_{ijk} E^j E^k + 4 \chi_{ijkl} E^j E^k E^l + \cdots, \tag{2}$$

respectively. In (1), μ_0 is the linear magnetic permeability, ϵ is the linear electric permittivity, and $\boldsymbol{P}_{NL}$ is the non-

Manuscript received March 4, 1987; revised June 15, 1987. This work was supported in part by the National Science Foundation under Grant ECS 8415387 and in part by the Air Force Office of Scientific Research under Grant AFOSR 840375.

The authors are with the Department of Electrical Engineering, Pennsylvania State University, University Park, PA 16802.

IEEE Log Number 8716532.

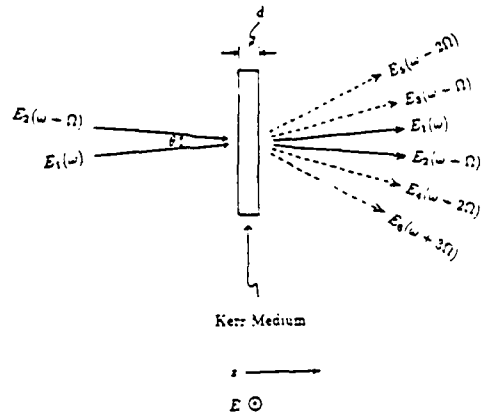

Fig. 1. Beam geometry for degenerate optical wave mixing. ω is the optical frequency of beam 1, $\omega + \Omega$ is the frequency of beam 2, and so on. Ω ($\ll \omega$) is a frequency shift introduced to induce a phase shift ϕ between the refractive index and the intensity gratings. ϕ and Ω are related by the response time of the medium, $\phi = 0$ and $\Omega = 0$. Beam 1 is considered as the pump beam, while beam 2 the probe beam. Beams 3-6 are the diffracted beams generated by the optically induced index gratings. Number of diffracted beams is not limited to four. All the beams are equally distant at the far field.

linear component of the medium polarization. In (2), χ_{ij} is the linear susceptibility, d_{ijk} and χ_{ijkl} are the second-order and third-order nonlinear susceptibility, respectively, and so on. The subscripts and superscripts represent the Cartesian coordinates. The convention of summation over repeated indexes is assumed here.

To reduce (1) to a set of first-order differential equations, we make the following assumptions:

1) All the waves are assumed to be plane waves, z dependent only, and for simplicity, linearly polarized in the same direction, i.e., we have

$$E_j = \tfrac{1}{2}\left(\mathcal{E}_j \exp\left[i(\omega_j t - k_{zj})\right] + \text{c.c.}\right), \qquad j = 1, 2, \cdots, 6 \tag{3a}$$

and the nonlinear polarization can be decomposed into their electric field counterparts as

$$P_j = \tfrac{1}{2}\left(\mathcal{P}_j \exp\left[i(\omega_j t - k_{zj} z)\right] + \text{c.c.}\right), \qquad j = 1, 2, \cdots, 6 \tag{3b}$$

where ω_j is the frequency and k_{zj} is the z component of the wave vector of the jth beam.

2) The rate of the electric field change satisfies the slowly varying envelope approximation [14]-[15], i.e.,

$$\left|k^2 \mathcal{E}\right| \gg \left|k \frac{\partial \mathcal{E}}{\partial z}\right| \gg \left|\frac{\partial^2 \mathcal{E}}{\partial z^2}\right|. \tag{3c}$$

From these assumptions, the second-order wave equation (1) can now be reduced to a set of first-order wave equations

$$\left(\frac{\partial}{\partial z} + \sqrt{\mu_0 \epsilon}\,\frac{\partial}{\partial t}\right)\mathcal{E}_j = -i\,\frac{\omega}{2}\sqrt{\frac{\mu_0}{\epsilon}}\,\mathcal{P}_j, \qquad j = 1, 2, \cdots, 6. \tag{4}$$

For practical reasons, let us express the effective degenerate third-order susceptibility $\chi^{(3)}$ in terms of the Kerr coefficient n_2 by

$$\chi^{(3)} = \tfrac{1}{3}\,\epsilon_0 n_0 n_2 \tag{5}$$

where the Kerr coefficient n_2 is defined as

$$n = n_0 + n_2 \langle E^2 \rangle \tag{6}$$

with n_0 being the linear index of refraction, $E (= E_1 + E_2 + E_3 + E_4 + E_5 + E_6)$ the total optical field, and $\langle E^2 \rangle$ the time average of E^2. In the nearly degenerate case, n_2 becomes a function of the frequency difference between the incident beams $\Omega = \omega_2 - \omega_1$ and the response time of the medium τ [9]:

$$n_2 = (n_{20}/\sqrt{1 + \tan^2 \phi})\, e^{i\phi} \tag{7}$$

where

$$\phi = \tan^{-1}(\Omega \tau) \tag{8}$$

and n_{20} is the value of the index change for the degenerate case. ϕ is the phase shift between the refractive index and the intensity gratings.

Finally, using (2) (retaining only the third-order term), (3a), (3b), (4), and (5), we obtain the following first-order coupled wave equations:

$$\begin{aligned}
\frac{d\mathcal{E}_1}{dz} = {} & -ig\left|\mathcal{E}_1\right|^2 \mathcal{E}_1 \\
& - 2ig\left[\left(\left|\mathcal{E}_2\right|^2 f_1 e^{-i\phi} + \left|\mathcal{E}_3\right|^2 f_1 e^{-i\phi} \right.\right. \\
& + \left|\mathcal{E}_4\right|^2 f_2 e^{-2i\phi} + \left|\mathcal{E}_5\right|^2 f_2 e^{2i\phi} \\
& \left.\left. + \left|\mathcal{E}_6\right|^2 f_3 e^{-3i\phi}\right)\mathcal{E}_1\right] - ig\left\{\mathcal{E}_2^2 \mathcal{E}_4^* f_3 \right. \\
& \cdot \exp\left[i(-3\phi - \Delta k_3 z)\right] \\
& + \mathcal{E}_2^* \mathcal{E}_3 \mathcal{E}_4 f_2 \exp\left[2i\Delta k_3 z\right]\left(f_1 e^{i\phi} + f_2 e^{-2i\phi}\right) \\
& + \mathcal{E}_1^* \mathcal{E}_2 \mathcal{E}_3 \exp\left[i\Delta k_3 z\right]\left(f_3 e^{3i\phi} + f_1 e^{-i\phi}\right) \\
& + \mathcal{E}_2 \mathcal{E}_4 \mathcal{E}_6^* \exp\left[i(\Delta k_3 z - \Delta k_5 z)\right] \\
& \cdot \left(f_1 e^{-i\phi} + f_2 e^{-2i\phi}\right) \\
& + \mathcal{E}_3^2 \mathcal{E}_5^* f_1 \exp\left[i(\phi + 2\Delta k_3 z - \Delta k_5 z)\right] \\
& + 2\mathcal{E}_4 \mathcal{E}_5 \mathcal{E}_1^* \exp\left[i(\Delta k_3 z + \Delta k_5 z)\right] f_2 \cos 2\phi \\
& + \mathcal{E}_5 \mathcal{E}_6 \mathcal{E}_2^* \exp\left[2i\Delta k_5 z\right]\left(f_2 e^{2i\phi} + f_3 e^{-3i\phi}\right) \\
& + \mathcal{E}_2 \mathcal{E}_5 \mathcal{E}_3^* \exp\left[i(\Delta k_3 z + \Delta k_5 z)\right] \\
& \cdot \left(f_2 e^{2i\phi} + f_1 e^{-i\phi}\right) \\
& \left. + \mathcal{E}_3 \mathcal{E}_6 \mathcal{E}_4^* \exp\left[i\Delta k_5 z\right]\left(f_1 e^{i\phi} + f_3 e^{-3i\phi}\right)\right\} \\
& - \tfrac{1}{2}\,\alpha \mathcal{E}_1
\end{aligned} \tag{9a}$$

$$\frac{d\mathcal{E}_2}{dz} = -ig|\mathcal{E}_2|^2\mathcal{E}_2 - ig\big[2(|\mathcal{E}_1|^2 f_1 e^{i\phi} + |\mathcal{E}_3|^2 f_2 e^{2i\phi} + |\mathcal{E}_4|^2 f_1 e^{-i\phi} + |\mathcal{E}_5|^2 f_3 e^{3i\phi} + |\mathcal{E}_6|^2 f_2 e^{-2i\phi})\mathcal{E}_2\big] - ig\big\{\mathcal{E}_1^2\mathcal{E}_3^* \cdot \exp[-i\Delta k_3 z] (f_1 e^{i\phi} - f_3 e^{-3i\phi}) + \mathcal{E}_1\mathcal{E}_4\mathcal{E}_2^* \exp[i\Delta k_3 z](f_3 e^{3i\phi} + f_1 e^{-i\phi}) + \mathcal{E}_3\mathcal{E}_4\mathcal{E}_1^* \exp[2i\Delta k_3 z](f_2 e^{2i\phi} + f_1 e^{-i\phi}) + \mathcal{E}_1\mathcal{E}_3\mathcal{E}_5^* \exp[i(\Delta k_3 z - \Delta k_5 z] \cdot (f_1 e^{i\phi} + f_2 e^{2i\phi}) + \mathcal{E}_4^2\mathcal{E}_6^* f_1 \exp[i(-\phi + 2\Delta k_3 z - \Delta k_5 z)] + \mathcal{E}_5\mathcal{E}_6\mathcal{E}_1^* \exp[2i\Delta k_5 z](f_3 e^{3i\phi} + f_2 e^{-2i\phi}) + \mathcal{E}_4\mathcal{E}_5\mathcal{E}_3^* e^{i\Delta k_5}(f_3 e^{3i\phi} + f_1 e^{-i\phi}) + 2\mathcal{E}_3\mathcal{E}_6\mathcal{E}_2^* \exp[i(\Delta k_3 z + \Delta k_5 z)] f_2 \cos 2\phi + \mathcal{E}_1\mathcal{E}_6\mathcal{E}_4^* \exp[i(-\Delta k_3 z + \Delta k_5 z)](f_1 e^{i\phi} + f_2 e^{2i\phi})\big\} - \tfrac{1}{2}\alpha\mathcal{E}_3 \quad (9b)$$

$$\frac{d\mathcal{E}_3}{dz} = -ig|\mathcal{E}_3|^2\mathcal{E}_3 - ig\big[2(|\mathcal{E}_1|^2 f_1 e^{-i\phi} + |\mathcal{E}_2|^2 f_2 e^{-2i\phi} + |\mathcal{E}_4|^2 f_3 e^{-3i\phi} + |\mathcal{E}_5|^2 f_1 e^{i\phi} + f_4 e^{-4i\phi})\mathcal{E}_3\big] - ig\big\{\mathcal{E}_1^2\mathcal{E}_2^* f_1 \cdot \exp[i(-\phi - \Delta k_3 z)] + \mathcal{E}_1\mathcal{E}_2\mathcal{E}_4^* \exp[-2i\Delta k_3 z](f_1 e^{-i\phi} + f_2 e^{-2i\phi}) + \mathcal{E}_1\mathcal{E}_4\mathcal{E}_6^* \exp[-i\Delta k_5 z](f_1 e^{-i\phi} + f_3 e^{-3i\phi}) + \mathcal{E}_2^2\mathcal{E}_6^* f_1 \exp[i(-\phi - \Delta k_3 z - \Delta k_5 z)] + \mathcal{E}_2\mathcal{E}_5\mathcal{E}_1^* \exp[i(-\Delta k_3 z + \Delta k_5 z)] \cdot (f_1 e^{i\phi} + f_2 e^{-2i\phi}) + \mathcal{E}_4\mathcal{E}_5\mathcal{E}_2^* \exp[i\Delta k_5 z](f_1 e^{i\phi} + f_3 e^{-3i\phi}) + 2\mathcal{E}_1\mathcal{E}_5\mathcal{E}_3^* \exp[i(-2\Delta k_3 z + \Delta k_5 z)] f_1 \cos\phi + 2\mathcal{E}_5\mathcal{E}_6\mathcal{E}_4^* \exp[2i(-\Delta k_3 z + \Delta k_5 z)] \cdot (f_1 e^{i\phi} + f_4 e^{-4i\phi})\big\} - \tfrac{1}{2}\alpha\mathcal{E}_3 \quad (9c)$$

$$\frac{d\mathcal{E}_4}{dz} = -ig|\mathcal{E}_4|^2\mathcal{E}_4 - ig\big[2(|\mathcal{E}_1|^2 f_2 e^{2i\phi} + |\mathcal{E}_2|^2 f_1 e^{i\phi} + |\mathcal{E}_3|^2 f_3 e^{3i\phi} + |\mathcal{E}_5|^2 f_4 e^{4i\phi} + |\mathcal{E}_6|^2 f_1 e^{-i\phi})\mathcal{E}_4\big] - ig\big\{\mathcal{E}_2^2\mathcal{E}_1^* f_1 \cdot \exp[i(\phi - \Delta k_3 z)] + \mathcal{E}_1\mathcal{E}_2\mathcal{E}_3^* \exp[-2i\Delta k_3 z](f_1 e^{i\phi} + f_2 e^{2i\phi}) + \mathcal{E}_1^2\mathcal{E}_5^* f_2 \exp[i(2\phi - \Delta k_3 z - \Delta k_5 z)] + \mathcal{E}_2\mathcal{E}_3\mathcal{E}_5^* \exp[-i\Delta k_5 z](f_1 e^{i\phi} + f_3 e^{3i\phi}) + \mathcal{E}_5\mathcal{E}_6\mathcal{E}_3^* \exp[2i(-\Delta k_3 z + \Delta k_5 z)] \cdot (f_4 e^{4i\phi} + f_1 e^{-i\phi}) + \mathcal{E}_3\mathcal{E}_6\mathcal{E}_1^* \exp[i\Delta k_5 z](f_3 e^{3i\phi} + f_1 e^{-i\phi}) + \mathcal{E}_1\mathcal{E}_6\mathcal{E}_2^* \exp[i(-\Delta k_3 z + \Delta k_5 z)] \cdot (f_2 e^{2i\phi} + f_1 e^{-i\phi}) + 2\mathcal{E}_2\mathcal{E}_6\mathcal{E}_4^* \exp[i(-\Delta k_3 z + \Delta k_5 z)] f_1 \cos\phi\big\} - \tfrac{1}{2}\alpha\mathcal{E}_4 \quad (9d)$$

$$\frac{d\mathcal{E}_5}{dz} = -ig|\mathcal{E}_5|^2\mathcal{E}_5 - ig\big[2(|\mathcal{E}_1|^2 f_2 e^{-2i\phi} + |\mathcal{E}_2|^2 f_3 e^{-3i\phi} + |\mathcal{E}_3|^2 f_1 \cdot e^{-i\phi} + |\mathcal{E}_4|^2 f_4 e^{-4i\phi} + |\mathcal{E}_6|^2 f_5 e^{-5i\phi})\mathcal{E}_5\big] - ig\big\{\mathcal{E}_1\mathcal{E}_2\mathcal{E}_6^* \exp[-2i\Delta k_5 z](f_2 e^{-2i\phi} + f_3 e^{3i\phi}) + \mathcal{E}_3\mathcal{E}_4\mathcal{E}_6^* \exp[i(2\Delta k_3 z - 2\Delta k_5 z)] \cdot (f_1 e^{-i\phi} + f_4 e^{-4i\phi}) + 2\mathcal{E}_1\mathcal{E}_3\mathcal{E}_2^* \exp[i(\Delta k_3 z - \Delta k_5 z)] \cdot (f_1 e^{-i\phi} + f_2 e^{-2i\phi}) + \mathcal{E}_1^2\mathcal{E}_4^* f_2 \exp[i(-2\phi - \Delta k_3 z - \Delta k_5 z)] + \mathcal{E}_2\mathcal{E}_3\mathcal{E}_4^* \exp[-i\Delta k_5 z](f_1 e^{-i\phi} + f_3 e^{-3i\phi}) + \mathcal{E}_3^2\mathcal{E}_1^* f_1 \exp[i(-\phi + 2\Delta k_3 z - \Delta k_5 z)]\big\} - \tfrac{1}{2}\alpha\mathcal{E}_5, \quad (9e)$$

$$\frac{d\mathcal{E}_6}{dz} = -ig|\mathcal{E}_6|^2\mathcal{E}_6$$
$$-ig\left[2(|\mathcal{E}_1|^2 f_3 e^{3i\phi} + |\mathcal{E}_2|^2 f_2 e^{2i\phi} + |\mathcal{E}_3|^2 f_4 \cdot e^{4i\phi} + |\mathcal{E}_4|^2 f_1 e^{i\phi} + |\mathcal{E}_5|^2 f_5 e^{5i\phi})\mathcal{E}_6\right]$$
$$-ig\Big\{\mathcal{E}_1\mathcal{E}_2\mathcal{E}_5^* \exp\left[-2i\Delta k_5 z\right](f_2 e^{2i\phi} + f_3 e^{3i\phi})$$
$$+ \mathcal{E}_3\mathcal{E}_4\mathcal{E}_5^* \exp\left[i(2\Delta k_3 z - 2\Delta k_5 z)\right] \cdot (f_1 e^{i\phi} + f_4 e^{4i\phi})$$
$$+ \mathcal{E}_1\mathcal{E}_4\mathcal{E}_3^* \exp\left[-i\Delta k_5 z\right](f_1 e^{i\phi} + f_3 e^{3i\phi})$$
$$+ \mathcal{E}_2\mathcal{E}_4\mathcal{E}_1^* \exp\left[i(\Delta k_3 z - \Delta k_5 z)\right] \cdot (f_1 e^{i\phi} + f_2 e^{2i\phi})$$
$$+ \mathcal{E}_2^2\mathcal{E}_3^* f_2 \exp\left[i(2\phi - \Delta k_3 z - \Delta k_5 z)\right]$$
$$+ \mathcal{E}_4^2\mathcal{E}_2^* f_1 \exp\left[i(\phi + 2\Delta k_3 z - \Delta k_5 z)\right]\Big\}$$
$$- \tfrac{1}{2}\alpha\mathcal{E}_6 \qquad (9f)$$

where α is the loss coefficient of the medium, f_α's are the factors associated with the medium response time and the frequency detuning and are defined as

$$f_\alpha = 1/\sqrt{1 + \tan^2(\alpha\phi)}, \qquad \alpha = 1, 2, \cdots, 5, \qquad (10a)$$

and g is the coupling constant defined as

$$g = \frac{\omega^2 n_0 n_{20}}{2k_z c^2} \qquad (10b)$$

with c being the speed of light in vacuum. Δk_3 and Δk_5 are the z components of the mismatched wave vectors given by

$$\Delta k_3 = 2k_1 - k_2 - k_3 \qquad (11a)$$

and

$$\Delta k_5 = 3k_1 - 2k_2 - k_5, \qquad (11b)$$

respectively.

III. Physical Meaning of the Wave Mixing Terms

Since each term in the coupled-wave equations derived in the last section is coupled to other terms, we must consider all the terms, at the same time, to obtain the actual "nonlinear" effect. In this section, we discuss the separate physical meaning of the self-phase modulation terms in Section III-A, the two-wave mixing terms in Section III-B, and finally, the forward DFWM terms in Section III-C.

A. Self-Phase Modulation Terms

The first term in each of (9a)–(9f) is the familiar self-phase modulation term. In the case of a single incident plane wave, only the phase of the wave is modulated by this term (see Section IV). Although the self-phase modulation terms are usually ignored, in our theory, they are explicitly included because these self-phase modulation terms play a major role in the phase matching conditions and the resulting wave mixing effects.

B. Two-Wave Mixing Terms

The terms in the square brackets of (9) are the familiar two-wave mixing terms that appear in other calculations [9]. The physical meaning of these terms can be illustrated, for example, by the first two-wave mixing term in (9b) ($-2ig|\mathcal{E}_1|^2\mathcal{E}_2$). This term leads to the process in which the pump beam $\mathcal{E}_1$ and the probe beam $\mathcal{E}_2$ form a grating proportional to $\mathcal{E}_1^*\mathcal{E}_2\,dz$. Then the pump beam is diffracted from this grating into the probe beam by an amount $d\mathcal{E}_2 = -2ig|\mathcal{E}_1|^2\mathcal{E}_2\,dz$. The phase difference between this infinitesimal change in the probe beam field and the probe beam field itself is $\phi - 90°$. Fig. 2 illustrates, in the vector diagrams, this relation for $\phi = 0$ and $\phi = 90°$. In Fig. 2(a) ($\phi = 0$), the infinitesimal change in the probe beam is always perpendicular to the probe beam itself. Hence, the intensity (magnitude) of the probe beam does not change, while the phase of the probe beam does change during the process. (However, due to the existence of other terms, the probe beam intensity change is, in fact, possible for $\phi = 0$.) On the other hand, in Fig. 2(b) ($\phi = 90°$), the infinitesimal change in the probe beam and the probe beam itself are always in parallel. Thus, the change in the intensity of the probe beam is possible, while the phase of the probe beam is not varied by this process.

It is interesting to note that if the phase shift ϕ is induced by moving grating or other techniques, cf. (7) and (8), then the condition $\phi = 90°$ corresponds to exactly $n_2 = 0$. Therefore, maximum energy exchange in the case of moving grating induced phase shift occurs at other than 90°. (In the case of a purely two-wave interaction, it can be readily shown that maximum energy exchange occurs at $\phi = 45°$.) *This is different from two-wave mixing in photorefractive crystals.* In the photorefractive media, this optimum energy exchange occurs when $\phi = 90°$, since in this case, the grating is not moving and so the coupling constant is not degraded by the finite response of the media.

C. Forward DFWM Terms

The terms in the curly brackets in (9) are the forward DFWM terms. They do not have a simple fixed phase difference as the two-wave mixing terms discussed above. For example, the first DFWM term of (9b) corresponds to the process in which the pump beam $\mathcal{E}_1$ and the diffracted beam $\mathcal{E}_3$ form a grating, and then part of the pump beam $\mathcal{E}_1$ is diffracted from this grating into the probe beam $\mathcal{E}_2$. The phase difference between the infinitesimal change $d\mathcal{E}_2$ in the probe beam resulted from this diffraction, and the probe beam itself $\mathcal{E}_2$ is $2\phi_1 - \phi_3 - \phi_2 + \phi - \Delta k_3 z$.

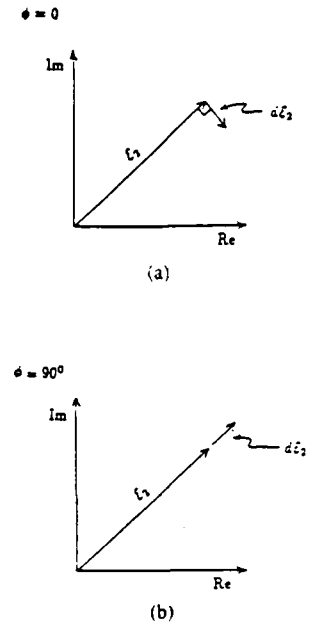

Fig. 2. Vector diagrams for the probe beam field and the change in the probe beam field: (a) $\phi = 0$, (b) $\phi = 90°$. Note only the phase of the probe beam is changed in (a) and only the magnitude of the probe beam is changed in (b).

Clearly, this phase difference can not be solely controlled by ϕ as in two-wave mixing terms. Furthermore, it contains a phase mismatching factor $\Delta k_3 z$ which can limit the efficiency of the energy transfer. As we can see in the following discussion, the phase mismatching can sometimes be compensated when all the wave mixing terms are considered simultaneously.

IV. Analytical Solutions

Equation (9) is a set of complicated equations. The general analytical solutions are difficult to obtain and may not be illustrative. However, in order to gain some insights into the process associated with these equations, we may simplify the physical situations such that analytical solutions can be more easily obtained. We can achieve this by assuming a nondepleted pump beam (namely, $|\mathcal{E}_1| >> |\mathcal{E}_2|, |\mathcal{E}_3|$, and so on) and a perfectly transparent medium (namely, $\alpha = 0$). Under these conditions, (9) can be simplified to yield

$$\frac{d\mathcal{E}_1}{dz} = -ig\mathcal{E}_1|\mathcal{E}_1|^2$$

$$\frac{d\mathcal{E}_2}{dz} = -ige^{i\phi}\left(2|\mathcal{E}_1|^2\mathcal{E}_2 + \mathcal{E}_1^2\mathcal{E}_3^* \exp\left[-i\Delta k_3 z\right]\right)$$

$$\frac{d\mathcal{E}_3}{dz} = -ige^{-i\phi}\left(2|\mathcal{E}_1|^2\mathcal{E}_3 + \mathcal{E}_1^2\mathcal{E}_2^* \exp\left[-i\Delta k_3 z\right]\right) \tag{12c}$$

where $\mathcal{E}_1$ is the pump beam, $\mathcal{E}_2$ is the probe beam, and $\mathcal{E}_3$ is the diffracted beam. Also, for simplicity, the medium response factor is assumed to be included in g.

Writing $\mathcal{E}_1 = |\mathcal{E}_1|e^{i\phi_1}$, (12a) can be readily solved by decomposing it into two equations, with one being a function of $|\mathcal{E}_1|$ only and the other a function of ϕ_1 only. Then we have

$$|\mathcal{E}_1|^2 = |\mathcal{E}_1(0)|^2 \tag{13d}$$

$$\phi_1 = -ig|\mathcal{E}_1(0)|^2 z. \tag{13b}$$

Without loss of generality, we have arbitrarily chosen the initial condition of $\phi_1(0) = 0$.

Now, using (13), we may proceed to solve (12b) and (12c) for the amplitudes of the probe beam $\mathcal{E}_2$ and the diffracted beam $\mathcal{E}_3$. We begin this with the following variable changes:

$$\mathcal{E}_2 \equiv \mathcal{E}_2' \exp\left(-ige^{i\phi}|\mathcal{E}_1(0)|^2 z\right) \tag{14a}$$

$$\mathcal{E}_3 \equiv \mathcal{E}_3' \exp\left(-ige^{-i\phi}|\mathcal{E}_1(0)|^2 z\right). \tag{14b}$$

Substitution of (14) in (12b) and (12c) gives

$$\frac{d\mathcal{E}_2'}{dz} = -ige^{i\phi}|\mathcal{E}_1(0)|^2(\mathcal{E}_3')^* \exp(i2pz) \tag{15a}$$

$$\frac{d\mathcal{E}_3'}{dz} = -ige^{-i\phi}|\mathcal{E}_1(0)|^2(\mathcal{E}_2')^* \exp(i2pz) \tag{15b}$$

where

$$p = g|\mathcal{E}_1(0)|^2(2e^{i\phi} - 1) - \frac{\Delta k_3}{2}. \tag{16}$$

Equation (15) can be solved by 1) taking the derivative of (15a), 2) eliminating $\mathcal{E}_3$ from the new second-order differential equation, and 3) solving this equation for $\mathcal{E}_3$ which can then be substituted into (15b) to obtain the solution for $\mathcal{E}_3$. This procedure yields

$$\mathcal{E}_2 = \mathcal{E}_2(0) \exp\left[-i\left(g|\mathcal{E}_1(0)|^2 + (\Delta k_3/2)\right)d\right] \cdot \left[\cosh(qd) - i\frac{p}{q}\sinh(qd)\right] \tag{17a}$$

$$\mathcal{E}_3 = -i\mathcal{E}_2^*(0) \exp\left[-i\left(g|\mathcal{E}_1(0)|^2 + (\Delta k_3/2)\right)d\right] \cdot \frac{p^{*2} + q^{*2}}{q^* g e^{-i\phi}|\mathcal{E}_1|^2}\sinh(q^* d) \tag{17b}$$

where d is the interaction length and

$$q = \sqrt{-p^2 + g^2|\mathcal{E}_1(0)|^4},$$

$$= \left[g^2|\mathcal{E}_1(0)|^4(4\sin^2\phi - (2\cos\phi - 1)^2 - 4\sin\phi(2\cos\phi - 1) + 1) - g|\mathcal{E}_1(0)|^2(2\cos\phi - 1)\Delta k_3 - (\Delta k_3^2/4) + 2i\sin\phi\Delta k_3 g|\mathcal{E}_1(0)|^2\right]^{1/2}$$

$$= \sqrt{\Delta k_3\left(g|\mathcal{E}_1(0)|^2 - \frac{\Delta k_3}{4}\right)}, \qquad \text{for } \phi = 0. \tag{18c}$$

In obtaining (17), we have used the initial condition

$$\mathcal{E}_3(0) = 0. \tag{19}$$

Equation (17b) indicates that the amplitude of the diffracted beam $\mathcal{E}_3$ is proportional to the complex conjugate of the incident probe beam amplitude $\mathcal{E}_2(0)$. It is well known that this nature of the forward DFWM can be used to perform the forward optical phase conjugation process [16]–[18]. From (17), we can also obtain the solutions in intensity:

$$I_2 = I_2(0)\left[\left|\cosh(qd)\right|^2 + |p|^2\left|\frac{\sinh(qd)}{q}\right|^2 - 2\,\mathrm{Re}\left(i\frac{p}{q}\sinh(qd)\cosh(q^*d)\right)\right]$$

$$I_3 = I_2(0)\,\frac{|p|^4 + |q|^4 + 2\,\mathrm{Re}(p^2q^{*2})}{4\eta^2g^2I_1^2(0)}\left|\frac{\sinh(qd)}{q}\right|^2, \tag{20b}$$

where

$$I_j = \frac{1}{2\eta}\left|\mathcal{E}_j\right|^2 \tag{21}$$

is the intensity of the jth beam, $\eta = \sqrt{\mu/\epsilon} \approx 377\ \Omega$, and Re (x) represents the real part of x.

From the following relations,

$$\left|\sinh x\right|^2 = \cosh\left[\mathrm{Re}\,(2x)\right] - \cos\left[\mathrm{Im}\,(2x)\right] \tag{22a}$$

$$\approx \tfrac{1}{2}\exp\left[\mathrm{Re}\,(2x)\right], \quad \text{for } x \gg 1 \tag{22b}$$

$$\left|\cosh x\right|^2 = \cosh\left[\mathrm{Re}\,(2x)\right] + \cos\left[\mathrm{Im}\,(2x)\right] \tag{22c}$$

$$\approx \tfrac{1}{2}\exp\left[\mathrm{Re}\,(2x)\right], \quad \text{for } x \gg 1 \tag{22d}$$

with Im (x) the imaginary part of x, and from (20) and (22), we observe that if Re $(qd) \gg 1$, the probe beam gain is approximately an exponential function of Re (qd). Define $\gamma = \mathrm{Re}\,(q)$. Then, from (18c) and (19), we see that if $\phi = 0$, and $8g\eta I_1(0)/\Delta k_3 > 1$,

$$\gamma(\phi = 0) = \sqrt{\Delta k_3\left(2g\eta I_1(0) - \frac{\Delta k_3}{4}\right)}. \tag{23}$$

Another interesting result is that if $\phi = 0$, $qd \sim 0$ (i.e., the medium thickness is thin) and $8g\eta I_1(0)/\Delta k_3 \gg 1$ (i.e., the crossing angle betwen the two input beams is small), (22) become

$$I_2 \approx I_2(0)\left(1 + 4\eta^2g^2I_1^2(0)d^2\right) \tag{24a}$$

$$I_3 \approx I_2(0)4\eta^2g^2I_1^2(0)d^2 \tag{24b}$$

which is similar to the solutions obtained in [13].

The above discussion indicates that we cannot consider each wave mixing separately, even when some of the terms (in this case, the two-wave mixing and the self-phase modulation terms) do not seem to directly contribute to the intensity change of the probe and the diffracted beams. This is because they could still change the phase matching condition. We may also draw the conclusion that in the case of $\phi = 0$, if the pump beam intensity is high enough or if the crossing angle between the input beams is small enough such that the phase matching is satisfied, an exponential-like probe beam amplification becomes possible.

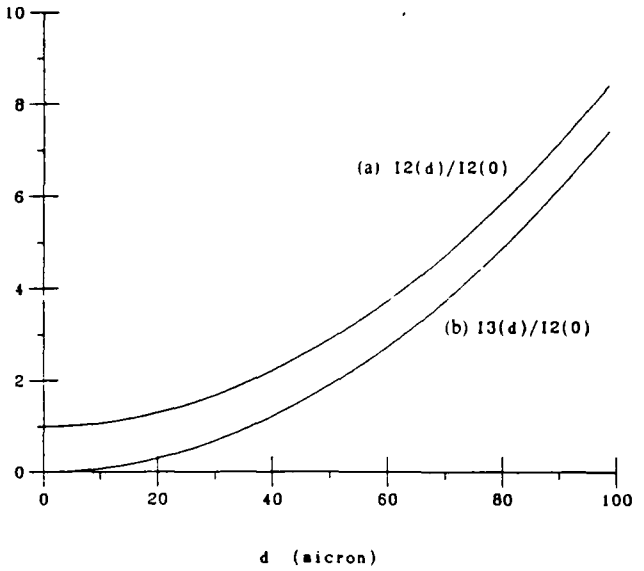

Fig. 3. Analytical solutions. (a) Probe beam gain versus interaction length. (b) Normalized intensity of diffracted beam versus interaction length. $n_2 = 2.3 \times 10^{-4}$ cm^2/W, $I_1(0) = 20$ W/cm^2, θ (angle between the incident beams) = 0.001 rad, $\phi = 0$, $\lambda = 514.5$ nm.

Fig. 3 is the plot of the probe beam gain [cf. (20)] and the normalized intensity of the diffracted beam as a function of the interaction length for $I_1(0) = 20$ W/cm^2, $n_2 = 2.3 \times 10^{-4}$ cm^2/W (typical value of n_2 for liquid crystals [19]), $d \le 100\ \mu$m, and $\lambda = 514.5$ nm. Fig. 4 is the plot of the same quantities versus the pump beam intensity $I_1(0)$. Since the medium is very thin ($d \le 100\ \mu$m), the square-law gain is observed here.

V. Numerical Solutions

The numerical solutions of the coupled-wave equations (9) are required if we remove those simplifying assumptions (nondepleted pump beam and perfectly transparent media, which may not be physically true) made in obtaining the analytical solutions. Furthermore, in the numerical analysis, we have included three more diffracted beams. Essentially, some new features not predictable by the analytical solutions may arise from the numerical solutions.

1) As a result of the pump depletion, the probe beam gain is also a function of the pump-to-probe beam ratio for a given pump beam intensity. In general, it increases with the pump-to-probe beam ratio and eventually approaches a constant (or saturation) (see Fig. 5).

2) If the initial exponential gain is high enough to compensate the exponential loss α, we expect to see the probe beam gain decreases after it reaches a maximum at a crit-

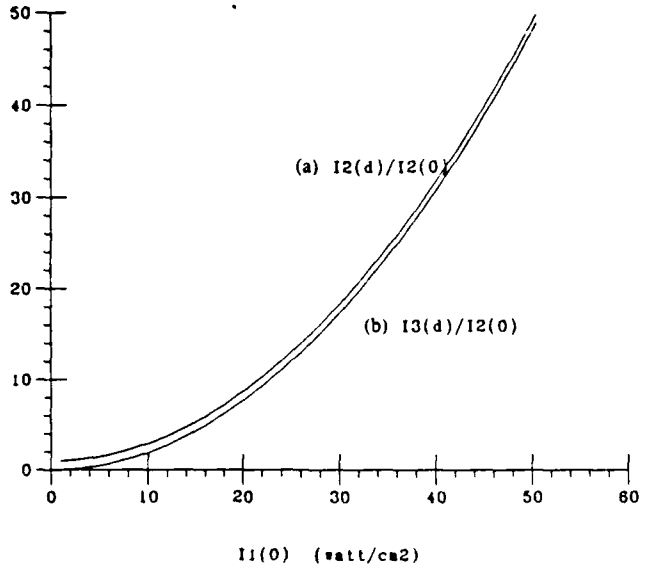

Fig. 4. Analytical solutions. (a) Probe beam gain versus pump beam intensity. (b) Normalized intensity of diffracted beam versus pump beam intensity. $d = 100\ \mu m$, $\phi = 0$.

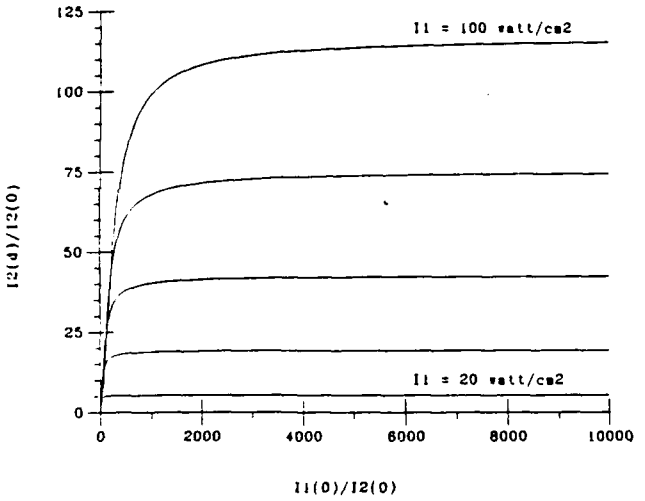

Fig. 5. Numerical solution. Probe beam gain versus pump-probe beam ratio. Note that the gain saturates in the limit of large pump-probe beam ratios. The difference between the pump beam intensities of two adjacent curves is 20 W/cm^2. $\alpha = 20.0\ cm^{-1}$, $d = 100\ \mu m$, $\phi = 0$.

ical interaction length (see Fig. 6). This is due to the depletion of the pump beam, the decrease of the pump-to-probe beam ratio, and the exponential loss. (Note that when the probe beam is amplified, the pump-to-probe beam ratio is decreased.)

3) Due to the presence of higher order diffracted beams, the energy of the probe beam can be depleted by other diffracted beams when the interaction length and the pump beam intensity are increased (cf. Fig. 7). In fact, as a result of this depletion, the maximum probe beam gain (cf. Fig. 8) occurs at different values of ϕ for different thicknesses as a result of these energy exchanges among the beams.

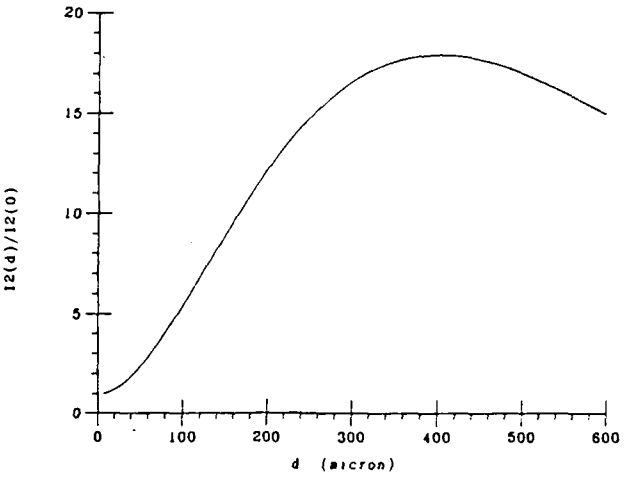

Fig. 6. Numerical solution. Probe beam gain versus interaction length. Note that this curve is different from the analytical curve in Fig. 1. The decrease of the probe beam gain beyond the so-called critical interaction length is due to the pump depletion and the medium loss. $\alpha = 20.0\ cm^{-1}$, $I_1(0) = 20$ W/cm^2, $I_2(0) = 0.1$ W/cm^2, $\phi = 0$.

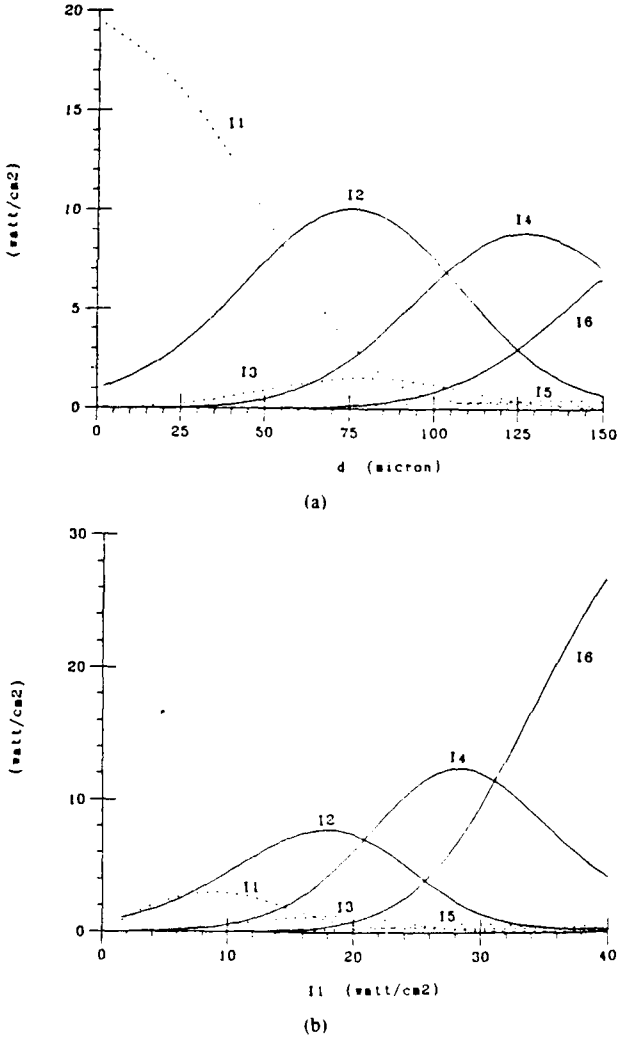

Fig. 7. Numerical solutions. Energy transfer due to nonzero phase shift ϕ. (a) Intensities of beams 1-6 versus interaction length $I_1(0) = 20$ W/cm^2, $I_2(0) = 1$ W/cm^2. (b) Intensities of beams 1-6 versus pump intensity. $d = 100\ \mu m$, $I_2(0) = 1$ W/cm^2, $\phi = 40°$ in both cases.

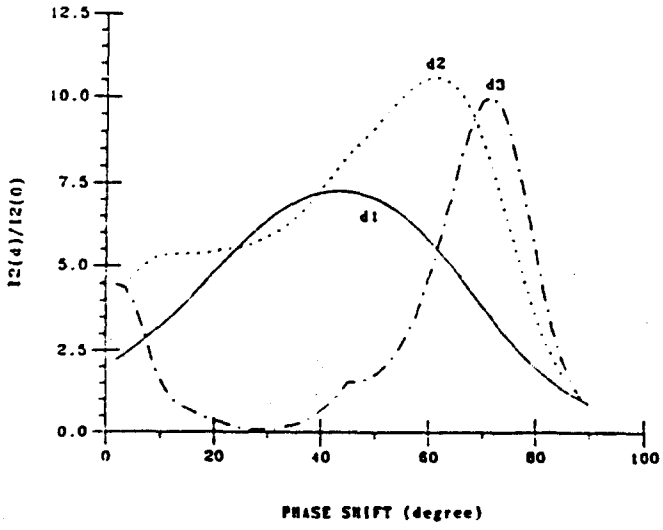

Fig. 8. Numerical solution. Probe beam gain versus phase shift for increasing medium thickness (d_1 = 50 μm, d_2 = 100 μm, d_3 = 150 μm). $I_1(0)$ = 20 W/cm^2, $I_2(0)$ = 1 W/cm^2.

VI. Conclusions

We have presented both analytical solutions (under the assumption of a nondepleted pump beam and a transparent medium) and numerical solutions of the first-order coupled-wave equations, taking into account all the degenerate third-order wave mixing terms (i.e., the forward DFWM, two-wave mixing, and self-phase modulation terms). Our analytical solutions show that under certain conditions, a phase matched probe beam amplification process can be achieved, even for a zero phase shift between the index and the intensity gratings. In general, this process has an exponential gain for a thick medium and a square-law gain for a thin medium. The numerical solutions show that the probe beam gain is a function of the pump-to-probe beam ratio and saturates when this ratio approaches infinity. Our analysis also shows that due to the depletion of the probe beam by some higher order diffracted beams, the maximum gain may not occur exactly at a 45° phase shift implied by the theory of two-wave mixing in Kerr media [9]. Some experimental results on this subject have been reported previously [20]. More experimental research concerning various aspects of this subject is currently being pursued in our laboratory and will be reported elsewhere.

References

[1] D. L. Staebler and J. J. Amodei, "Coupled-wave analysis of holographic storage in $LiNbO_3$," *J. Appl. Phys.*, vol. 43, p. 1042, 1972.

[2] N. V. Kukhtarev, V. B. Markov, S. G. Odulov, M. S. Soskin, and V. L. Vinetskii, "Holographic storage in electrooptic crystals. II. Beam coupling—Light amplification," *Ferroelec.*, vol. 22, p. 961, 1979.

[3] J. P. Huignard and A. Marrakchi, "Coherent signal beam amplification in two-wave mixing experiments with photorefractive $Bi_{12}SiO_{20}$ crystals," *Opt. Commun.*, vol. 38, p. 349, 1981.

[4] P. N. Günter, "Holography, coherent light amplification and optical phase conjugation with photorefractive materials," *Phys. Rep.*, vol. 93, p. 199, 1982 and references therein.

[5] M. B. Klein, "Beam coupling in undoped GaAs at 1.06 μm using the photorefractive effect," *Opt. Lett.*, vol. 9, p. 350, 1984.

[6] B. Fischer, J. O. White, M. Gronin-Golomb, and A. Yariv, "Nonlinear vectorial two-beam coupling and forward four-wave mixing in photorefractive materials," *Opt. Lett.*, vol. 11, p. 239, 1986.

[7] R. Y. Chiao, P. L. Kelley, and E. Garmire, "Stimulated four-photon interactions and its influence on stimulated Rayleigh-wing scattering," *Phys. Rev. Lett.*, vol. 17, p. 1158, 1966; R. L. Carman, R. Y. Chiao, and P. L. Kelley, "Observation of degenerate stimulated four-photon interaction and four-wave parametric amplification," *Phys. Rev. Lett.*, vol. 17, p. 1281, 1966.

[8] D. I. Stasel'ko and V. G. Sidorovich, "Efficiency of light-beam conversion by dynamic three-dimensional phase holograms," *Sov. Phys. Tech. Phys.*, vol. 19, p. 361, 1974; "Efficiency of light-beam transformation by dynamic phase holograms. I," *Sov. Phys. Tech. Phys.*, vol. 21, p. 205, 1976; V. G. Sidorovich and D. I. Stasel'ko, "Transformation of light beams by dynamic correctors using three-dimensional displacement phase holograms," *Sov. Phys. Tech. Phys.*, vol. 19, p. 1593, 1975; "Light-wave propagation in amplitude dynamic holograms with recording in media with saturable amplification and absorption," *Opt. Spectrosc.*, vol. 38, p. 695, 1975; "Parameters of light beams corrected by dynamic three-dimensional phase holograms," *Sov. Phys. Tech. Phys.*, vol. 20, p. 1614, 1976; V. G. Sidorovich, "Diffraction efficiency of three-dimensional phase holograms," *Sov. Phys. Tech. Phys.*, vol. 21, p. 742, 1976; "Theory of the transformation of light fields by amplitude three-dimensional holograms recorded in amplifying media," *Opt. Spectrosc.*, vol. 42, p. 395, 1977.

[9] P. Yeh, "Exact solution of a nonlinear model of two-wave mixing in Kerr media," *J. Opt. Soc. Amer. B*, vol. 3, p. 747, 1986.

[10] J. P. Huignard and A. Marrakchi, "Coherent signal beam amplification in two-wave mixing experiments with photorefractive $Bi_{12}SiO_{20}$ crystals," *Opt. Commun.*, vol. 38, p. 249, 1981.

[11] J. P. Huignard and J. P. Herriau, "Frequency shifters for photorefractive crystals," *Appl. Opt.*, vol. 24, p. 4285, 1985.

[12] G. C. Valley, "Two-wave mixing with an applied field and a moving grating," *J. Opt. Soc. Amer.*, vol. B1, p. 868, 1984 and references therein.

[13] A. Maruani, "Propagation analysis of forward degenerative four-wave mixing," *IEEE J. Quantum Electron.*, vol. QE-16, p. 558, 1980.

[14] See, for example, Y. R. Shen, *The Principles of Nonlinear Optics*. New York: Wiley Interscience, 1984.

[15] J. F. Reintjes, *Nonlinear Optical Parametric Processes in Liquids and Gases*. New York: Academic, 1984.

[16] R. A. Fisher, *Optical Phase Conjugation*. New York: Academic, 1983 and references therein.

[17] C. V. Heer and N. C. Griffen, "Generation of a phase-conjugate wave in the forward direction with thin Na-vapor cells," *Opt. Lett.*, vol. 4, p. 239, 1979.

[18] A. L. Smirl and T. F. Boggess, "Generation of a forward-traveling phase-conjugate wave in germanium," *Opt. Commun.*, vol. 34, p. 463, 1980.

[19] I. C. Khoo, P. Y. Yan, T. H. Liu, S. Shepard, and J. Y. Hou, "Theory and experiment on optical transverse intensity bistability in the transmission through a nonlinear thin (nematic liquid crystal) film," *Phys. Rev. A*, vol. 29, p. 2756, 1984.

[20] I. C. Khoo and T. H. Liu, "Probe beam amplification via two- and four-wave mixings in a nematic liquid crystal film," *IEEE J. Quantum Electron.*, vol. QE-23, p. 171, 1987.

Tsuen-Hsi Liu [redacted]. He received the B.S. degree from National Cheng-Kung University, Tainan, Taiwan, in 1978, and the M.S. degree from Wayne State University, Detroit, MI, in 1984, both in physics. He will receive the Ph.D. degree in electrical engineering from the Pennsylvania State University, University Park, PA, in 1987.

His graduate research included optical bistable devices, optical phase conjugation, beam amplification, and nonlinear optics in liquid crystals.

Mr. Liu is a student member of the IEEE LEOS, OSA, and SPIE. He is a recipient of a GTE Fellowship in 1987.

Iam-Choon Khoo (M'85-SM'86), for a photograph and biography, see p. 272 of the February 1987 issue of this JOURNAL.

Four wave mixing with gain using liquid crystal films

I. C. Khoo, T. H. Liu, R. R. Michael, G. M. Finn and J. Y. Hou

Electrical Engineering Department, Pennsylvania State University
121 Electrical Engineering East, University Park, PA 16802

Abstract

The extraordinarily large thermal and orientational nonlinearities of nematic liquid crystal is studied in the context of amplified reflection in four wave mixing. Greater than 100% reflection in wavefront conjugation can be obtained.

Introduction

Four wave mixings and related wavefront conjugation and other interesting real time imaging processes have been studied by various workers using a variety of nonlinear materials[1]. In highly nonlinear media such as $BaTiO_4$ and BSO, the large nonlinearities enable probe (or image) beam amplification and self-oscillations with the use of low power cw lasers[2,3].

In this paper, we will investigate the two mechanisms for optical nonlinearities in nematic liquid crystals in the context of probe beam gain or wavefront conjugation reflection amplification, namely, the thermal nonlinearity[4] associated with the ordinary (dn_o/dT) and the extraordinary (dn_e/dT) rays, and the orientational nonlinearity[5]. The mechanism and dynamics of these nonlinearities have been discussed in details recently, and thus our principal discussions here are on the specific conditions whereby these beam amplifications can be realized.

Discussion

Consider a homeotropically aligned nematic liquid crystal film illuminated by two linearly polarized (in the y-direction) lasers with propagation constant $\vec{k}_1$ and $\vec{k}_2$. The lasers interfere with one another and, through some absorption in the nematic, set up a temperature grating in the x direction with a grating constant Λ [$\Lambda = 2\pi \mid \vec{k}_1 - \vec{k}_2 \mid^{-1}$]. Realistically, of course, the temperature (and therefore the refractive index) grating build up and decay are three-dimensional problems, which are further complicated by the lasers finite beam width, the different thermal conductivities of the glass and nematics, as well as the anisotropy in the thermal conductivities and refractive indices. Nevertheless, without much loss of physical insights, one can consider the simpler soluble case where the laser beam is assumed to be a plane wave (true for beam size on the order of a few mm while d and Λ are on the order of about 100 μms), and the heat diffusion is assumed to be along the x-direction (which is a valid assumption for $\Lambda \ll d$). For $\Lambda \sim d$, then heat diffusion from the nematics to the glass walls (along the z direction) can also be taken into account. However, once we know how the mechanisms and dynamics of the process in the one-dimensional case, the two- or three-dimensional problems do not really provide any newer insights.

In the one-dimensional case, the equation governing the temperature distribution is given by

$$\rho c \frac{\partial \Delta T}{\partial t} - K \frac{\partial^2 \Delta T}{\partial x^2} = \alpha I_{op} \tag{1}$$

where the optical intensity I_{op} is given by

$$I_{op} = I_1 + I_2 + 2\sqrt{I_1 I_2} \cos \frac{2\pi}{\Lambda} x \tag{2}$$

$$= I_1 \left[1 + \frac{I_2}{I_1} + 2\sqrt{\frac{I_2}{I_1}} \cos \frac{2\pi x}{\Lambda} \right] \tag{3}$$

We are interested in the case where $I_2 \ll I_1$, so equation (3) may be rewritten as

$$I_{op} = I_1[1 + m \cos \frac{2\pi x}{\Lambda}] \tag{4}$$

where $m = 2\sqrt{I_2/I_1}$. In equation (1), ρ is the density of the nematic, c the heat capacity, K the thermal conductivity and α the light absorption constant.

There are two distinct time scales, namely, transient and steady state, which allow one to clearly determine a set of conditions governing high wave mixing efficiency. For a given grating constant Λ, the characteristic heat diffusion time is given by $\tau = \frac{\rho c}{k(2\pi/\Lambda)^2}$. For a typical nematic like PCB (Pentyl-Biphenyl), $\rho \sim 1$, $c \sim 2$ Joule $°C^{-1} gm^{-1}$ $k = 10^{-3}$ Joule/cm sec °C. For $\Lambda = 100$ μm, e.g. we have $\tau = [3.6]$ ms. We shall henceforth refer to the steady state case as occurring when the time $t \gg \tau$, while the transient case is for $t \ll \tau$.

In the steady state case, $\frac{\partial}{\partial t} = 0$, and we have

$$\Delta T_{SS} = \frac{2\alpha\sqrt{I_1 I_2}}{K(2\pi/\Lambda)^2} \cos \frac{2\pi}{\Lambda} x + c_1 \tag{5}$$

where c_1 is an overall rise in the background temperature. On the other hand, for $t \ll \tau$, we have

$$\Delta T_{TS} = \frac{\tau_\ell \, 2\alpha}{\rho c} \sqrt{I_1 I_2} \cos(\frac{2\pi}{\Lambda})x + c_2 \tag{6}$$

where c_2 is the overall background rise in temperature due to an optical illumination for a duration τ_ℓ. The maximum temperature rise at the intensity maxima from (5) and (6) are, respectively

$$\Delta T_{SS} = 2\alpha\sqrt{I_1 I_2} \, (\frac{\Lambda}{2\pi})^2/K \tag{7}$$

and

$$\Delta T_{TS} = 2\alpha\sqrt{I_1 I_2} \, (\frac{\tau_\ell}{\rho c}) \tag{8}$$

ΔT_{TS} is comparable to ΔT_{SS} if $\tau_\ell \sim \tau$.

The change in the refractive index due to the rise in temperature is given by

$$\Delta n = n(T_o + \Delta T) - n(T_o) \tag{9}$$

where T_o is the initial temperature of the sample.

Assuming that the first terms on the R.H.S. of (5) and (6) are small compared to the overall rise in temperature c_1 and c_2, we have for the steady state case

$$\Delta n_{SS} = \frac{dn}{dT}\Big|_{T_o + c_1} \Delta T_{SS} \tag{10}$$

And for the transient case

$$\Delta n_{TS} = \frac{dn}{dT}\Big|_{T_o + c_2} \Delta T_{TS} \tag{11}$$

As we remarked before, dn/dT for both ordinary and extraordinary rays are larger in magnitude factor of more than 30 times near T_c. In the thin phase grating case ($d \ll \Lambda$), the first order diffraction efficiency from the phase grating is proportional to $(\Delta n)^2$. Efficient wave mixings, therefore, can be obtained by setting the temperature $(T_o + c_1)$ or $(T_o + c_2)$ at near T_c (c.f. figure 2).

Secondly, in the steady case, it is obvious that the wave mixing efficiency will also increase with larger grating constant (which is also observed experimentally). Furthermore, since $dn_{||}/dT$ is in general larger than $dn_{\perp}/dT$, a higher diffraction efficiency can be obtained if one uses a planar sample ($\theta = 0$). In general, the diffraction efficiency is an order of magnitude larger than if one probes $dn_{||}/dT$.

Referring to figure 1 (see also figure 3) for a reconstructing beam $\vec{k}_3 = -\vec{k}_1$, the image (or generated) beam $\vec{k}_F$ will be in the direction $-\vec{k}_2$. The ratio of intensity of the beam 4 to beam 2, i.e. the reflectivity will increase as the parameters discussed in the preceding paragraph are maximized. As reported in a recent preliminary study, amplified reflection can be obtained in MBBA (Methoxy-benzylidene-butylaniline) sample (which absorbs considerably at the 5145 A laser line) at incident laser power on the watt range. Using an appropriate geometry that accounts for the scattered noise and the coherence of the laser, self oscillations are also observed. In a typical experiment involving a 75 μm sample (and $dn_1/\partial T$), a pump beam of ~ 1 Watt in power [beam size 1 mm^2] and a probe beam with a power of 1/200 that of the pump, a reflectivity of 1% is obtained for a wave mixing angle of 1/200 radian at room temperature (22°C). For the same mixing angle, the reflectivity increases by about 30 times near T_c. By decreasing the wave mixing angle to about 1/450 radian, a reflectivity of more than unity can be obtained.

Four wave mixing in liquid crystals using reorientational nonlinearities have been studied in various context. In our first experiment on wavefront conjugation[6], the aberration correction capability is demonstrated. Recently, we have also demonstrated the possibility of noise removal in wavefront conjugation using partially coherent laser[7]. Fundamental studies of the four wave mixing efficiencies based on reorientational nonlinearity have also appeared. In this paper therefore, we will investigate the conditions where amplified wavefront conjugation (or reflection) may be obtained.

As shown in the previous study, the reorientational effect induced by two intersecting laser is described by the Free energy density

$$f = \frac{1}{2} K_2\left(\frac{\partial\theta}{\partial x}\right)^2 + \frac{1}{2} K_2\left(\frac{\partial\theta}{\partial z}\right)^2$$

$$- \frac{\Delta\epsilon}{8\pi} [E_1^2+E_2^2+2E_1E_2\cos(\frac{2\pi}{\Lambda}x)]\sin(2\theta)\sin(2\theta),$$

where K_e is the elastic constant. Under the hard boundary conditions that $\theta=0$ at $Z=0$ and at $z=d$, and assuming an infinite plane wave in the direction, the solution for θ is

$$\theta=[C_1+C_2\cos(\frac{2\pi}{\Lambda}x)]\ g(z), \tag{13}$$

where C_1 and C_2 are to be obtained by the variational method, i.e., by setting $\partial F/\partial C_1=0$ and $\partial F/\partial C_2=0$, while $g(z)$ is the normalized function $g(z)=4(zd-z^2)/d^2$.

From the two conditions $\partial F/\partial C_1=0$ and $\partial F/\partial C_2=0$, we obtain

$$C_1 = \frac{3\Delta\epsilon d^2}{64\pi K}(E_1^2+E_2^2)\sin(2\theta) \tag{14}$$

and

$$C_2 = \frac{15\Delta\epsilon d^2E_1E_2\sin(2\theta)}{16\pi K(q^2d^2+10)} \ . \tag{15}$$

where $q = (\frac{2\pi}{\Lambda})$

Inserting (4) and (5) into (3) gives

$$\theta = \frac{3\Delta\epsilon\sin(2\theta)}{16\pi K}\left(E_1^2+E_2^2+\frac{20E_1E_2\cos(qx)}{q^2d^2+10}\right)(zd-z^2) \ . \tag{16}$$

For optical fields propagating as shown in Fig. 1, the effective dielectric constant is given by

$$\varepsilon_{eff} = \frac{\varepsilon_{\perp}\varepsilon_{\parallel}}{\varepsilon_{\parallel}\cos^2(\beta+\theta)+\varepsilon_{\perp}\sin^2(\beta+\theta)} \tag{17}$$

$$\simeq \varepsilon(\beta)+\delta\varepsilon(\theta)+\delta\varepsilon(\theta^2) \tag{18}$$

for $\Delta\varepsilon/\varepsilon_{\parallel} \simeq \Delta\varepsilon/\varepsilon_{\perp} \ll 1$ and $\theta \ll 1$. From (7) and (8), we obtain

$$\varepsilon(\phi)=\varepsilon_{\perp}\left(1+\frac{\Delta\varepsilon}{\varepsilon}\sin(2\beta)\right), \tag{19}$$

$$\delta\varepsilon(\theta)=\theta\,\frac{\varepsilon_{\perp}\Delta\varepsilon\theta}{\varepsilon_{\parallel}}\sin(2\beta), \tag{20}$$

$$\delta\varepsilon(\theta^2)=\theta^2\,\frac{\varepsilon_{\perp}\Delta\varepsilon}{\varepsilon_{\parallel}}\cos^2\beta, \tag{21}$$

In conjunction with (6) we note that θ, and therefore $\delta\varepsilon(\theta)$ and $\delta\varepsilon(\theta^2)$, are vanishing for $\phi=0$. For finite ϕ, $\delta\varepsilon(\theta^2)$ is much smaller than $\delta\varepsilon(\theta)$ and thus may be neglected. From equations (20) and (16), one can see that the laser induced dielectric constant change $\delta\varepsilon(\theta)$ is maximal at $\beta=45°$.

Secondly, the nonlinearity varies inversely as $(d^2 + \Lambda^2)$, where d is the sample thickness, and Λ the grating constant. In our recent study on wavefront conjugation (c.f. figure 3), an amplified reflection that traverse back along E_1 [beam c] can be obtained under the following conditions: $\beta = 22°$; $d \sim \Lambda \sim 200$ μm; $E_1 \sim E_3 = 0.5$ watt; $E_2 \leq 0.01$ watt; beam-size = 2 mm^2. It is obvious from the rather modest powers involved that the reorientational nonlinearity is a good candidate for wavefront conjugation with gain studies.

It is also clear from these studies that the use of lasers at much longer wavelength would be ideal, or conversely, nematic liquid crystal films are ideally suited for wavefront conjugation using infrared lasers (e.g. CO_2). With $\lambda CO_2 = 10.6$ μm versus the 0.5145 μm of argon laser line, the wave mixing angle can be increased by 20 times (i.e. a wave mixing angle of 1/20 radian (= 3°)) while amplified reflection can still be observable. Moreover, the reorientational effect is not wavelength sensitive. Experiments with infra-red lasers are currently under way and will be reported in a longer article elsewhere.

Acknowledgement

This research is supported by a grant from the National Science Foundation under grant no. ECS8415397 and by the Air Force Office of Scientific Research under grant no. AFOSR840375

References

1. For a good list of references, see "Optical Phase Conjugation," ed. R. Fisher (Academic, New York 1983).
2. See, for example, J. Feinberg and R. W. Hellwarth, Opt. Lett. 5, 519 (1980); B. Fisher, M. Cronin-Golomb, J. P. White and A. Yariv, Opt. Lett. 6, 519 (1981).
3. H. Rajbenbach and J. P. Huignard, Opt. Lett. 10, 137 (1985).
4. I. C. Khoo and S. Shepard, J. Appl. Phys. 54, 5491 (1985). I. C. Khoo and R. Normandin, Optics Letts. 9, 285 (1984); IEEE JQE 21, 329 (1985). See also H. Hsiung, L. P. Shi and Y. R. Shen, Phy. Rev. A30, 1453 (1984).
5. See, for example, I. C. Khoo and Y. R. Shen, Optical Engineering 24, 579 (1985) and references therein.
6. I.C. Khoo and S. L. Zhuang, IEEE JQE 18, 246 (1982)
7. E. N. Leith, H. Chen, Y. Cheng, G. Swanson and I. C. Khoo Proceedings of 5th Rochester Conference on coherence and Quantum Optics (Plenum, NY 1984).

Figure Captions

Fig. 1. Schematic of lasers propagating in (a) a homeotropically aligned nematic liquid crystal film and (b) a planar nematic film. The $\hat{x}$-direction is perpendicular to the plane of the paper; z-direction is parallel to $\hat{n}$. For thermal effect, $\delta = 0$ or 90°. For orientational effect, $\delta = 22°$.

Fig. 2. Observed dependence of the thermal grating diffraction as a function of the temperature.

Fig. 3. A typical wavefront conjugation set up.

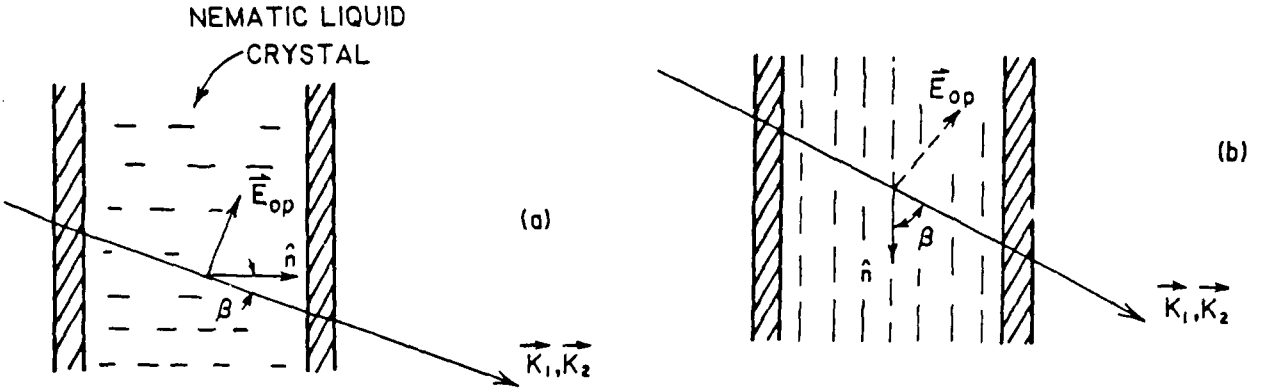

FIGURE 1

FIGURE 2

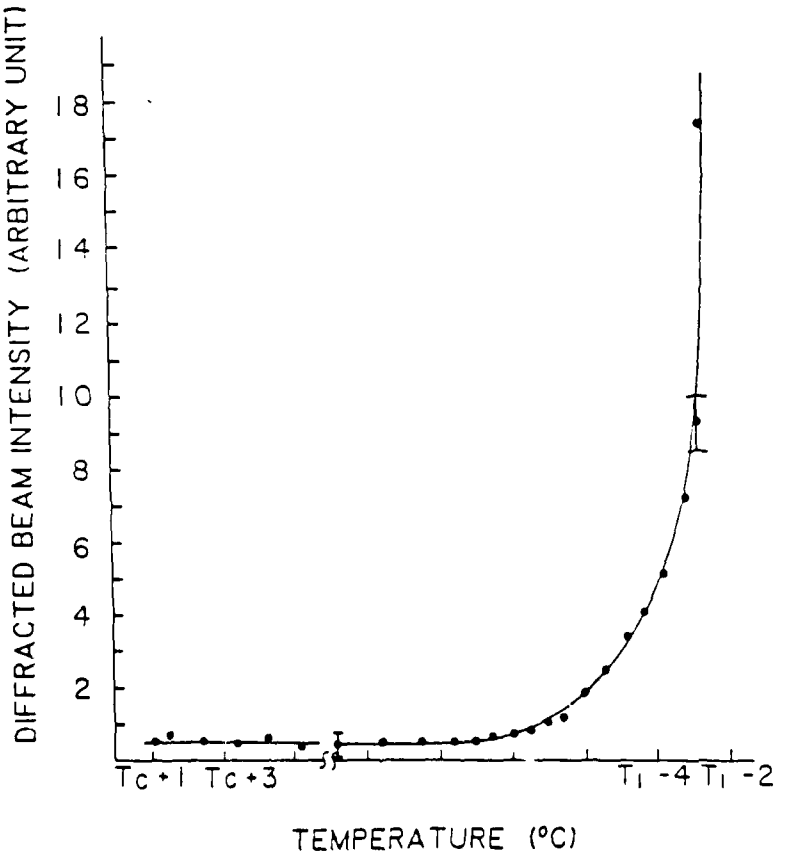

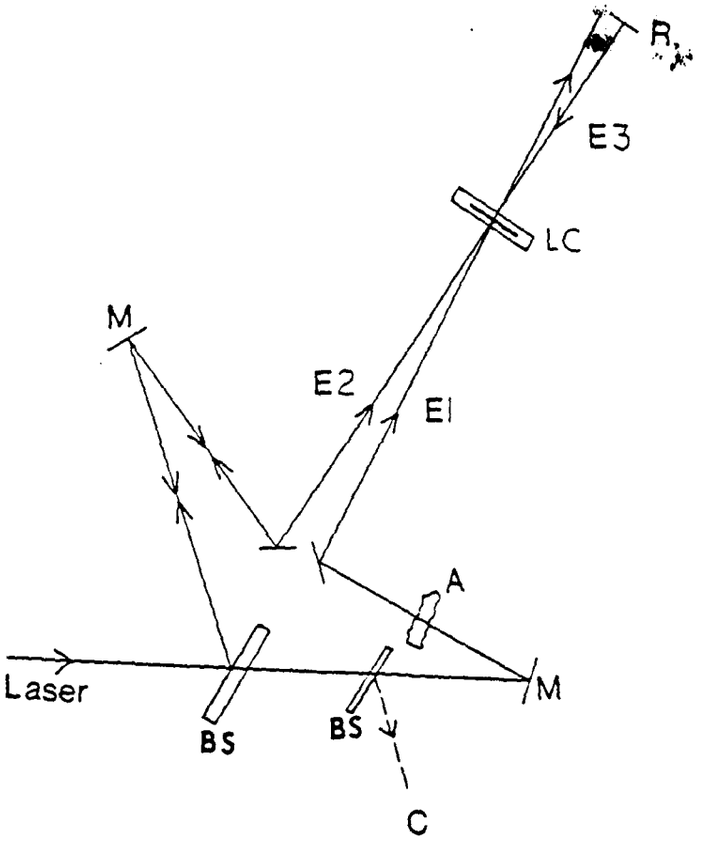

FIGURE 3